



BMBF funding measure GROW – Water as a global resource

Ein globales Werkzeug zur Charakterisierung von Dürren
und Quantifizierung ihrer Wirkungen auf Wasserressourcen
(GlobeDrought)

A global-scale tool for characterising droughts and quantifying
their impact on water resources (GlobeDrought)



Schlussbericht

Projektkoordination	Prof. Dr. Stefan Siebert Department für Nutzpflanzenwissenschaften der Georg-August-Universität Göttingen
Projektlaufzeit	01.08.2017 – 31.12.2020
Förderkennzeichen	02WGR1457A bis F




Gemeinsamer Schlussbericht der Teilvorhaben

FKZ
02WGR1457A

Rheinische Friedrich Wilhelms
Universität Bonn

Institut für Geodesie und
Geoinformation
Prof. Dr. Jürgen Kusche
(Projektleitung)


Zentrum für Fernerkundung der
Landoberfläche
PD Dr. Olena Dubovyk


UNIVERSITÄT **BONN**

FKZ
02WGR1457B


Johann Wolfgang Goethe-Universität
Frankfurt am Main


Institut für Physische Geographie
Prof. Dr. Petra Döll (Projektleitung)


GOETHE
UNIVERSITÄT
FRANKFURT AM MAIN

FKZ
02WGR1457C


Universität der Vereinten Nationen
Institut für Umwelt und menschliche
Sicherheit
Dr. Michael Hagenlocher
(Projektleitung)


UNITED NATIONS
UNIVERSITY


UNU-EHS
Institute for Environment
and Human Security


FKZ
02WGR1457D

Remote sensing Solutions GmbH
Dr. Jonas Franke (Projektleitung)


RSS
remote sensing
SOLUTIONS


FKZ
02WGR1457E

Welthungerhilfe
Daniel Rupp (Projektleitung)


welt
hunger
hilfe

FKZ
02WGR1457F

Georg-August-Universität Göttingen
Institut für
Nutzpflanzenwissenschaften
Prof. Dr. Stefan Siebert
(Projektleitung)


GEORG-AUGUST-UNIVERSITÄT
GÖTTINGEN

Das diesem Bericht zugrundeliegende Vorhaben wurde mit Mitteln des Bundesministeriums für Bildung und Forschung unter dem Förderkennzeichen 02WGR1457A-F gefördert. Die Verantwortung für den Inhalt dieser Veröffentlichung liegt bei den Autoren.











Berichtsblatt

1. ISBN oder ISSN	2. Berichtsart (Schlussbericht oder Veröffentlichung) Schlussbericht
3. Titel Ein globaleskaliges Werkzeug zur Charakterisierung von Dürren und Quantifizierung ihrer Wirkungen auf Wasserressourcen (GlobeDrought)	
4. Autor(en) [Name(n), Vorname(n)] Siebert, Stefan; Nouri, Hamideh; Eyshi Rezaei, Ehsan; Kusche, Jürgen; Dubovyk, Olena; Döll, Petra; Herbert, Claudia; Hagenlocher, Michael; Franke, Jonas; Rupp, Daniel	5. Abschlussdatum des Vorhabens 31.12.2020
	6. Veröffentlichungsdatum 01.11.2021
	7. Form der Publikation Elektronisches Dokument
8. Durchführende Institution(en) (Name, Adresse) Universität Göttingen, DNPW, Von-Siebold-Str. 8, 37075 Göttingen Universität Bonn, IGG, Nussallee 17, 53115 Bonn Universität Bonn, ZfL, Genscherallee 3, 53113 Bonn Universität Frankfurt am Main, IPG, Altenhöferallee 1, 60438 Frankfurt am Main Universität der Vereinten Nationen, EHS, Platz der Vereinten Nationen 1, 53113 Bonn Remote Sensing Solutions GmbH, Dingolfinger Str. 9, 81673 München Deutsche Welthungerhilfe e. V., Friedrich-Ebert-Str. 1, 53173 Bonn	9. Ber. Nr. Durchführende Institution
	10. Förderkennzeichen 02WGR1457A – 02WGR1457F
	11. Seitenzahl 154
12. Fördernde Institution (Name, Adresse) Bundesministerium für Bildung und Forschung (BMBF) 53170 Bonn	13. Literaturangaben 104
	14. Tabellen 2
	15. Abbildungen 44 + Anhang
16. Zusätzliche Angaben	
17. Vorgelegt bei (Titel, Ort, Datum)	
18. Kurzfassung Im Rahmen des Projektes erfolgte eine räumlich explizite Beschreibung von Dürreerisiken durch Betrachtung der Komponenten Dürregefahr, Exposition und Verwundbarkeit für landwirtschaftliche Systeme sowie die Wasserversorgung. Die gewonnenen Informationen wurden auf globaler Ebene sowie für die Projektregion südliches Afrika (Südafrika, Zimbabwe) in einem Dürreinformationssystem verfügbar gemacht. Die Verknüpfung von satelliten-gestützter Fernerkundung mit hydrologischer Modellierung und Ertragsmodellierung sowie mit der Analyse von Niederschlagsdaten führte zu hochaufgelösten Indikatoren für meteorologische, hydrologische und agronomische Dürregefahren. Die Exposition von Anbaukulturen im Bewässerungs- und Regenfeldbau wurde separat berücksichtigt. Treiber, räumliche Muster sowie Dynamiken von Verwundbarkeit der betrachteten Sektoren gegenüber Dürren wurden analysiert. Dazu wurden systematische Erhebungen unter Experten weltweit zu Verwundbarkeitsindikatoren sowie deren Gewichtung durchgeführt. Die Ergebnisse der Dürreerisikoanalyse wurden durch Vergleich mit Informationen zu bekannten Dürrewirkungen (z.B. Ertragsausfälle, monetäre Verluste, Beeinträchtigung der Versorgung mit Trinkwasser und Nahrungsmitteln) aus globalen und regionalen Datenbanken validiert. Zudem wurden zwei Validierungsworkshops mit globalen und regionalen Anwendern durchgeführt. Die im Projekt gewonnenen Daten und Erkenntnisse sind bereits in externe Informationssysteme eingeflossen, z.B. in das Global Drought Observatory (GDO) des Joint Research Centers der Europäischen Kommission in Ispra, das Politiker, Entscheidungsträger sowie die Bevölkerung in Europa über Dürreerisiken informiert. Um die Verbreitung von Methoden und Daten zu fördern, erfolgte die Veröffentlichung wesentlicher Ergebnisse in Fachzeitschriften unter Einbeziehung ausgewählter regionaler sowie globaler Partner. Gemeinsam mit Forscher(innen) aus dem SaWaM-Projektverbund wurde ein Konzept zur saisonalen Dürrevorhersage basierend auf Bias-korrigierten Ensemblevorhersagen entwickelt und durch Verknüpfung globaler Modelle mit globaler Klimadatenprozessierung erfolgreich demonstriert.	
19. Schlagwörter Dürregefahren, Verwundbarkeit, Dürreerisiko, Landwirtschaft, Wasserversorgung, Globale Analyse, Südafrika, Zimbabwe, Indien, USA, Modellierung, Fernerkundung, Risikoanalyse, Informationssystem	
20. Verlag	21. Preis

Document Control Sheet

1. ISBN or ISSN	2. type of document (e.g. report, publication) Final report
3. title A global-scale tool for characterising droughts and quantifying their impact on water resources (GlobeDrought)	
4. author(s) (family name, first name(s)) Siebert, Stefan; Nouri, Hamideh; Eysli Rezaei, Ehsan; Kusche, Jürgen; Dubovyk, Olena; Döll, Petra; Herbert, Claudia; Hagenlocher, Michael; Franke, Jonas; Rupp, Daniel	5. end of project 31.12.2020
	6. publication date 01.11.2021
	7. form of publication Online publication
8. performing organization(s) (name, address) University of Göttingen, DNPW, Von-Siebold-Str. 8, 37075 Göttingen University of Bonn, IGG, Nussallee 17, 53115 Bonn University of Bonn, ZfL, Genscherallee 3, 53113 Bonn University of Frankfurt am Main, IPG, Altenhöferallee 1, 60438 Frankfurt am Main University of the United Nations, EHS, Platz der Vereinten Nationen 1, 53113 Bonn Remote Sensing Solutions GmbH, Dingolfinger Str. 9, 81673 München Deutsche Welthungerhilfe e. V., Friedrich-Ebert-Str. 1, 53173 Bonn	9. originator's report no.
	10. reference no. 02WGR1457A – 02WGR1457F
	11. no. of pages 154
12. sponsoring agency (name, address) Bundesministerium für Bildung und Forschung (BMBF) 53170 Bonn	13. no. of references 104
	14. no. of tables 2
	15. no. of figures 44 + Appendix
16. supplementary notes	
17. presented at (title, place, date)	
18. abstract The project performed a spatial analysis of drought risks by integrating the components drought hazard, exposure and vulnerability for irrigated and rainfed agricultural systems and the water supply sector. The results of a global analysis and more detailed regional assessments for South Africa and Zimbabwe have been made available to the public in a drought information system. Indicators for meteorological, hydrological and agronomic drought hazards were obtained at high spatial resolution by combining satellite remote sensing, precipitation data analysis and hydrological and crop modeling. The exposure of irrigated and rainfed crops was explicitly considered. To analyze drivers, spatial patterns and temporal dynamics of drought vulnerability, expert surveys were performed systematically resulting in vulnerability indicators and their weights for the sectors considered in the project. The results of the drought risk analysis were validated by comparing computed drought hazard and exposure to drought impacts such as yield losses, economic losses or the number of affected people reported in global and regional data bases. In addition, two validation workshops were organized with participation of global and regional stakeholders. The information and data sets developed by the project groups have already been used by external scientists, for example by the Global Drought Observatory of the Joint Research Centre of the European Commission to inform policy makers and citizens across Europe about current drought risk. To facilitate knowledge dissemination and reuse of our products, several scientific articles were published together with regional and global end users of our products. A concept for a global drought forecasting system based on bias-corrected seasonal ensemble weather forecasts was developed together with researchers from the SaWaM-project and demonstrated successfully.	
19. keywords Drought hazard, vulnerability, drought risk, crop production, water supply, global assessment, South Africa, Zimbabwe, India, USA, modeling, remote sensing, risk analysis, information system	
20. publisher	21. price

Authors / project members

Authors (bold) / project members	Institution	
Prof. Dr. Jürgen Kusche Helena Gerdener Dr. Olga Engels	University of Bonn, Institute of Geodesy and Geoinformation, Nussallee 17, 53115 Bonn	 UNIVERSITÄT BONN 
PD Dr. Olena Dubovyk Dr. Valerie Graw Dr. Gohar Ghazaryan Dr. Javier Gonzales Simon König	University of Bonn, ZfL, Genscherallee 3, 53113 Bonn	 UNIVERSITÄT BONN 
Prof. Dr. Petra Döll Claudia Herbert Eklavyya Popat	University of Frankfurt, Institute of Physical Geography Altenhöferallee 1, 60438 Frankfurt am Main	 GOETHE UNIVERSITÄT FRANKFURT AM MAIN
Dr. Michael Hagenlocher Isabel Meza Dr. Erick Tambo Annika Min Dr. Emmanuel Cheo Dr. Zita Sebesvari Zeinab El Maadawi Yannick Urs Schillinger Dr. Yvonne Walz	University of the United Nations, Institute for Environmental and Human Security, Platz der Vereinten Nationen 1, 53113 Bonn	  UNITED NATIONS UNIVERSITY UNU-EHS Institute for Environment and Human Security
Dr. Jonas Franke Dr. Tobias Landmann Natalie Cornish Maximilian Schwarz	Remote Sensing Solutions GmbH, Dingolfinger Str. 9, 81673 München	
Daniel Rupp Dr. Heinz Peters Katharina Wietler Jasmin Koottummel	Deutsche Welthungerhilfe e. V., Friedrich-Ebert-Str. 1, 53173 Bonn	
Prof. Dr. Stefan Siebert Dr. Hamideh Nouri Dr. Ehsan Eyshi Rezaei Malte Weller Anja Wrobel	University of Göttingen, Department of Crop Sciences, Von-Siebold-Str. 8, 37075 Göttingen	 GEORG-AUGUST-UNIVERSITÄT GÖTTINGEN

Zusammenfassung

Aufgabenstellung

Ziel des Gesamtvorhabens GlobeDrought war die stakeholder-unterstützte Entwicklung eines Informationssystems zur umfassenden Charakterisierung von Dürreereignissen und ihrer Auswirkungen auf Wasserressourcen, die Produktivität im Pflanzenbau, den Handel mit Nahrungsmitteln, die Ernährungssicherheit und den Bedarf an internationaler Nahrungsmittelhilfe. Analysen sollten auf globaler Skala sowie, mit höherem Detail, für besonders von Dürren betroffene Regionen durchgeführt werden und dabei sowohl das historische Dürreerisiko umfassen, als auch den aktuellen Dürrezustand. In Zusammenarbeit mit dem GRoW-Projekt SaWaM sollte zudem die Eignung von 7-monatigen, globalen, bias-korrigierten ECMWF-Wettervorhersagen für die Dürreprojektion getestet werden.

Voraussetzungen unter denen das Projekt durchgeführt wurde

Der Stand der Forschung zu Beginn des Vorhabens war dass Dürreinformationssysteme entweder Fernerkundungsinformationen und Niederschlagsdaten basierten während Pflanzenwachstumsmodellierung und hydrologische Modellierung selten zum Einsatz kamen. Ansätze aus der Fernerkundung haben dabei den Vorteil einer hohen räumlichen Auflösung aber den Nachteil von nur relativ kurzen verfügbaren Zeitreihen. Modelle zur Berechnung von Indikatoren für hydrologische oder agronomische Dürren können lange Zeiträume abdecken und sehr detailliert sogar Kulturarten unterscheiden, verfügen aber üblicherweise über eine geringe räumliche Auflösung. In den meisten Fällen beschränkten sich verfügbare Dürreinformationssysteme auf Dürregefahren, während eine Integration von Informationen zu Exposition und Verwundbarkeiten zum Dürreerisiko selten durchgeführt wurde.

Ablauf des Vorhabens

Zu Beginn des Projektes wurde in Zusammenarbeit mit allen Partnern und unter Beteiligung der Stakeholder zunächst die Projektregionen ausgewählt und ein Konzept zur Abbildung von Dürregefahren, Dürreexposition, Verwundbarkeit sowie der Integration zum Dürreerisiko einschließlich der dafür nötigen Indikatoren entwickelt sowie Bestandteile des zu entwickelnden Dürreinformationssystems definiert. Grundlage bildete eine umfangreiche Literaturstudie zum gegenwärtigen Stand des Wissens in der Dürreerisikoanalyse. Auf einem Projektworkshop wurden im Co-Designprozess mit den regionalen Partnern die zu untersuchenden Sektoren (Bewässerungs- und Regenfeldbau, Wasserversorgung) definiert. Dürregefahren wurden analysiert, in dem prozessbasierte Modelle (WGHM, GCWM, Simplace) mit Fernerkundungsinformationen kombiniert wurden. So konnten Speicheränderungen im globalen hydrologischen Modell WGHM durch Assimilation von Speicheränderungen aus GRACE-Schwerefelddaten angepasst werden. Daten

optischer Fernerkundungssensoren zur Vegetationsaktivität und Evapotranspiration wurden genutzt um Aussat und Erntetermine in Pflanzenwachstumsmodellen anzupassen, Bewässerungs- und Regenfeldbau zu unterscheiden und modellierte Evapotranspiration zu validieren. Informationen zu geeigneten Indikatoren zur Verwundbarkeiten der untersuchten Sektoren sowie zur Gewichtung der Indikatoren wurden durch Auswertung systematischer Expertenbefragungen gewonnen. Informationen zu Dürregefahren, Exposition und Verwundbarkeit wurden schliesslich zum Dürreisiko integriert. Solche integrierten Dürreisikoanalysen wurden mit globaler Abdeckung sowie für die Projektregionen Simbabwe und Südafrika publiziert. Einzelne regionale Studien deckten auch das Missouri-Einzugsgebiet in den USA sowie Teile Indiens ab. Die wesentlichen Ergebnisse des Projektes werden im GlobeDrought – Dürreinformationssystem dargestellt. Schliesslich wurde in Zusammenarbeit mit dem GRoW-Projekt SaWaM (Prof. Kunstmann, KIT, Campus Alpin) eine Prozesskette zur Generierung saisonaler Dürrevorhersagen entwickelt und am Beispiel des Jahres 2018 getestet und demonstriert.

Ergebnisse und Zusammenarbeit mit anderen Forschungseinrichtungen

Es wurde gezeigt dass Dürregefahren räumlich und zeitlich stark variieren, weshalb die Abbildung in hoher raumzeitlicher Auflösung nötig ist. Auf Grund von großen Unterschieden in der Verwundbarkeit der Systeme können ähnliche Dürregefahren zu stark unterschiedlichem Dürreisiko führen. Somit spielt die Verringerung der Verwundbarkeit eine entscheidende Rolle beim Dürremanagement mit dem Ziel der Beschränkung der Dürrewirkungen. Es wurde gezeigt dass die entwickelten Modelle und Indikatoren generell die in Datenbanken berichteten Dürrewirkungen auf die Produktion landwirtschaftlicher Güter sowie die Wasserversorgung sehr gut abbilden können. Für den Zeitraum mit Datenverfügbarkeit konnte auch eine hohe Konsistenz von Modellergebnissen mit Daten der Fernerkundung sowohl regional als auch global belegt werden. Die Ergebnisse der experimentellen, 7-monatigen Dürrevorhersage zeigten deutliche Unterschiede in der Qualität der Vorhersagen für das Jahr 2018 mit überwiegend guten Prognosen für die Südhalbkugel sowie Südeuropa. Demgegenüber wurde die starke Dürre in Mittel- und Osteuropa nicht gut vorhergesagt.

Die Projektgruppen betrieben während der Laufzeit des Projektes eine intensive Zusammenarbeit untereinander sowie mit potentiellen Nutzern der globalen oder regionalen Produkte. Dies ist auch durch zahlreiche gemeinsame Publikationen dokumentiert. Neben vier großen Projektworkshops wurden auch kleinere Treffen mit den Nutzern der regionalen oder globalen Produkte und Daten organisiert. Inhaltliche Erkenntnisse sowie methodische Grundlagen wurden auch durch 12 Webinare und Online-Kurse unter Mitwirkung aller Projektpartner an eine breite Öffentlichkeit kommuniziert. Die Projektgruppen beteiligten sich intensiv an Querschnittsaktivitäten im GRoW-Verbund und präsentierten Konzepte und Ergebnisse auf den gemeinsamen Tagungen und Workshops.

Table of contents

List of tables	10
List of figures	11
Abstract	14
Introduction	15
1 Development of tools and methods for drought risk analysis	19
1.1 Defining the system to be studied	19
1.2 Defining drought impacts to be studied	20
1.3 Linking of hydrological and crop models	21
1.3.1 Concept of coupling WaterGAP and SIMPLACE.....	22
1.3.2 Combining WaterGAP and GCWM to calculate drought hazard for irrigated agriculture	24
1.4 Linking process based modeling with remote sensing.....	25
1.4.1 Improving trends in simulated water storages by using changes in total water storage obtained from GRACE	25
1.4.2 Improving sowing and harvest dates in SIMPLACE by remote sensing information	25
1.4.3 Combining drought hazard simulated with process based crop models with drought indicators derived by remote sensing	26
1.5 Development and application of drought hazard indicators	26
1.5.1 Hydrological drought hazard affecting the water supply	26
1.5.2 Development of drought hazard indicators for rainfed and irrigated crop production	38
1.6 Drought exposure analysis.....	42
1.6.1 Global scale analysis	42
1.6.2 Regional analysis.....	43
1.7 Development of drought vulnerability indicators and indices	43
1.7.1 Global scale analysis of vulnerability to drought.....	44
1.7.2 Regional analysis of vulnerability to drought	45
1.8 Integration of hazard, exposure and vulnerability to drought risk.....	47
1.9 Validation of drought hazards and drought risk	48
2 Results of the drought risk analysis at global scale	49
2.1 Hydrological drought hazard	49
2.2 Drought hazard for agricultural systems.....	50
2.2.1 Irrigated crop production systems	50
2.2.2 Rainfed crop production systems.....	51

2.2.3	Remote sensing based hazard analyses for crop production in general.....	52
2.2.4	Comparison of simulated and remotely sensed drought hazard.....	54
2.3	Exposure to drought.....	55
2.4	Vulnerability of agricultural systems to drought	56
2.5	Drought risk of agricultural systems	56
2.5.1	Drought risk for irrigated systems.....	56
2.5.2	Drought risk for rainfed systems.....	57
2.5.3	Drought risk for agricultural systems (irrigated and rainfed combined)	57
3	Results of the drought risk analysis for regional case studies	59
3.1	South Africa	59
3.1.1	Drought hazard and exposure.....	61
3.1.2	Vulnerability and risk of rainfed and irrigated systems.....	66
3.2	Zimbabwe	69
3.2.1	Drought hazard and exposure.....	70
3.2.2	Drought vulnerability and drought risk.....	73
4	Experimental early warning and forecasting.....	76
5	Dissemination of results and knowledge to the general public.....	79
5.1	Development of the Integrated Drought Tool.....	79
5.2	Knowledge dissemination by webinars and electronic lectures	81
	References	83
	Appendix	90
	Appendix A1 - Time series of global drought hazard 1981-2018	90
	1. Rainfed agricultural systems.....	90
	2. Irrigated agricultural systems.....	109
	Appendix A2 - Time series of global drought risk at country level (2000-2018).....	128
	1. Rainfed agricultural systems.....	128
	2. Irrigated agricultural systems.....	137
	Appendix A3 - Drought impact analysis: regional anomalies in domestic food supply, net trade and production of cereals, oil crops and pulses.....	146
	Appendix A4 - List of project publications.....	153



List of tables

Table 1. Characteristics of streamflow drought hazard indicators suitable for global-scale assessments and their inherent assumptions about habituation of people or other biota.....29

Table 2. Online courses provided by the GlobeDrought Learning Platform..... 81

List of figures

Figure 1. An integrated assessment of drought risk	20
Figure 2. Participants of the 1 st GlobeDrought stakeholder workshop (top) and ranking of drought impacts performed by the participants for selected potential case study regions (bottom).....	21
Figure 3. Flow chart of data exchange between WaterGAP and SIMPLACE	24
Figure 4. Data availability for remote sensing and process based modeling.....	25
Figure 5. Schematic for computing four types of drought hazard indicators, indicating 1) magnitude of the drought at a certain time as deficit and/or anomaly or 2) severity of the drought event, i.e. the cumulative magnitude of drought since drought onset. Both, magnitude and severity, can be expressed in terms of frequency/probability to compare the drought of interest to other droughts. The grey boxes indicate decisions made when computing the indicators. Indicators in bold have already been applied in the literature. Assumptions about the habituation of people and ecosystems determine the selection of the type of indicator, the averaging period and the threshold (see Table 1)	28
Figure 6. Global comparison of overall drought severity during 1986-2015 based on the probability of exceedance p for two streamflow drought hazard indicators: Cumulative streamflow deficit indicator with monthly Q80 as threshold (CDQI-Q80) (a) and cumulative relative deviation from mean monthly streamflow with -50% as threshold (cumulative RDQI1-50%) (b). A high value denotes a high sum of severity compared to other grid cells. A value of 0.8 in grid cell i , for example, means that in 80% of all grid cells the sum of severities of all drought events during 1986-2015 was smaller than in grid cell i . Greenland was excluded from the analysis	32
Figure 7. Country-level drought conditions as indicated by HP anomaly HPA3 (a) and relative reduction HPR3 (b) in August 2003	35
Figure 8. Probabilistic forecast for the year 2019 based on the drought hazard indicator ADQI-Q80, lfm and ERA5 climate data at the WaterGAP calibration station Mainz, Rhine River, Germany..	38
Figure 9. Workflow in the remote sensing based drought risk analyses performed for the Missouri River Basin, South Africa and Zimbabwe (upper left, Fig. 1 in Schwarz et al., 2020), the global scale (upper right, Fig. 1 in Ghazaryan et al., 2020) and for Zimbabwe (bottom left, Fig. 2 in Frischen et al., 2020)	39
Figure 10. The overall workflow of the drought risk assessment for agricultural systems performed at global scale (Fig. 1 in Meza et al., 2020)	47
Figure 11. The overall workflow of the drought risk assessment for agricultural systems performed at regional scale for South Africa (Fig. 2 in Meza et al., 2021)	48
Figure 12. Frequency of occurrence (%) of mild (a), moderate (b), severe (c), extreme (d) or no (e) streamflow drought during the period 1981–2010 as defined by the indicator QDAI (Fig. 6 in Popat and Döll, 2021). Grid cells where for any calendar month there are at least 6 months with $Q_{ant} = 0$ are indicated as int, and grid cells which are not computed due to land cover are indicated as nc	50
Figure 13. Long-term drought hazard of irrigated crop production systems (Fig. 2b in Meza et al., 2020)	51
Figure 14. Long-term drought hazard of rainfed crop production systems (Fig. 3b in Meza et al., 2020)	52
Figure 15. Pearson's correlation coefficient (r) estimated for a maize yield anomaly (based on gridded yield data) with land surface temperature (LST), evaporative stress index (ESI), and normalized difference vegetation index (NDVI) anomalies (peak of the growing season) (Fig. 2a in Ghazaryan et al., 2020)	53
Figure 16. Maximum number of consecutive months with the ESI anomaly < -1 in the period 2001-2017 (non-cropland areas are masked based on the MODIS land cover, Fig. 4a in Ghazaryan et al., 2020)	54
Figure 17. Pearson's correlation coefficient between the crop drought indicator (CDI) for rainfed crops simulated with the Global Crop Water Model and MODIS-based CDI for period 2001-2019.....	54

Figure 18. Exposure to drought for irrigated (top) and rainfed (bottom) agricultural systems in period 1981–2016 (Fig. 4 in Meza et al., 2020)	55
Figure 19. Vulnerability to drought for irrigated and rainfed agricultural systems in period 1981–2016 (Fig. 3c in Meza et al., 2020).....	56
Figure 20. Drought risk for irrigated agricultural systems in period 1981–2016 (Fig. 2a in Meza et al., 2020)	57
Figure 21. Drought risk for rainfed agricultural systems in period 1981–2016 (Fig. 3a in Meza et al., 2020)	57
Figure 22. Drought risk for crop production systems (irrigated and rainfed combined) in period 1981–2016 (Fig. 4a in Meza et al., 2020)	58
Figure 23. South Africa: a) Köppen-Geiger climate classification map for South Africa (1980–2006) (Beck et al., 2018). b) South African provinces. c) and d) Rainfed and irrigated areas per municipality, respectively. e) Ratio between irrigated and total agricultural area per municipality. f) Irrigated and rainfed agriculture in South Africa at pixel level. Maps are based on data from the national land use/land cover dataset 2018 (Thompson, 2019). (Fig. 1 in Meza et al., 2021)	60
Figure 24. Drought hazard and combined hazard/exposure for rainfed (top row) and irrigated (bottom row) cropping systems across South Africa at grid and local municipality levels in the period 1981–2018. Black lines indicate provincial boundaries (Fig. 3 in Meza et al., 2021)	61
Figure 25. Drought hazard/exposure for rainfed cropping systems across local municipalities of South Africa in the period 1981–2018. Black lines indicate provincial boundaries (Fig. 4 in Meza et al., 2021)	62
Figure 26. Drought hazard/exposure for the irrigated cropping system across local municipalities of South Africa for the period 1981–2018. Black lines indicate provincial boundaries (Fig. 5 in Meza et al., 2021)	63
Figure 27. Correlation coefficient between drought exposure of rainfed systems obtained by modeling and remote sensing (Fig. 6 in Meza et al., 2021).....	63
Figure 28. Time series of rainfed drought hazard (positive values indicate drought) and cereal yield and production anomaly in South Africa in the period 1981 to 2018. The r values show the Pearson correlation coefficient (Fig. S6 in Meza et al., 2021).....	64
Figure 29. Drought hazard in South Africa for agricultural, grass- and shrubland in the nondrought season 2013/2014 (left) and the drought season 2015/2016 (right, Fig. 3 in Schwarz et al., 2020)	65
Figure 30. Drought vulnerability and risk in South Africa at local municipality level for rainfed (top row) and irrigated agriculture (bottom row). Tendency to dark blue shows lower levels of vulnerability and risk, the tendency to red shows higher vulnerability or risk values. Black lines indicate provincial boundaries (Fig. 7 in Meza et al., 2021)	67
Figure 31. Local municipalities contrasted with drought risk for rainfed (x axis) and irrigated (y axis) systems. The size of the bubbles represent the amount of crop dependent population by local municipality (Fig. 8 in Meza et al., 2021)	69
Figure 32. Farming systems map for Zimbabwe showing irrigated and rainfed cropland in period 2013–2018 (Fig. 4 in Landmann et al., 2019).....	70
Figure 33. Seasonal vegetation health index (VHI) composites (1989–2019) based on NOAA AVHRR and VIIRS data used to identify drought hazard for agricultural systems in Zimbabwe (Fig. 3 in Frischen et al., 2020)	71
Figure 34. Average number of drought years during 1989–2019 for agricultural systems in Zimbabwe at district level (Fig. 4 in Frischen et al., 2020)	71
Figure 35. Drought hazard in Zimbabwe for agricultural, grass- and shrubland in the nondrought year 2013/2014 (left) and the drought year 2015/2016 (right; Fig. 4 in Schwarz et al., 2020)	72
Figure 36. Vulnerability of agricultural systems in Zimbabwe to drought per district (left) and province (right, bottom). Province boundaries and province names are shown in the map top right (Fig. 6 in Frischen et al., 2020)	73

Figure 37. Drought risk of agricultural systems in Zimbabwe (left) and separation into drought risk for rainfed agriculture (top right) and irrigated agriculture (bottom right; Fig. 7 in Frischen et al., 2020)... 74

Figure 38. Spatial explicit drought hazard, vulnerability and risk for South Africa and Zimbabwe (exemplary) for the growing seasons December to March 2013/14 (non-drought period) and 2015/16 (drought period), respectively (Fig. 6 in Schwarz et al., 2020) 75

Figure 39. Comparison of the drought hazard indicator for rainfed crops simulated with ensemble climate forecasts (ENS) and historical climate in period 1986-2015 (HIS) for the forecast period March 2018 – September 2018 with results obtained from the standard model run with ERA5 data for 2018 (black bold line) for selected countries..... 77

Figure 40. Comparison of the drought hazard indicator for irrigated crops simulated with ensemble climate forecasts (ENS) and historical climate in period 1986-2015 (HIS) for the forecast period March 2018 – September 2018 with results obtained from the standard model runs with ERA5 data for 2018 (black bold line) for selected countries..... 78

Figure 41. The portal interface showing the indicator Accumulated Drought Severity, which is a hazard indicator which can be seen from the left panel. The panel furthermore shows that is dat set is a Global' data set and relevant for rainfed agriculture 79

Figure 42. Participants overview of the online Zimbabwe stakeholder meeting, facilitated in September 2020..... 80

Figure 43. Stakeholders' survey results on the usefulness of the Globe Drought portal that was developed in this sub project. The criteria 'usefulness for decision makers' attained the highest score (4.8)..... 80

Figure 44. Landing page of the GlobeDrought Learning Platform 82

Abstract

The project performed a spatial analysis of drought risks by integrating the components drought hazard, exposure and vulnerability for irrigated and rainfed agricultural systems and the water supply sector. The results of a global analysis and more detailed regional assessments for South Africa and Zimbabwe have been made available to the public in a [drought information system](#).

Indicators for meteorological, hydrological and agronomic drought hazards were obtained at high spatial resolution by combining satellite remote sensing, precipitation data analysis and hydrological and crop modeling. Methods were developed to assimilate remote sensing data obtained by the Gravity Recovery and Climate Experiment (GRACE) into the global hydrological model WaterGAP and to combine remote sensing and crop model based drought hazard and drought impact assessments. The exposure of irrigated and rainfed crops was explicitly considered. To analyze drivers, spatial patterns and temporal dynamics of drought vulnerability, expert surveys were performed systematically resulting in vulnerability indicators and their weights for the sectors considered in the project.

The results of the drought risk analysis were validated by comparing computed drought hazard and exposure to drought impacts such as yield losses, economic losses or the number of affected people reported in global and regional data bases. In addition, two validation workshops were organized with participation of global and regional stakeholders.

The information and data sets developed by the project groups have already been used by external scientists, for example by the Global Drought Observatory of the Joint Research Centre of the European Commission to inform policy makers and citizens across Europe about current drought risk. To facilitate knowledge dissemination and reuse of our products, several scientific articles were published together with regional and global end users of our products. 12 online courses consisting of webinars and electronic lectures were developed and integrated into the [GlobeDrought Learning Platform](#). These courses describe drought impacts and introduce into drought risk analysis. By the end of the project, more than 600 people had signed up to the platform.

GlobeDrought researchers contributed to cross-cutting activities bringing together the scientists of the 12 research projects funded by the measure Global Resource Water (GRoW) targeting on the improvement of the water footprint concept, providing recommendations on how to achieve the Sustainable Development Goals (SDGs) and on policy advice to improve water resource management. A concept for a global drought forecasting system based on bias-corrected seasonal ensemble weather forecasts was developed and presented at the GRoW final workshop together with researchers from the GRoW SaWaM-project.

Introduction

Droughts exceed all other natural hazards in terms of the number of people affected (FAO, 2018). It has been estimated that since 1900 more than 11 million people have died as a consequence of drought and more than 2 billion have been affected by drought (FAO, 2013).

Drought generally refers to a lack of water compared to normal conditions (Van Loon et al., 2016) and this lack can be detected as decline of the water volume in storage components (soil, aquifers, rivers, lakes, reservoirs) or as decline in the fluxes between storages (rainfall, evapotranspiration, runoff, river discharge). Depending on the total storage capacity and the dynamics of fluxes in- and out of the storages, drought dynamics can be very different with relatively fast responses in soil and atmosphere and relatively slow changes in aquifers. Therefore, analysis of drought has to consider distinct time scales, that are relevant for the processes and components considered. Drought analysis also needs to be spatially explicit because major water fluxes such as rainfall and evapotranspiration are very heterogeneously so that, at larger extent, regions with drought coincide with wet conditions elsewhere. To describe the present drought status it is therefore needed to monitor the changes in the hydrological cycle for long time periods with time steps reflecting the dynamics of the processes and storages studied and with a spatial resolution reflecting their heterogeneity.

Because of the diversity in storages and fluxes potentially affected by drought, major direct and indirect impacts on human and natural systems and their properties, including terrestrial and freshwater ecosystems, agricultural systems, public health, water supply, water quality, food security, energy, or economy have been reported. Drought impacts can hardly be generalized across sectors and affected systems because distinct storages and fluxes are considered relevant. While soil moisture is in particular relevant for agriculture and terrestrial ecosystems, reservoir storage and river temperature is more relevant for energy production while drinking water supply is mainly affected by groundwater levels and reservoir storage.

Agriculture (crops, livestock, fisheries, aquaculture, and forestry) absorbed 23 percent of all damage and loss caused by medium- to large-scale natural disasters in period 2006-2016. Drought affects the agriculture sector disproportionately, 83 percent of all damage and loss caused by drought was absorbed by agriculture (FAO, 2018). Consequently, studying drought impacts on agricultural systems can be considered extremely relevant.

Drought events and associated hazard are characterized in terms of their frequency, severity, duration, and extent (Zargar et al., 2011). However, drought impacts depend not only on the severity and duration of the hazard but also on the coping and adaptive capacity of the system or sector affected. For example, a local soil moisture drought may have considerable impact on the food supply of subsistence

farmers in developing countries while it will hardly affect food availability of people living in developed countries characterized by integration into domestic and international trade and efficient transport and storage infrastructure. Today it is widely acknowledged that drought risk, i.e. the likelihood of adverse impacts or consequences, is not driven only by drought hazard but results from the interaction of hazard, exposure, and vulnerability (IPCC 2012, 2014).

The complexity of processes affected by drought and the differences in their spatial and temporal characteristics resulted in a large number of different methods and approaches to monitor the drought status and to analyse drought risks. Networks of sensors performing direct measurements of relevant water fluxes or storages such as soil moisture sensors, automated weather stations, eddy covariance flux towers or river gauges are mainly used for monitoring. Indirect measurements performed by remote sensing inform about vegetation and land surface properties, moisture content of the topsoil, water levels in reservoirs and major rivers or changes in the earth gravity field. This information is used for drought monitoring but also to detect drought impacts. Process based hydrological or crop models can be applied for long time periods and also for scenario based projection and are mainly used to quantify drought hazard and to integrate specific changes in water storages and water fluxes to describe the response of complex systems such as river networks or crop production systems. Information from sensing and modeling is then transformed to indicators describing the drought status of a system at a specific time and location compared to the status expected based on long-term time series of the measured or modeled data. Numerous drought information systems have been developed for specific sectors and regions informing inhabitants, politicians and decision makers. Most of the present information systems are designed to inform a specific sector, are either based on sensing or on modeling and miss integration of drought vulnerability information. Therefore, they mainly inform about drought hazards or indicate drought risk for specific regions where it can be assumed that vulnerability is homogenous and does not change much in time.

Objectives of the project GlobeDrought, funded by the German Ministry of Education and Research under the funding measure [Water as a Global Resource \(GRoW\)](#) were (i) to perform a spatial analysis of drought risks by integrating the components drought hazard, exposure and vulnerability for irrigated and rainfed agricultural systems and the water supply sector at global scale and for specific, heavily affected regions, (ii) to analyze drought impacts and (iii) to develop a drought information system providing access to the information created in the project and supporting thereby drought risk management.

The GlobeDrought project was coordinated by the [Division Agronomy at the Department of Crop Sciences, University of Göttingen](#) (UG). UG was also responsible for the hazard analysis of rainfed and irrigated agricultural systems using regional and global crop water models.

The [Astronomical, Physical and Mathematical Geodesy Group at the Institute of Geodesy and Geoinformation, University of Bonn](#) (UB-IGG) processed GRACE satellite data to derive total water storage changes at global scale and developed methods to assimilate these data into the global hydrological model WaterGAP to analyze hydrological droughts. UB-IGG also developed drought indicators directly based on total water storage change and performed analyses of meteorological drought using indicators such as SPI.

[The Center for Remote Sensing of Land Surfaces at the University of Bonn](#) (UB-ZFL) contributed to the project by using optical remote sensing to derive drought impacts on the vegetation, in particular agricultural crops. UB-ZFL performed analyses at global scale and for the regions South Africa and Zimbabwe. In addition, methods were tested to link remote sensing based drought indicators to process based crop models and to improve essential input data used by the model, such as sowing dates of agricultural crops.

[The Hydrology Group at the Institute of Physical Geography, University of Frankfurt am Main](#) (UF) developed methods to analyze hydrological drought based on simulation results of the global hydrological model WaterGAP. The indicators and data developed at UF were in particular relevant to study drought hazard for water supply and irrigated agricultural systems. UF contributed to global scale assessments and to regional assessments for South Africa. In addition, methods were developed to couple the hydrological model WaterGAP with the crop model SIMPLACE and to use total water storage changes from GRACE for improving streamflow simulation results of WaterGAP.

[The Institute for Environmental and Human Security at the University of the United Nations](#) (UNU-EHS) developed methods to analyze the vulnerability of the sectors studied to drought and performed the integration of indicators for hazard, exposure and vulnerability to analyze drought risk. UNU-EHS performed studies at global and regional level and supported the coordination of the project by organizing the project and stakeholder workshops. In addition, UNU-EHS developed and maintained the project website and developed the electronic courses in collaboration with all project partners.

[Remote Sensing Solutions GmbH](#) (RSS) developed the GlobeDrought information system providing access to the data developed in the project. RSS developed methods to distinguish irrigated and rainfed agricultural systems based on remote sensing imagery and applied these methods for Zimbabwe and South Africa to support the regional drought risk assessments performed in the project. In addition, RSS performed a drought risk assessment using high resolution remote sensing data for the project regions.

[Deutsche Welthungerhilfe e.V.](#) (WHH) contributed considerably to the stakeholder involvement and evaluated the GlobeDrought products and results from the



Final report – Introduction

perspective of a potential user. WHH considerably contributed to the regional case studies, in particular to the drought risk analyses for Zimbabwe and acted as the link to other NGOs involved in humanitarian aid such as the [Start network](#).

1 Development of tools and methods for drought risk analysis

1.1 Defining the system to be studied

Numerous meteorological, hydrological, and agricultural drought indicators have been introduced to assess the physical characteristics of drought impacts or operate a drought early warning system throughout the years. Over 150 different drought indices convey the variety of definition, perception, spatial extension and application of drought indicators (Niemeyer, 2008; Rojas, 2018; Sánchez et al., 2018; Tian et al., 2018; Zhao et al., 2017). However, most of these indicators are spatially limited to regional or national extents; very few apply to the global scale while mainly address meteorological or hydrological drought. In this research, our definition of drought is a temporary recurrent climatic feature of abnormal dry weather, long enough to cause a significant impact on the sector to be studied. Drought should be appropriately differentiated from aridity, which refers to long-term moisture deficiency and dryness when the water demand is continuously larger than water supply (Scheff, 2019; Sohoulane Djebou, 2017; Vicente-Serrano et al., 2010).

Recent severe droughts in southeastern Brazil (2014–2017), California (2011–2017), the Caribbean (2013–2016), northern China (2010–2011), Europe (2011, 2015, 2018), India (2016, 2019), the Horn of Africa (2011–2012), South Africa (2015–2016, 2018) and Vietnam (2016) have clearly shown that the risk of negative impacts associated with droughts is not only linked to the severity, frequency and duration of drought events but also to the degree of exposure, susceptibility and lack of coping capacity of a given socioecological system (SES). To improve the monitoring, assessment, understanding and ultimately proactive management of drought risk effectively, we need to acknowledge that the root causes, patterns and dynamics of exposure and vulnerability need to be considered alongside climate variability in an integrated manner (Meza et al., 2020).

To comprehend and define the effect of drought events on the agricultural sector and, in a broader vision, the food security of nations and potential needs for international food aid, we developed, for the first time, an integrated drought risk assessment approach. Our integrated drought risk assessment approach brings together data from different sources, for different sectors or impacts and disciplines. This information is systematically structured into the components hazard, exposure and vulnerability and then integrated to analyse drought risk (Figure 1). The spatio-temporal variability in drought risk at global and regional extent helps us to identify leverage points for reducing impacts and properly anticipate, adapt and move towards resilient agricultural and water supply systems. Drought risk is defined as the probability or likelihood for a specific drought impact. Hazard is a deviation of the situation in a specific year or month



$$\text{DROUGHT RISK INDEX} = \text{HAZARD} \times \text{EXPOSURE} \times \text{VULNERABILITY}$$

Figure 1. An integrated assessment of drought risk

from the long-term mean. Exposure refers to the elements located in areas that could be adversely affected by drought hazard. Vulnerability refers to the predisposition to be adversely affected due to the sensitivity or susceptibility of a system and its elements to harm, coupled with a lack of coping and adaptive capacity. The overall workflow of the drought risk assessment, integrating hazard, exposure and vulnerability to risk is described in detail in section 1.8.

1.2 Defining drought impacts to be studied

Before drought indicators for hazard, exposure and vulnerability can be selected, it is required to define the drought impacts or sectors that will be studied. The selection of drought impacts to be studied in GlobeDrought was performed at the 1st stakeholder workshop (May 03-04, 2018 at UNU in Bonn) as an element of the co-design process. Based on the priority ranking conducted by the participants from the regional case study areas NE Brazil, W India, Missouri basin, South Africa and Zimbabwe (Figure 2), drought impacts on agricultural systems and water supply were considered most relevant and selected for further study in GlobeDrought.



Regional Drought Impact Importance

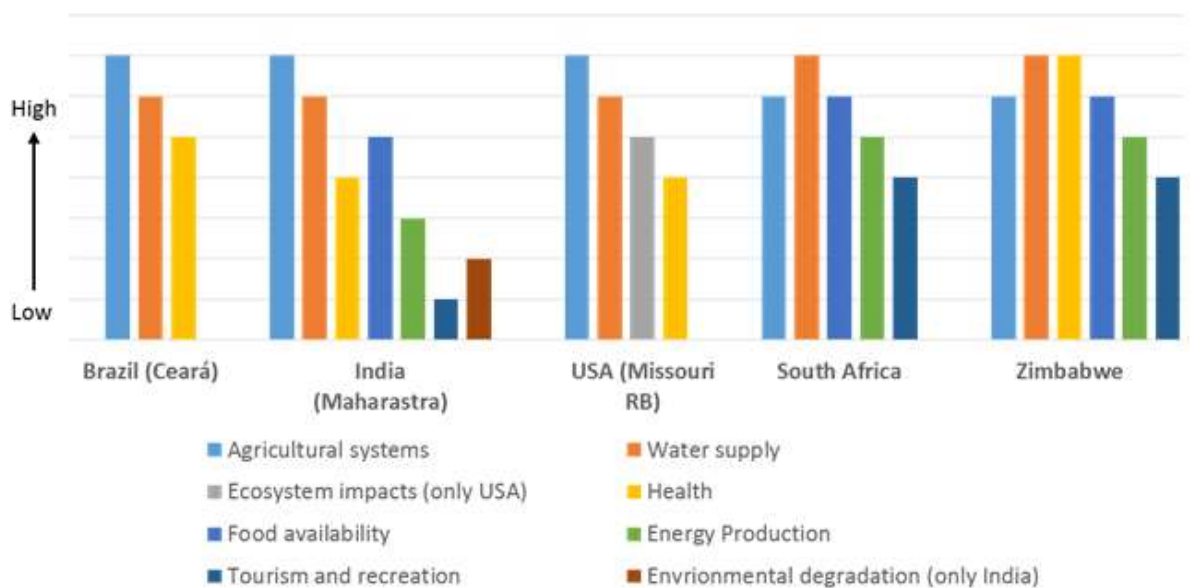


Figure 2. Participants of the 1st GlobeDrought stakeholder workshop (top) and ranking of drought impacts performed by the participants for selected potential case study regions (bottom)

1.3 Linking of hydrological and crop models

The global hydrological model WaterGAP (Müller Schmied et al., 2021) and the crop models GCWM (Siebert and Döll, 2010) and Simplace (Eyshi Rezaei et al., 2021) were applied in GlobeDrought to study the impact of drought on the water supply sector and on agricultural systems including food supply. Drought risk on water supply is usually investigated by monitoring changes in water storages such as reservoirs or aquifers determining the water availability. Hydrological models such as WaterGAP are designed to quantify these water storages and their changes. Drought impacts on agricultural systems are mainly induced by constraints in crop water supply resulting in reduced crop productivity. The underlying physiological relationship is the linear response of biomass production to crop transpiration. The models GCWM and Simplace are perfect tools to assess the relationship between actual evapotranspiration (AET) of specific crops and their potential

evapotranspiration (PET) and thus between crop water use and crop water requirement. Consequently they reproduce the basic response of crops to drought and using this relationship for assessing drought hazard is advancing previous research which was mainly based on indirect indicators such as anomalies in precipitation or soil moisture. For some drought impacts it is also useful to link hydrological and crop models. In irrigated agriculture, for example, farmers can ensure crop water supply independently of precipitation as long as enough irrigation water is available. Consequently, it is needed to combine the modeling of water availability (hydrological models) with the modeling of crop water requirements (crop models) to investigate drought impacts on irrigated crop production. In GlobeDrought, two different approaches were tested for this purpose. A direct coupling of WaterGAP with SIMPLACE was tested in a regional assessment considering one specific crop (maize). In this approach, described in section 1.3.1, there is a direct exchange of information between the two models throughout the simulations. Alternatively, a soft link between WaterGAP and GCWM was tested by using the output of the models generated by independent simulations for calculation drought hazard (section 1.3.2).

1.3.1 Concept of coupling WaterGAP and SIMPLACE

The impact of meteorological drought on crop production can be alleviated by irrigation but only if sufficient water is available from either groundwater or surface water bodies. Thus, a crop model is required to simulate crop water requirement as a function of crop, soil, climate and water application by irrigation, while a hydrological model is required to simulated water availability from streamflow and groundwater. To take into account limited water supply for irrigation, which can be expected to be particularly limited during drought events, it is necessary to couple a crop model to a hydrological model that also simulated runoff from non-cropland as well as groundwater storage and streamflow as affected by non-irrigation water use. Examples of coupling crop growth and hydrologic models include Bithell and Brasington (2009) and Boegh et al. (2004).

The objective of coupling the crop yield model SIMPLACE and the global hydrological model WaterGAP was 1) to improve the computation of hydrological drought hazard indicators and 2) to provide water availability data for irrigation to SIMPLACE such that in SIMPLACE the impact of the availability of blue water on yield decreases of irrigated crops could be taken into account. In an uncoupled run, SIMPLACE is presumed to underestimate the impacts of drought on crop yield for irrigated crops and WaterGAP would have some differences in the values of available streamflow for irrigation when compared to observed data.

For a coupled approach, vegetation land cover of croplands is identified in WaterGAP's 0.5° grid cells via up-scaled spatial resolution input from SIMPLACE. The temporal resolution of both models is kept at daily scale, and model outputs are

exchanged with a daily time step. This exchange and adaptation of each parameter value, in each model, comes with its own complexities and inconsistencies. In SIMPLACE, return flows from irrigation are taken into account in the soil water balance, while in WaterGAP, return flows are included in net abstractions from surface water and groundwater. Hence, the respective equations in WaterGAP to compute runoff, streamflow into downstream cells and net abstractions from surface water and groundwater need to be adapted. Moreover, daily streamflow in WaterGAP is not only impacted by water demand for irrigation, but for all water use sectors (domestic, livestock, manufacturing and thermal power). The following data exchange is required between the models:

1) Data provided by SIMPLACE to WaterGAP:

- Actual evapotranspiration (reduced by the fraction resulting from return flows into soil)
- Total runoff from cropland
- Soil moisture
- Water withdrawals and water consumption for irrigation from surface water and groundwater

2) Data provided by WaterGAP to SIMPLACE:

- Available streamflow (adjusted by the amount of water allocated to non-irrigation water use sectors)

Data exchange between the models can be achieved through the concept of in-memory “common coupling”. Common coupling is a coordinated type of pairing, where both the models are coupled through a common global variance, which facilitates automatic or semi-automatic exchange of data (Yu and Ramaswamy 2011). “Protocol Buffer” (<https://developers.google.com/protocol-buffers/>) is proposed to be used as the common global variance for common coupling between WaterGAP and SIMPLACE. It is an open-sourced, language neutral, platform neutral automated mechanism for serializing structured data provided by Google. The flow of data exchange between WaterGAP and SIMPLACE is illustrated in Figure 3. The proposition is to dock both models on to one server, facilitating efficient communication between them and controlling initiations through a shell script. To ensure that both models exchange data only at the required time step, a concept of ReadWriteLock locking mechanism needs to be introduced in the same code.

There is one pivotal difference between SIMPLACE and WaterGAP that poses a challenge for the coupling: While WaterGAP computes, for each time step, the water balance of all grid cells according to a routing order defined by the drainage direction map, SIMPLACE computes the water balance for the whole time series grid cell by grid cell. During implementation of the described coupling approach, it became evident that restructuring SIMPLACE according to the computation sequence of WaterGAP results in unreasonably high computational time. Hence, there is currently no feasible technical solution for the coupling of these two models.

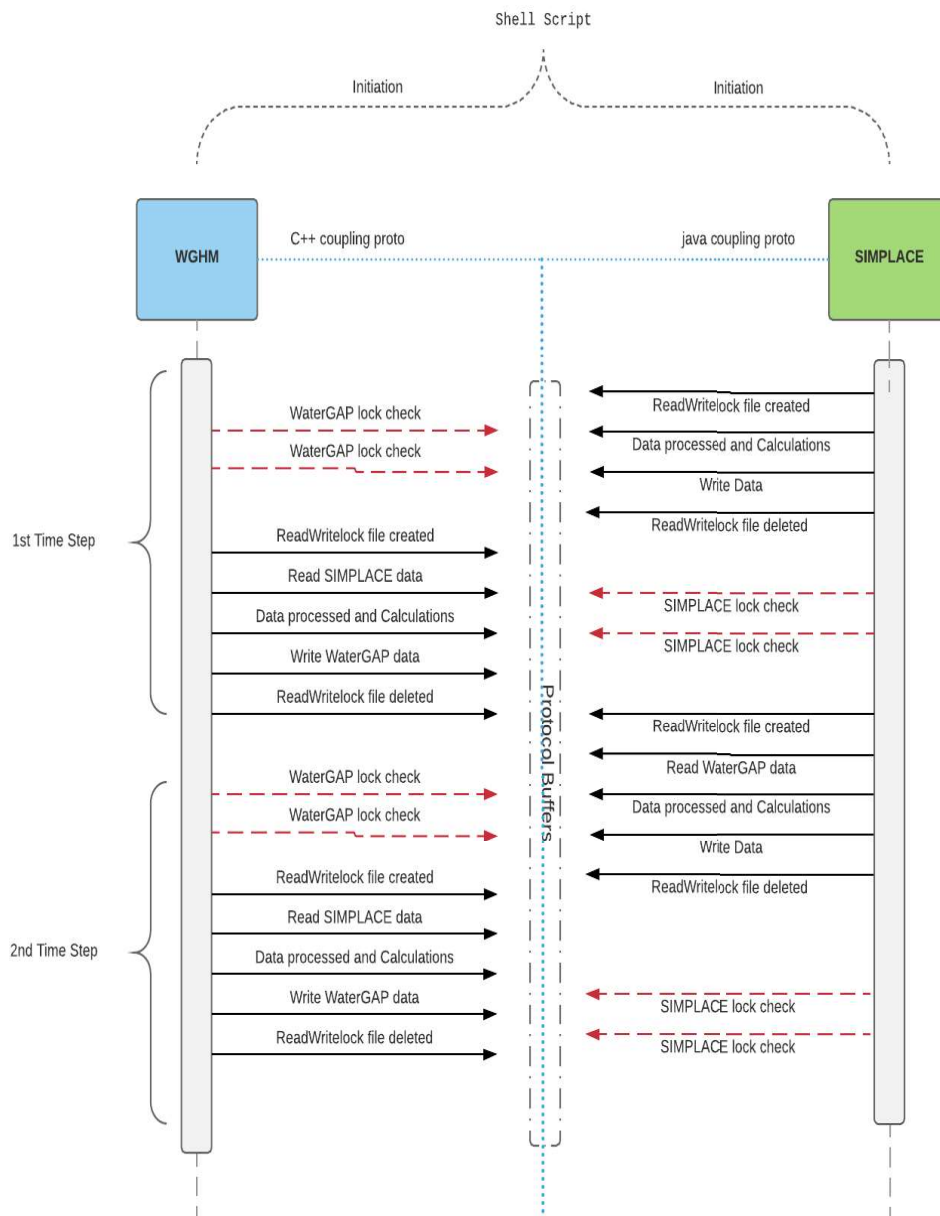


Figure 3. Flow chart of data exchange between WaterGAP and SIMPLACE

1.3.2 Combining WaterGAP and GCWM to calculate drought hazard for irrigated agriculture

Similar to the simulations at regional scale described before, it was also needed to combine information for stream flow (derived from WaterGAP) and irrigation water requirement (derived from GCWM) for the simulation of drought hazard for irrigated agriculture (see section 1.5.2). Stream flow is used as an indicator of water availability for irrigation. Drought hazard for irrigated agriculture was analyzed by studying anomalies in the difference between water availability and water requirement.

1.4 Linking process based modeling with remote sensing

Objective of GlobeDrought is to analyse drought risk for historical periods, present drought risk and to provide ensemble-based forecast of potential risk. In addition the drought assessments were performed at global scale and for selected regions. The combination of these goals requires to compute drought hazard at high spatial resolution (regional studies), global extent (global assessment), for a long period stretching from at least 30 years ago (to define the historical distribution of drought indicators needed for the baseline) to 8 month in the future (for seasonal forecasts). The characteristics of available models and data shows that the required coverage in space and time is only achievable by combining remote sensing and modeling (Figure 4). Remote sensing offers the advantage of using data at very high spatial resolution but with limited coverage in time. Process based models can perform simulations for long time periods including projections of future conditions but have limitations in either spatial resolution or spatial extent. To combine models with remote sensing it is needed to identify variables that can be simulated with the models and derived by remote sensing. In GlobeDrought process based models (WaterGAP, GCWM, Simplace) and remote sensing (GRACE, MODIS) were linked for three processes: changes in water storages, determination of sowing and harvest dates of crops and qualifying drought stress of crops.

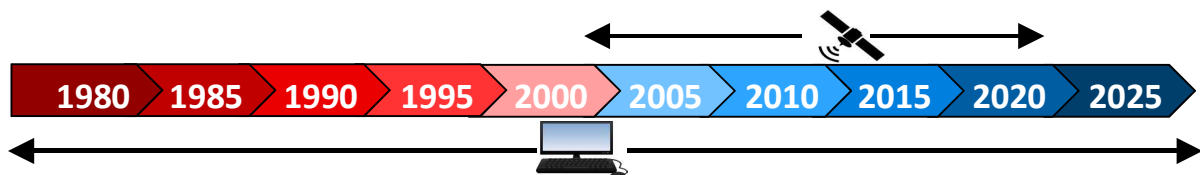


Figure 4. Data availability for remote sensing and process based modeling

1.4.1 Improving trends in simulated water storages by using changes in total water storage obtained from GRACE

To improve simulations of changes in surface- and subsurface water storages in the WaterGAP model, total water storage changes obtained from GRACE were assimilated into the model. The use of this independent data source can in particular improve the representation of long-term trends in water storages in the model (Schumacher et al., 2018).

1.4.2 Improving sowing and harvest dates in SIMPLACE by remote sensing information

Appropriate sowing and harvest dates are essential to simulate crop water requirements and crop drought stress realistically, in particular for more detailed crop models applied in semi-arid regions. Unfortunately, little is known about representative sowing dates in African countries, in particular about the spatial and interannual variability in sowing dates. Therefore, often fix sowing dates or rules based on the precipitation distribution are used in crop models. Using remote sensing to identify the phenology of crops such as maize (Viña et al. 2004) constitutes a promising approach. The impact of the choice of the sowing date on maize drought stress and maize yield was therefore tested for South Africa by comparing simulation results obtained by the LINTUL-5 crop model implemented in the SIMPLACE modeling platform which was applied during the period 2001–2016 with fix sowing dates, application of a precipitation rule, and use of the MODIS global vegetation phenology (MCD12Q2) product (Xiao et al. 2013) to derive the sowing date based on the greenup date (Eyshi Rezaei et al., 2021). Maize is the most important field crop in South Africa and relevant for both, subsistence farming and commercial agriculture.

1.4.3 Combining drought hazard simulated with process based crop models with drought indicators derived by remote sensing

To validate the drought hazard indicator for rainfed crops in the regional study for South Africa and at global scale, the simulated AET/PET ratio for rainfed conditions was validated using the remotely sensed AET/PET ratio in the period 2001-2019. AET and PET values were extracted from the Moderate Resolution Imaging Spectroradiometer (MODIS) product (MOD16A2.006) which provides data at 500m spatial resolution (Running et al., 2017). The dataset is derived from meteorological reanalysis data coupled with remotely sensed products of land cover and vegetation properties (Huang et al., 2017). The dataset was preprocessed based on the quality control layer, and pixels with low quality were excluded. The original data set provided the AET and PET in 8 days intervals, which were summed up to yearly values. The drought hazard indicator for rainfed crops was recalculated for model results and remote sensing observations considering the reference period 2001-2018 to account for the limited availability of remote sensing observations. The Pearson correlation coefficient was calculated between model and remote sensing based drought hazard at the municipality level (South Africa) or at pixel level (global scale) to test for the agreement between simulated and remotely sensed drought hazard.

1.5 Development and application of drought hazard indicators

1.5.1 Hydrological drought hazard affecting the water supply

Drought monitoring requires a sound understanding of the underlying concepts of drought risk including the applied indicators. Especially drought hazard, as one

component of drought risk, has many facets and is thus difficult to define. Previous research has revealed that there is often no common understanding among stakeholders about drought hazard concepts (Steinemann et al., 2015).

During the stakeholder workshops of the GlobeDrought project, it also became apparent that there are still open questions on the suitability and meaningfulness of different drought hazard indicators. One major focus of the sub-project was therefore to develop a transparent description and classification scheme for (hydrological) drought hazard indicators taking into account the different levels of drought characterization (Figure 5; Herbert and Döll, 2021, in preparation) and assumptions about the habituation of people and ecosystems to the streamflow regime (Table 1).

Threshold-based and standardized hydrological drought hazard indicators

Streamflow drought hazard indicators are generally classified into threshold-based and standardized indicators (Van Loon, 2015). The threshold level method (TLM) was first applied by Yevjevich (1967), who defined that a drought event begins when streamflow falls below a certain threshold, and that the drought severity is equivalent to the cumulative streamflow deficit since the onset of the drought event. Standardized indicators such as the Standardized Precipitation Index (SPI) (McKee et al., 1993) or the Standardized Streamflow Index (SSI) (Vicente-Serrano et al., 2012) can be described as dryness probability as they indicate how unusually dry the current month is regarding streamflow as compared to normal conditions. SSI is computed similar to the method introduced in McKee et al. (1993) for SPI. For instance, SSI1 for January (Jan) 2015 is computed as (with Q: streamflow): $[Q(\text{Jan}2015) - \text{mean monthly } Q(\text{Jan})] / \text{standard deviation}[Q(\text{Jan})]$. A value of SSI1 = -1 [-] denotes that monthly streamflow is one standard deviation below the median of the respective calendar month. A value of -0.84 is equivalent the 20th percentile of monthly discharge (Q80).

Following the TLM, we computed and analyzed the cumulative streamflow deficit indicators CDQI-Q50, CDQI-Q80, and the latter combined with a method that takes into account drought conditions in highly seasonal flow regimes, CDQI-Q80-HS (Table 1). With CDQI-Q50, a deficit is defined to occur if monthly streamflow is lower than the 50th percentile (median) of the calendar month streamflow (or lower than the 20th percentile in case of CDQI-Q80). The cumulative streamflow deficit is normalized against mean annual streamflow. A value of 2 [-], for example, indicates that the cumulative streamflow deficit in a certain month is twice the mean annual streamflow.

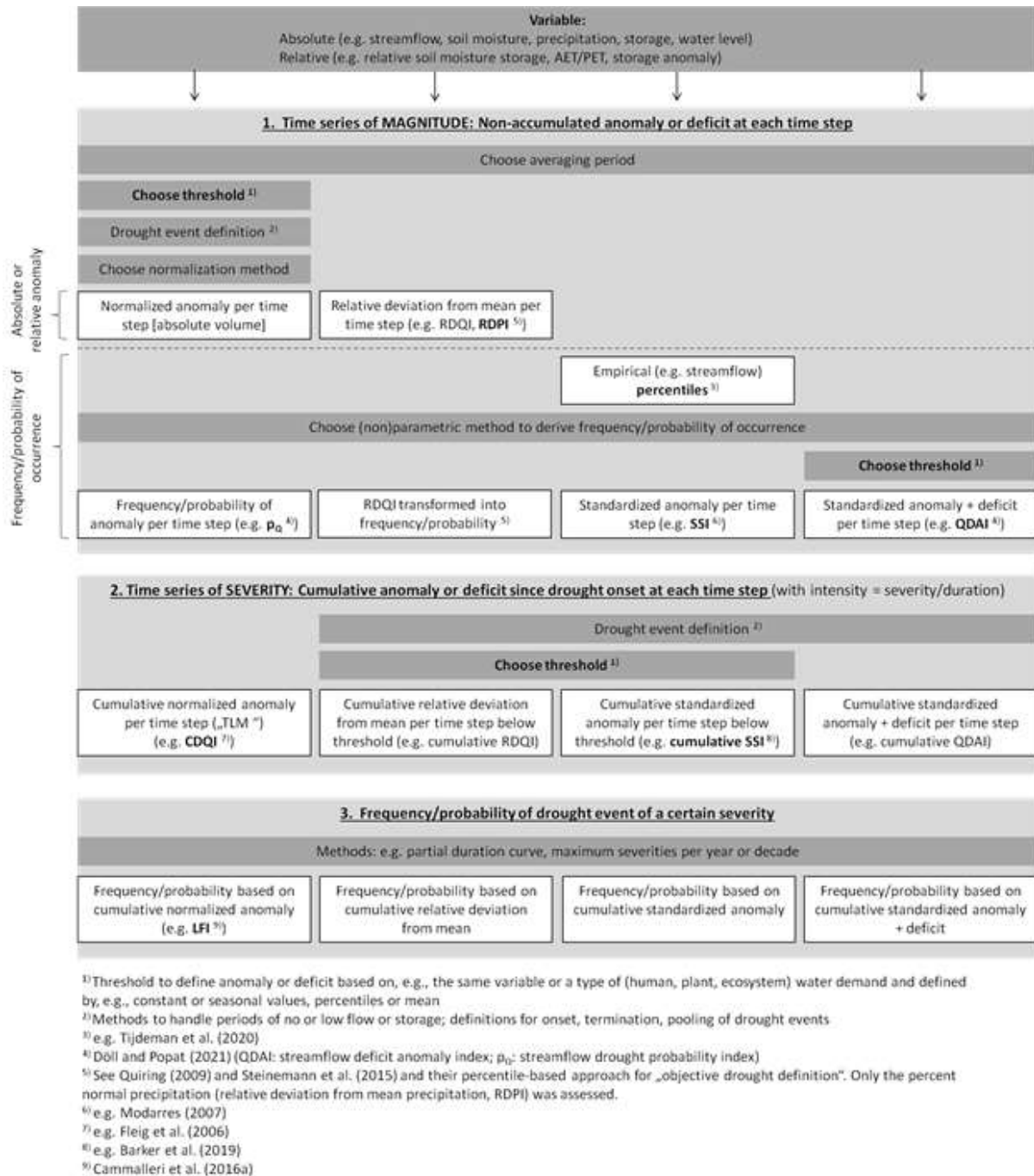


Figure 5. Schematic for computing four types of drought hazard indicators, indicating 1) magnitude of the drought at a certain time as deficit and/or anomaly or 2) severity of the drought event, i.e. the cumulative magnitude of drought since drought onset. Both, magnitude and severity, can be expressed in terms of frequency/probability to compare the drought of interest to other droughts. The grey boxes indicate decisions made when computing the indicators. Indicators in bold have already been applied in the literature. Assumptions about the habituation of people and ecosystems determine the selection of the type of indicator, the averaging period and the threshold (see Table 1)

Table 1. Characteristics of streamflow drought hazard indicators suitable for global-scale assessments and their inherent assumptions about habituation of people or other biota

Assumed habituation <i>People, other biota accustomed to:</i>	Indicator	Prominent, hydrology-related characteristics
Interannual variability	SPI12	Often used as proxy for hydrological drought hazard. However, processes in altered flow regimes cannot be characterized.
	SPEI12	Often used as proxy for hydrological drought hazard. However, processes in altered flow regimes cannot be characterized. Better suited in climate change impact assessments than SPI12 as it uses not only precipitation, but also temperature as input.
	SSI12	Suitable in study regions with access to reservoirs, which buffer potential monthly streamflow deficits.
Seasonality and interannual variability	SSI1	Suitable in study regions without access to reservoirs.
	CDQI-Q80	The study region is in drought 20 % of the time. With Q80 (per calendar month) as a rather low threshold, streamflow drought hazard might be underestimated in regions with high vulnerability and interannual variability.
	CDQI-Q80-HS	The study region is in drought at least 20 % of the time. An existing drought continues during a pre-defined low-flow season even if Q80 is exceeded, as it can be assumed that the region will not recover from the drought during the low-flow season.
Seasonality	CDQI-Q50	The study region is in drought 50 % of the time. Using such a high threshold can be beneficial in highly vulnerable regions where people cannot even cope with small reductions in median monthly streamflow.
	CDQI-WUs	An indicator of water deficit rather than drought hazard. The health of river ecosystems is not taken into account.
	CDQI-WUs-EFR	EFR based on Qant ¹⁾ : The river ecosystem has adjusted to the altered flow regime over the last decades, which is considered the “new normal status”. EFR based on Qnat ²⁾ : the natural flow regime is the aspired status.
	RDQ1	Suitable in study regions without large surface water storages.
Mean annual conditions	RDQ12	Suitable in study regions with large surface water storages, which buffer monthly streamflow fluctuations.

¹⁾ Qant: Modeled anthropogenic streamflow altered by human water use and dams

²⁾ Qnat: Naturalized modeled streamflow

A direct comparison between CDQI-Q80 and SSI1 is not possible. While the former indicates the severity of the current drought event, i.e. the cumulative streamflow deficit since the onset of the drought event., negative values of SSI represent the drought magnitude, i.e. the non-accumulated streamflow deficit at the considered time step (see Figure 5). On the other hand, going one computational step backwards with CDQI-Q80, i.e. the time series of monthly deficits, and going one

step further with SSI1, i.e. the time series of cumulative standardized deficits below a threshold of -0.84 ($= Q80$), reveals that both indicators are basically the same (given that $Q80$ for CDQI is derived from the probability density function used to compute SSI1). Therefore, we argue that the differentiation between TLM-based and standardized indicators might be misleading. Figure 5 depicts the computational steps that distinguish four different types of drought hazard indicators such as CDQI- $Q80$ (left) and SSI1 (third column): Computation of 1) drought magnitude (non-accumulated anomaly or deficit at each time step), 2) drought severity (cumulative anomaly or deficit since drought onset at each time step) and 3) probability of a drought event of a certain severity. For each of the four indicator-specific “flow schemes”, a threshold needs to be selected in one of the steps in order to define drought onset and termination. When selecting indicators of drought hazard, one should be aware which level of drought characterization it represents (e.g. monthly anomaly vs. severity of drought event).

Through the selected methods and criteria to define drought events, any drought hazard indicator implies assumptions about the habituation and thus vulnerability of people and the ecosystem at risk. With the rather high threshold $Q50$ in CDQI- $Q50$, it is assumed that people and the river ecosystem are accustomed to seasonality but not interannual variability. This means that people and ecosystems are used to the fact that streamflow is generally lower in, e.g., August compared to March, but they may suffer in years where streamflow in August is below mean (or rather median) conditions. Especially in semi-arid regions, where interannual variability is high and where people are often vulnerable to drought, a lower threshold than $Q50$ (e.g. $Q80$) might not capture or underestimate streamflow drought hazard. However, CDQI- $Q50$ is less suitable in humid regions where interannual variability in streamflow, and often vulnerability to drought, is low. Here, indicators with a lower percentile, such as $Q80$, would be more meaningful.

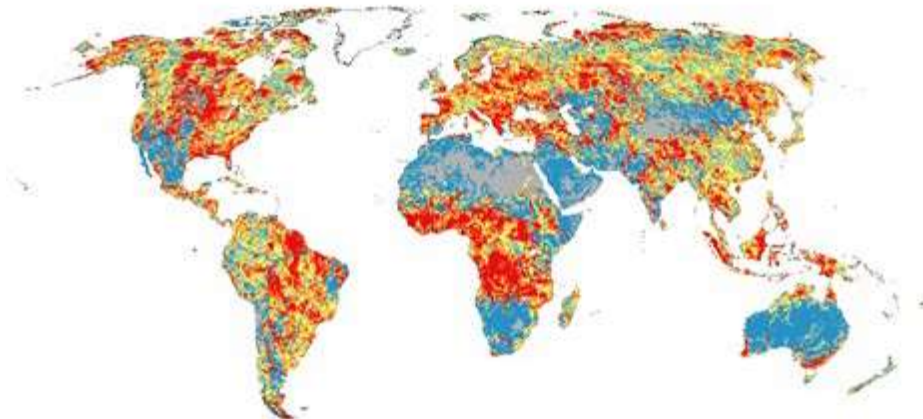
Similar to using low percentiles as threshold (as in CDQI- $Q80$), the concept of SSI1 is based on the assumption that people and biota are used to seasonality and interannual variability. In regions where this is not the case, relative deviations from mean streamflow might be better suited to capture the drought hazard (implicitly assuming that people are used to the mean instead of variability). Comparing a humid (low interannual variability) with a semi-arid (high interannual variability) region, the same negative SSI1 (e.g. -0.84) value would correspond to a much stronger negative deviation from mean streamflow in the semi-arid area (e.g. -50%) compared to the humid area (e.g. -20%). Hence, although SSI1 has the advantage of being comparable among regions with different flow regimes, it might underestimate streamflow drought hazard in semi-arid areas. Regarding the accumulation period of one month, SSI1 has the advantage of identifying the onset of a drought as opposed to longer accumulation periods (e.g. SSI12) where deviations from normal conditions are smoothed and the identification of a drought is delayed. However, since SSI1 can only quantify the current status of drought hazard,

it is more suitable for the assessment of drought hazard for irrigated agricultural systems and water supply systems in regions without surface water storages (reservoirs and lakes).

CDQI-Q80-HS is a new indicator developed within the GlobeDrought framework. It combines CDQI-Q80 with a method that takes into account drought conditions in highly seasonal flow regimes. It allows an existing drought to continue during a pre-defined low-flow season even if streamflow exceeds the calendar month Q80 (Table 1). For each grid cell, the low-flow season is defined to encompass all calendar months in which the mean monthly flow during the reference period is less than 20 % of the mean monthly flow averaged over all calendar months. A drought event that has built up outside of the low-flow season will continue throughout the low-flow season; the cumulative deficit is reduced by the streamflow surplus over the calendar month Q80. The rationale behind this approach is that people and the ecosystem cannot recover from a drought during the low-flow season if flow during this season is only a small percentage of total streamflow in each year. The indicator can add additional value in regions with high seasonal streamflow variability where people strongly rely on water storage in man-made reservoirs that needs to be replenished by streamflow.

While drought hazard and vulnerability to drought are independent components of drought risk, drought hazard indicators imply assumption about habituation to different types of temporal streamflow variability, i.e. about the type of temporal streamflow dynamics that people and ecosystems are used to. Table 2 lists the implicit assumptions about habituation of humans and other biota for the indicators computed within GlobeDrought as well as selected unique characteristics relevant in hydrology-related assessments. In addition to the above described indicators, Table 2 includes RDQI1 and RDQI12 (relative deviation from mean streamflow averaged over one month and 12 months, respectively) and the newly developed water deficit indicators CDQI-WUs and CDQI-WUs-EFR. These are computed similar to CDQI-Q80, but using as thresholds mean monthly surface water use WUs, and in case of the latter WUs plus mean monthly environmental flow requirements, EFR = 80 % of mean monthly discharge.

a) p based on CDQI-Q80



b) p based on cumulative RDQI1-50%

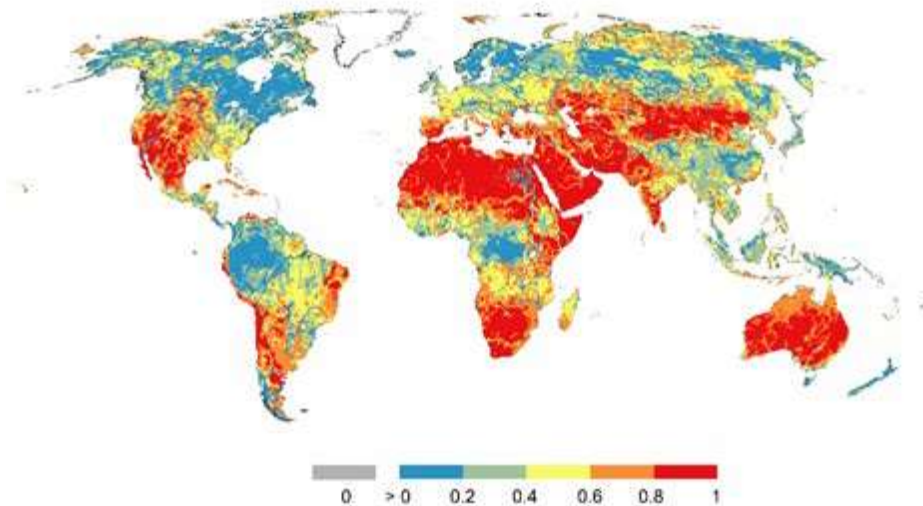


Figure 6. Global comparison of overall drought severity during 1986-2015 based on the probability of exceedance p for two streamflow drought hazard indicators: Cumulative streamflow deficit indicator with monthly Q80 as threshold (CDQI-Q80) (a) and cumulative relative deviation from mean monthly streamflow with -50% as threshold (cumulative RDQI1-50%) (b). A high value denotes a high sum of severity compared to other grid cells. A value of 0.8 in grid cell i , for example, means that in 80% of all grid cells the sum of severities of all drought events during 1986-2015 was smaller than in grid cell i . Greenland was excluded from the analysis

Figure 6 shows a global comparison of the cumulative drought severity during 1986-2015, transferred into the probability of exceedance p , for CDQI-Q80 (top) and the cumulative relative deviation from mean monthly streamflow with a threshold of -50% (cumulative RDQI1-50%) (bottom). The figure illustrates that the conceptualization and selection of a drought hazard indicator can lead to very different patterns of drought severity. RDQI generally leads to a higher level of severity in dry areas with high interannual variability (e.g. northern Africa, Australia and Arabian Peninsula). The figure highlights the need to provide a suite of hazard

indicators with different assumed types of habituation of the people/ecosystem at risk for a global-scale drought monitoring, since at the global scale, it is unknown which streamflow conditions are perceived as normal. In conclusion, rather than differentiating between TLM and standardized indicators, drought hazard indicators should be classified according to the inherently assumed type of habituation: 1) percentile-based indicators (e.g. CDQI-Q80, SSI1), suitable in case of habituation to interannual variability and seasonality of streamflow and 2) indicators showing the relative deviation from mean conditions, suitable in case of habituation to seasonality only, while suffering from interannual variability of streamflow.

Defining drought hazard indices combining water deficit and anomaly characteristics

According to the Australian Bureau of Meteorology, “drought is a prolonged, abnormally dry period when the amount of available water is insufficient to meet our normal use (BoM, 2018)”. This definition describes drought as both an anomaly (“less water than normal”) and a deficit (“less water than required”), reflecting general non-expert notions of drought. However, most experts define drought only as an anomaly, for example, as “a lack of water compared to normal conditions which can occur in different components of the hydrological cycle” (van Loon et al., 2016, p.3633). Also, most drought indices only consider the anomaly aspect.

During the GlobeDrought project, we developed and related two drought hazard indicators that combine both the deficit and anomaly aspects: one for soil moisture drought and the other for streamflow drought (Popat and Döll, 2021). In the soil moisture deficit anomaly index (SMDAI), which describes the drought hazard for vegetation, the deficit is calculated as the difference between the soil moisture at field capacity (that which should allow optimal, non-water-limited plant growth) and the actual soil moisture. The SMDAI slightly modifies and simplifies the DSI introduced by Cammalleri et al. (2016). Another difference from Cammalleri et al. (2016) is that the SMDAI is computed globally, using the output of WaterGAP, rather than just for Europe. The streamflow deficit anomaly index QDAI is, to our knowledge, the first-ever streamflow drought indicator that combines both the anomaly and deficit aspects of streamflow drought. In the case of QDAI, the deficit is computed by comparing actual streamflow to the combined human and environmental surface water demand per grid cell. QDAI focuses on determining the drought hazard for the water supply for humans, including domestic, industrial, and irrigation water demand. QDAI is constructed similarly to SMDAI and computed globally using WaterGAP.

We found that the values of the combined deficit-anomaly drought indices are often broadly similar to purely anomaly-based indices. However, the deficit anomaly indices provide more differentiated spatial and temporal patterns that help to distinguish the degree and nature of the actual drought hazard to vegetation health

or the water supply. Like all hydrological drought indicators that reflect streamflow anomaly, QDAI needs to be interpreted carefully in case of highly intermittent streamflow regimes. QDAI can be made relevant for stakeholders with different perceptions about the importance of ecosystem protection, by adapting the approach for computing the amount of water that is required to remain in the river for the well-being of the river ecosystem.

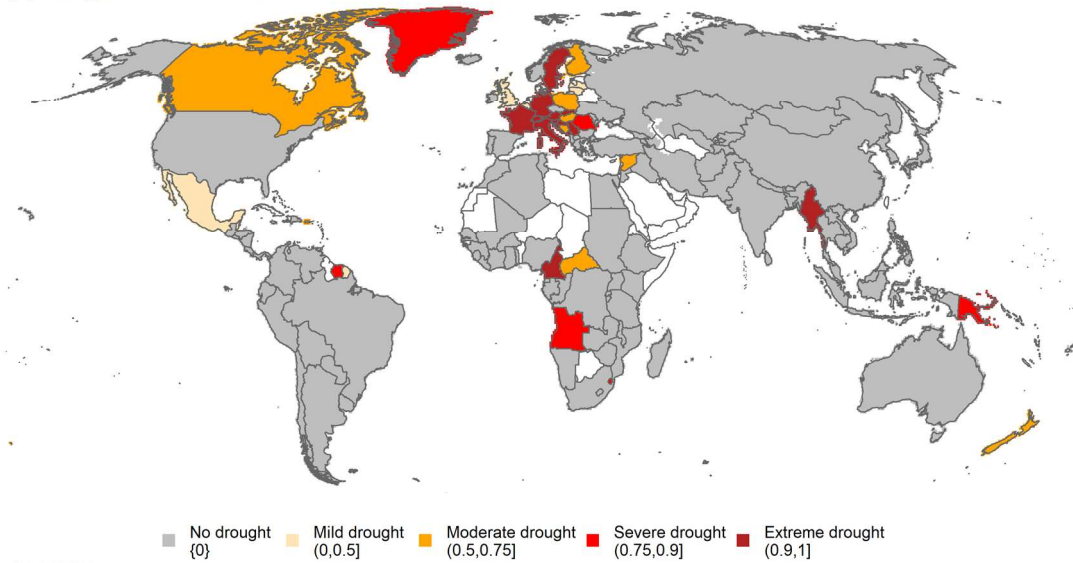
The term “drought hazard” can be defined as the source of a potential adverse effect of an unusual lack of water on humans or ecosystems. In this sense, SMDAI and QDAI are drought hazard indicators, even if they include some elements of vulnerability to drought. Both SMDAI and QDAI are well applicable in drought risk studies. In local drought risk studies, additional indicators of ecological or societal vulnerability should be added. In regional or global drought risk studies, the inclusion of grid-scale values of QDAI and SMDAI would be beneficial as both indices contain spatially highly resolved information on vulnerability, while most other vulnerability indicators represent spatial averages of much larger spatial units such as countries.

Analyzing the impact of streamflow drought hazard on hydroelectricity production

Electricity production by hydropower is negatively affected by streamflow drought. To understand, monitor and manage risks of less than normal streamflow for hydroelectricity production (HP) at the global scale, an HP model was developed that simulates time series of monthly HP worldwide and thus enables analyzing and monitoring the impact of drought on HP (Wan et al., 2020). The HP model is based on a new global hydropower database (GHD), containing 8748 geo-localized plant records, and on monthly streamflow values computed by WaterGAP.

Within the framework of GlobeDrought, four new indices of HP decrease due to streamflow drought were developed: HPA3 indicates how unusually low a HP reduction is compared to normal conditions. The approach roughly follows the SPI method with a 3-month averaging period. HPR3 shows the relative HP reduction compared to the long-term mean. A comparison of both indicators (Figure 7) in August 2003 reveals that, e.g., the extreme drought conditions in different countries as indicated by HPA3 correspond to very different relative reductions (HPR3) between 0.2-0.4 (European countries), 0.1-0.2 (Myanmar), and (Cameroon). Hence, both indicators have a different informative value on drought conditions and can be used complementary in drought assessment. Both indices were further modified by multiplying them by rHP (HP-to-total-electricity-production ratio). The resulting EPA3 and EPR3 indices (Wan et al., 2020, their Figure 10) provide information about to what extent HP reduction during drought affects the whole electricity production. However, due to the small contribution of HP to total EP, the negative impact becomes rather small.

(a) Drought classes and HPA3



(b) HPR3

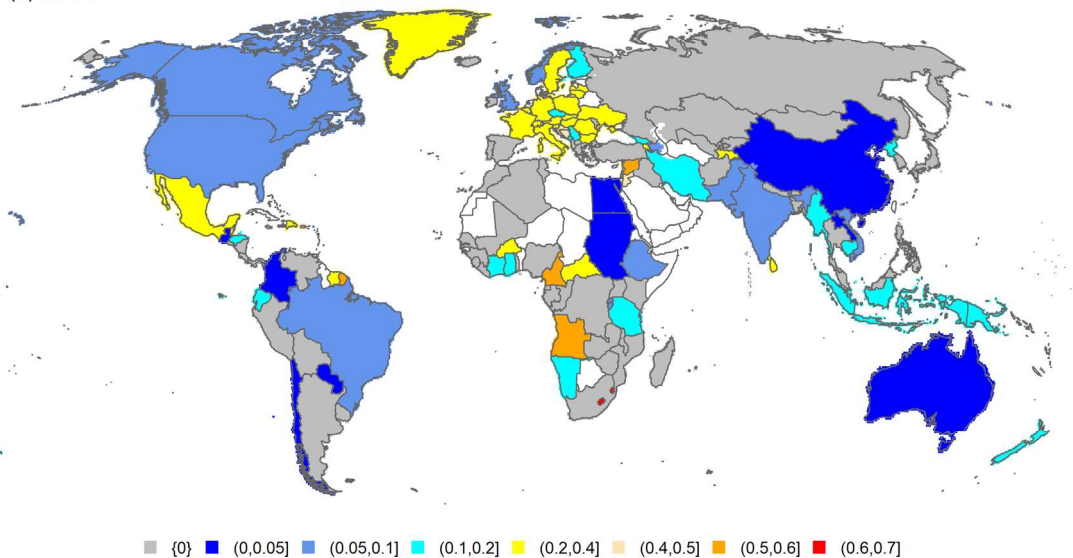


Figure 7. Country-level drought conditions as indicated by HP anomaly HPA3 (a) and relative reduction HPR3 (b) in August 2003

The HP model can capture the interannual variability of country-scale HP that was caused by both (de)commissioning of hydropower plants and streamflow variability. It can also simulate the streamflow drought and its impact on HP reasonably well. A drought risk analysis for period 1975–2016 revealed the reduction of HP that is exceeded in 1 out of 10 years. 71 out of 134 countries with hydropower suffer from a reduction of more than 20% of average HP, and 20 countries from a reduction of more than 40%.

Analyzing patterns of hydrological drought based on total water storage change obtained from GRACE

Change in water storages can also be detected by the GRACE satellite because any water flux is related to a mass flux altering the earth gravity field. Therefore, distinct drought indices based on Total Water Storage Anomalies (TWSA) obtained from GRACE were tested for their ability to reproduce hydrological droughts observed in historical years in NE Brazil, West India and South Africa (Gerdener et al., 2020).

Near-real time monitoring of hydrological drought hazard

With WaterGAP, near-real time monitoring of hydrological drought hazard is currently possible at a monthly time scale, i.e. near-real time drought hazard indicators can be computed for the preceding month with a delay of approximately seven days. As some scripts are not adapted to the specific requirements yet, only the conceptualization of near-real time monitoring is described below (to be completed in March 2021). All process steps can be started within one shell script. Among the five water use sectors in WaterGAP (irrigation, domestic, livestock, manufacturing and thermal power), only irrigation water demand is updated in a near-real time monitoring, since it is the only climate-dependent water use. As for the other water use sectors, annual values, currently available until 2016, are assumed to remain constant after 2016. The process chain for near-time WaterGAP computations of hydrological drought indicators is as follows:

- 1) Download of ERA5T climate data at day 5 in each month for the preceding month
- 2) Climate data check (plausibility, NaN values, etc.)
- 3) Computation of irrigation water demand for the last month

Irrigation water use in WaterGAP is computed by the Global Irrigation Model (GIM) based on annual time series of the area equipped for irrigation (AEI) and the ratio between area actually irrigated (AAI) and AEI (sources of data and scaling procedures are described in Müller Schmied et al., 2021). As AAI/AEI ratios are only available until 2005 or 2008 (depending on the country), the values are assumed to remain constant after 2005 and 2008, respectively. Since GIM can only be applied for a whole year, the future months in the current year need to be filled with placeholders.

- 4) Computation of net water abstractions for the last month

The linking model Groundwater-SurfaceWater Use (GWSWUSE) computes the fractions of all five sectoral water abstractions and consumptive water use in each grid cell that stem from either groundwater or surface water bodies (lakes, reservoirs

and river). From these values, net abstractions from surface water and groundwater are computed.

5) Run hydrological module of WaterGAP (WGHM) for the last month

Variant 5a) Run WGHM in “annual mode” (standard) from 1901 until current year (use “placeholders” for future months of the current year)

Variant 5b) Run WGHM in “monthly mode”: WGHM can be started at any month. Storages are initialized with the values of the last day of the preceding month. For simulation of January 2021, for example, storages are initialized with the values from 31 December 2020.

6) Post-processing of WaterGAP output

Computation of monthly hydrological drought hazard indicators, mapping and upload of maps to public server, upload of relevant model output and indicators to public server.

Probabilistic seasonal forecast of hydrological drought hazard

In the framework of GlobeDrought, it was not the goal to compute actual seasonal forecasts of hydrological drought indicators by driving WaterGAP with an ensemble of actual meteorological seasonal forecast. As planned, we only simulated the generation of an ensemble forecast of hydrological drought indicators by driving WaterGAP not with actual seasonal forecasts of climate variables but by historic climate data where each of 30 historic years was considered as one ensemble member of a seasonal forecast. The aim was to derive methods for seasonal forecast analysis and communication. We used the drought hazard indicator ADQI-Q80, Ifm and ERA5 climate data to simulate a seasonal forecast starting at the end of 2018. To this end, 30 WaterGAP model runs were conducted until 31 December 2018, where the climate data input until 2018 was the standard ERA5 time series, while the year 2019 was simulated with the climate data of one of the 30 climate years 1989-2018 as alternative climate forcing. The resulting range of possible streamflow drought hazard in 2019 is shown in Figure 8 for the WaterGAP calibration station in Mainz, Rhine River, Germany. The drought hazard range of the probabilistic forecast in 2019 is not the same as the actual drought hazard range during 1989-2018. This is due to the fact that a) streamflow in January 2019 depends on water storages in December 2018 and b) the accumulated deficit in January 2019 depends on the deficit in December 2018. For instance, drought hazard in 2017 is not the same as in the probabilistic forecast year 2017 (yellow line in Figure 8), since water storages as well as accumulated deficits were different in December 2016 and 2018. Moreover, the probabilistic forecasts based on the drought years 2003 and 2011 are highlighted in red (2011) and dark red (2003). In

addition to station-specific (or grid-cell specific) analyses, seasonal forecast results should be summarized in global maps, e.g. showing the following:

- Percentage of ensemble runs per grid cell that exceed a certain drought hazard threshold (maps can be compared for different indicators and different drought hazard thresholds),
- Mean indicator over all ensemble members.

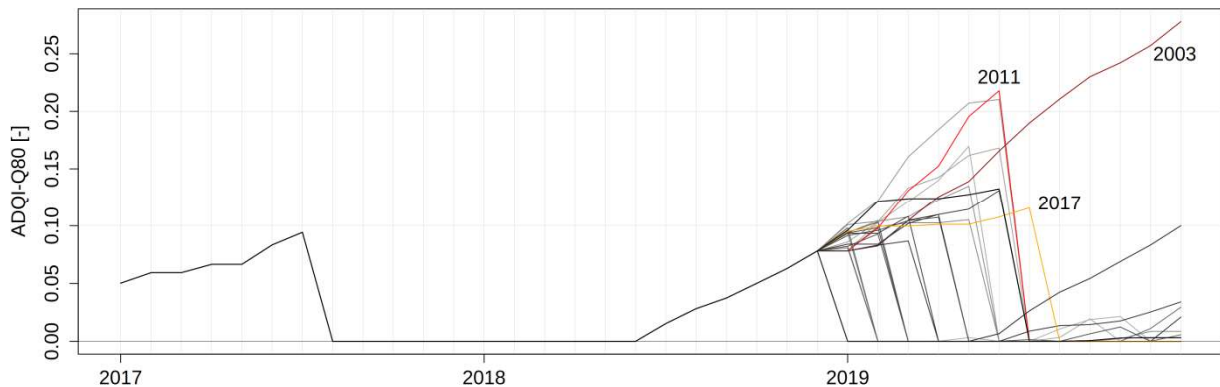


Figure 8. Probabilistic forecast for the year 2019 based on the drought hazard indicator ADQI-Q80, lfm and ERA5 climate data at the WaterGAP calibration station Mainz, Rhine River, Germany

1.5.2 Development of drought hazard indicators for rainfed and irrigated crop production

Drought hazard indicators were developed in GlobeDrought based on remote sensing and based on crop water modelling. Remote sensing based indicators have the advantages of a very high spatial resolution and that the drought indicators are based on reflections of the land surface that is really be measured at a specific location and time. Disadvantages are that observations are limited to the more recent period since 2001 (MODIS) or 1989 (NOAA AVHRR) and that it is usually not possible to distinguish specific crops or irrigated and rainfed crops. In contrast, models can be applied for a longer period than remote sensing but are more limited with regard to the spatial resolution. They can distinguish specific crops and irrigated versus rainfed conditions but the accuracy of the simulations is constrained a lot by the uncertainty in the input data for cropping patterns, climate and soil and the assumptions made for the begin and end of the growing seasons.

Remote sensing based drought hazard analyses

Mainly remote sensing based drought hazard analyses were performed for Zimbabwe (Frischen et al., 2020), the case study regions Missouri basin, Zimbabwe and South Africa (Schwarz, 2020) and at global scale (Ghazaryan et al., 2020). The

workflow in the analyses and the data processing steps are illustrated in Figure 9. Although the three studies used different methods with distinct complexity, all approaches successfully determined drought hazard. Drought hazard patterns agreed also well for study regions and years considered in more than one assessment. The hazard analysis performed for Zimbabwe (Frischen et al., 2020) was based on anomalies in the Normalized Difference Vegetation Index (NDVI) and temperature, combined in the Vegetation Health Index (VHI). The study for the Missouri River Basin, South Africa and Zimbabwe (Schwarz et al., 2020) combined five hazard indicators in a logistic regression model to estimate the probability of

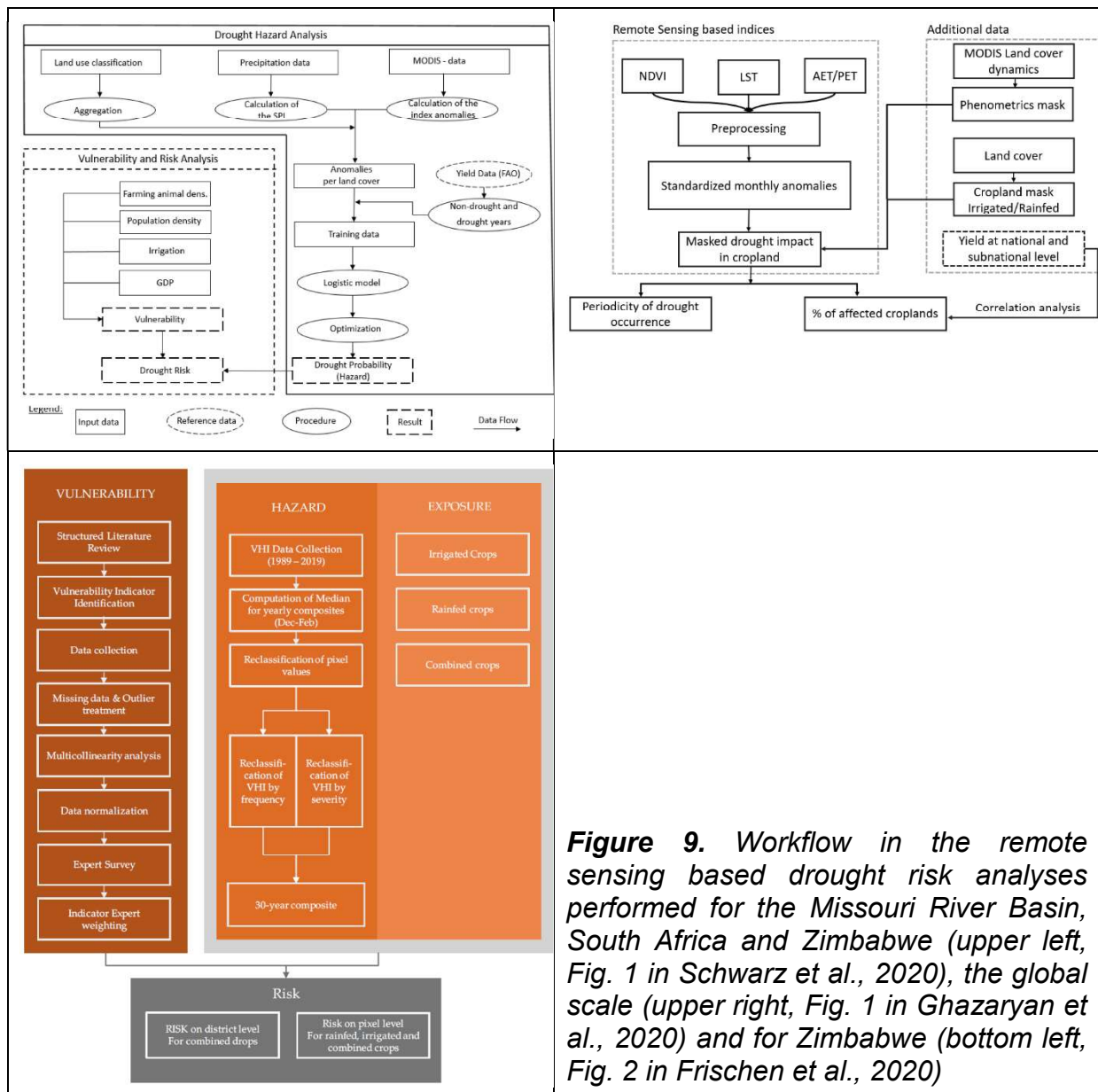


Figure 9. Workflow in the remote sensing based drought risk analyses performed for the Missouri River Basin, South Africa and Zimbabwe (upper left, Fig. 1 in Schwarz et al., 2020), the global scale (upper right, Fig. 1 in Ghazaryan et al., 2020) and for Zimbabwe (bottom left, Fig. 2 in Frischen et al., 2020)

drought, namely precipitation anomaly (SPI), NDVI, Normalized Difference Infrared Index (NDII), Albedo and Land Surface Temperature (LST). The logistic regressions were performed separately for the three regions. Consequently, the variables and coefficients considered in the final regression model differed. The global scale study (Ghazaryan et al., 2020) tested anomalies of the three indices NDVI, LST and AET/PET ratio for their correlation with yield anomalies to derive drought hazard and the percentage of cropland affected by drought. Since the three indices were treated separately in the correlations, an objective was also to find out which of the indices was most suitable to predict negative yield anomalies as usually caused by drought.

Drought hazard analyses based on process based crop water modeling

In addition to the remote sensing based assessments described before, two studies were performed to estimate drought hazard based on the output of process based models. One study was performed at global scale (Meza et al., 2020) and one study for South Africa (Meza et al., 2021). The Global Crop Water Model (GCWM) was applied for period 1981-2018 to estimate drought stress of rainfed crops or water requirements of irrigated crops. In addition, WaterGAP was used to simulate streamflow anomalies which were used as indicator of water availability for irrigation. Drought hazard is defined as a deviation of the situation in a specific year or month from long-term mean conditions in the 30-year reference period from 1986 to 2015. For the global study (Meza et al., 2020) the two models were still forced with different climate input covering the period 1981-2016. WaterGAP 2.2d, was forced by the WFDEI-GPCC climate data set (Weedon et al., 2014), which was developed by applying the forcing data methodology developed in the EU project WATCH on ERA-Interim reanalysis data. GCWM used the CRU-TS 3.25 climate data set (Harris et al., 2014) as input. CRU-TS 3.25 was developed by the Climate Research Unit of the University of East Anglia by interpolation of weather station observations and is provided as a time series of monthly values. Pseudo-daily climate was generated by the GCWM as described in Siebert and Döll (2010). For the subsequent regional study for South Africa (Meza et al., 2021), both models were adjusted to use daily climate input data for period 1981-2018 obtained from the ERA5 global reanalysis product (Hersbach et al., 2020).

Drought hazard for irrigated agricultural systems

The irrigated hazard index $CH_IrrigAg_y$ (-) is defined based on the annual difference between the water resource available for irrigation and irrigation water requirement. The water resource available for irrigation was simulated using the WaterGAP model (Müller-Schmied et al., 2021) as annual sum of discharge Q at a spatial resolution of 30 arcmin. The irrigation water requirement IWR was simulated using GCWM as the volume of water needed to increase the AET of irrigated crops to their PET (Siebert and Döll, 2010). Drought hazard for irrigated crops $CH_IrrigAg_y$ was computed as:

$$CH_IrrigAg_y = \frac{(Q-IWR)_{med} - (Q_y - IWR_y)}{Q_{med}} \quad (1)$$

where $(Q - IWR)_{med}$ is the median of the difference between discharge and irrigation water requirement ($m^3 yr^{-1}$) in the reference period 1986-2015 (Meza et al., 2021). Q_y and IWR_y are discharge and irrigation water requirements in year y ($m^3 yr^{-1}$), and Q_{med} is the median of the annual discharge in the reference period 1986-2015 ($m^3 yr^{-1}$). Positive values of $CH_IrrigAg_y$ indicate drought, while negative values indicate that the difference between water resources and water demand for irrigation is larger than usual (wetness). Both models (GCWM and WaterGAP) used the same soil and climate input data and the same simulation period (1981-2018). The outputs of GCWM (for crops grown in South Africa) were aggregated to 30 arcmin to match the spatial resolution used by WaterGAP. A similar analysis was performed also at global scale (Appendix A1). The long-term hazard for irrigated conditions at grid level was computed as the frequency of the years with an irrigated hazard index $CH_IrrigAg_y$ of bigger than 0.5 meaning that the deficit in the annual difference between discharge and irrigation requirement exceeded half of the long-term median of annual discharge. A long term hazard for irrigated conditions of 0.2 means then that such a deficit occurs every 5 years.

Drought hazard for rainfed agricultural systems

The rainfed hazard indicator was computed using the ratio between actual evapotranspiration (AET) and potential (PET) evapotranspiration of crops in the crop growing season for the period 1981-2018. AET refers to the amount of water consumed by a crop and evaporated from the soil under actual soil moisture calculated by performing a soil water balance in daily time steps, while PET assumes no limitation in crop water availability. The ratio is highly associated with crop yield and is widely used as a drought indicator for cropland (Peng et al., 2019). The Global Crop Water Model (GCWM) (Siebert and Döll, 2010) was employed to simulate AET and PET for specific crops grown in South Africa based on prescribed crop calendars and cropping patterns derived from the the MIRCA2000 dataset (Portmann et al., 2010). A similar analysis was also performed at global scale (Appendix A1). The spatial resolution of GCWM's is five arcmin (8.3 km). Drought hazard in specific years was defined as deviation from the long-term mean condition in the reference period 1986-2015 (Meza et al., 2020; Meza et al., 2021). The annual hazard indicator for rainfed agricultural systems CH_RfAg_y was calculated as:

$$CH_RfAg_y = 1 - \frac{AET_y/PET_y}{\underline{AET}/\underline{PET}} \quad (2)$$

where AET_y and PET_y are annual sums of actual and potential evapotranspiration of all cultivated crops in year y ($m^3 yr^{-1}$). \underline{AET} and \underline{PET} are the long-term annual mean of actual and potential evapotranspiration ($m^3 yr^{-1}$) in the reference period 1986-2015.

Consequently, positive values of CH_RfAgy represent conditions dryer than usual, while negative values indicate wet years. The long term hazard during the study period at grid level was computed as the frequency (percentile rank) of years in which the AET/PET ratio was at least 10% lower than the mean AET/PET ratio in the reference period 1986-2015 (Meza et al., 2020). A long-term hazard of 0.5 means therefore that in every second year the AET/PET ratio is lower than 90% of the long-term mean AET/PET ratio.

1.6 Drought exposure analysis

Following the definitions of the Intergovernmental Panel on Climate Change put forward in their Fifth Assessment Report (IPCC, 2014), exposure is defined as the elements located in areas that could be adversely affected by drought hazard. The distinct exposure of irrigated and rainfed agricultural systems to drought was considered by weighting grid-cell-specific hazards with the harvested area of irrigated and rainfed crops.

1.6.1 Global scale analysis

The monthly irrigated and rainfed crop areas' (MIRCA2000) data set (Portmann et al., 2010) was used when aggregating grid-cell-specific hazards to exposure at a national scale. MIRCA2000 was also used to inform the models used in the hazard calculations about growing areas and growing periods of irrigated and rainfed crops. The data set refers to the period centered around the year 2000; time-series information is not available at a global scale. To maximize the representativeness of the land use, the reference period and evaluation period used in this study were centered around the year 2000. Grid specific drought hazard was then weighted with harvested area when computing the mean hazard per country (Meza et al., 2020). The combined drought exposure of rainfed and irrigated cropping systems was evaluated at the country level by averaging the harvested-area weighted drought exposure of irrigated and rainfed cropping systems. As described before, distinct methods were used to calculate hazard and exposure of irrigated and rainfed systems so that a direct comparison of the exposure values is not meaningful. In addition, the frequency distributions differed considerably, with a harvested-area weighted global mean of the drought exposure of 0.455 for irrigated systems and 0.189 for rainfed systems. To ensure a more similar weight of rainfed and irrigated drought exposure, country-specific exposures were divided by the global mean, and then the integrated exposure was calculated as harvested-area weighted mean:

$$\text{Exp}_{\text{tot}} = ((\text{AH}_{\text{rf}} \cdot \text{Exp}_{\text{rf}} / 0.189) + (\text{AH}_{\text{irr}} \cdot \text{Exp}_{\text{irr}} / 0.455)) / \text{AH}_{\text{tot}} \quad (3)$$

with Exp_{tot} , Exp_{rf} and Exp_{irr} being the exposure of the whole, rainfed and irrigated cropping systems to drought and AH_{tot} , AH_{rf} and AH_{irr} being the harvested area of all crops, rainfed crops and irrigated crops.

1.6.2 Regional analysis

The estimation of exposed agricultural land in the regional studies for South Africa was based on the South African National Land Cover dataset 2018 (Thompson, 2019), from which irrigated and rainfed land were extracted as separate classes. The SANLC 2018 map has 20 meters spatial resolution and was generated using multi-seasonal Sentinel 2 satellite time series data acquired during the period 01 January 2018 to 31 December 2018 with 90.14% accuracy (Thompson, 2019). Rainfed systems are mostly located in the North Eastern provinces, as well as in Northern and Western Cape (DAFF 2018). The hazard indicators - CH_RfAgy and CH_IrrigAgy - were aggregated from pixel to municipality level as average of the pixel values, using the rainfed or irrigated area within each pixel derived from the SANLC 2018 dataset for weighting. From this point, the combined components of hazard and exposure are referred to as 'hazard/exposure'. For the studies in Zimbabwe, a land cover map separating irrigated and rainfed cropland was developed as part of the GlobeDrought project (Landmann et al., 2019) because alternative products have not been available.

1.7 Development of drought vulnerability indicators and indices

According to the Intergovernmental Panel on Climate Change (IPCC, 2014), vulnerability is the predisposition to be adversely affected as a result of the sensitivity or susceptibility of a system and its elements to harm, coupled with a lack of coping and adaptive capacity. The assessment of drought vulnerability is complex because it depends on both biophysical and socioeconomic drivers (Naumann et al., 2014). Due to this complexity, the most common method to assess vulnerability in the context of natural hazards and climate change is using composite indicators or index-based approaches (Beccari, 2016; de Sherbinin et al., 2019). Although their usefulness for policy support has also been subject to criticism (Hinkel, 2011; Beccari, 2016), it is widely acknowledged that composite indicators can identify generic leverage points for reducing impacts at the regional to global scale (De Sherbinin et al., 2019; UNDRR, 2019). In some studies performed by GlobeDrought in which the hazard and exposure analysis was mainly based on remote sensing (Ghazaryan et al., 2020; Schwarz et al., 2020) vulnerability to drought was analysed by using a simplified methodology based on just a few indicators (Figure 9). In contrast, a very detailed vulnerability analysis based on a large number of indicators was performed for the global drought risk study (Meza et al., 2020) and the two regional assessments for Zimbabwe (Frischen et al., 2020) and South Africa (Meza et al., 2021). These advanced vulnerability assessments are described in this section in more detail.

Following the workflow to calculate composite indicators proposed by the Organisation for Economic Co-operation and Development (OECD, 2008) and Hagenlocher et al. (2018), the methodological key steps on which the vulnerability

assessment is based are (1) the definition of the conceptual framework, (2) identification of valid indicators, (3) data acquisition and preprocessing, (4) analysis and imputation of missing data, (5) detection and treatment of outliers, (6) assessment of multicollinearities, (7) normalization, (8) weighted aggregation, and (9) visualization.

1.7.1 Global scale analysis of vulnerability to drought

An initial set of vulnerability indicators for agricultural systems was identified based on a recent review of existing drought risk assessments (Hagenlocher et al., 2019). In total 64 vulnerability indicators, including social, economic and physical indicators; farming practices; and environmental, governance, and crime and conflict factors, were selected and classified by socioecological susceptibility (SOC_SUS, ENV_SUS), a lack of coping capacity (COP) and a lack of adaptive capacity (AC) following the risk framework of the IPCC (IPCC, 2014). Indicator weights, which express the relevance of the identified indicators to characterizing and assessing the vulnerability of agricultural systems to droughts, were identified through a global survey of relevant experts (n=78), the majority of whom have worked in academia and for governmental organizations with more than 5 years of work experience (Meza et al., 2019). In total, 46 of the 64 indicators were considered relevant by the experts, comprising susceptibility, coping- and adaptive-capacity indicators. However, since adaptive capacity is only relevant when assessing future risk scenarios and less relevant to current risk, indicators related to adaptive capacity and indicators that could be measured with the same data source due to the similarity in what they represent were removed. For instance agriculture (% of GDP) and dependency on agriculture for livelihood (%) were averaged into one income indicator, and the variables GDP per capita (PPP – purchasing-power parity) and population below the national poverty line (%) both refer to poverty and therefore were also averaged to a combined indicator. This resulted in a set of 26 indicators as part of the vulnerability assessment.

Following data acquisition, the data were preprocessed by transforming absolute to relative values and standardized when necessary (e.g., travel time to cities ≤ 30 min – population, divided by the total population). Descriptive statistics were used to evaluate the degree of missing data. The imputation of missing values was done with data from previous years and using secondary sources following Naumann et al. (2014) in cases where the r value lay between -1.0 and -0.9 or 1.0 and 0.9 using a Spearman correlation matrix and scatter diagram for visual interpretation. Following suggestions by Roth et al. (1999), Peng et al. (2006) and Enders (2003), listwise and pairwise deletion thresholds were selected when $>30\%$ of data were missing on a country level and when $>20\%$ of data were missing on the indicator level. After the deletion, 168 countries and 26 indicators were considered for the final analysis. To detect potential outliers, scatter plots and box plots for each indicator were created. Potential outliers were further examined using triangulation with other

sources and past years. On this basis, outliers were identified in only one indicator (i.e., fertilizer consumption – kg ha⁻¹ of arable land) and treated using winsorization following Field (2013). Multicollinearities were identified using a Spearman correlation matrix for the different vulnerability components (social susceptibility, environmental susceptibility and a lack of coping capacity). Following the rule proposed by Hinkel et al. (2011), any values higher than $r > 0.9$ or smaller than $r < -0.9$ were considered very highly correlated. The correlation was considered only if it was significant at the 0.05 level (two-tailed). Two indicators for the lack of a coping-capacity component and two from social susceptibility (e.g., healthy life expectancy at birth – years – and disability-adjusted life) showed high and significant correlations. However, no indicators were excluded on this basis due to the difference in concepts they represented and their relevance at the global level. In order to render the indicators comparable, the final selected indicators were normalized to a range from 0 to 1 using min–max normalization (Naumann et al., 2014; Carrão et al., 2016):

$$Z_i = (X_i - X_{\min}) / (X_{\max} - X_{\min}) \quad (4)$$

where Z_i is the normalized score for each indicator score X_i . For variables with negative cardinality to the overall vulnerability the normalization was defined as

$$Z_i = 1 - (X_i - X_{\min}) / (X_{\max} - X_{\min}) \quad (5)$$

Finally, the normalized indicator scores were aggregated into vulnerability components (SOC_SUS, ENV_SUS, COP) using weighted arithmetic aggregation based on (using the example of SOC_SUS)

$$\text{SOC_SUS} = \sum W_i Z_i \quad (6)$$

where W_i is the weights for each normalized data set, and Z_i is the weights as obtained from the global expert survey. Therefore, weights were normalized to add up to 1. The vulnerability components of socioecological susceptibility (SE_SUS) were combined using an average, which was then combined with COP to obtain a final vulnerability index (VI) score:

$$\text{VI} = (V(\text{SE_SUS}) + V(\text{COP})) / 2 \quad (7)$$

1.7.2 Regional analysis of vulnerability to drought

Drought impacts are often associated with drought hazard severity, but the degree of the impact is mediated by the vulnerability of the exposed agricultural system, i.e. its susceptibility and the (lack of) capacity to cope with drought events (IPCC, 2014; World Bank, 2019). While an array of methods for assessing vulnerability to natural hazards exists, indicator-based approaches are amongst the most common to

represent the multi-dimensional nature of vulnerability (Hagenlocher et al., 2019; de Sherbinin et al., 2019). For the regional assessment in South Africa, composite indicators were developed according to the impacted sector: i) irrigated agriculture and ii) rainfed agriculture, considering a wide array of environmental, social, and economic indicators.

Relevant indicators were identified through a combination of literature review and expert consultation. The review was conducted based on pre-defined search terms in Web of Science and Scopus. The selected articles ($n = 17$) were coded with MAXQDA software (VERBI Software 2019) to extract suitable indicators. Later, these indicators were compared and complemented with the ones identified by Hagenlocher et al. (2019) in their review of existing drought risk assessments, and within South Africa at a local municipality level by Walz et al. (2018) and a quaternary catchment level by Jordaan et al. (2017a, 2017b). In total, 44 suitable indicators for rainfed and irrigated systems in South Africa were identified. To assess which of those 44 indicators are the most relevant for representing vulnerability of these two systems towards drought, an online expert survey was conducted as a joint effort with the National Disaster Management Centre (NDMC) of South Africa. A total of 33 experts representing all provinces of South Africa participated in this survey. They selected 36 relevant indicators for irrigated systems and 40 for rainfed. These experts were from multiple sectors including academia ($n=4$), private sector ($n=5$), NGO ($n=1$), Government ($n=20$), international organizations ($n=1$) and others ($n=2$).

Open-source data for the selected indicators was retrieved (e.g. Statistics from South Africa (STATS SA), National Treasury, World Bank) in order to ensure that the final results can be validated and reproduced in a different context - as recommended by Naumann et al. (2014). Following the methodological suggestions by Hagenlocher et al. (2018), Meza et al. (2020), Nauman et al. (2014), and OECD (2008), statistical operations were performed to prepare an indicator dataset to perform the vulnerability assessment: i.e., i) imputation of missing data, ii) normality test, iii) outlier detection and treatment, iv) multicollinearity assessment, v) normalization and vi) expert weighted aggregation.

After data acquisition and statistical data processing, 22 indicators were used to perform the vulnerability assessment for irrigated systems and 24 for rainfed. The selected vulnerability indicators were normalized to make them comparable. A linear min-max normalization was applied to create a range between 0 (lowest vulnerability) to 1 (highest vulnerability) (Beccari, 2016; Carrão et al., 2016).

The final step to build the composite vulnerability index (CVI) for each agricultural system (irrigated and rainfed) was the weighted arithmetic aggregation for each vulnerability component (SOC-ENV_SUS and lack of COP) based on the normalised indicators (Z_i) and the weights obtained from the expert survey (W_i).

$$CVI_{irrigated} = \sum_{i=1}^n (Z_i * W_i) \quad CVI_{rainfed} = \sum_{i=1}^n (Z_i * W_i) \quad (8)$$

1.8 Integration of hazard, exposure and vulnerability to drought risk

The final drought risk index was calculated in the studies performed by GlobeDrought by multiplying the indices for drought hazard and exposure by vulnerability (Figures 9-11). At the pixel level, the presence of hazard and vulnerability point to a certain drought risk, independent of how much crop area is contained in the specific pixel. At the aggregated level, the different crop areas in the specific pixels must be considered; therefore exposure was calculated as harvested-area weighted mean of the pixel-level hazard and then multiplied by vulnerability to calculate drought risk at the country level.

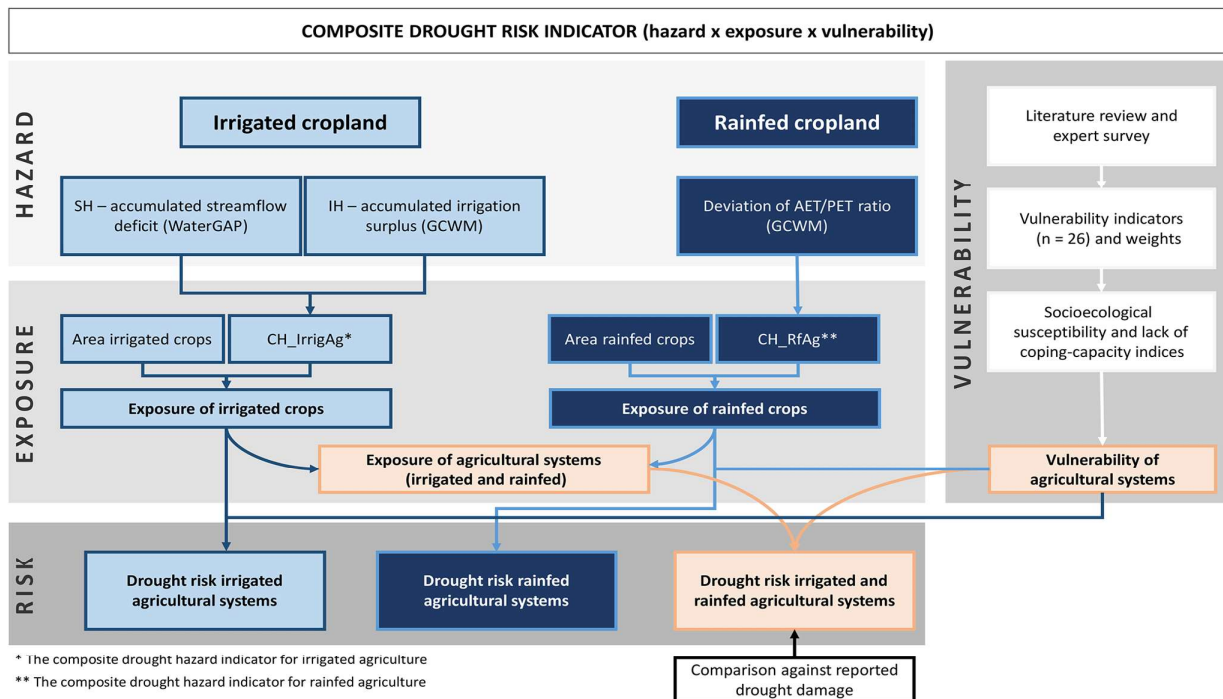


Figure 10. The overall workflow of the drought risk assessment for agricultural systems performed at global scale (Fig. 1 in Meza et al., 2020)

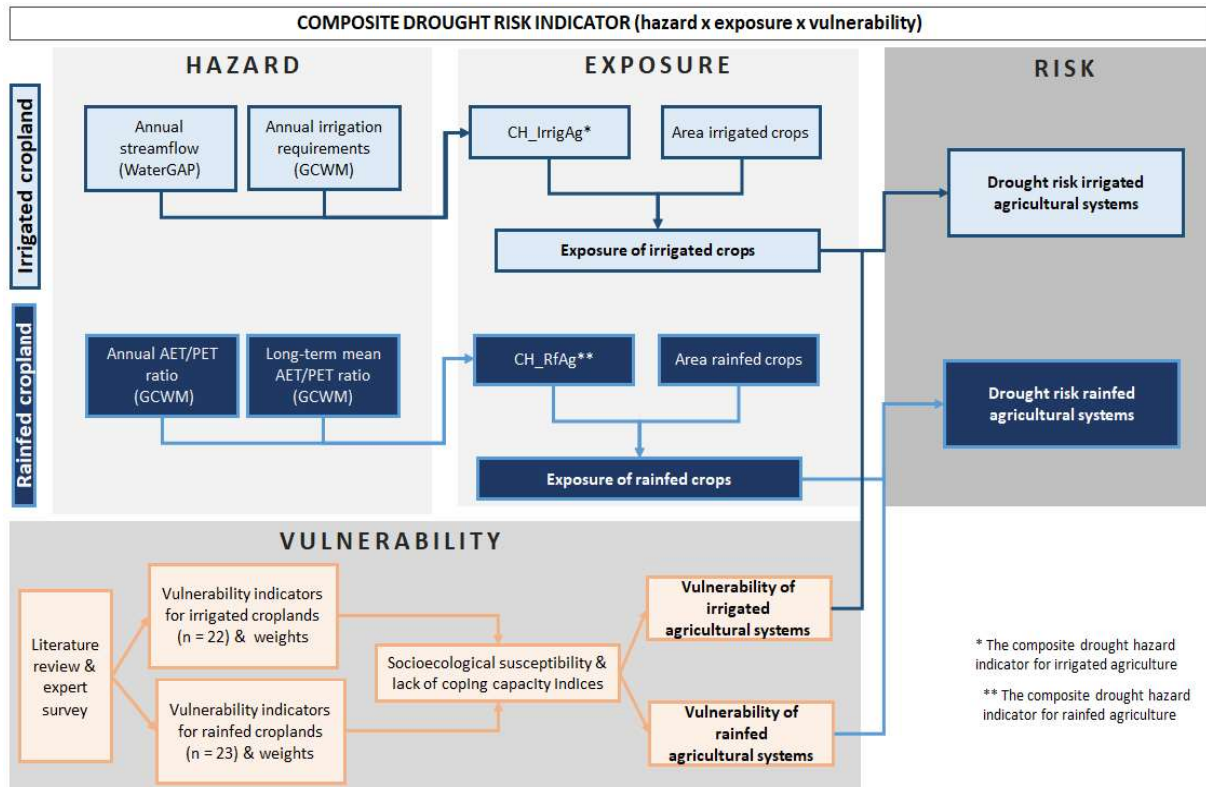


Figure 11. The overall workflow of the drought risk assessment for agricultural systems performed at regional scale for South Africa (Fig. 2 in Meza et al., 2021)

1.9 Validation of drought hazards and drought risk

The outcomes of the risk assessment for irrigated and rainfed systems were compared against drought impact data from different sources, against drought hazard shown in local observational early warning systems, against anomalies in reported crop yields and against similar drought indices derived with independent data.

Drought impact data were extracted from the international Emergency Events Database (EM-DAT) of the Centre for Research on the Epidemiology of Disasters (CRED). EM-DAT systematically collects reports of drought events and drought impacts from various sources, including UN agencies, NGOs, insurance companies, research institutes and press agencies. A drought event is registered in EM-DAT when at least one of the following criteria applies: 10 or more people are dead, 100 or more people are affected, or a declaration of a state of emergency or a call for international assistance is made. The number of drought events within the period 1980–2016 at country level and global extent was used as an input for the comparison (Meza et al., 2020).

Drought hazard calculated in the GlobeDrought project was also compared against estimates derived from national drought information systems such as the US Drought Monitor (Schwarz et al., 2020) or of the Global Drought Observatory of the

European Commission. Hydrological drought hazard was evaluated using reported river discharge (Schumacher et al., 2018).

Drought hazard for agricultural systems was compared against reported crop yields (Eyshi Rezaei et al., 2021; Meza et al., 2021). In regions with strong limitations in crop water supply a high correlation between the drought hazard indicators and yield anomalies should be expected with large negative yield anomalies in dry years.

Finally, we also did cross-validations of drought hazard estimates from process based models with estimates for the same variable derived from remote sensing. For example, the ratio between AET and PET used to calculate drought hazard for rainfed crops derived from process based models (Meza et al. 2020, 2021) is similar to the Evaporative Stress Index (ESI) computed from MODIS data (Ghazaryan et al., 2020). Therefore, strong correlations between simulated and remotely sensed AET/PET ratios should be expected in particular for regions where vegetation growth is constrained by soil water availability and where we find large inter-annual variability in AET/PET ratios.

2 Results of the drought risk analysis at global scale

2.1 Hydrological drought hazard

Seven innovative indicators for hydrological drought hazard were developed in this project. The streamflow drought hazard indicator ADQI-Q80,lfm is based on the widely used threshold-level method, but it implies a low-flow method that allows an existing drought to continue during a pre-defined low-flow season even if the threshold to terminate the drought (Q80) is exceeded. The rationale behind this approach is that people and the ecosystem cannot recover from a drought during the low-flow season if flow during this season is only a small percentage of total streamflow in each year. The indicator can add value in regions with high seasonal streamflow variability where people strongly rely on water storage in man-made reservoirs that needs to be replenished by streamflow. Moreover, two new water deficit indicators were developed, ADQI-WUs and ADQI-WUs-EFR that take into account mean monthly surface water use, and in case of the latter also mean monthly environmental flow requirements, EFR, which are assumed to be 80 % of mean monthly discharge. Finally, the new indicators QDAI and SMDAI combine the anomaly and deficit aspects of a drought for the variables streamflow and soil moisture. For the first time in a drought monitoring system, these indicators take into account that unusually low streamflow only translates into a high drought hazard if the water demand of people/biota cannot be satisfied. On the other hand, low streamflow anomalies can be perceived as strong drought hazard if they occur during periods of high water demand (see section 1.5.1 for details). Selected indicators (ADQI-Q50, ADQI-Q80, ADQI-Q80,lfm, SSI1, SSI12, QDAI and SMDAI) were made available through the [Integrated Drought Tool](#).

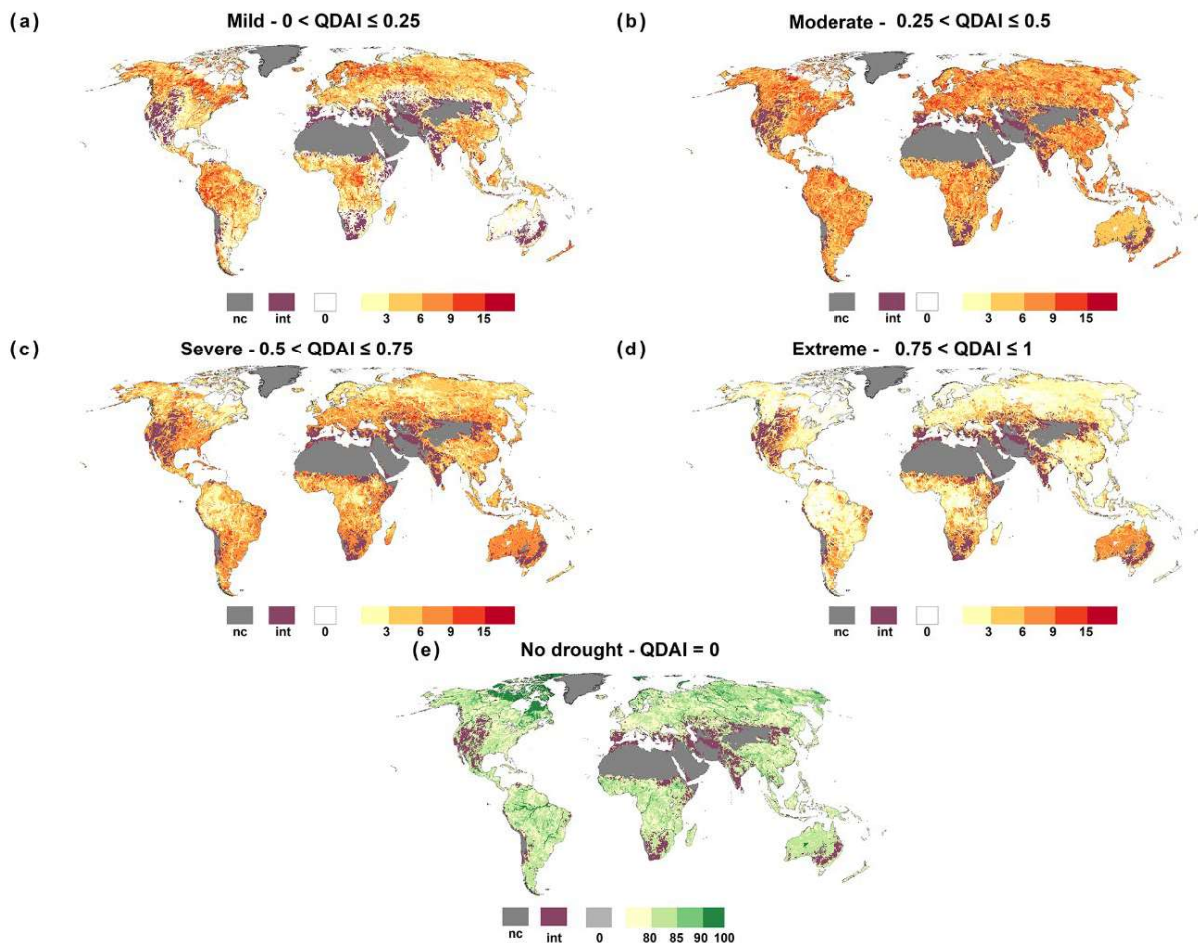


Figure 12. Frequency of occurrence (%) of mild (a), moderate (b), severe (c), extreme (d) or no (e) streamflow drought during the period 1981–2010 as defined by the indicator QDAI (Fig. 6 in Popat and Döll, 2021). Grid cells where for any calendar month there are at least 6 months with $Q_{ant} = 0$ are indicated as int, and grid cells which are not computed due to land cover are indicated as nc

We found that the large majority of the land surface is affected by streamflow drought (Figure 12). Mild and moderate droughts prevail in temperate and tropical climate while severe and extreme streamflow droughts occur more frequently in sub-tropical climate. This has direct implications for the stability of the water supply in these regions because the indicator QDAI is not only accounting for streamflow anomalies but also for deficits (Popat and Döll, 2021).

2.2 Drought hazard for agricultural systems

2.2.1 Irrigated crop production systems

High drought hazard for irrigated crops was calculated for most semi-arid regions characterized by large interannual variability in streamflow and irrigation requirement such as in the Western part of the US, Northeast Brazil, Argentina, Middle East, or Western India. However, drought risk for irrigated crops is also high in large parts of

Southern and Eastern Europe. Drought hazard for irrigated production systems is low for humid regions such as most tropical regions or regions with a low interannual variability in water resources and irrigation requirement such as Northern Africa and the Arabian Peninsula (Figure 13). Extended regions with high drought hazard were detected for each year in the observation period but spatial patterns differed a lot between the years. In many regions such as the Western part of the US or Western India multi-year droughts were detected (Appendix A1).

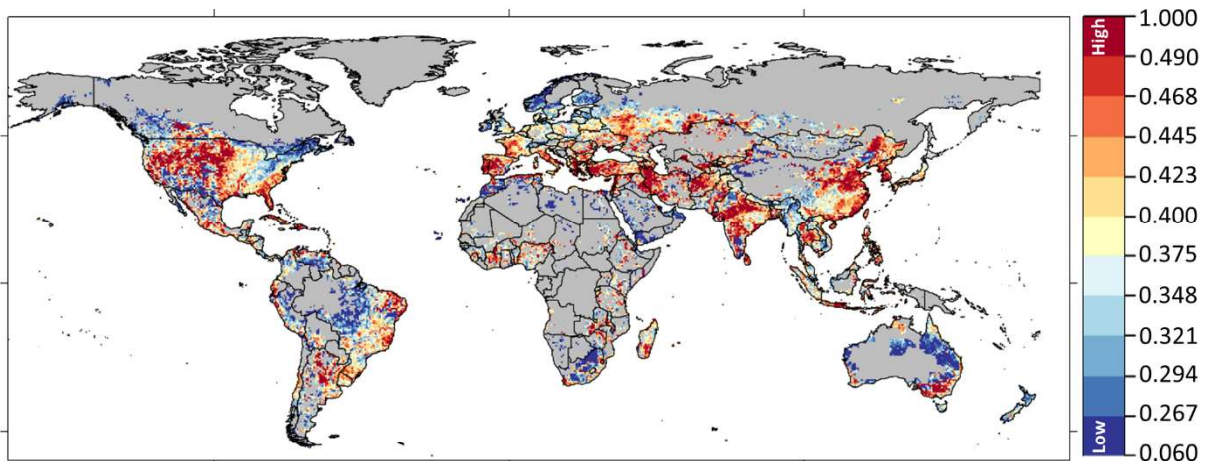


Figure 13. Long-term drought hazard of irrigated crop production systems (Fig. 2b in Meza et al., 2020)

2.2.2 Rainfed crop production systems

A high long-term hazard indicating frequent drought events was detected for most arid and semi-arid regions such as Western US, North Mexico, Northeast Brazil, Chile, Peru, Argentina, Southern Africa, Southern Russia, the Sahel-Zone, Central Asia, North India, North China Middle East and Australia (Figure 14). These are regions where irrigation is used at the large scale to reduce exposure to soil moisture droughts. However, not all farmers have access to irrigation infrastructure so that rainfed systems are frequently affected by drought. Spatial patterns of drought hazard for rainfed systems differ considerably between years but we also identified years in which most of the major agricultural production areas were affected by drought such as the years 2012, 1987, 2015, 2018 and 2002. In contrast, the major crop production regions were not or little affected by drought in years 1993, 1985, 1997, 1996 and 1998 (Appendix A1). For severe drought events occurring in larger regions the drought hazard maps were validated by inspection of anomalies in production, net trade and supply of cereals, pulses and oilcrops (Appendix A4). The comparison shows that production declined considerably in most of the selected drought events compared to the two preceding and subsequent years. Net trade reduced mainly when drought was observed in major crop exporting regions such as Australia, although the effect always happened here in the year subsequent to the

drought. Sharp declines in food supply became visible in regions where subsistence farming is prevailing such as Southern Africa while in developed regions reduced production was buffered by storage or trade (Appendix A4).

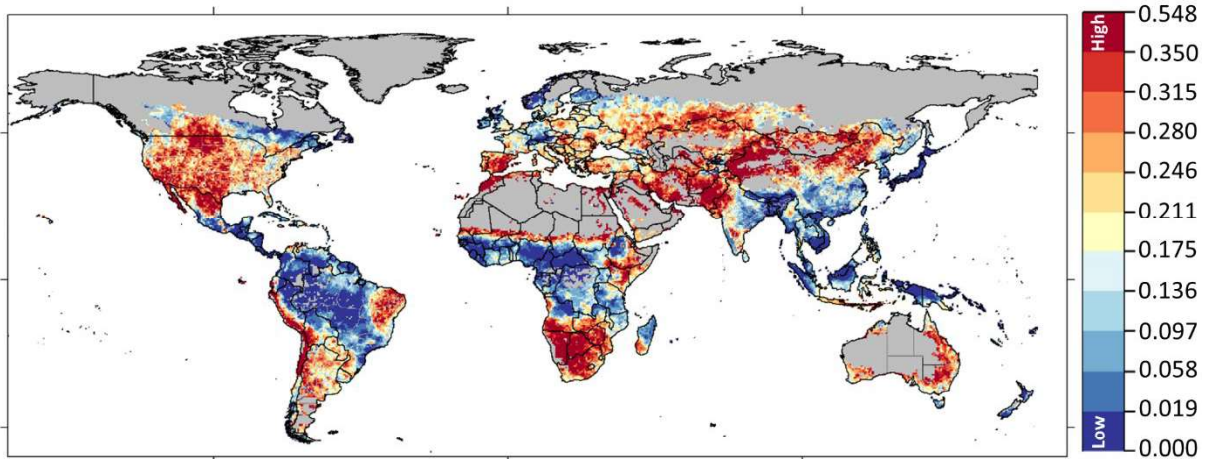


Figure 14. Long-term drought hazard of rainfed crop production systems (Fig. 3b in Meza et al., 2020)

2.2.3 Remote sensing based hazard analyses for crop production in general

The analysis of spatiotemporal patterns of drought and the relationship with yield anomalies at global scale showed that all three tested indicators (NDVI, LST and ESI) were correlated with negative yield anomalies (Figure 15). All indices could identify past drought events, such as the drought in the USA in 2012, Eastern Africa in 2016–2017, and South Africa in 2015–2016 (Ghazaryan et al., 2020). Anomalies in the ESI had higher correlations with maize and wheat yield anomalies than other indices (Figure 15). This finding is in particular relevant because the index ESI is similar to the drought hazard indicator for rainfed crop production systems used in the modeling studies (see previous section) and both indices can easily be translated into each other. Therefore the underlying AET / PET ratio was identified as powerful indicator for agricultural drought which can be obtained by modeling and remote sensing and therefore be used in studies combining modeling with remote sensing or to compare the results. The area affected by reduced AET / PET was mapped at global scale but a separation of irrigated and rainfed cropland could not be made because time series of irrigated and rainfed crop shares have not been available. However, such a comparison was possible for the US (Iowa) and South Africa (Free State Province) and showed that in many years a reduced ESI was found for both, rainfed and irrigated pixels. This points to constraints in water supply for irrigated fields resulting in deficit irrigation or even rainfed cultivation in years of severe hydrological drought. (Ghazaryan et al., 2020).

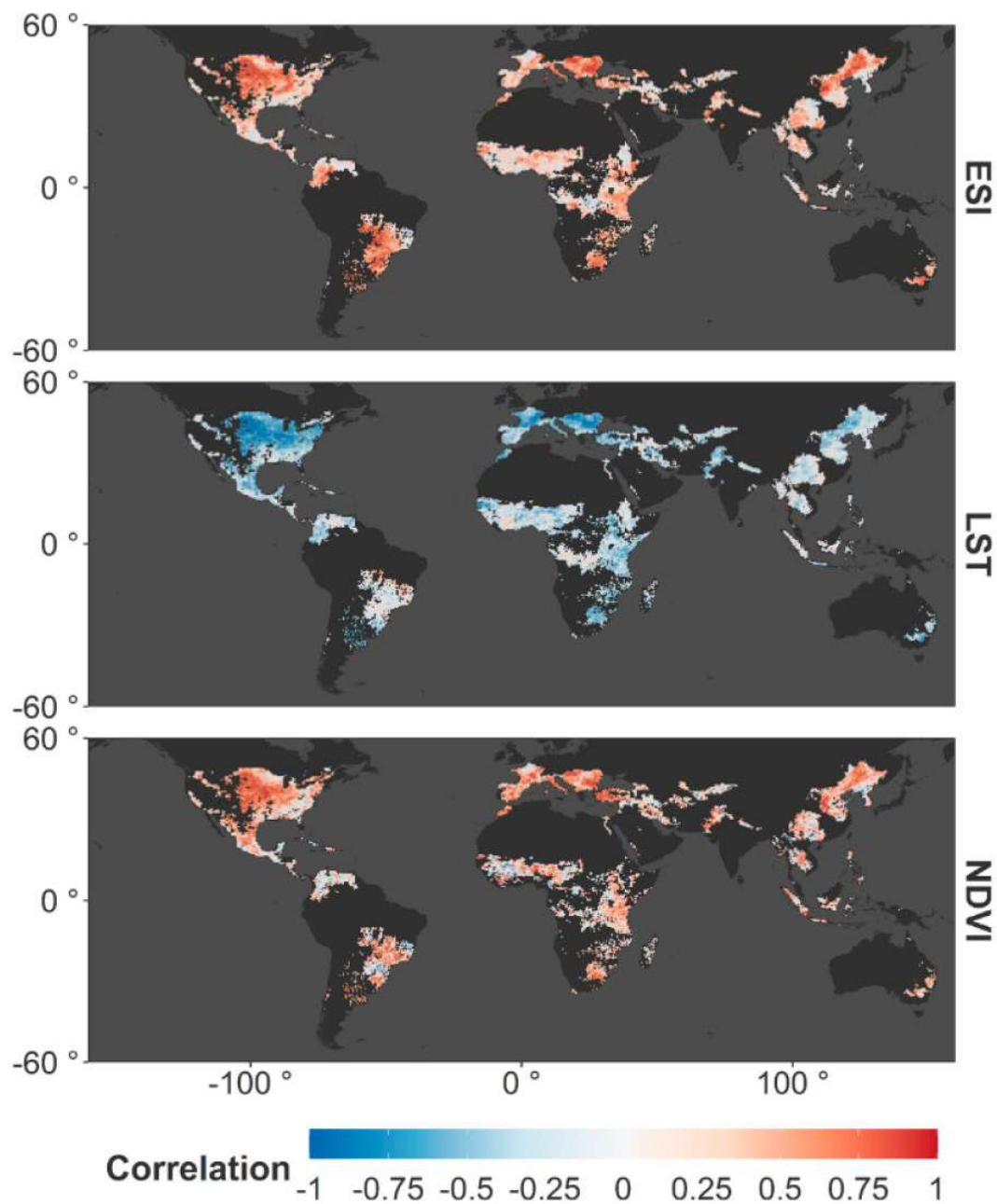


Figure 15. Pearson's correlation coefficient (r) estimated for a maize yield anomaly (based on gridded yield data) with land surface temperature (LST), evaporative stress index (ESI), and normalized difference vegetation index (NDVI) anomalies (peak of the growing season) (Fig. 2a in Ghazaryan et al., 2020)

The duration of droughts (in months) was also analyzed based on anomalies in the ESI (Figure 16). The spatial patterns in the duration of EVI-anomalies agree quite well with the patterns in drought hazard for rainfed and irrigated systems derived by modeling (Figures 13, 14).

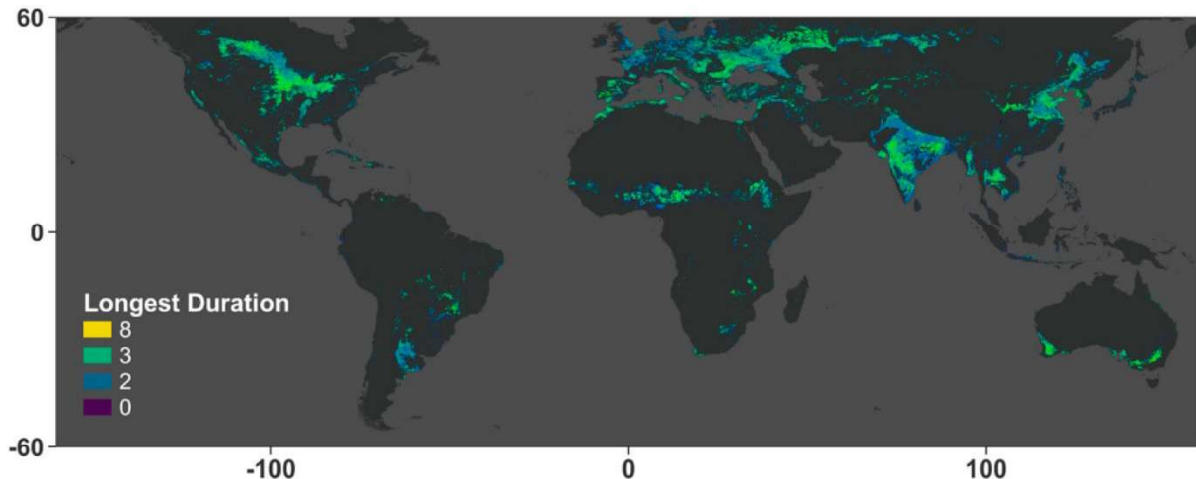


Figure 16. Maximum number of consecutive months with the ESI anomaly <-1 in the period 2001-2017 (non-cropland areas are masked based on the MODIS land cover, Fig. 4a in Ghazaryan et al., 2020)

2.2.4 Comparison of simulated and remotely sensed drought hazard

The comparison of the crop drought indicator for rainfed crops simulated with GCWM to the indicator derived from MODIS satellite imagery for period 2001-2019 showed a high agreement ($r > 0.5$) for all the regions with a high long-term drought hazard (Figures 14, 17). In contrast, correlations were low in humid or tropical regions such as West Africa, the Amazon basin, Southeast Asia or Northern Russia (Figure 17). The reason for the low agreement in these humid regions is the low inter-annual variability of the drought index making high positive correlations less likely.

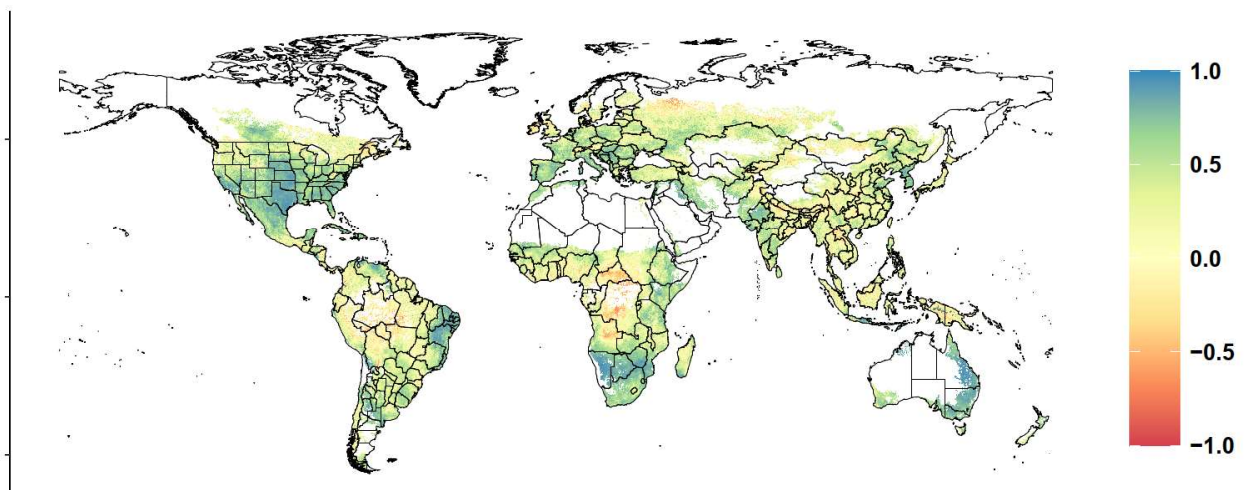


Figure 17. Pearson's correlation coefficient between the crop drought indicator (CDI) for rainfed crops simulated with the Global Crop Water Model and MODIS-based CDI for period 2001-2019

2.3 Exposure to drought

Exposure to drought was analyzed by aggregating pixel level harvested area weighted mean drought hazard to country level (Meza et al., 2020). The analysis shows that regions with low exposure of rainfed and irrigated crops to drought tend to be tropical and subarctic regions following the Köppen–Geiger climate classification (1980–2016; Beck et al., 2018). There are significant regional differences when comparing irrigated and rainfed drought exposure. Rainfed crops in Southern Africa are highly exposed to drought while the exposure of irrigated crops is relatively low (Figure 18). In contrast, exposure of irrigated crops to drought is higher than the one of rainfed crops in countries such as Iran, Turkey, China and Australia (Figure 18). A reason might be that these are large countries in which irrigated crops grow in the more arid regions which are more frequently affected by drought. Countries with high exposure for both, rainfed and irrigated crop production systems are the US, Australia, Iran, Syria and Pakistan. In contrast, low exposure for both, rainfed and irrigated crop production systems were found for countries in tropical West Africa (Central African Republic, Gabun, Congo, Liberia, Sierra Leone Guinea and Guinea-Bissau), Colombia, Norway, Myanmar and Laos (Figure 18).

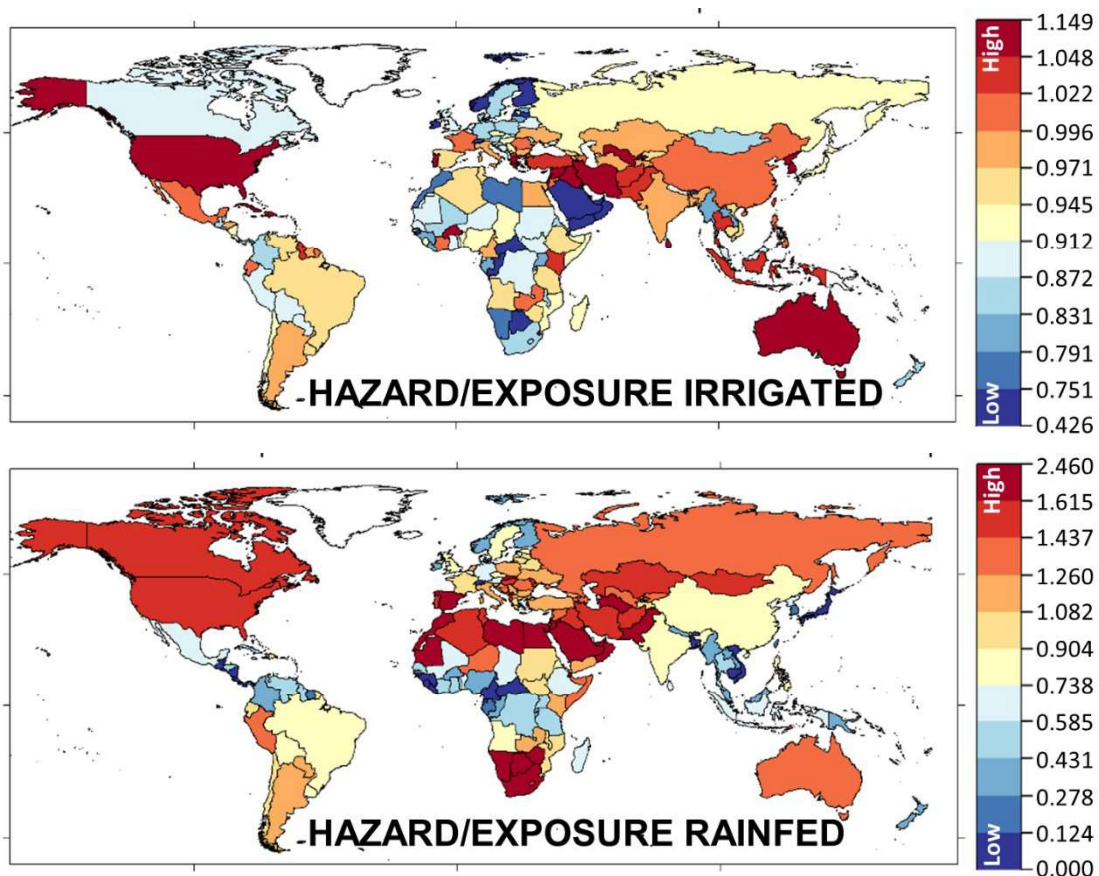


Figure 18. Exposure to drought for irrigated (top) and rainfed (bottom) agricultural systems in period 1981-2016 (Fig. 4 in Meza et al., 2020)

2.4 Vulnerability of agricultural systems to drought

Countries with particular high vulnerability to drought were detected mainly in sub-Saharan Africa (Mali, Niger, Chad, Sudan, Central African Republic, Congo DR, Angola, Mosambique, Zimbabwe and Madagascar), Asia (Iraq, Yemen, Afghanistan, Myanmar) and Latin America (Paraguay) while vulnerability to drought was low in developed countries such as the US, Canada, Western Europe, Australia but also in China (Figure 19). There were cases where countries such as Namibia presented high socioecological susceptibility in contrast with high coping capacity, reducing its overall vulnerability. The drought risk in countries such as Lesotho and Mauritania that have, in contrast, limited coping capacities is notably higher (Meza et al., 2020).

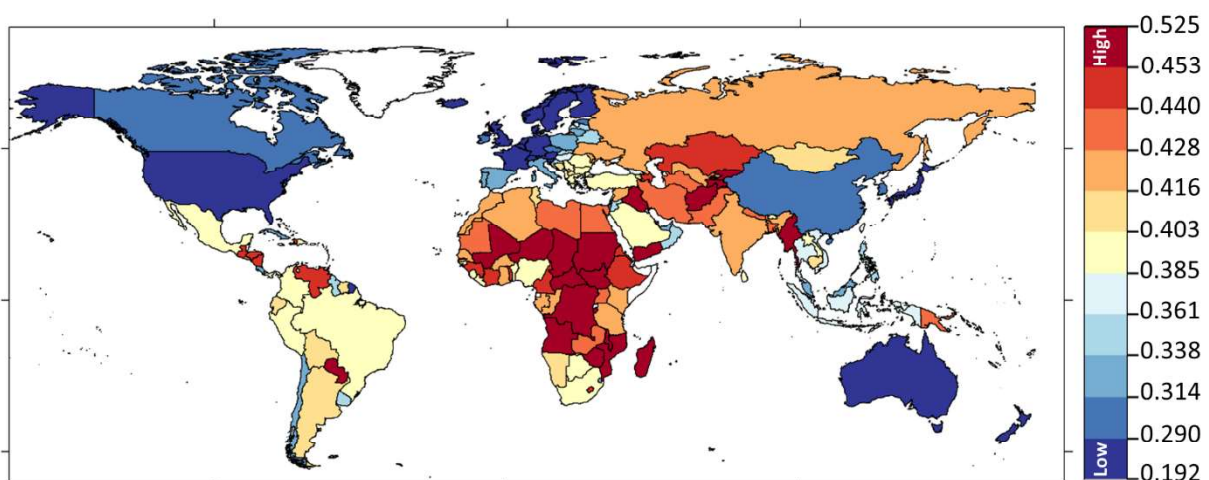


Figure 19. Vulnerability to drought for irrigated and rainfed agricultural systems in period 1981-2016 (Fig. 3c in Meza et al., 2020)

2.5 Drought risk of agricultural systems

2.5.1 Drought risk for irrigated systems

The drought risk for irrigated agricultural systems varies significantly among continents and countries. Especially large countries such as the USA, Brazil, China and Australia show a high variation at the country level due to varying climatic conditions. Drought hazard and exposure was highest in regions with a high density of irrigated land and high irrigation water requirements such as the western part of the USA, central Asia, northern India, northern China and southern Australia. Vulnerability was high particularly in sub-Saharan Africa but also in some countries in central Asia and the Middle East and low in general for industrialized and high-income countries. The combination of hazard and vulnerability to risk resulted in the highest values for large parts of western, central and southern Asia; eastern Africa; and the eastern part of Brazil. Low-risk areas include western Europe, the USA, Australia, New Zealand and most parts of China (Figure 20).

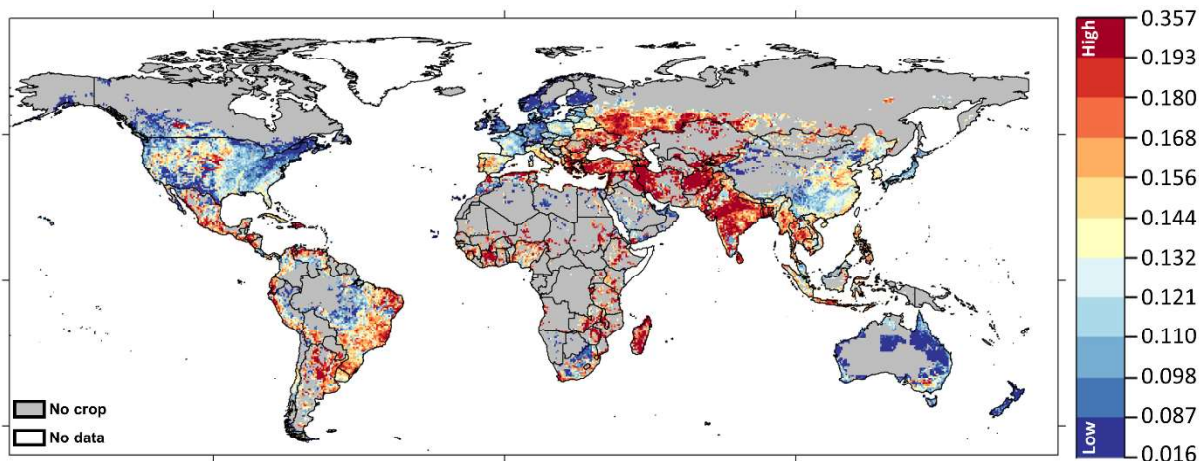


Figure 20. Drought risk for irrigated agricultural systems in period 1981-2016 (Fig. 2a in Meza et al., 2020)

2.5.2 Drought risk for rainfed systems

High levels of risk (dark yellow to red color scheme) for rainfed agricultural systems are observed in southern Africa, in southeastern Europe, in northern Mexico, in northeastern Brazil, at the western coast of South America, in southern Russia and in western Asia (Figure 21). Although drought hazard and exposure were high in the US and Australia (Figures 14, 18) the drought risk is relatively low (Figure 21) because of the low vulnerability (Figure 19). Drought risk is also low in general in Western Europe, Southeast Asia and in the humid tropics (Figure 21).

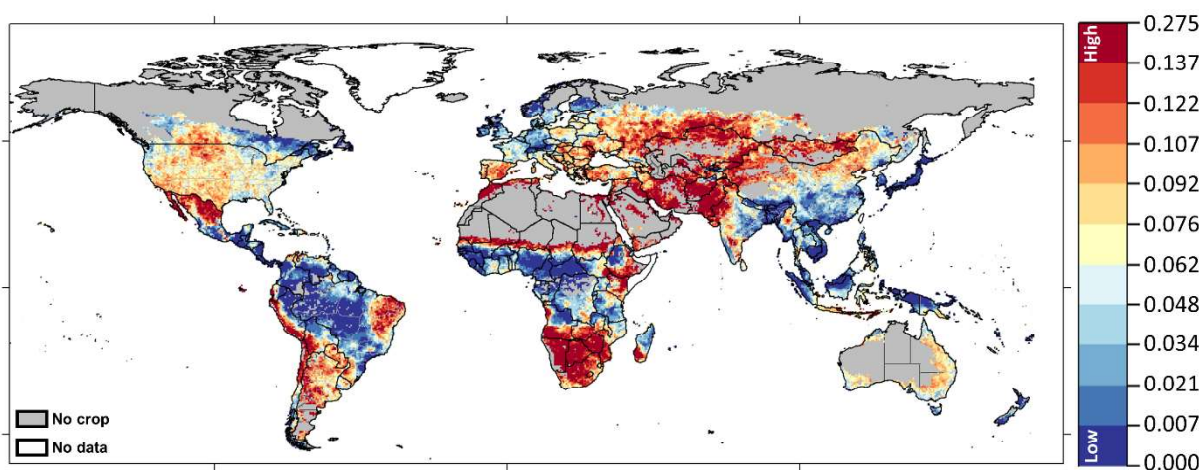


Figure 21. Drought risk for rainfed agricultural systems in period 1981-2016 (Fig. 3a in Meza et al., 2020)

2.5.3 Drought risk for agricultural systems (irrigated and rainfed combined)

Although the drought hazard was computed differently for the different agricultural systems, the countries with high risk of drought to both farming systems are Botswana, Namibia and Zimbabwe (Figure 22). These countries share the same

Final report – 2 Results of the drought risk analysis at global scale

relevant indicators that define their high vulnerability: a high soil and land degradation rate, a low literacy rate and low total renewable water in combination with high drought hazard and exposure. In addition, high total risk was computed for countries in Northern Africa (Morocco, Algeria, Niger, Lybia and Tunesia), Asia (Iran, Afghanistan; Mongolia, Kazakhstan) and for the Russian Federation (Figure 22). The attempt to calculate hazard, exposure and risk for the whole crop production sector by assigning a similar weight to the hazard exposures for rainfed and irrigated systems must be viewed critically, and results should be analyzed with care. A potential way to derive specific weights for rainfed and irrigated exposure could be validating not only calculated hazard and exposure but also vulnerability and risk, with information about drought impacts separately, for both irrigated and rainfed systems (Meza et al., 2020). Such an attempt has been made recently yielding indicators for vulnerability to drought separately for irrigated and rainfed systems and distinguishing different years (Appendix A2).

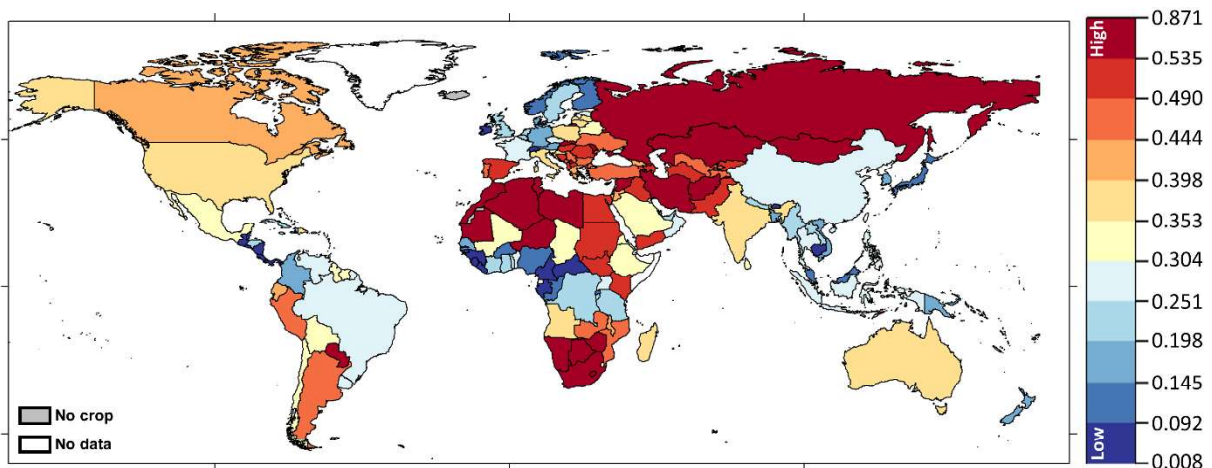


Figure 22. Drought risk for crop production systems (irrigated and rainfed combined) in period 1981-2016 (Fig. 4a in Meza et al., 2020)

3 Results of the drought risk analysis for regional case studies

3.1 South Africa

South Africa is located in the southern part of Africa, spreading over 122 million ha with approximately 12% croplands (FAO, 2020a). The country is composed of nine provinces and has a wide range of climates from arid to subtropical, temperate, and mediterranean (Figure 23). About 91% of South African territory is arid or semi-arid, with only 10% of the land generating half of the annual run-off (Le Maitre, 2018). The country has uneven rainfall distribution with a mean annual rainfall of 550 mm and annual mean temperature of 18°C (FAO, 2020a). The potential annual mean evaporation for the whole country is about three times greater than its annual rainfall, 1800mm per year (WWF, 2018).

The agricultural economy comprises technically developed commercial farming on the one hand and more subsistence-based production in the remote rural areas on the other hand (Waldner et al., 2017). The dominant activities include: i) intensive crop production and mixed farming in areas characterised by winter and summer rainfall, ii) cattle ranching in the bushveld and iii) sheep farming in the arid regions (Waldner et al., 2017). Climate--soil combinations leave only 12% of the country suitable for crop production; of which 22% is considered as high potential land in terms of production capacity (Waldner et al., 2017; WWF, 2018). In general, rainfed agriculture prevails in South Africa, accounting for the majority of the harvested area (Fig. 1) (Hardy et al., 2011). This means that only 1.35 million ha (8.5%) of the potentially arable land is irrigated (DAFF 2019). Nevertheless, irrigated agriculture contributes 30% to agricultural production (FAO, 2020c). Irrigation systems in South Africa can be permanent, supplementary, or occasional. Most commercial irrigation occurs across large river basins (e.g. Orange, Lower Vaal, Fish) and in the Western Cape region (FAO, 2016).

South Africa has been frequently affected by droughts in the last four decades. Major drought periods include 1982-1984, 1991-1992, 1994-1995, 2004-2005, 2008-2009, 2015-2016, and the most recent in 2018-2020 (Mahlalela et al., 2020; FAO, 2019; Walz et al., 2020, Unganai et al., 1998). During those years, drought not only impacted the environment, but also the social and the economic systems. The 1992 drought affected around 250,000 people, with an estimated 50,000 jobs losses in the agriculture sector, and 20,000 additional jobs losses in related sectors (AFRA, 1993). In 2007-2008, the South African government spent over R285 million (19 million US dollars) on drought relief measures for the agricultural sector, primarily on the purchase and supply of subsidised fodder depending on farms' sizes (Ngaka, 2012). Recent droughts such as the one in 2015-2016 revealed the cascading impacts of the drought. The BFAP (2016) reported that the area of maize planted for the 2016-17 season was 25% lower than the area planted in the 2015-16 season, which was reflected in the year-on-year declines in seasonally adjusted sectoral GDP. In

addition to the direct impact on agriculture, general economic indicators pointed to an aggravated situation (e.g. input providers were hard hit due to the lack of purchasing power in the agricultural sector; given the suppliers' import propensity and the local currency depreciation (BFAP, 2016). Inflationary pressures resulting, inter alia, from drastic increases in food prices drove up interest rates, which had a negative effect on farming enterprises' debt servicing costs and further restricted access to credit in the sector (BFAP, 2016).

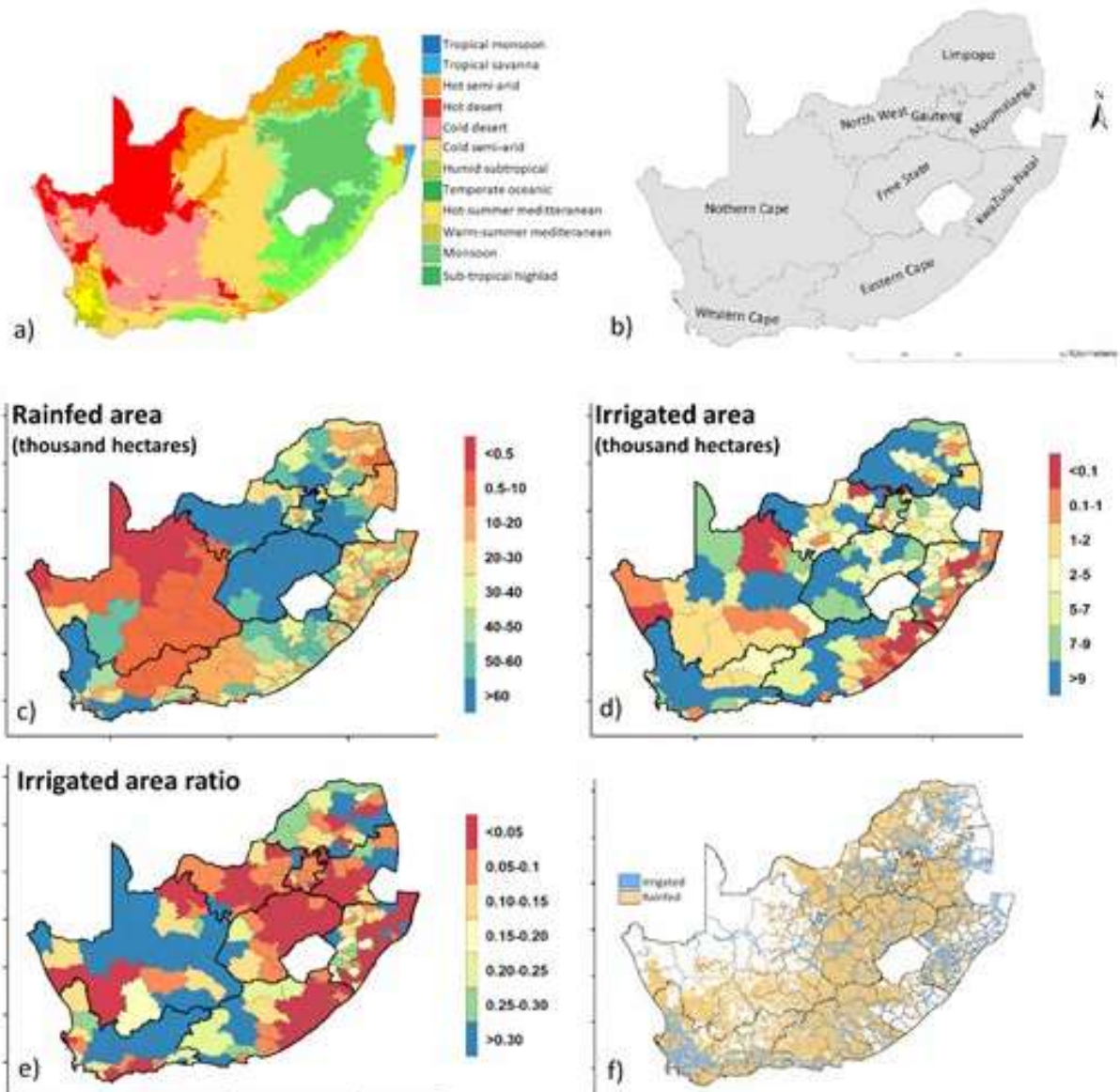


Figure 23. South Africa: a) Köppen-Geiger climate classification map for South Africa (1980-2006) (Beck et al., 2018). b) South African provinces. c) and d) Rainfed and irrigated areas per municipality, respectively. e) Ratio between irrigated and total agricultural area per municipality. f) Irrigated and rainfed agriculture in South Africa at pixel level. Maps are based on data from the national land use/land cover dataset 2018 (Thompson, 2019). (Fig. 1 in Meza et al., 2021)

3.1.1 Drought hazard and exposure

Our results demonstrate a large variability in drought hazard and exposure among provinces and local municipalities. The most extreme drought hazard/exposure for rainfed conditions is observed in the North Cape, North West and Limpopo provinces during the study period (Figure 24). On the other hand, the lowest hazard and exposure in the period 1981-2018 is computed for Kwazulu province (Figure 24). Western and central parts of Eastern Cape and Mpumalanga provinces also have a low level of rainfed drought hazard/exposure (Figure 24). The time series analysis of drought hazard and exposure showed that 1992 and 2016 were the driest years during the study period under rainfed conditions (Figure 25). The year 2000 and 2006 are classified as wettest years across South Africa (Fig. 25). The frequency of dry years for rainfed systems remarkably increased after year 2010 (Meza et al., 2021).

In general, the irrigated systems are less often affected by drought than rainfed systems, with larger areas exposed to drought in Limpopo and Eastern Cape provinces of South Africa (Figure 24). These areas have semi-arid to arid climates and are characterised with less annual precipitation than the rainfed growing areas of the country. For irrigated croplands, larger areas were affected by drought

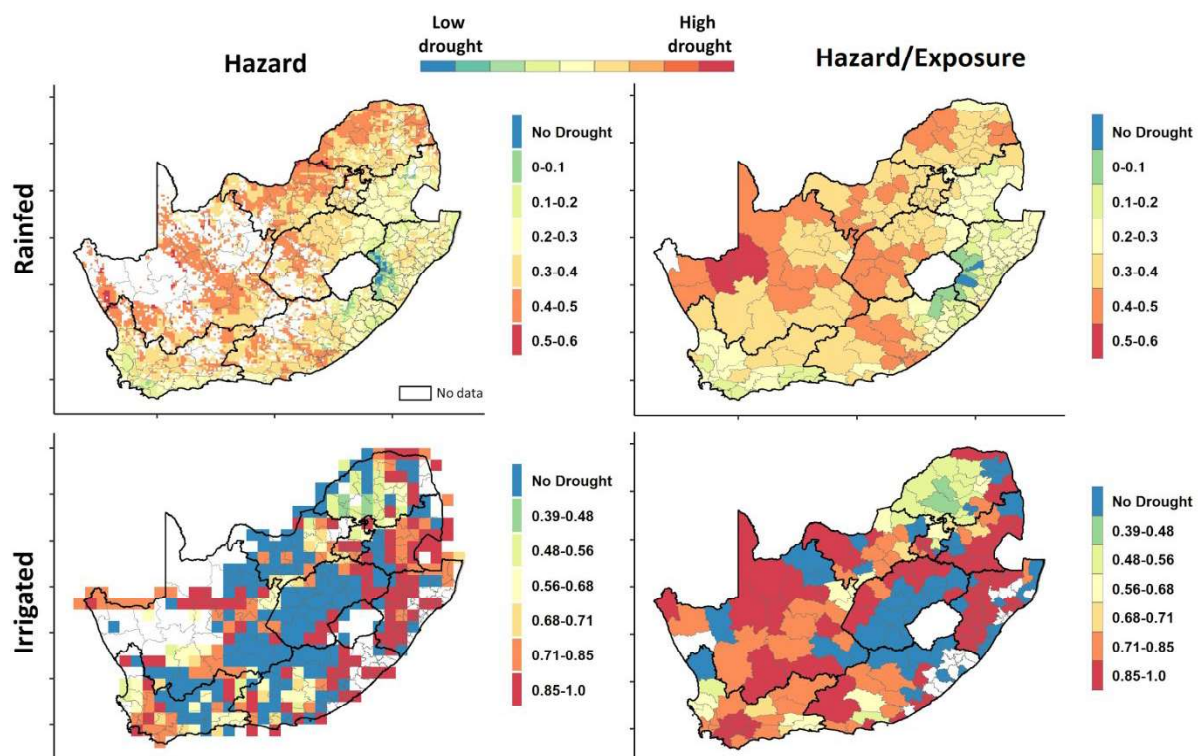


Figure 24. Drought hazard and combined hazard/exposure for rainfed (top row) and irrigated (bottom row) cropping systems across South Africa at grid and local municipality levels in the period 1981-2018. Black lines indicate provincial boundaries (Fig. 3 in Meza et al., 2021)

hazard/exposure since 2012, even in areas that have low share of irrigated croplands, such as north western municipalities in the Northern Cape (Figures 24 and 26). Despite smaller areas of hazard/exposed irrigated land compared to rainfed areas, the impacts can be significant due to the number of affected people. Roughly about 230,000 irrigation farmers were affected, mostly smallholders often with very small plots for self-consumption (FAO, 2016). The highest hazard/exposure was found in years 2015-2016 and the lowest in year 2001 (Figure 26).

The accuracy of simulated hazard/exposure for rainfed agricultural systems was tested by comparing modelling outputs with remotely sensed exposure data in the period 2001-2018 (Figure 27). There was a strong correlation (0.5 to 0.9) between remotely sensed and simulated drought exposure for rainfed conditions for most of the municipalities across South Africa. The lowest correlation (0 to 0.2) was obtained in a limited number of municipalities mainly in KwaZulu-Natal and Eastern Cape provinces, which are largely covered by natural grasslands. The annual drought signal obtained by remote sensing may therefore deviate considerably from the conditions in the cropping period considered in the model.

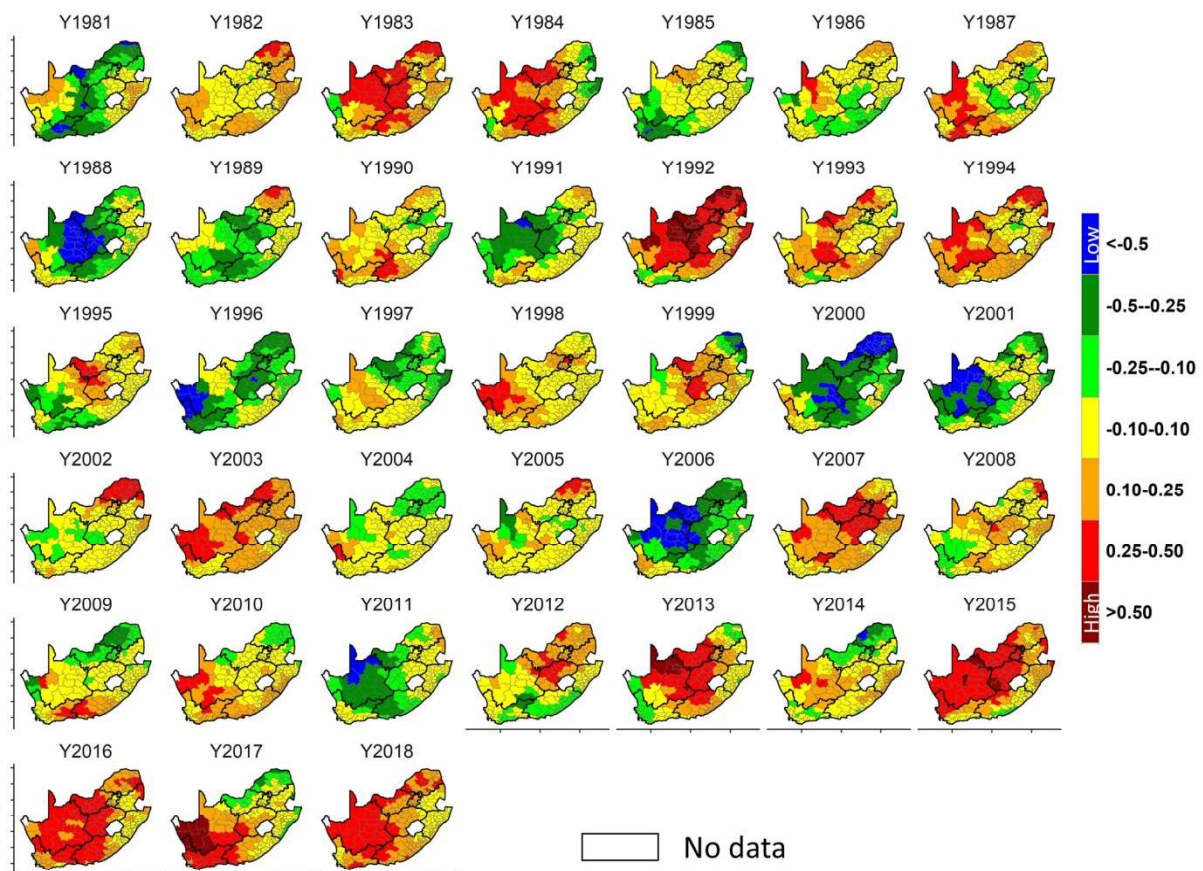


Figure 25. Drought hazard/exposure for rainfed cropping systems across local municipalities of South Africa in the period 1981-2018. Black lines indicate provincial boundaries (Fig. 4 in Meza et al., 2021)

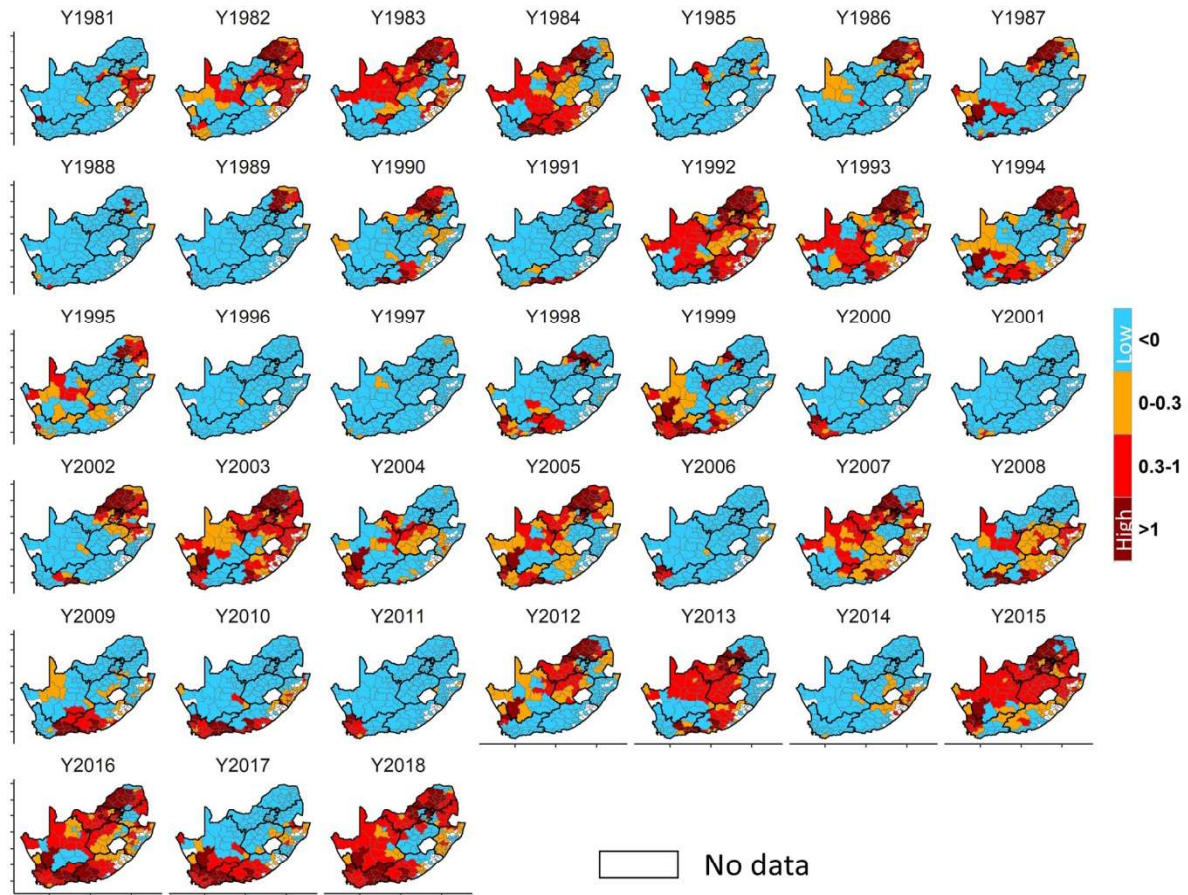


Figure 26. Drought hazard/exposure for the irrigated cropping system across local municipalities of South Africa for the period 1981-2018. Black lines indicate provincial boundaries (Fig. 5 in Meza et al., 2021)

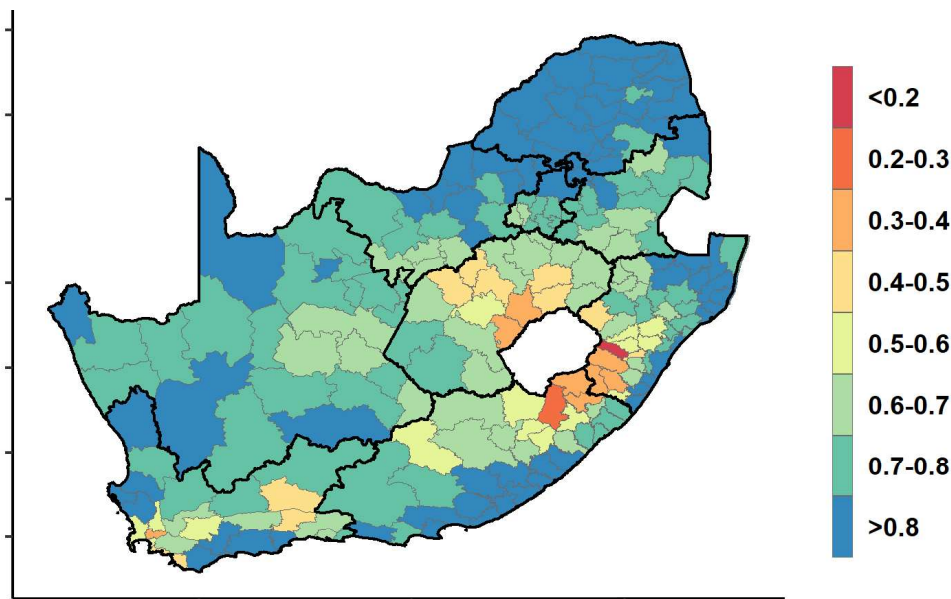


Figure 27. Correlation coefficient between drought exposure of rainfed systems obtained by modeling and remote sensing (Fig. 6 in Meza et al., 2021)

Moreover, we assessed the relationships between annual drought exposure simulated for rainfed systems and yield/production reported at the country scale (FAO, 2021). The correlation coefficient among simulated drought exposure and reported yield and production were -0.32 and -0.41, respectively (Figure 28) which means that drought resulted in lower yields and production. The model reproduced the drought for the years (1992-2015-2016) which showed the largest yield/production reduction. It is important to note that the FAO yield/production data did not distinguish between rainfed and irrigated systems. Therefore we expected even higher correlations when separate data would become available.

Drought hazard for combined (irrigated and rainfed) agriculture was also determined by using remote sensing (Schwarz et al., 2020). Drought hazard was estimated based on a regression model which included the variables albedo, LST, NDII, NDVI

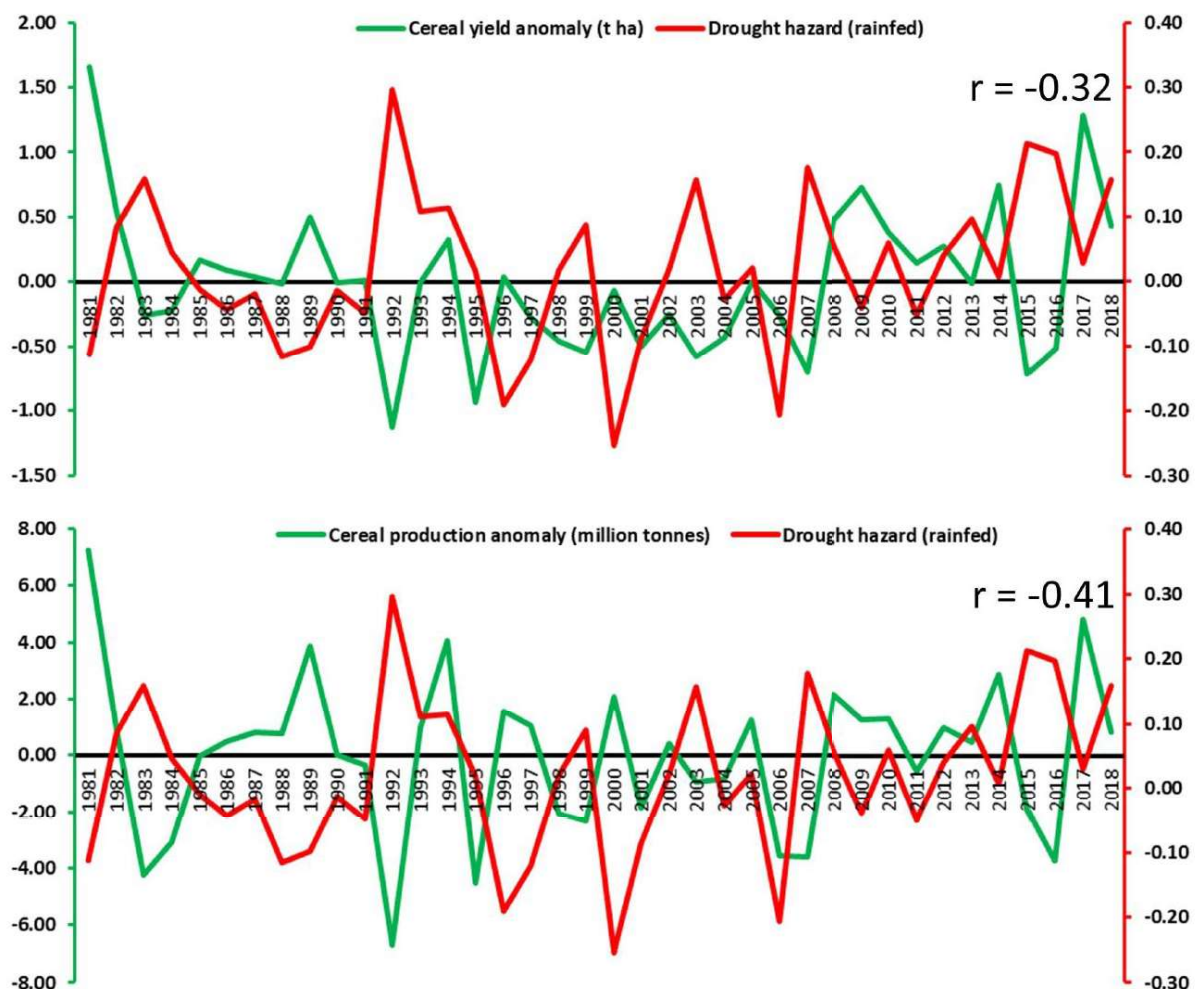


Figure 28. Time series of rainfed drought hazard (positive values indicate drought) and cereal yield and production anomaly in South Africa in the period 1981 to 2018. The r values show the Pearson correlation coefficient (Fig. S6 in Meza et al., 2021)

and SPI3. The high resolution remote sensing based estimate (Figure 29) shows good agreement with the model based estimates (Figures 25, 26) for the relatively wet year 2014 and the dry season 2015-2016.

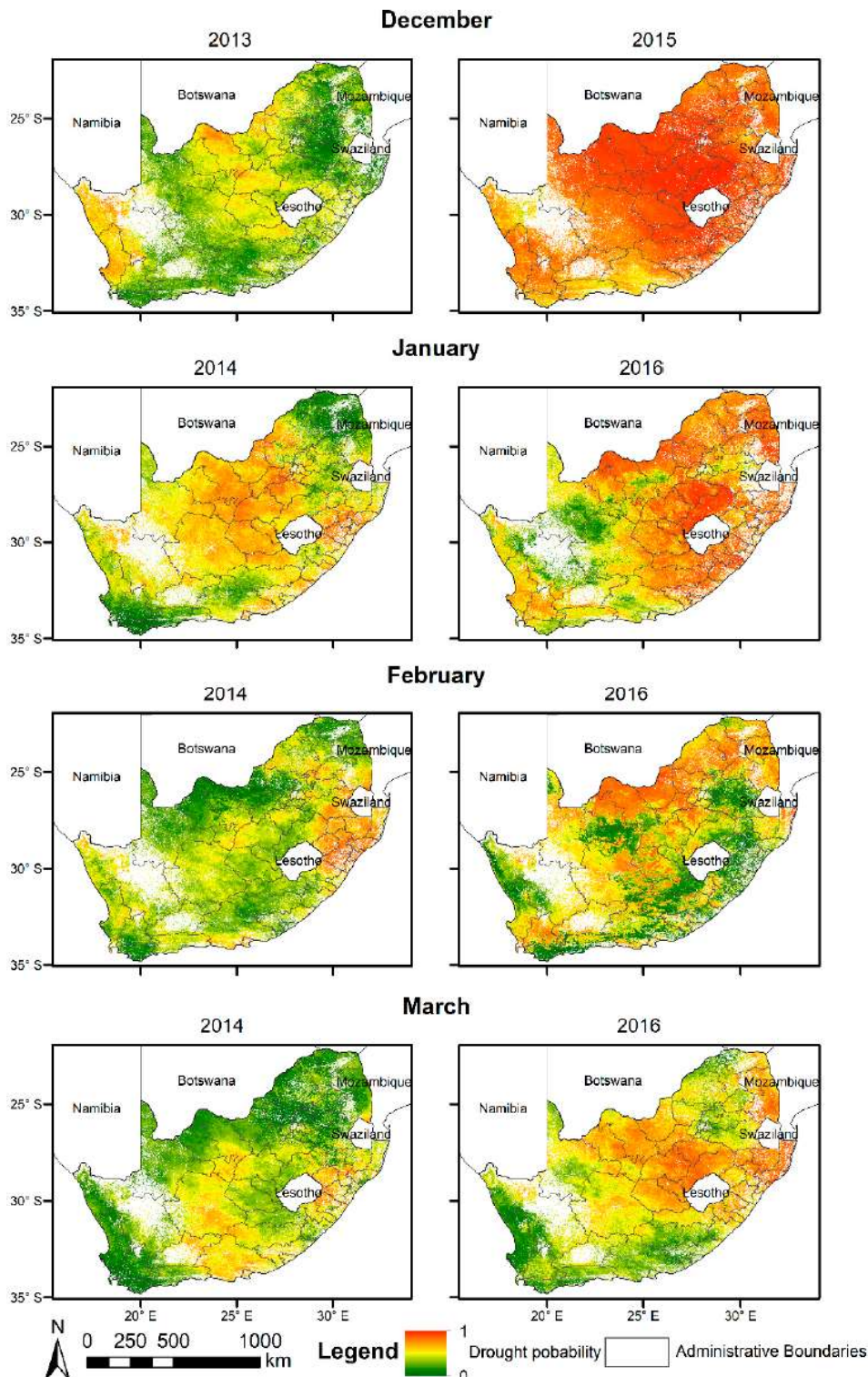


Figure 29. Drought hazard in South Africa for agricultural, grass- and shrubland in the nondrought season 2013/2014 (left) and the drought season 2015/2016 (right, Fig. 3 in Schwarz et al., 2020)

3.1.2 Vulnerability and risk of rainfed and irrigated systems

The vulnerability assessment shows heterogeneity across the country (Figure 30) for both systems. Our assessment highlights that crops under rainfed systems are more vulnerable to drought than irrigated systems.

According to the expert consultations, the most relevant vulnerability indicator for irrigated systems is unemployment rate (%). This is also recognized as a relevant indicator by the scientific community in the South African context as the country suffers from deep structural unemployment having a direct impact on poverty levels (Chibba and Luiz, 2011). Agriculture proved to be the best way to reduce rural poverty according to the rural development literature, besides, in most developing countries, agriculture and agriculture-related activities provide most of the rural employment (Machethe, 2004). Irrigation schemes have had great impact in South Africa, not only in food production but also alleviating poverty. One notable example is the one caused by the Great Depression by resettling of returning soldiers that reduced the unemployment rate in the country (FAO, 2016). Irrigated agriculture employs between 10% and 15% of the total agricultural workforce (DWA, 2002).

The most relevant indicators for rainfed systems according to the experts are: area equipped for irrigation expressed as percentage of total area, and households with an alternative to farm income (%). Access to irrigation infrastructure can help farmers increase their coping capacities to drought since due to rapid climate change, irregular rainfall patterns and water shortages are becoming a common issue (Asadieh and Krakauer, 2017; Trenberth et al., 2014). Irrigation infrastructure systems can allow crops to be uniformly supplied with water according to their needs. Despite the advantages of irrigation systems, in South Africa, the expansion of irrigation systems is limited by water availability (FAO, 2016). Furthermore, irrigation schemes have performed poorly. Poor performance mainly resulted from inefficient and non functioning infrastructure, inappropriate planning and design, insufficiency of training to raise awareness, improper land tenure arrangements, and the lack of both input and output markets (Machethe, 2004; Gidi, 2013; Fanadzo et al., 2010). The ability to irrigate at least parts of the land can stabilize farm income in drought periods and thereby also reduce the vulnerability of the rainfed sector. Low harvests threaten the households that only depend on their farm income (~97%); this could result from a drought period that requires compromising their entire livelihoods. Having an alternative income may increase their coping capacities as they do not depend solely on the agricultural income derived from crop sales (Meza et al., 2021).

The vulnerability maps display high values particularly on irrigated systems for the Western Cape municipalities and for rainfed agricultural systems in KwaZulu-Natal. Our findings underline that determining factors of vulnerability vary depending on the sector which is susceptible to the negative impacts of drought. For instance, the main indicators which shape the vulnerability for irrigated systems and are potential

entry points for the drought risk reduction is the lack of environmental awareness, poor water quality, and low total dam storage capacity. In the South African context this is due to the limited access to extension services (e.g geographically remote farmers tend to have little network coverage), and very limited financial resources to invest in technologies or utilities (Meza et al., 2021). Resulting in a lack of accessible, relevant, and practical information to share, as well as few or no opportunities to expand the irrigation farmers capacities (FAO, 2020b).

For rainfed agricultural systems, the key indicators shaping the socio-environmental susceptibility and the coping capacities of the local municipalities are the small fertilizer application rate, the lack of area equipped for irrigation, and land degradation. This last indicator is relevant for both systems; land degradation is linked to different factors in the context of agricultural systems in South Africa, one of them is the lack of environmental awareness led to unsustainable farming practices (Rotheret al., 2008; Schulze, 2016).

The drought risk assessment highlights its context-specificity and how different communities of a country experience different levels of risk. Drought risk varies substantially for rainfed and irrigated systems (Figure 30). There is a high-risk

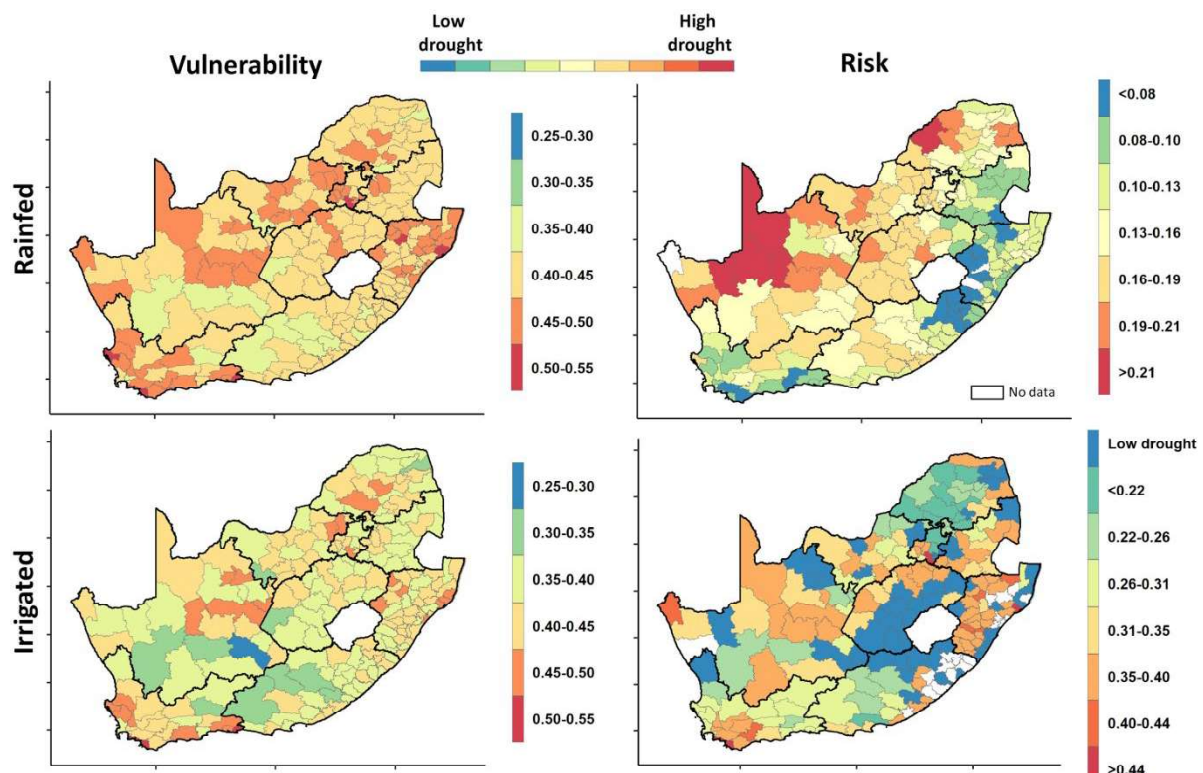


Figure 30. Drought vulnerability and risk in South Africa at local municipality level for rainfed (top row) and irrigated agriculture (bottom row). Tendency to dark blue shows lower levels of vulnerability and risk, the tendency to red shows higher vulnerability or risk values. Black lines indicate provincial boundaries (Fig. 7 in Meza et al., 2021)

pattern towards the North provinces for rainfed agricultural systems. Meanwhile, high-risk hotspots for irrigated agricultural systems can be found in some local municipalities of KwaZulu-Natal (e.g. uMhlathuze, Endumeni local municipalities), Western Cape (e.g. Overstrand, Swellendam) and Gauteng (e.g. Midvaal) provinces (Meza et al., 2021).

When analysing the risk for rainfed systems, among the local municipalities in the Northern Cape, Emthanjeni has the lowest risk score than other provinces despite its high hazard and exposure levels; it is explained by a lower social susceptibility (e.g. overall quality of water services, less population have experienced crime and theft of livestock), and higher coping capacities (e.g. access to credits). In contrast, the local municipality of Raymond Mhlaba in the Eastern Cape has lower vulnerability than other provinces, but its high hazard and exposure scores result in a high risk.

In order to identify priority areas for disaster risk management, the risk assessment of each agricultural system was plotted against the crop dependent population in each local municipality (Figure 31). The comparison shows that the local municipalities with higher irrigated and rainfed systems are not among the highest in terms of crop dependent population. The city of Johannesburg presents a higher crop dependency, but also has high risk for both systems. Its drought hazard and exposure are high, and the vulnerability analysis reveals that their lack of environmental awareness, fertilization rate and land degradation are key factors contributing to their overall very high risk; highlighting the relevance to take actions in this municipality. Johannesburg, the largest city in South Africa, is facing enormous challenges which reflect on the drought vulnerability level. Challenges like urbanisation's impact on the soil and water quality and availability, and facing non-sustainable growth paths (SACN, 2016) have significant impacts on the magnitude of Johannesburg's vulnerability toward drought.

In contrast, the city of Tshwane has a high number of crop dependent population, but it presents a medium rainfed risk and very low irrigated risk. Its medium risk is explained by its medium-low vulnerability as a result of better performance in nutrition level, good water quality and road density, among others.

The Northern-Cape province has the lowest population dependent on crops. However, it is one of the provinces with more local municipalities on high rainfed risk, as this province has arid climate which exposes rainfed crops to high drought hazard. In contrast, the KwaZulu-Natal province has a higher amount of population dependent on crops, but more local municipalities are at high risk for irrigated systems (Meza et al., 2021).

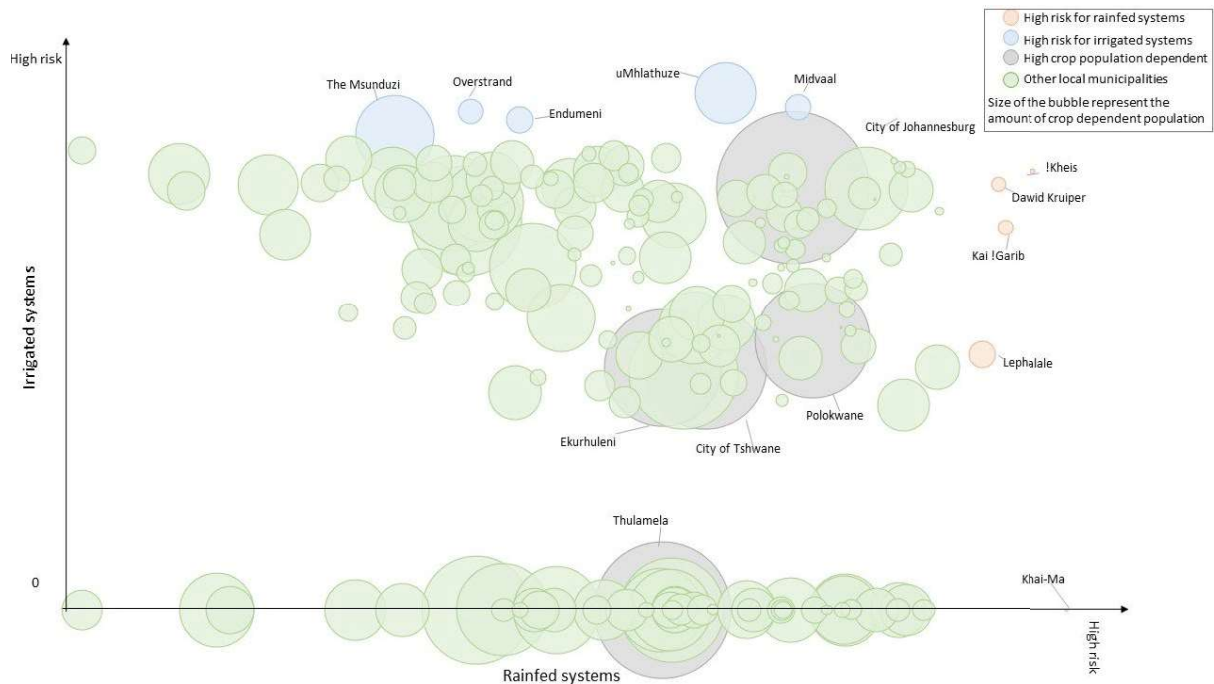


Figure 31. Local municipalities contrasted with drought risk for rainfed (x axis) and irrigated (y axis) systems. The size of the bubbles represent the amount of crop dependent population by local municipality (Fig. 8 in Meza et al., 2021)

3.2 Zimbabwe

Zimbabwe is among the countries in southern Africa that are heavily affected by droughts (Figures 20-22). Agriculture accounts for approximately 12% of the country's Gross Domestic Product (GDP) (World Bank, 2020). About 70% of the population directly depends on agricultural outputs (UN Zimbabwe, 2020), and more than 60% conducts rainfed subsistence and semisubsistence agriculture (Makaudze and Miranda, 2010). Since recent information on the extent of irrigated and rainfed cropland has not been available for Zimbabwe, an assessment based on optimizing harmonic functions fitted to cloudcorrected Landsat NDVI time-series was performed for period 2013-2018 by the GlobeDrought project (Landmann et al., 2019). The result of the assessment shows that rainfed cropland is found scattered across the whole country while irrigated agriculture is concentrated in the North and the Southeast of the country (Figure 32). The dataset classifying irrigated and rainfed cropland, was then used in subsequent drought risk studies for Zimbabwe (Frischen et al., 2020; Schwarz et al., 2020). These drought risk studies mainly used remote sensing to detect drought hazard but additional socio-economic information to specify vulnerability and risk. In Frischen et al. (2020) a comprehensive vulnerability assessment was performed which included 32 indicators identified by an extensive literature review.

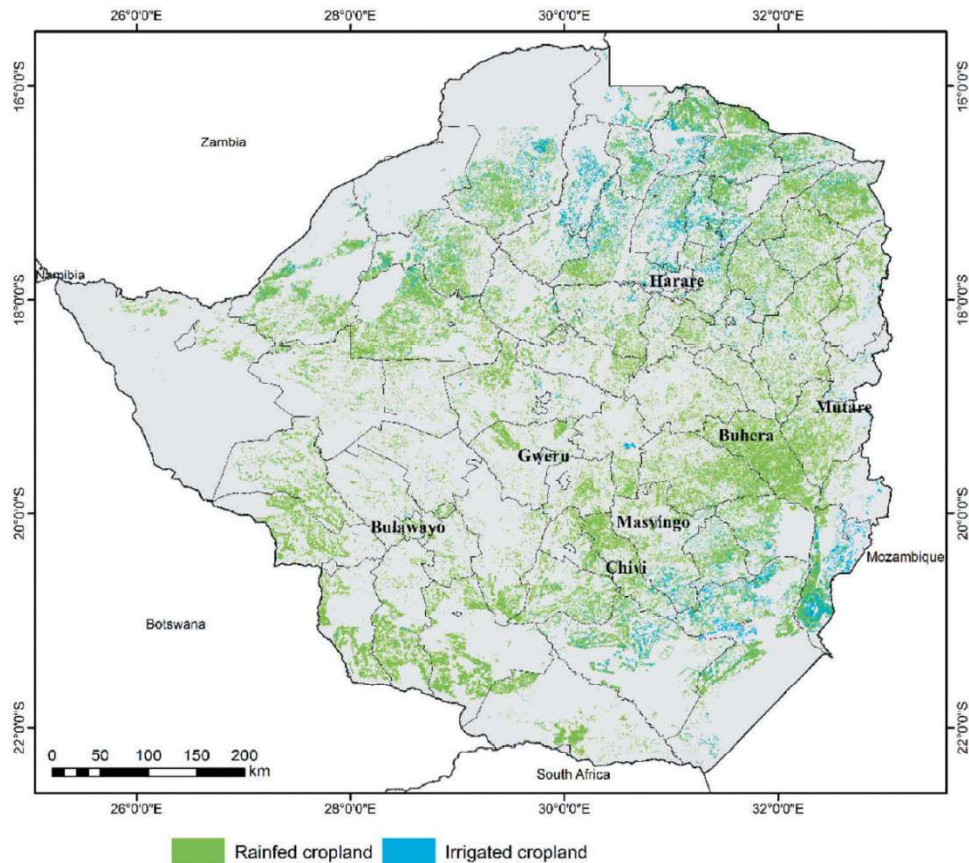


Figure 32. Farming systems map for Zimbabwe showing irrigated and rainfed cropland in period 2013-2018 (Fig. 4 in Landmann et al., 2019)

3.2.1 Drought hazard and exposure

The seasons 1991-1992, 1994-1995, 2002-2003 and 2015-2016 were identified as periods with extreme drought hazard (Frischen et al., 2020; Figure 33). The five districts with the highest average number of drought events were Beitbridge (7.05 droughts in 30 years), Hwange (6.91), Bulilima (6.90), Buhera (6.84), and Tsholotsho (6.70). The five districts with the lowest average of drought events were Mutasa (1.99), Zaka (2.36), Morondera (2.69), Wedza (2.74), and Nyanga (2.89) (Figure 34). At provincial level, Matabeleland South and Matabeleland North indicated the highest average of drought events, followed by the Midlands Province, Mashonaland West, Mashonaland Central, and Manicaland. Masvingo and Mashonaland East have the lowest average of drought events (Frischen et al., 2020). The high drought hazard in season 2015-2016 and the low hazard in season 2013-2014 was confirmed in the drought assessment performed for Zimbabwe based on albedo, LST, NDII, NDVI and SPI3 (Schwarz et al., 2020; Figure 35).

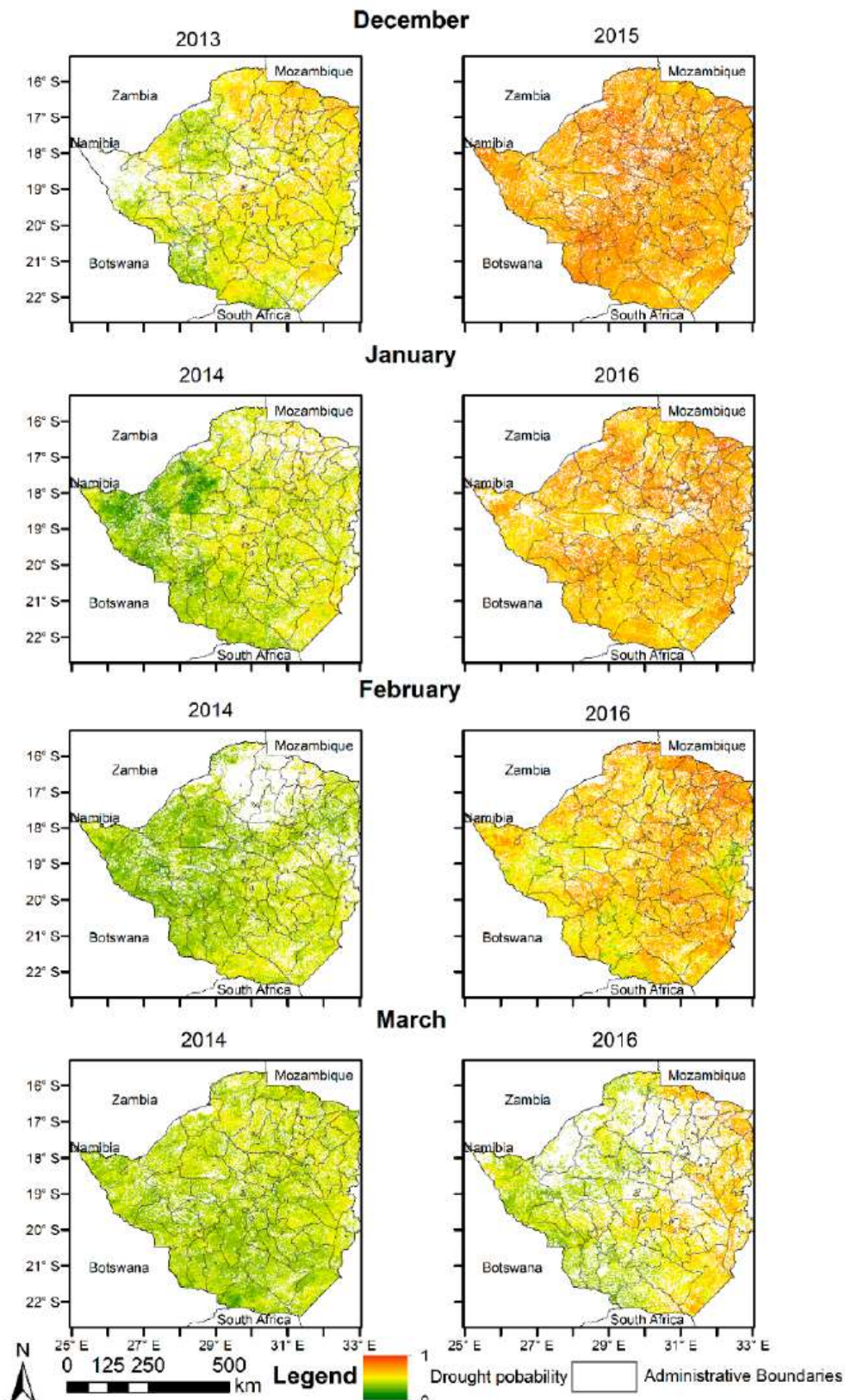


Figure 35. Drought hazard in Zimbabwe for agricultural, grass- and shrubland in the nondrought year 2013/2014 (left) and the drought year 2015/2016 (right; Fig. 4 in Schwarz et al., 2020)

3.2.2. Drought vulnerability and drought risk

A very detailed and comprehensive drought vulnerability assessment based on 32 different indicators derived from the literature was performed for Zimbabwe (Frischen et al., 2020). The result shows a diverse vulnerability pattern at district level but a consistent gradient from high vulnerability in the Southwest to low vulnerability in the Northeast at province level (Figure 36). Low vulnerability was particularly observed in Manicaland, which also performs comparably well in all social indicators. Contrastingly, provinces with high vulnerability scores are Matabeleland South, Matabeleland North, and Masvingo (Figure 36). These provinces are characterized by remoteness, with a bad state of public infrastructure including transportation, electricity, and sanitation and health facilities. The provinces additionally indicate a high state of land degradation and limited natural vegetation cover, given the low annual rainfalls (Frischen et al., 2020).

An index for drought risk in irrigated and rainfed agriculture was then derived by multiplying, at pixel level, the indices for hazard/exposure by vulnerability (Figure 37). The highest drought risk for irrigated systems agricultural systems is observed in Chipinge, whereas a high drought risk to rainfed agriculture occurs in multiple

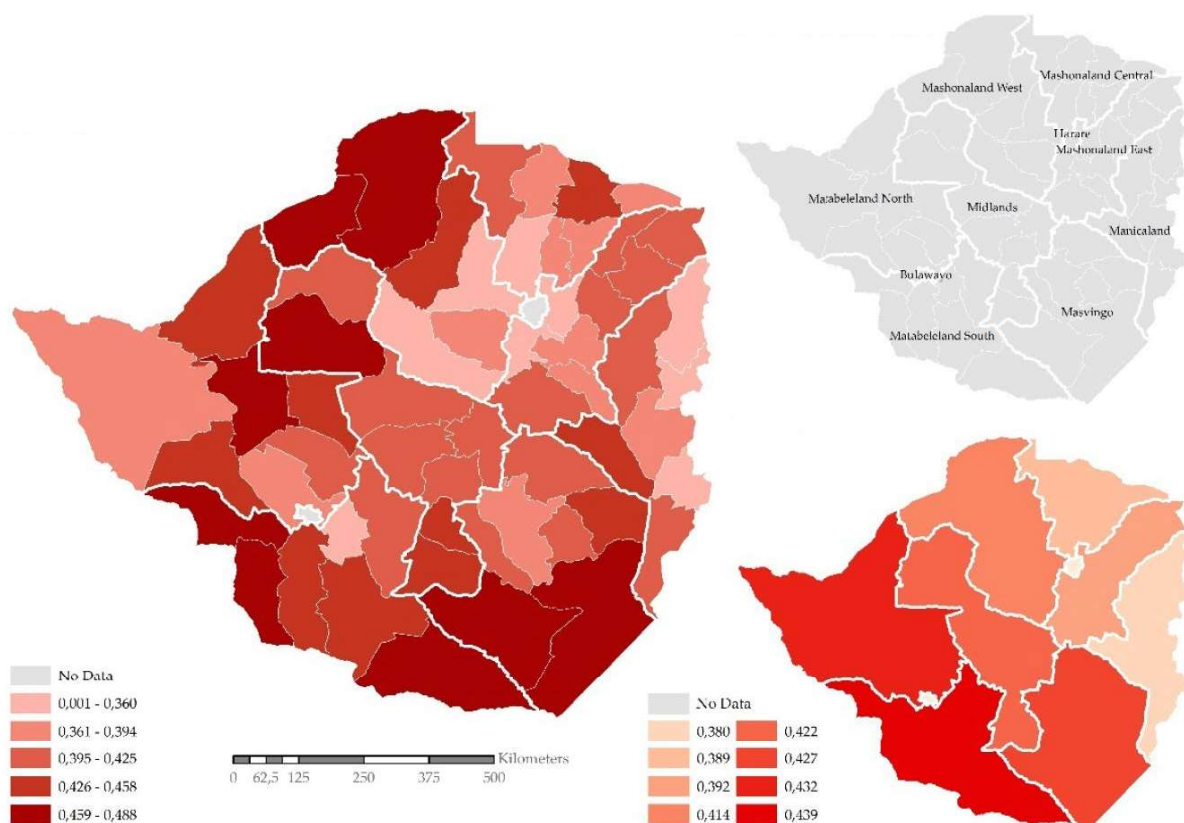


Figure 36. Vulnerability of agricultural systems in Zimbabwe to drought per district (left) and province (right, bottom). Province boundaries and province names are shown in the map top right (Fig. 6 in Frischen et al., 2020)

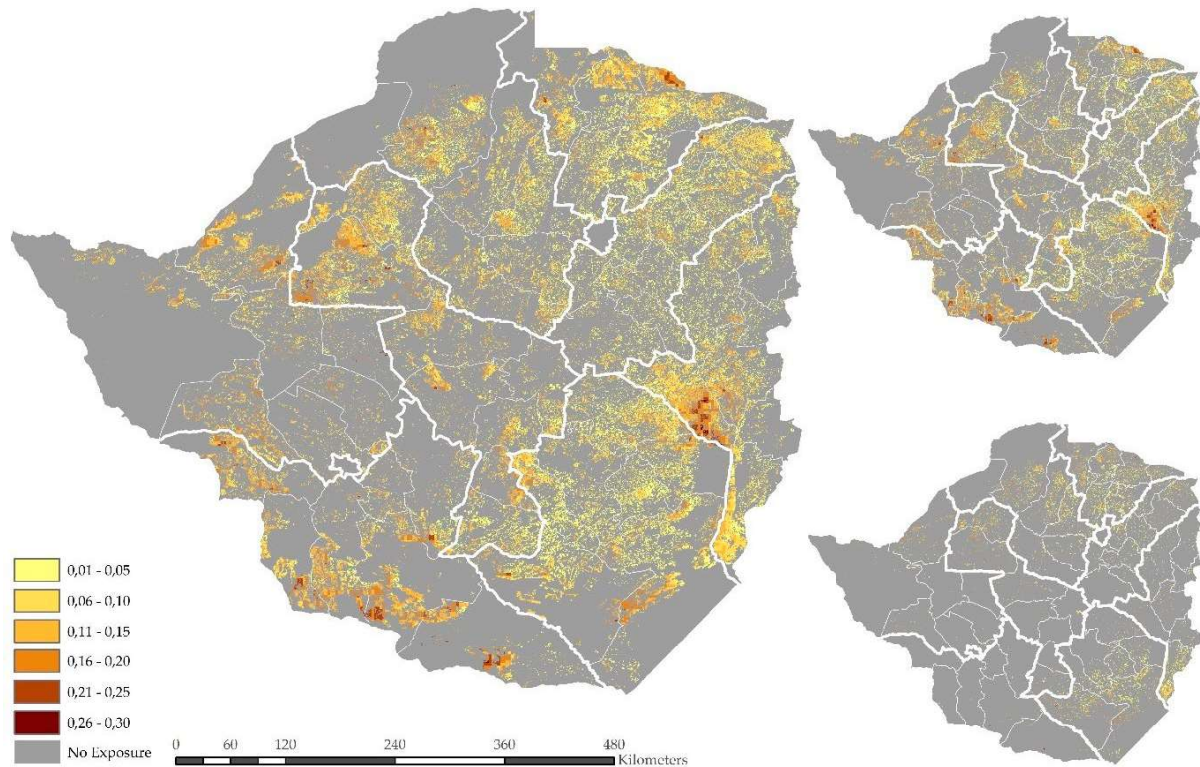


Figure 37. Drought risk of agricultural systems in Zimbabwe (left) and separation into drought risk for rainfed agriculture (top right) and irrigated agriculture (bottom right; Fig. 7 in Frischen et al., 2020)

districts, including Buhera (Manicaland), Mount Darwin (Mashonaland Central), Gokwe South (Midlands), Beitbridge, Gwanda, Matobo, and Mangwe (Matabeleland South). Mashonaland East and Manicaland are generally less at risk to severe and extreme drought. Beitbridge and Bulilima indicate the highest risk of severe droughts. Mangwe, Matobo, Gwanda, Mwenezi, and Chiredzi show the highest risk to extreme drought (Frischen et al., 2020).

The drought assessment performed by Schwarz et al. (2020) for the seasons 2013-2014 and 2015-2016 detects a bit different spatial patterns of drought risk with high risk in the Northeast and low risk in the Southwest of Zimbabwe (Figure 38). Reasons for the differences are the specific drought hazard pattern in season 2015-2016 (see also Figures 33 and 35) and the different results of the vulnerability assessment (Figures 36 and 38). Instead of 32 vulnerability indicators considered by Frischen et al. (2020), the study undertaken for seasons 2013-2016 used only four vulnerability indicators, namely population density, GDP, livestock density and irrigation (Figure 9). This shows that a careful selection of indicators is essential to identify reasonable spatial patterns in drought vulnerability.

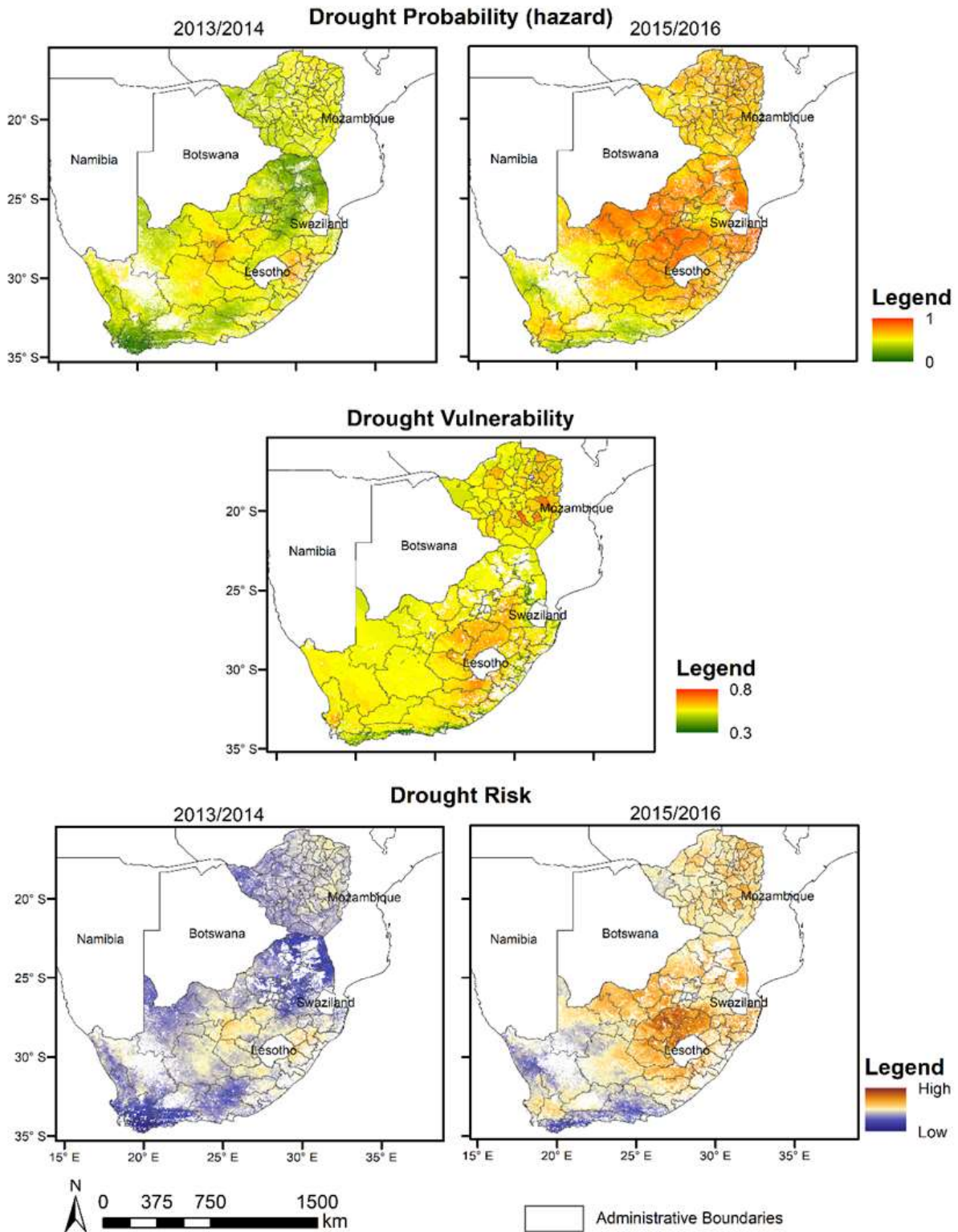


Figure 38. Spatial explicit drought hazard, vulnerability and risk for South Africa and Zimbabwe (exemplary) for the growing seasons December to March 2013/14 (non-drought period) and 2015/16 (drought period), respectively (Fig. 6 in Schwarz et al., 2020)

4 Experimental early warning and forecasting

To expand the GlobeDrought information system by an early warning component, several modifications had to be made to the models used in GlobeDrought to provide real time estimates and seasonal forecasts of drought hazard. Most importantly, the climate input data for the models used before only covered the period until year 2016 and could therefore not be used for simulations of the near realtime drought hazard. In the first phase of the project GCWM was forced with CRU-TS 3.25 climate input (Harris et al., 2014) while WaterGAP used WFDEI-GPCC (Weedon et al., 2014). The global assessment of historical drought hazard (Meza et al., 2020) was performed with this climate input. These climate input data have been replaced by ERA5 global reanalysis data (Hersbach et al., 2020) in both models. The data become updated frequently and allow therefore simulations in almost real time. A workflow was developed to download the variables required by the two models and to aggregate the data from hourly to daily time steps. Consequently, the models had to be adjusted to work with climate data at native daily time steps. Some assessments performed in the second phase of the project (e.g. Meza et al., 2021) have already been based on this new climate input and on the improved model versions.

To enable seasonal forecast simulations of drought hazard, a workflow was developed in collaboration with the GRoW SaWaM project (KIT RKH Garmisch, Prof. Kunstmann) to analyze drought hazard simulated with global bias-corrected seasonal climate forecasts. The data provided by KIT RKH consisted of forecasts spanning 7 months with daily time steps and included data for 51 ensemble members. These data were used to simulate actual and potential evapotranspiration of rainfed crops (GCWM), irrigation water requirement of irrigated crops (GCWM) and streamflow (WaterGAP) for each of the ensemble members. Then the drought hazard indicators for rainfed and irrigated agricultural systems (Meza et al., 2021) were calculated. To demonstrate the workflow and to evaluate the results, simulations were performed by using ensemble forecasts released beginning of March 2018 (covering the period March 2018 – September 2018) and beginning of May 2018 (covering the period May 2018 – November 2018). Then the results were compared to model runs performed with the standard ERA5 reanalysis product for year 2018, which was considered as the reference. In addition, the results of the ensemble forecasts were compared to simulations based on the climatology. Here, the models used the standard ERA5 climate input until the begin of the forecast period (01 March 2018 or 01 May 2018) and switched then to climate input from a historical year. The 30-year historical period 1986-2015 has been used as input for the model simulations based on the climatology, resulting in 30 ensemble members for the climatology runs.

According to the simulations with the standard ERA5 data for year 2018 high drought hazard for rainfed crop production was detected for Western Europe, Central Europe, Eastern Europe, Southern Russia, Southern Canada, Australia and Argentina while very low hazard was observed for Southern Europe and the Eastern

part of the USA (Appendix A1). For irrigated crop production systems, high drought hazard was detected for Southwestern USA, Northeast Brazil, Southern China, the Middle East region, Australia and Argentina while in particular low hazard was calculated for Eastern USA, Europe, India, Southeast Asia and Western Africa (Appendix A1). The results of the model runs with ensemble forecasts (ENS) was therefore compared to the results with the climatology (HIS) and the model run with

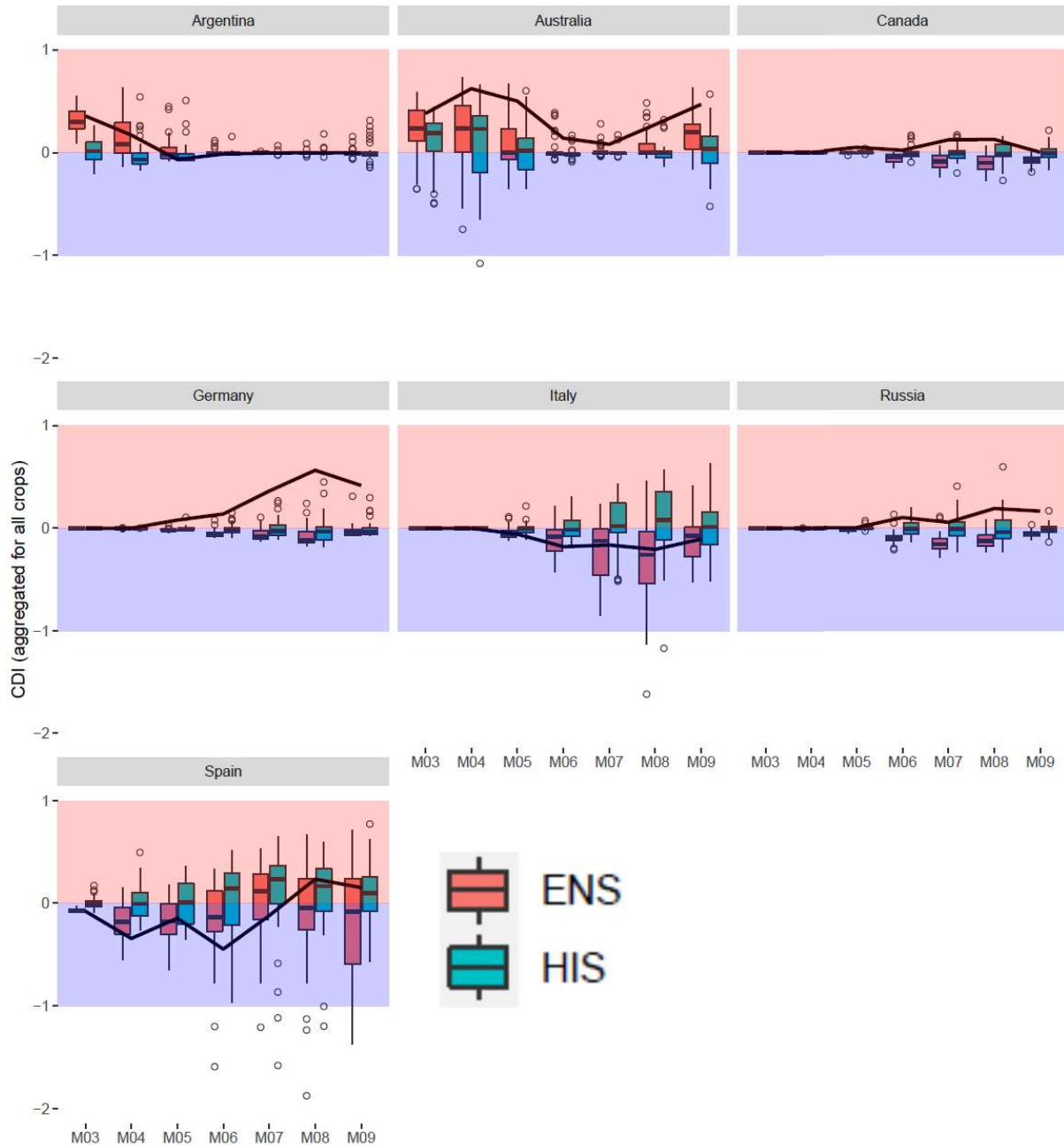


Figure 39. Comparison of the drought hazard indicator for rainfed crops simulated with ensemble climate forecasts (ENS) and historical climate in period 1986-2015 (HIS) for the forecast period March 2018 – September 2018 with results obtained from the standard model run with ERA5 data for 2018 (black bold line) for selected countries

standard ERA5 data for 2018 for selected countries affected by drought (Argentina, Australia, Canada, Germany, Russia) and for countries with relatively wet conditions in year 2018 (Italy, Spain).

The results of the comparison show that the model simulations using the bias corrected ensemble forecasts reproduced the reference hazard better than the model runs with the climatology for Argentina, Australia, Italy and Spain. In contrast, the forecasts could not reproduce the severe drought in Germany in both cases, model runs with ensemble forecasts and model runs with climatology (Figures 39, 40). The results show clearly that bias corrected seasonal ensemble forecasts have a huge potential to improve seasonal drought forecasts of soil moisture and streamflow and related drought hazard indicators. However, more research is needed to evaluate this potential more systematically across time periods, regions, drought indicators and the forecast length and to improve the efficiency of the forecasting system to reduce processing time before such systems maybe used in operational mode.

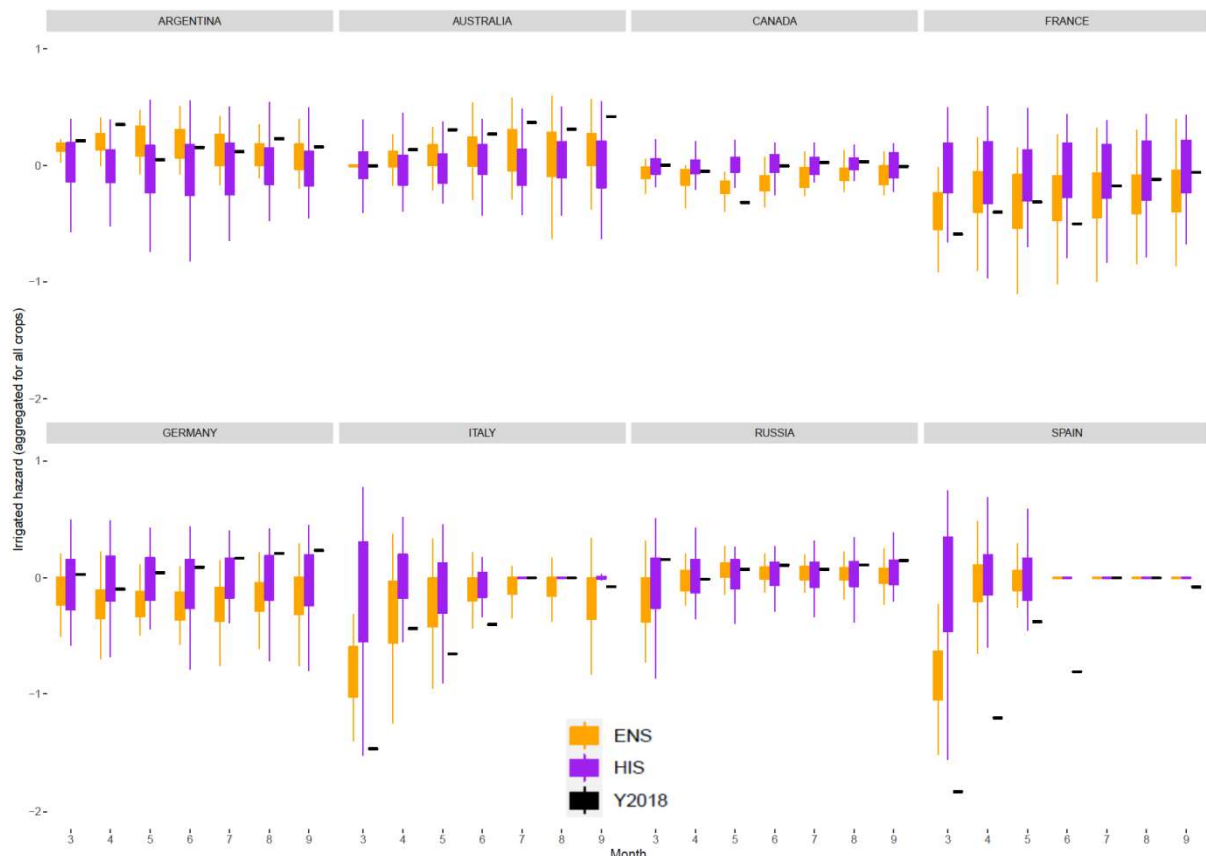


Figure 40. Comparison of the drought hazard indicator for irrigated crops simulated with ensemble climate forecasts (ENS) and historical climate in period 1986-2015 (HIS) for the forecast period March 2018 – September 2018 with results obtained from the standard model runs with ERA5 data for 2018 (black bold line) for selected countries

5 Dissemination of results and knowledge to the general public

5.1 Development of the Integrated Drought Tool

To visualize the datasets for drought hazard, vulnerability and risk created in the project GlobeDrought developed the [Integrated Drought Tool](#) (Figure 41). The portal provides access to more than 26 geospatial data sets and can be used for visualization and displaying statistics. Users can select the scale of the drought assessment (global, South Africa, Zimbabwe) and the sector affected by drought (irrigated agriculture, rainfed agriculture, water supply). According to the selections made by the users, corresponding indicators for drought hazard, exposure, vulnerability, risk or impact are displayed and can be selected. For each of the indicators available in the drought information system, metadata explaining data sources and methods used to compute the indicators can be displayed (Figure 41).

The portal was introduced to various stakeholders, specifically in Zimbabwe, in order to validate products and get feedback to its usability. One main outreach and stakeholder activity was the stakeholder workshop in Zimbabwe, which was facilitated online (Figure 42). The survey results from this workshop showed that the portal is considered to be utmostly useful for a number of use cases in the region, foremostly food security mitigation measures and to support finance-based forecasting. Future commercialization opportunities were assessed through discussions with insurance companies (e.g. Hagelschaden), German Helmholtz Research Centers (GFZ and UFZ) and numerous agri-business conglomerates in Brazil (sugar cane and palm oil processing companies).

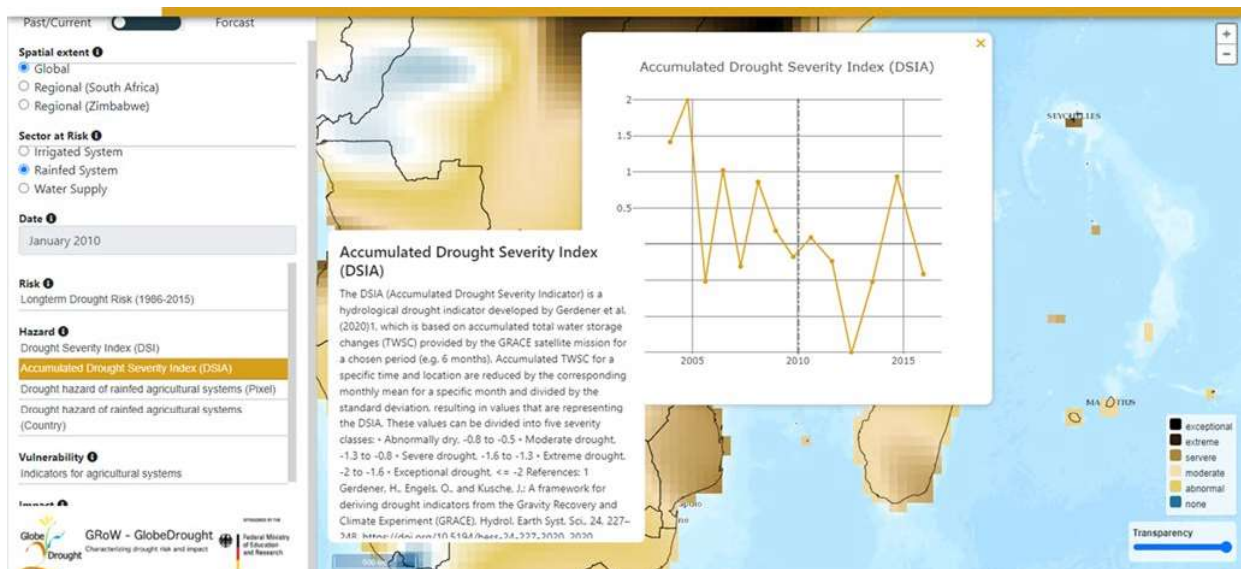


Figure 41. The portal interface showing the indicator Accumulated Drought Severity, which is a hazard indicator which can be seen from the left panel. The panel furthermore shows that its data set is a 'Global' data set and relevant for rainfed agriculture

It is anticipated to develop a commercially viable integrated drought service for an array of customers in the future. In the Zimbabwe stakeholder workshop, the usefulness of the portal for decision makers was assessed and the result (Figure 43) clearly illustrates an above average rating for all three criteria.

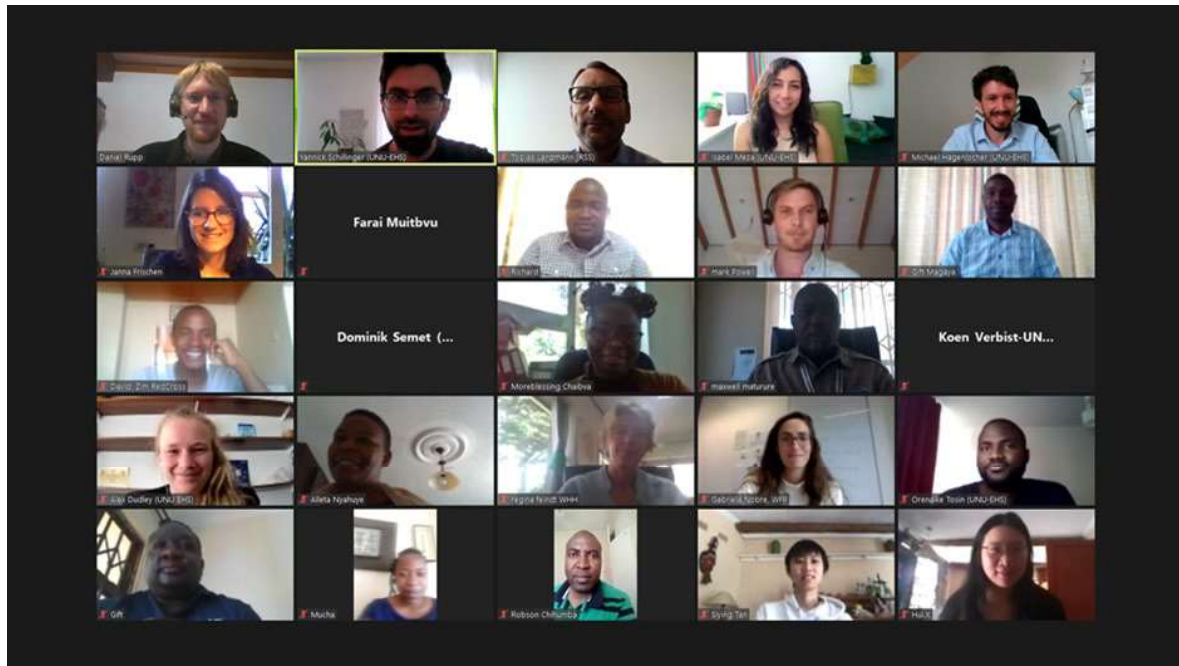


Figure 42. Participants overview of the online Zimbabwe stakeholder meeting, facilitated in September 2020

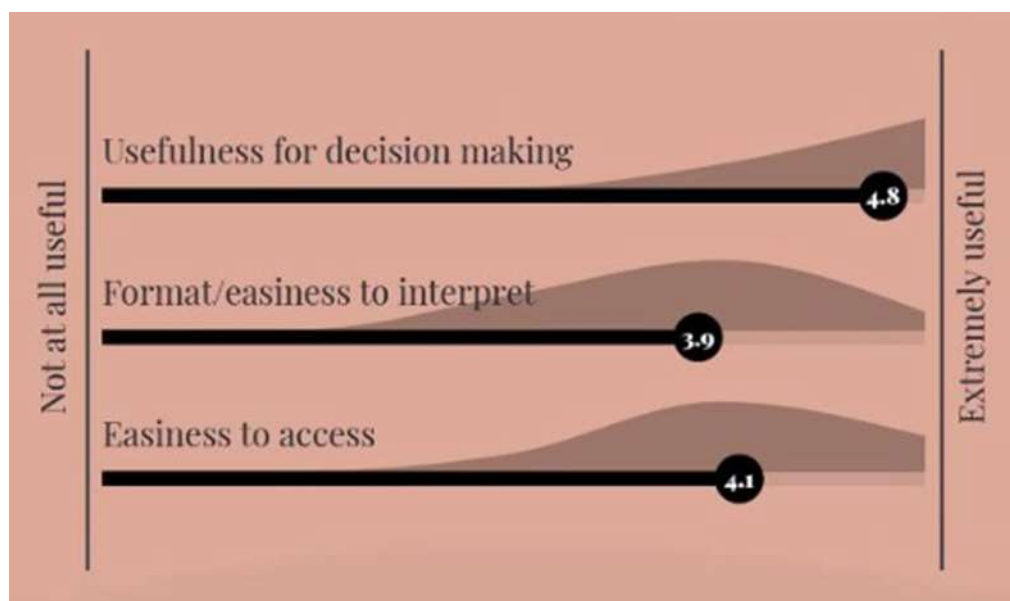






Figure 43. Stakeholders’ survey results on the usefulness of the Globe Drought portal that was developed in this sub project. The criteria ‘usefulness for decision makers’ attained the highest score (4.8)

5.2 Knowledge dissemination by webinars and electronic lectures

The [GlobeDrought Learning Platform](#) (Figure 44) was set up and deployed in 2018 with capabilities to manage learners, course content, discussions, assessment, and certification. It was later configured with learning blocks according to the developed learning strategy. By the end of the project, over 600 people had signed up to the platform. The Learning Platform provides access to online courses (Table 2) and to webinars developed and recorded during the project time. All webinars were announced on the website and through the newsletter. They were integrated in the learning platform together with the lecture videos and discussion forums on each of the topics. In total, 11 webinars were hosted, featuring experts from all of the project partners as well as strategic co-hosts from Oxford University Environmental Change Institute, CGIAR, Save Somali Women & Children, GFZ German Research Centre for Geosciences, University of Freiburg, FAO, UNCCD, and WMO. In aggregate, these webinars were attended by over 300 participants. Recordings of the webinars were made available on the Learning Platform where they were viewed over 800 times. All project partners contributed to the webinars and electronic lectures.

Table 2. Online courses provided by the GLOBEDROUGHT Learning Platform

	1) GLOBEDROUGHT Course		2) GLOBEDROUGHT – Characterizing and assessing drought risk and drought impacts at the global and regional level
	3) Drought impacts I: Migration		4) Drought impacts II: Gender / women
	5) Drought hazards I: Meteorological droughts		6) Drought hazards II: Hydrological droughts
	7) Innovation: Total water storage change analysis from GRACE and hydrological modeling		8) Detecting drought and vegetation health with remote sensing
	9) Understanding and assessing risk of drought impacts		10) Drought impacts III: Agricultural systems
	11) Drought impacts IV: Food Security		12) Droughts and the post-2015 agenda

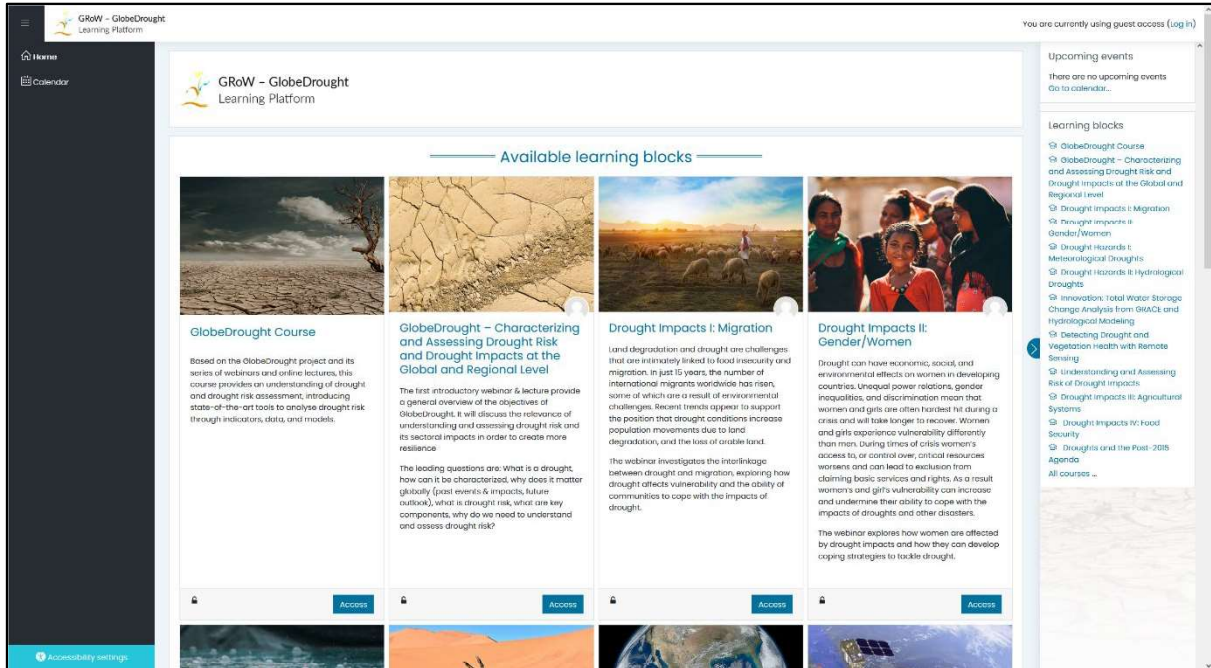


Figure 44. Landing page of the GlobeDrought Learning Platform

References

- AFRA (Association for Rural Advancement) (1993). Drought relief and rural communities. Special Rep. No. 9. Pietermaritzburg, South Africa.
- Asadieh, B. and Krakauer, N.Y. (2017). Global change in streamflow extremes under climate change over the 21st century. *Hydrol. Earth Syst. Sci.* 21, 5863–5874.
- Barker, L. J., Hannaford, J., Parry, S., Smith, K. A., Tanguy, M., Prudhomme, C. (2019). Historic hydrological droughts 1891–2015: systematic characterisation for a diverse set of catchments across the UK, *Hydrol. Earth Syst. Sci.* 23, 4583–4602.
- Beccari, B. (2016). A Comparative Analysis of Disaster Risk, Vulnerability and Resilience Composite Indicators. *PLoS Curr.* 8, doi: 10.1371/currents.dis.453df025e34b682e9737f95070f9b970.
- Beck, H.E., Zimmermann, N.E., McVicar, T.R., Vergopolan, N., Berg, A., Wood, E.F. (2018). Present and future Köppen-Geiger climate classification maps at 1-km resolution. *Scientific Data* 5, 180214.
- BFAP (Bureau for Food and Agricultural Policy) (2016). Policy brief on 2015/2016 drought. http://www.nstf.org.za/wp-content/uploads/2016/06/Agri-SA-Drought-Report_CS4.pdf (accessed 23.11.2020).
- Bithell, M. and Brasington, J. (2009). Coupling agent-based models of subsistence farming with individual-based forest models and dynamic models of water distribution. *Environmental Modelling & Software* 24, 173–190.
- Boegh, E., Thorsen, M., Butts, M.B, Hansen, S., Christiansen, J.S, Abrahamsen, P. et al. (2004). Incorporating remote sensing data in physically based distributed agro-hydrological modelling. *Journal of Hydrology* 287, 279–299.
- BoM (2018). What is drought? <http://www.bom.gov.au/climate/drought/> (accessed 23.06.2020).
- Cammalleri, C., Micale, F., Vogt, J. (2016). A novel soil moisture-based drought severity index (DSI) combining water deficit magnitude and frequency. *Hydrol. Process.* 30, 289–301.
- Cammalleri, C., Vogt, J., Salamon, P. (2017). Development of an operational low-flow index for hydrological drought monitoring over Europe. *Hydrological Sciences Journal* 62, 346-358.
- Carrão, H., Naumann, G., Barbosa, P. (2016). Mapping global patterns of drought risk: An empirical framework based on sub-national estimates of hazard, exposure and vulnerability. *Global Environmental Change* 39, 108–124.
- Chibba, M. and Luiz, J.M. (2011). Poverty, Inequality and Unemployment in South Africa: Context, Issues and the Way Forward: POVERTY, INEQUALITY AND UNEMPLOYMENT IN SOUTH AFRICA. *Economic Papers: A journal of applied economics and policy* 30, 307–315. <https://doi.org/10.1111/j.1759-3441.2011.00129.x>
- DAFF (2018). Abstract of agricultural statistics. South African Department of Agriculture, Forestry and Fisheries. <http://www.daff.gov.za/Daffweb3/Portals/0/Statistics%20and%20Economic%20Analysis/Statistical%20Information/Abstract%202018.pdf> (Accessed 10.07.2020).
- DAFF (2019). Abstract of agricultural statistics. South African Department of Agriculture, Forestry and Fisheries. <https://www.dalrrd.gov.za/Portals/0/Statistics%20and%20Economic%20Analysis/Statistical%20Information/Abstract%202019.pdf> (Accessed 05.01.2021).
- de Sherbinin, A., Bukvic, A., Rohat, G., Gall, M., McCusker, B., Preston, B., Apotsos, A., Fish, C., Kienberger, S., Muhonda, P., Wilhelmi, O., Macharia, D., Shubert, W., Sliuzas, R., Tomaszewski, B.,

- Zhang, S., (2019). Climate vulnerability mapping: A systematic review and future prospects. WIREs Clim Change. <https://doi.org/10.1002/wcc.600>.
- DWA (2002). Governing Board Induction Manual. Department of Water Affairs.
- Enders CK. (2003). Using the Expectation Maximization Algorithm to Estimate Coefficient Alpha for Scales With Item-Level Missing Data. Psychol Meth. 8, 322–337.
- Eyshi Rezaei, E., Ghazaryan, G., González, J., Cornish, N., Dubovyk, O. Siebert, S. (2021). The use of remote sensing to derive maize sowing dates for large-scale crop yield simulations. Int J Biometeorol 65, 565–576.
- Eyshi Rezaei, E., González, J., Graw, V., Cornish, N., Siebert, S. (2018). Combination of crop models and remote sensing for simulation of drought impacts on crop yield. doi:10.13140/RG.2.2.17166.41280.
- Fanadzo, M., Chiduzza, C., Mnkeni, P.N.S., Van der Stoep, L., Steven, J. (2010). Crop production management practices as a cause for low water productivity at Zanyokwe Irrigation Scheme. WSA 36. <https://doi.org/10.4314/wsa.v36i1.50904>.
- FAO (2013). Drought. FAO Land and Water, <https://www.fao.org/3/aq191e/aq191e.pdf> (accessed 05.08.2018)
- FAO (2016). AQUASTAT Country Profile –South Africa. Food and Agriculture Organization of the United Nations (FAO). Rome, Italy.
- FAO (2018). FAO: The impact of disasters and crises on agriculture and food security. <http://www.fao.org/3/l8656EN/i8656en.pdf> (accessed 01.07.2019).
- FAO (2019). GIEWS Update. Southern AfricaDry weather conditions reduce agricultural production prospects in 2019. Available at https://reliefweb.int/sites/reliefweb.int/files/resources/ca3071en_0.pdf (accessed 07.10.2020).
- FAO (2020a). Country profile, South Africa <http://www.fao.org/3/x9751e/x9751e07.htm> (accessed 1.8.2020).
- FAO (2020b). Digital Agriculture Profile South Africa, <http://www.fao.org/3/cb2506en/CB2506EN.pdf> (accessed 1.2.2021).
- Field, A. (2013). Discovering statistics using IBM SPSS statistics (4th edition). London: Sage.
- Fleig, A. K., Tallaksen, L. M., Hisdal, H., Demuth, S. (2006). A global evaluation of streamflow drought characteristics, Hydrol. Earth Syst. Sci., 10, 535–552.
- Frischen, J., Meza, I., Rupp, D., Wietler, K., Hagenlocher, M. (2020). Drought risk to agricultural systems in Zimbabwe: A spatial analysis of hazard, exposure, and vulnerability. Sustainability 12, 752.
- Gerdener, H., Engels, O., Kusche, J. (2020). A framework for deriving drought indicators from the Gravity Recovery and Climate Experiment (GRACE). Hydrology and Earth System Sciences 24, 227–248.
- Ghazaryan G., Dubovyk O., Kussul N., Schellberg, J. (2020). Local Scale Agricultural Drought Monitoring with Satellite-based Multi-sensor Time-series. GIScience & Remote Sensing. 57, 511-524.

- Gidi, L. S. (2013). Rural households' livelihood strategies and opportunities with regard to farming: A case of Intsika Yethu Local Municipality. University of Fort Hare, Department of Agricultural Economics and Extension. Alice, South Africa.
- Hagenlocher, M., Renaud, F. G., Haas, S., Sebesvari, Z. (2018). Vulnerability and risk of deltaic social-ecological systems exposed to multiple hazards, *Sci. Total Environ.* 631–632, 71–80.
- Hagenlocher, M.; Meza, I.; Anderson, C.C.; Min, A.; Renaud, F.G.; Walz, Y.; Siebert, S.; Sebesvari, Z. (2019). Drought vulnerability and risk assessments: State of the art, persistent gaps, and research agenda. *Environ. Res. Lett.* 14, 1–13.
- Hardy, M., Dziba, L., Kilian, W., Tolmay, J. (2011). Rainfed farming systems in South Africa. In: Tow, P., Cooper, I., Partridge, I., Birch, C. (Eds.), *Rainfed Farming Systems*. Springer, Netherlands, Dordrecht, 395–432 https://doi.org/10.1007/978-1-4020-9132-2_16.
- Harris, I., Jones, P., Osborn, T., Lister, D. (2014). Updated high-resolution grids of monthly climatic observations – the CRU TS3.10 Dataset. *Int. J. Climatol.* 34, 623–642.
- Herbert, C. and Döll, P. (2021). Analyzing the informative value of alternative global-scale hazard indicators for monitoring drought risk for human water supply and river ecosystems (in preparation, submission to *Nat. Hazards Earth Syst. Sci* in November 2021).
- Hersbach, H., Bell, B., Berrisford, P., Hirahara, S., Horányi, A., Muñoz-Sabater, J., Nicolas, J., Peubey, C., Radu, R., Schepers, D., Simmons, A., Soci, C., Abdalla, S., Abellan, X., Balsamo, G., Bechtold, P., Biavati, G., Bidlot, J., Bonavita, M., Chiara, G., Dahlgren, P., Dee, D., Diamantakis, M., Dragani, R., Flemming, J., Forbes, R., Fuentes, M., Geer, A., Haimberger, L., Healy, S., Hogan, R.J., Hólm, E., Janisková, M., Keeley, S., Laloyaux, P., Lopez, P., Lupu, C., Radnoti, G., Rosnay, P., Rozum, I., Vamborg, F., Villaume, S., Thépaut, J. (2020). The ERA5 global reanalysis. *Q.J.R. Meteorol. Soc.* 146, 1999–2049.
- Hinkel, J. (2011). Indicators of Vulnerability and Adaptive Capacity. *Towards a Clarification of the Science-Policy Interface*. *Global Environment Change* 21, 198–208.
- Huang, L., He, B., Han, L., Liu, J., Wang, H., Chen, Z., (2017). A global examination of the response of ecosystem water-use efficiency to drought based on MODIS data. *Science of The Total Environment* 601–602, 1097–1107.
- IPCC (2012). *Managing the Risks of Extreme Events and Disasters to Advance Climate Change Adaptation*. A Special Report of Working Groups I and II of the Intergovernmental Panel on Climate Change ed CB Field et al (Cambridge: Cambridge University Press)
- IPCC (2014). *Climate Change 2014: Impacts, Adaptation, and Vulnerability*. Part B: Regional Aspects. Contribution of Working Group II to the Fifth Assessment Report of the Intergovernmental Panel on Climate Change. (V. R. Barros, C. B. Field, D. J. Dokken, M. D. Mastrandrea, K. J. Mach, T. E. Bilir, ... L. L. White, Eds.). New York - Cambridge: Cambridge University Press.
- Jordaan, A.J., Sakulski, D.M., Muyambo, F. (2017a). Vulnerability, adaptation to and coping with drought: the case of commercial and subsistence rain fed farming in the Eastern Cape. Volume I. <http://www.wrc.org.za/Knowledge%20Hub%20Documents/Research%20Reports/TT%20716-17.pdf>. (Accessed 05.09.2020)
- Jordaan, A.J., Sakulski, D.M., Muyambo, F. (2017b). Vulnerability, adaptation to and coping with drought: the case of commercial and subsistence rain fed farming in the Eastern Cape. Vol. II. <http://www.wrc.org.za/Knowledge%20Hub%20Documents/Research%20Reports/TT%20716-2-17.pdf> (Accessed 29.10.2020)

- Landmann, T., Eidmann, D., Cornish, N., Franke, J., Siebert, S. (2019). Optimizing harmonics from Landsat time series data: The case of mapping rainfed and irrigated agriculture in Zimbabwe. *Remote Sensing Letters* 10, 1038-1046.
- Le Maitre, DC., Seyler, H., Holland, M., Smith-Adao, L., Nel, JL., Maherry, A., Witthüser, K. (2018). Identification, Delineation and Importance of the Strategic Water Source Areas of South Africa, Lesotho and Swaziland for Surface Water and Groundwater, Report No. TT 743/1/18, Pretoria: Water Research Commission.
- Machethe, C.L. (2004). Agriculture and poverty in South Africa: Can agriculture reduce poverty, in: *Overcoming Underdevelopment Conference Held in Pretoria*. Citeseer, p. 29.
- Mahlalela, P.T., Blamey, R.C., Hart, N.C.G., Reason, C.J.C. (2020). Drought in the Eastern Cape region of South Africa and trends in rainfall characteristics. *Clim Dyn* 55, 2743–2759.
- Makaudze, E.M. and Miranda, M.J. (2010). Catastrophic drought insurance based on the remotely sensed normalized difference vegetation index for smallholder farmers in Zimbabwe. *Agrekon* 49, 418–432.
- McKee, T.B., Doesken, N.J., Kleist, J. (1993). The relationship of drought frequency and duration to time scale. In: *Proceedings of the Eighth Conference on Applied Climatology*, Anaheim, California, 17–22 January 1993. Boston, American Meteorological Society, 179–184.
- Meza, I., Eyshi Rezaei, E., Siebert, S., Ghazaryan, G., Nouri, H., Dubovyk, O., Gerdener, H., Herbert, C., Kusche, J., Popat, E., Rhyner, J., Jordaan, A., Walz, Y., Hagenlocher, M. (2021). Drought risk for agricultural systems in South Africa: Drivers, spatial patterns, and implications for drought risk management. *Science of The Total Environment* 799, 149505.
- Meza, I., Hagenlocher, M., Naumann, G., Vogt, J., Frischen, J. (2019). *Drought Vulnerability Indicators for Global-Scale Drought Risk Assessments*. Publications Office of the European Union: Luxembourg.
- Meza, I., Siebert, S., Döll, P., Kusche, J., Herbert, C., Eyshi Rezaei, E., Nouri, H., Gerdener, H., Popat, E., Frischen, J., Naumann, G., Vogt, J.V., Walz, Y., Sebesvari, Z., Hagenlocher, M. (2020). Global-scale drought risk assessment for agricultural systems. *Nat. Hazards Earth Syst. Sci.* 20, 695-712.
- Modarres, R. (2007). Streamflow drought time series forecasting, *Stoch. Environ. Res. Ris. Assess.* 21, 223–233.
- Müller Schmied, H., Cáceres, D., Eisner, S., Flörke, M., Niemann, C., Peiris, T. A., Popat, E., Portmann, F. T., Reinecke, R., Schumacher, M., Shadkam, S., Telteu, C. E., Trautmann, T., Döll, P. (2021). The global water resources and use model WaterGAP v2.2d: Model description and evaluation. *Geoscientific Model Development* 14, 1037–1079.
- Naumann, G., Barbosa, P., Garrote, L., Iglesias, A., Vogt, J. (2014). Exploring drought vulnerability in Africa: an indicator based analysis to be used in early warning systems. *Hydrology and Earth System Sciences* 18, 1591–1604.
- Ngaka, M. (2012). Drought preparedness, impact and response: A case of the Eastern Cape and Free State provinces of South Africa. *Jàmbá: Journal of Disaster Risk Studies* 4, 1-10.
- Niemeyer, S. (2008). New drought indices, in: López-Francos, A. (Ed.), *Drought management: scientific and technological innovations*. Zaragoza : CIHEAM, 267-274.
- OECD (2008). *Handbook on Constructing Composite Indicators: Methodology and User Guide*. <https://doi.org/10.1787/9789264043466-en>.

- Peng, C.-Y. J., Harwell, M., Liou, S.-M., Ehman, L. H. (2006). Advances in missing data methods and implications for educational research. In: S. Sawilowsky (Ed.), Real data analysis. Greenwich, CT: Information Age, 31-37.
- Peng, L., Zeng, Z., Wei, Z., Chen, A., Wood, E.F., Sheffield, J. (2019). Determinants of the ratio of actual to potential evapotranspiration. *Glob Change Biol* 25, 1326–1343.
- Popat, E. and Döll, P. (2021): Soil moisture and streamflow deficit anomaly index: an approach to quantify drought hazards by combining deficit and anomaly. *Nat. Hazards Earth Syst. Sci.* 21, 1337–1354.
- Portmann, F.T., Siebert, S., Döll, P. (2010). MIRCA2000-Global monthly irrigated and rainfed crop areas around the year 2000: A new high-resolution data set for agricultural and hydrological modeling. *Global Biogeochem. Cycles* 24, GB1011.
- Quiring, S. M. (2009). Developing Objective Operational Definitions for Monitoring Drought. *Journal of Applied Meteorology and Climatology* 48, 1217–1229.
- Rojas, O. (2018). Agricultural extreme drought assessment at global level using the FAO-Agricultural Stress Index System (ASIS). *Weather and Climate Extremes*.
- Roth, P. L., Switzer III, F. S., Switzer, D. M. (1999). Missing data in multiple item scales: A Monte Carlo analysis of missing data techniques. *Organizational research methods* 2, 211-232.
- Rother, H., Hall, R., London, L. (2008). Pesticide use among emerging farmers in South Africa: contributing factors and stakeholder perspectives. *Development Southern Africa* 25, 399-424.
- Running, S., Mu, Q., Zhao, M. (2017). MOD16A2 MODIS/Terra Net Evapotranspiration 8-Day L4 Global 500m SIN Grid V006. <https://doi.org/10.5067/MODIS/MOD16A2.006>
- SACN (2016). State of South African Cities Report 2016. <http://www.socr.co.za/wp-content/uploads/2016/06/SoCR16-Main-Report-online.pdf> (Accessed 01.02.2021).
- Sánchez, N., González-Zamora, Á., Martínez-Fernández, J., Piles, M., Pablos, M. (2018). Integrated remote sensing approach to global agricultural drought monitoring. *Agricultural and Forest Meteorology* 259, 141-153.
- Scheff, J. (2019). A unified wetting and drying theory. *Nature Climate Change* 9, 9-10.
- Schulze, R.E. (2016). On Observations, Climate Challenges, the South African Agriculture Sector and Considerations for an Adaptation Handbook. In: Schulze, R.E. (Ed.) Handbook for Farmers, Officials and Other Stakeholders on Adaptation to Climate Change in the Agriculture Sector within South Africa. Section A: Agriculture and Climate Change in South Africa: Setting the Scene, Chapter A1.
- Schumacher, M., Forootan, E., van Dijk, A. IJM., Müller Schmied, H., Crosbie, R. S., Kusche, J., Döll, P. (2018). Improving drought simulations within the Murray-Darling Basin by combined calibration/assimilation of GRACE data into the WaterGAP Global Hydrology Model. *Remote Sensing of Environment* 204, 212-228.
- Schwarz, M., Landmann, T., Cornish, N., Wetzels, K.-F., Siebert, S., Franke, J. (2020). A Spatially Transferable Drought Hazard and Drought Risk Modeling Approach Based on Remote Sensing Data. *Remote Sensing* 12, 237.
- Siebert, S., and Döll, P. (2010). Quantifying blue and green virtual water contents in global crop production as well as potential production losses without irrigation. *Journal of Hydrology* 384, 198–217.

- Sohoulande Djebou, D.C. (2017). Bridging drought and climate aridity. *Journal of Arid Environments* 144, 170-180.
- Steinemann, A., Iacobellis, S.F., Cayan, D.R. (2015). Developing and Evaluating Drought Indicators for Decision-Making. *J. Hydrometeorol.* 16, 1793–1803.
- Thompson, M.W. (2019). South African National Land-Cover (SANLC) 2018. Department of Environmental Affairs of the Republic of South Africa, https://www.environment.gov.za/projectsprogrammes/egis_landcover_datasets (accessed 07.08.2020).
- Tian, L., Yuan, S., Quiring, S.M. (2018). Evaluation of six indices for monitoring agricultural drought in the south-central United States. *Agricultural and Forest Meteorology* 249, 107-119.
- Tijdeman, E., Stahl, K., Tallaksen, L. M. (2020). Drought Characteristics Derived Based on the Standardized Streamflow Index: A Large Sample Comparison for Parametric and Nonparametric Methods. *Water Resour. Res.* 56, e2019WR026315.
- Trenberth, K. E., Dai, A., Van der Schrier, G., Jones, P. D., Barichivich, J., Briffa, K. R., Sheffield, J. (2014). Global warming and changes in drought. *Nature Climate Change* 4, 17–22.
- UNDRR (2019). Global Assessment Report on Disaster Risk Reduction 2019, Chapter 6: Special Section on Drought. <https://gar.undrr.org/report-2019>, UN, New York
- Unganai, L.S., Kogan, F.N. (1998). Drought Monitoring and Corn Yield Estimation in Southern Africa from AVHRR Data. *Remote Sensing of Environment* 63, 219–232.
- UN Zimbabwe (2010). Country Analysis Report for Zimbabwe. <http://www.zw.one.un.org/sites/default/files/Country%20Analysis%20Report%20for%20Zimbabwe%202010.pdf> (accessed on 21.01.2020)
- Unganai, L.S. and Kogan, F.N. (1998). Drought Monitoring and Corn Yield Estimation in Southern Africa from AVHRR Data. *Remote Sensing of Environment* 63, 219-232.
- van Loon, A. F., Stahl, K., Di Baldassarre, G., Clark, J., Rangecroft, S., Wanders, N., Gleeson, T., van Dijk, A. I. J. M., Tallaksen, L. M., Hannaford, J., Uijlenhoet, R., Teuling, A. J., Hannah, D. M., Sheffield, J., Svoboda, M., Verbeiren, B., Wagener, T., Van lanen, H. A. J. (2016). Drought in a human-modified world: reframing drought definitions, understanding, and analysis approaches, *Hydrol. Earth Syst. Sci.* 20, 3631–3650.
- van Loon, A.F. (2015). Hydrological drought explained, *WIREs Water* 2, 359-392, <https://doi.org/10.1002/wat2.1085>.
- VERBI Software. (2019). *MAXQDA 2020*, computer program, VERBI Software, Berlin.
- Vicente-Serrano, S.M., Beguería, S., López-Moreno, J.I. (2010) A Multiscalar Drought Index Sensitive to Global Warming: The Standardized Precipitation Evapotranspiration Index. *Journal of Climate* 23, 1696-1718.
- Viña, A., Gitelson, A.A., Rundquist, D.C., Keydan, G.P., Leavitt, B., Schepers, J. (2004). Monitoring Maize (*Zea mays* L.) Phenology with Remote Sensing. *Agron. J.* 96, 1139–1147.
- Waldner, F., Hansen, M.C., Potapov, P.V., Löw, F., Newby, T., Ferreira, S., Defourny, P. (2017). National-scale cropland mapping based on spectral-temporal features and outdated land cover information. *PLoS ONE* 12, e0181911.
- Walz, Y., Dall, K., Graw, V., León, J., Haas, S., Kussul, N., Jordaan, A. (2018). Understanding and reducing agricultural drought risk: Examples from South Africa and Ukraine.

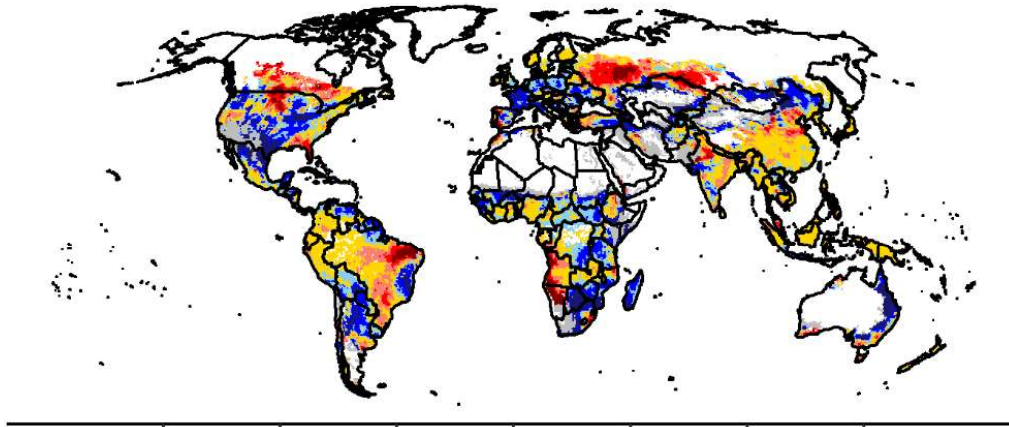
- Walz, Y., Min, A., Dall, K., Duguru, M., Villagran de Leon, J.-C., Graw, V., Dubovyk, O., Sebesvari, Z., Jordaan, A., Post, J. (2020). Monitoring progress of the Sendai Framework using a geospatial model: The example of people affected by agricultural droughts in Eastern Cape, South Africa. *Progress in Disaster Science* 5, 100062. <https://doi.org/10.1016/j.pdisas.2019.100062>.
- Wan, W., Zhao, J., Popat, E., Herbert, C., Döll, P. (2020). Analyzing and Monitoring the Impact of Streamflow Drought on Hydroelectricity Production: A Global-Scale Study (in review in *Water Resources Research*). <https://www.essoar.org/doi/10.1002/essoar.10503337.1> (accessed 18.11.2020).
- Weedon, G. P., Balsamo, G., Bellouin, N., Gomes, S., Best, M. J., and Viterbo, P. (2014). The WFDEI meteorological forcing data set: WATCH forcing data methodology applied to ERAInterim reanalysis data, *Water Resour. Res.* 50, 7505–7514.
- World Bank, (2019). *Assessing Drought Hazard and Risk: Principles and Implementation Guidance*. Washington, DC: World Bank.
- World Bank. (2020). *Global - Dams Database | Data Catalog [WWW Document]*. <https://datacatalog.worldbank.org/dataset/global-dams-database>. (Accessed 01.12.2021).
- WWF (2018). *Agriculture: Facts and Trends, South Africa* [online]. World Wide Fund. http://awsassets.wwf.org.za/downloads/facts_brochure_mockup_04_b.pdf (Accessed 06.07.2020).
- Xiao, W., Sun, Z., Wang, Q. et Yang, Y. (2013). Evaluating MODIS phenology product for rotating croplands through ground observations. *Journal of Applied Remote Sensing* 7, 73562.
- Yevjevich, V. (1967). *An objective approach to definitions and investigations of continental hydrological droughts*. Colorado State University, Fort Collins, Hydrology Paper
- Yu, L., and Ramaswamy, S. (2011). Examining the Relationships between Software Coupling and Software Performance: A Cross-platform Experiment. *J. Comput. Inf. Technol.* 19, 1-10.
- Zargar, A., Sadiq, R., Naser, B., Khan, F.I. (2011). A review of drought indices. *Environmental Reviews* 19, 333-349.
- Zhao, H., Xu, Z., Zhao, J., Huang, W. (2017). A drought rarity and evapotranspiration-based index as a suitable agricultural drought indicator. *Ecological Indicators* 82, 530-538.

Appendix

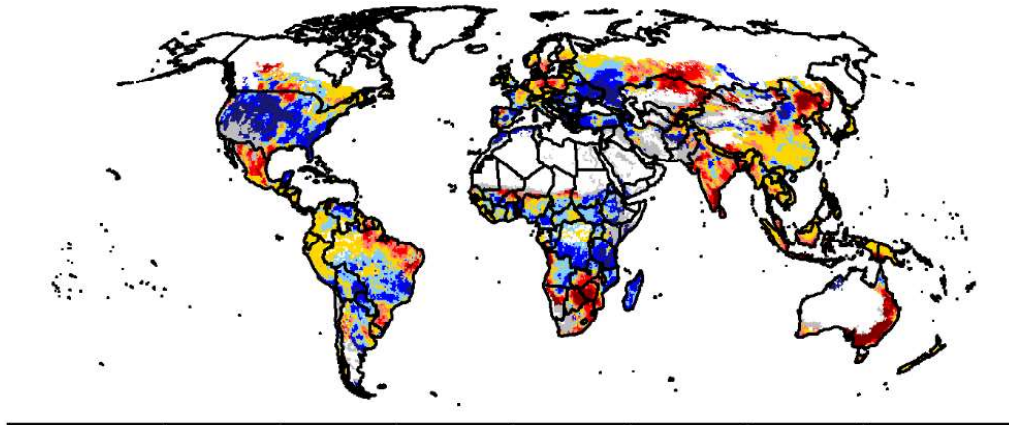
Appendix A1 - Time series of global drought hazard 1981-2018

1. Rainfed agricultural systems

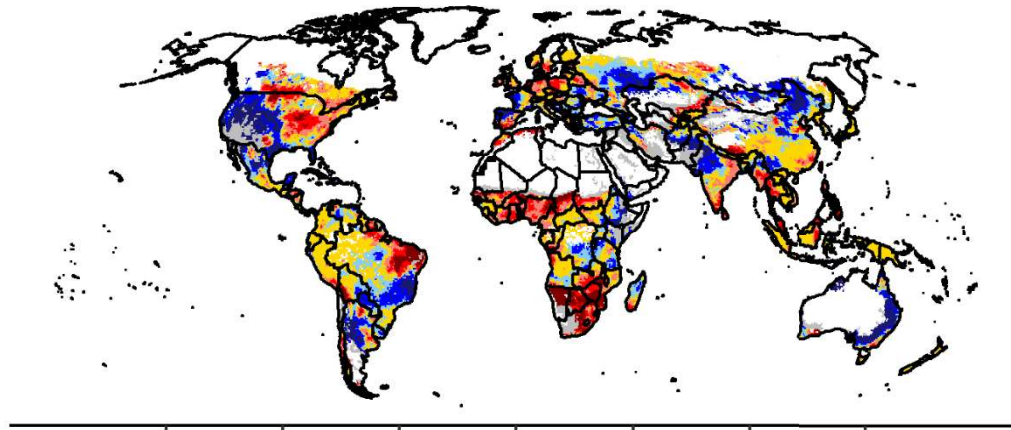
Year 1981



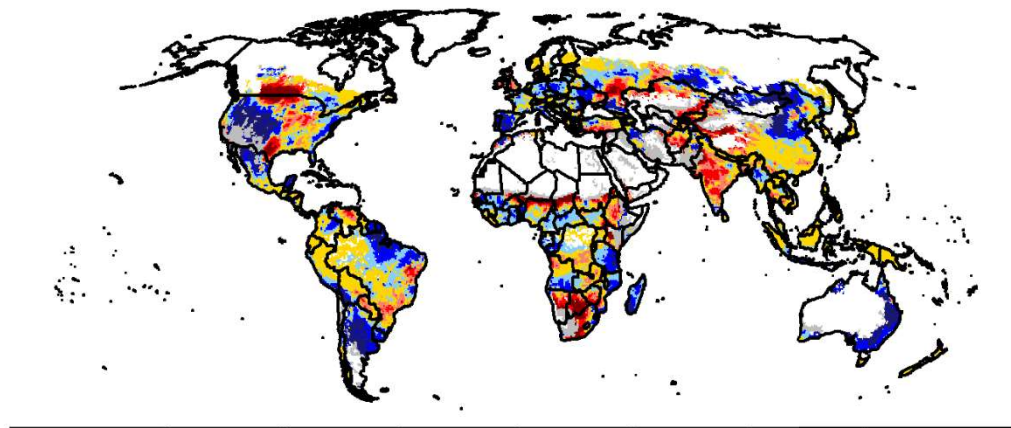
Year 1982



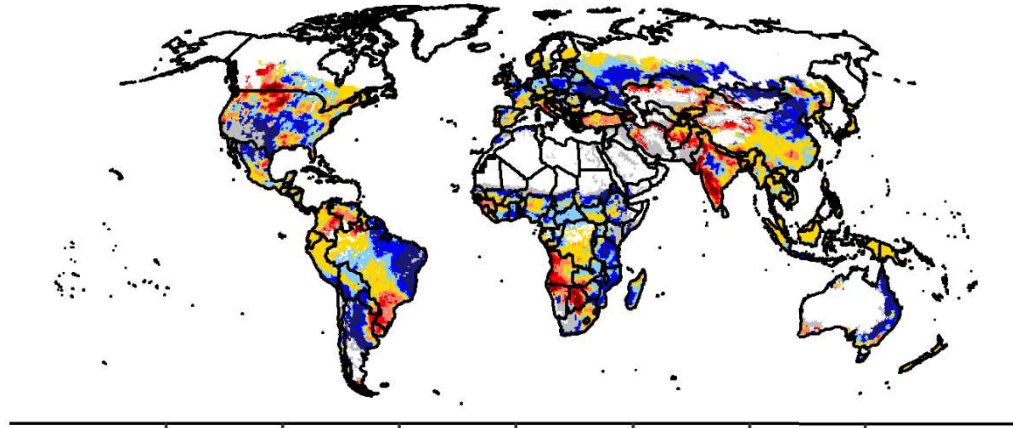
Year 1983



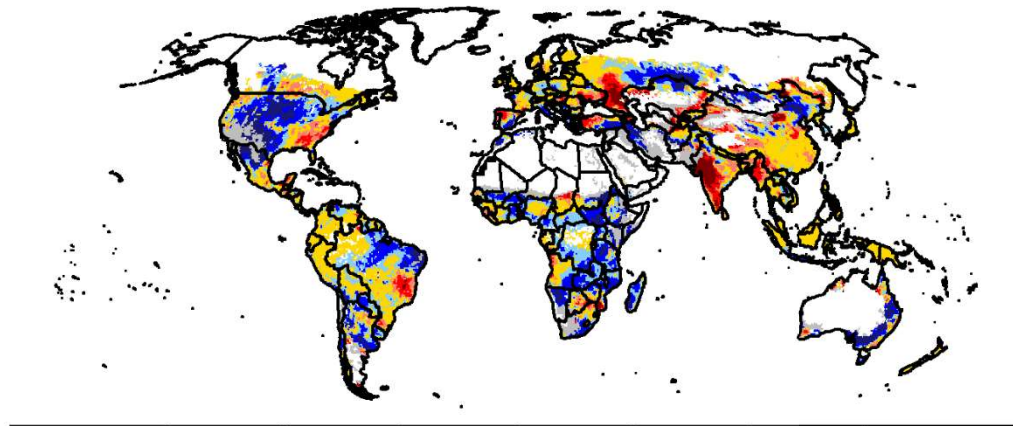
Year 1984



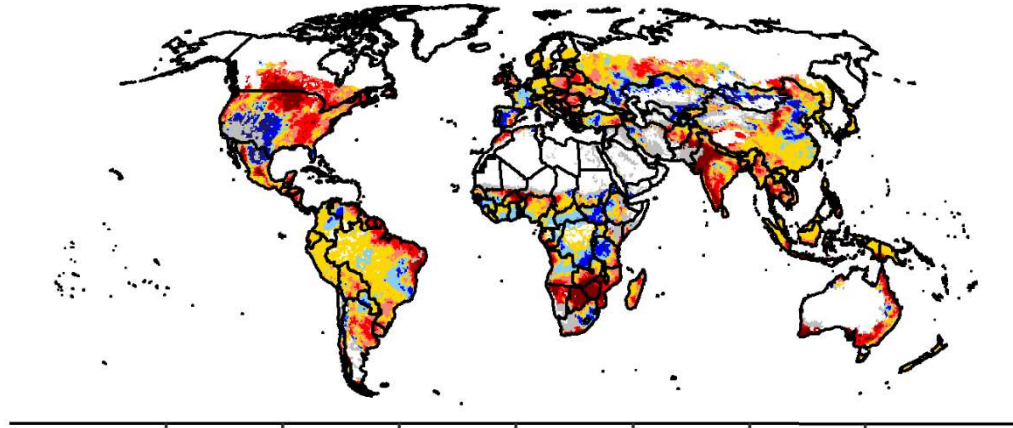
Year 1985



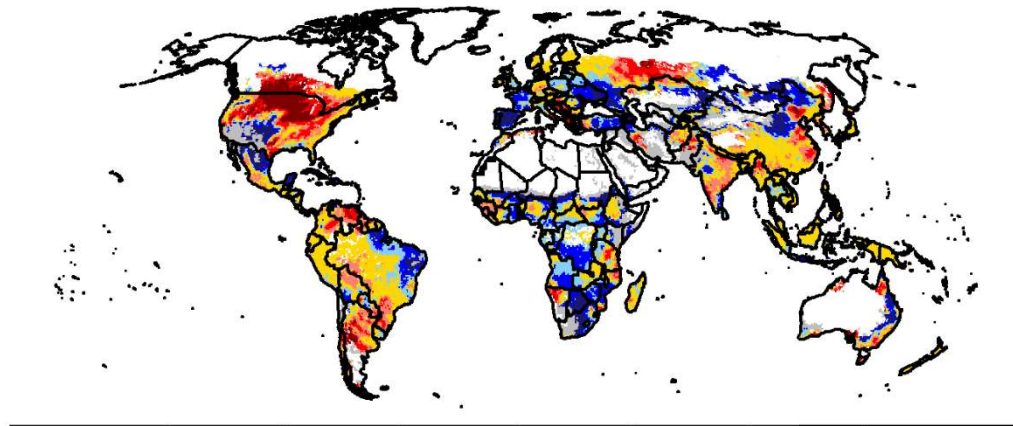
Year 1986



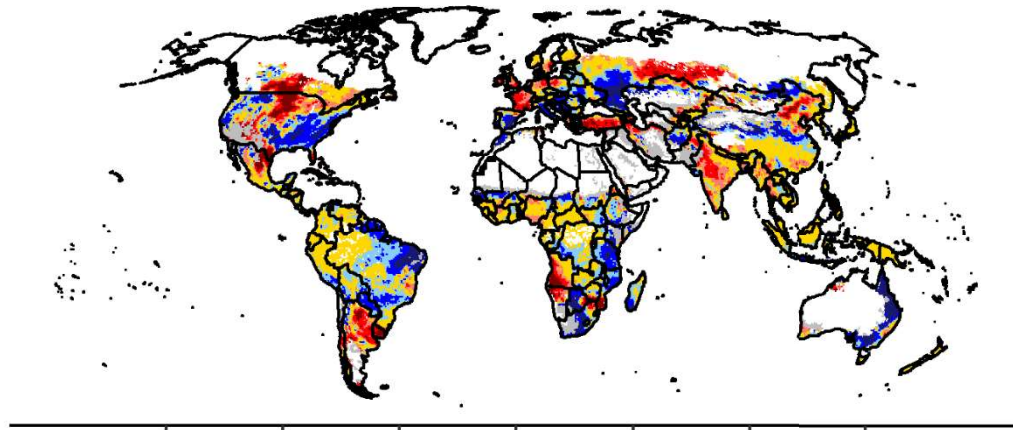
Year 1987



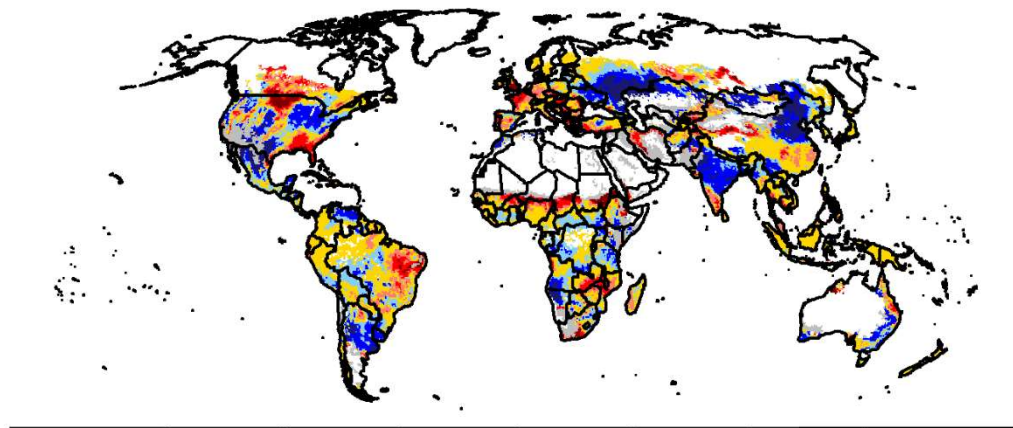
Year 1988



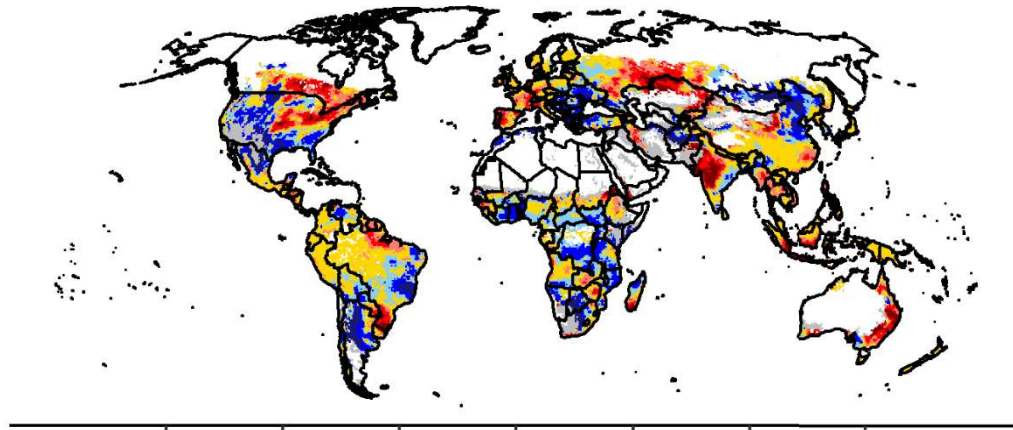
Year 1989



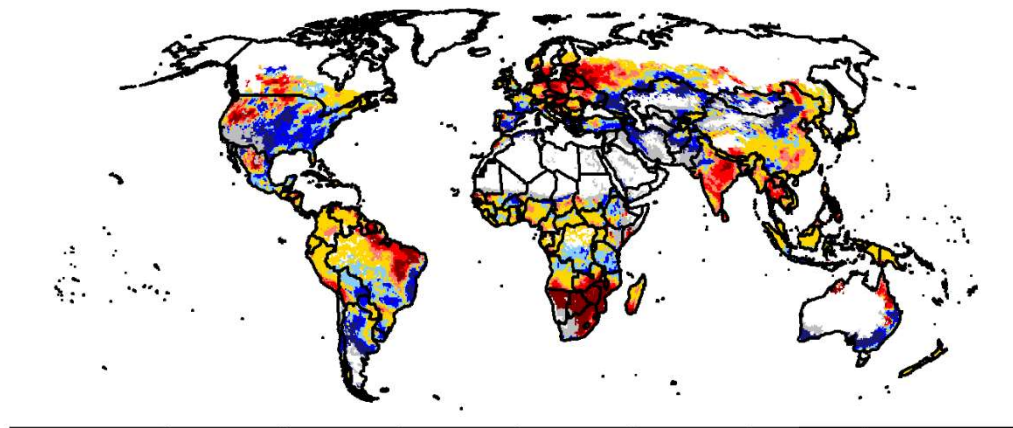
Year 1990



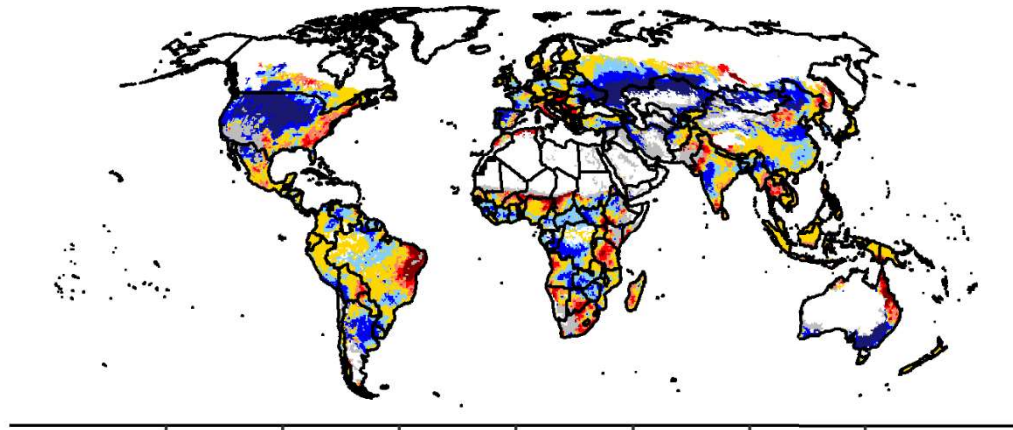
Year 1991



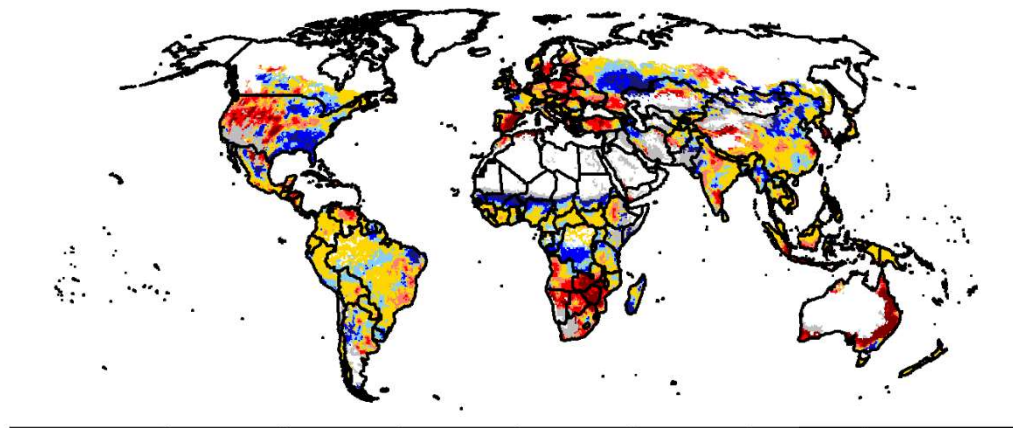
Year 1992



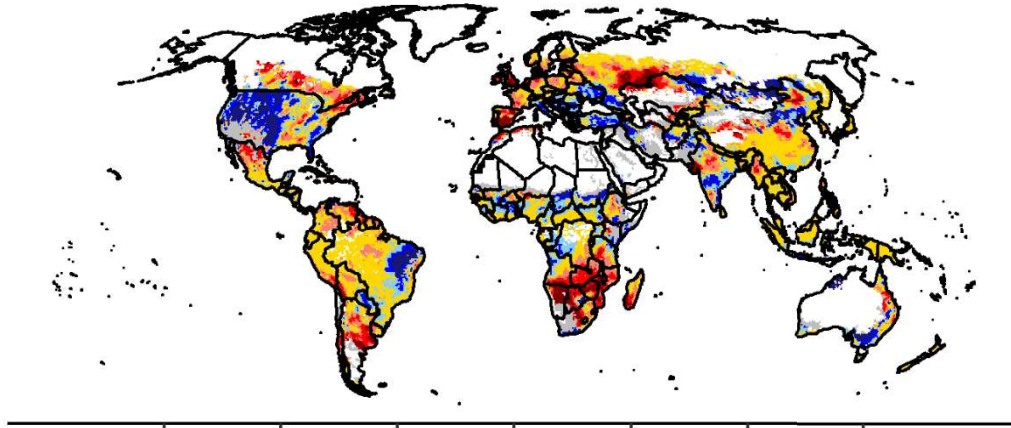
Year 1993



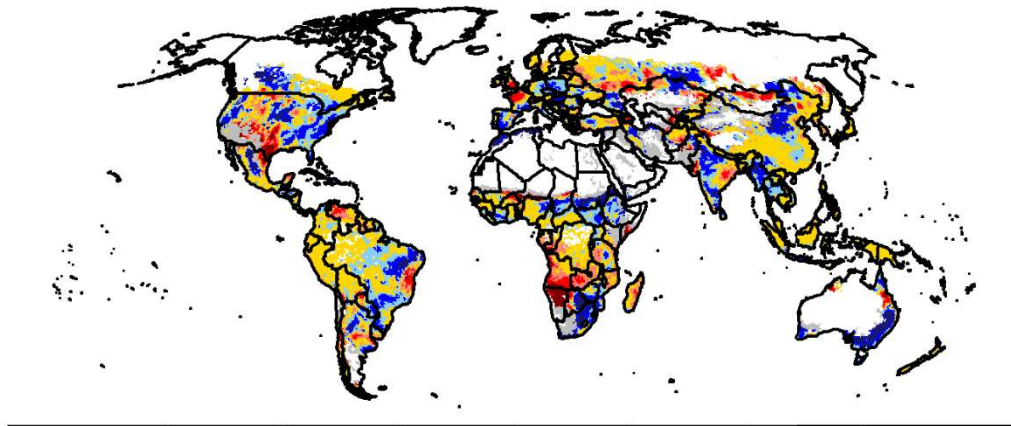
Year 1994



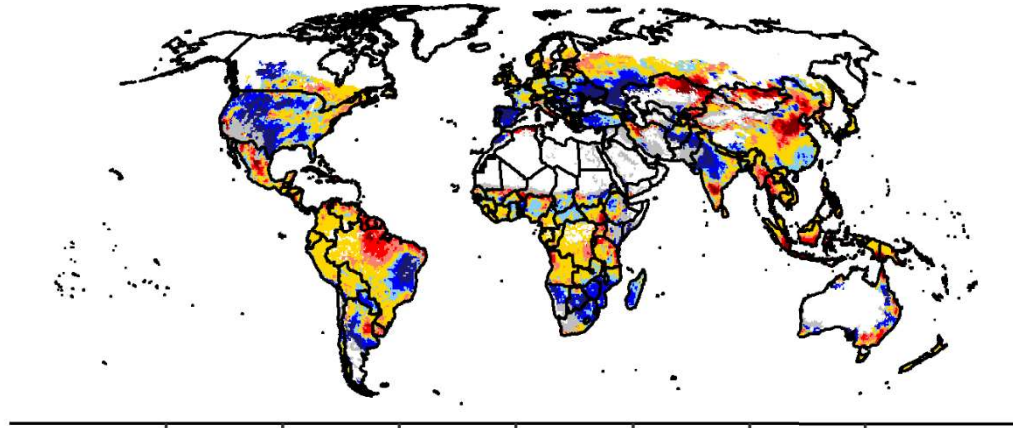
Year 1995



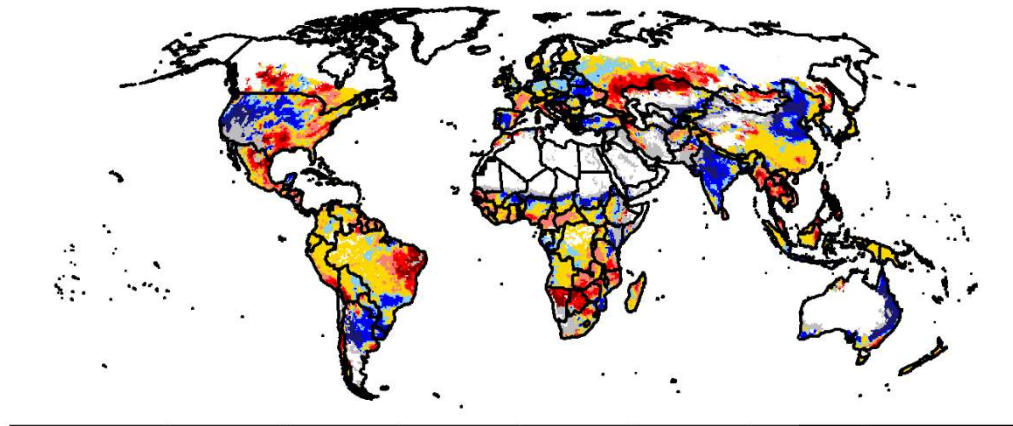
Year 1996



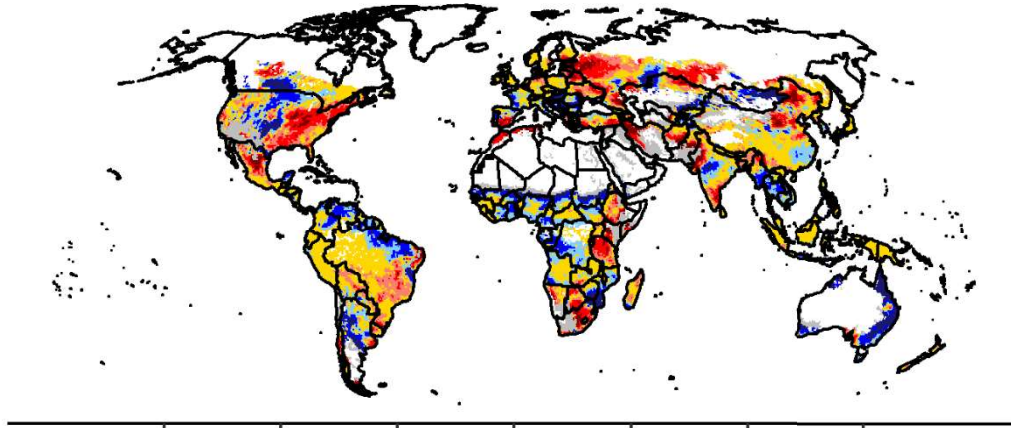
Year 1997



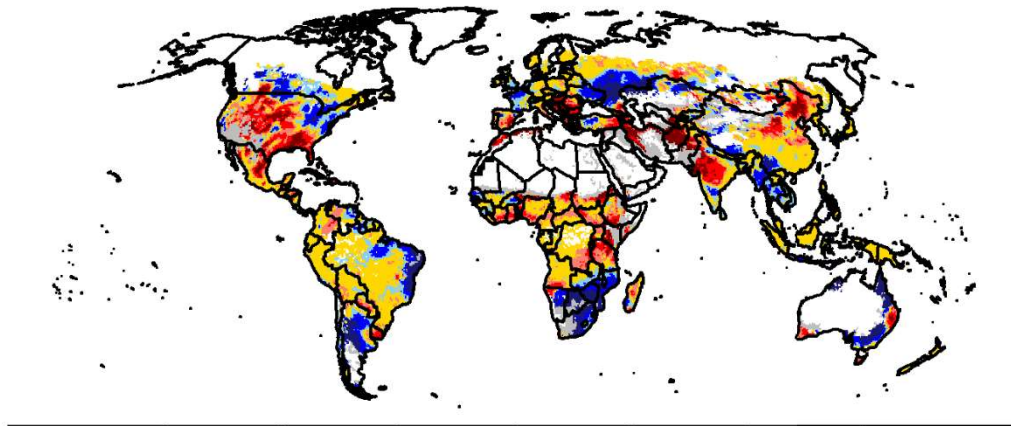
Year 1998



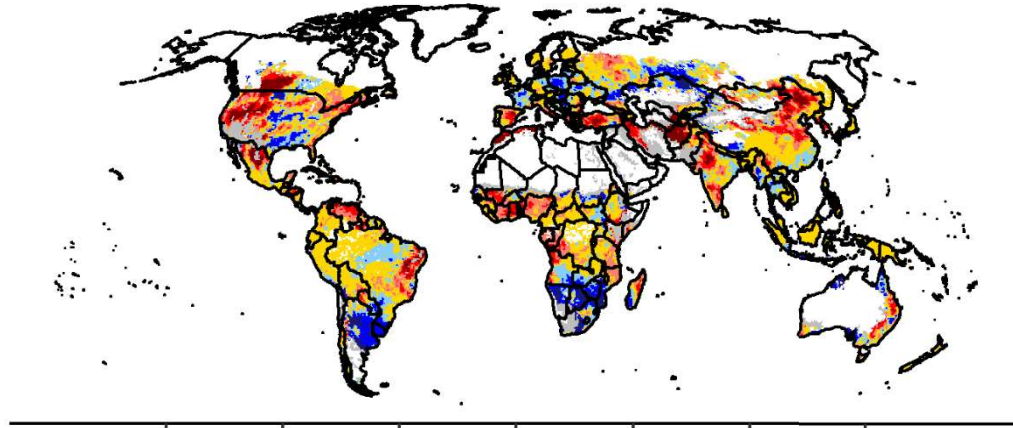
Year 1999



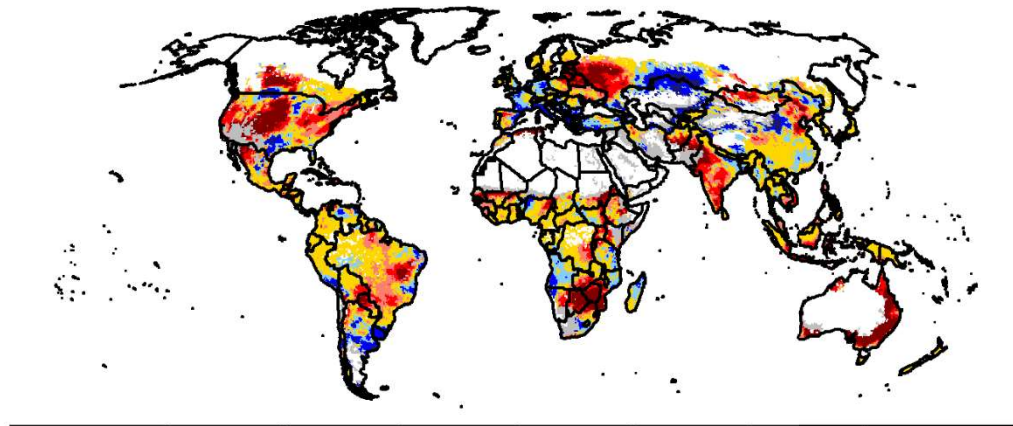
Year 2000



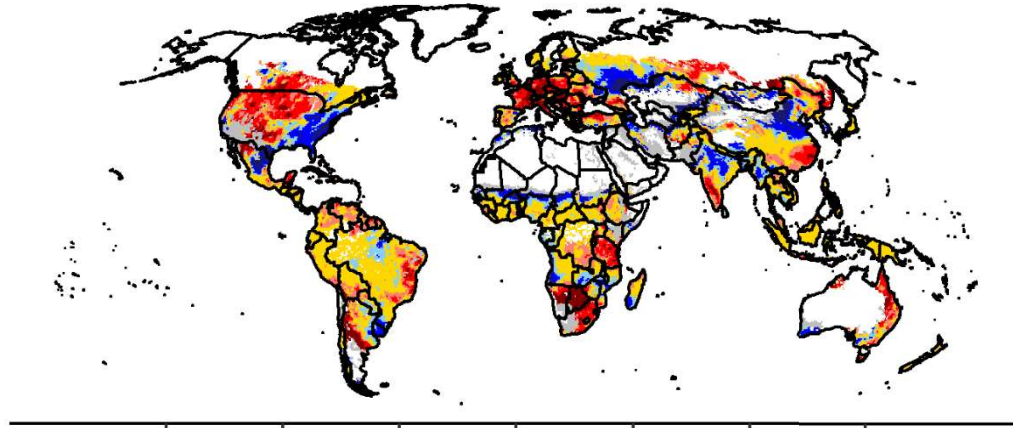
Year 2001



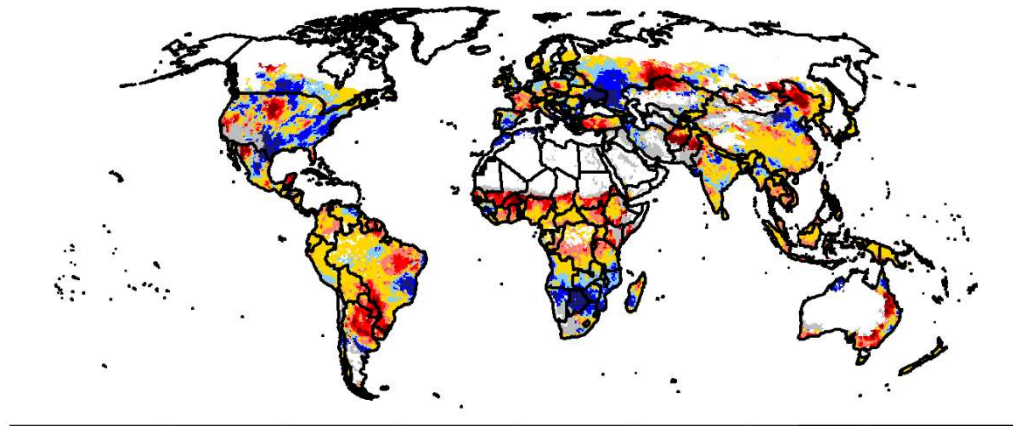
Year 2002



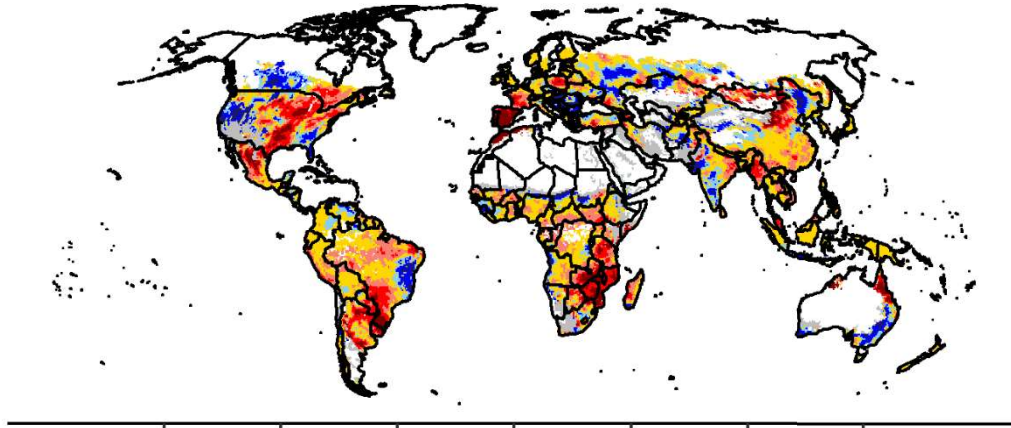
Year 2003



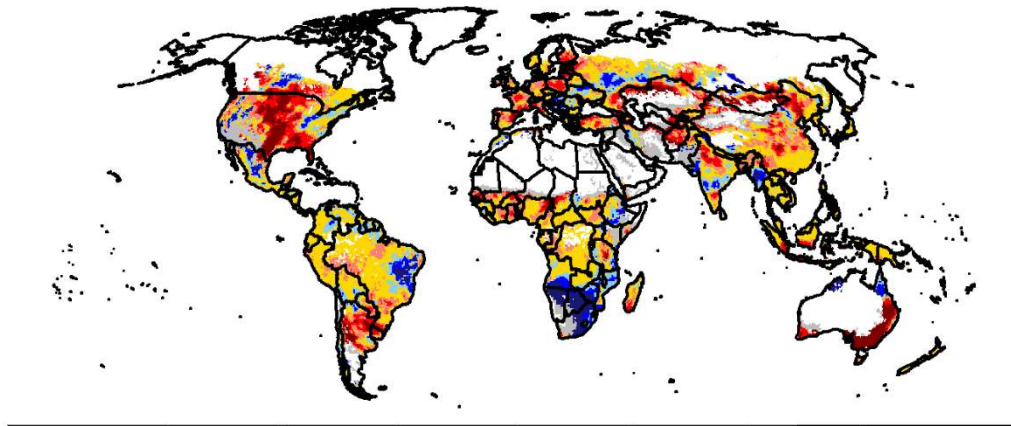
Year 2004



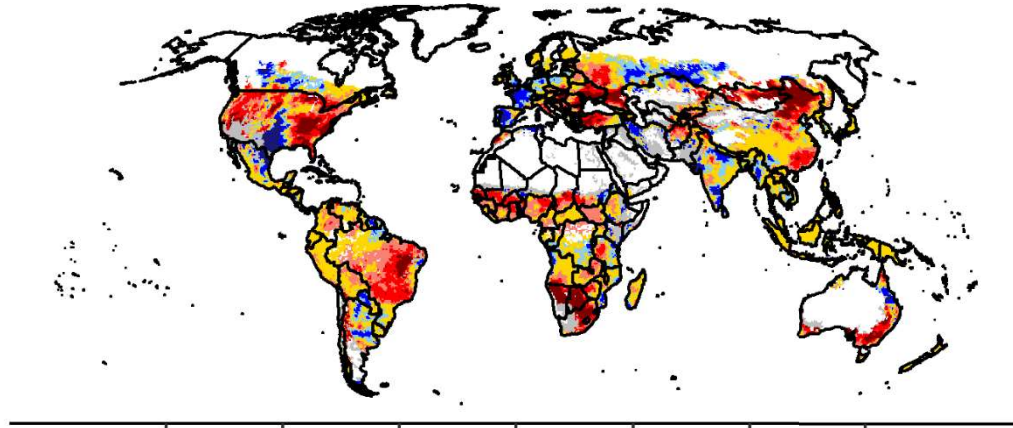
Year 2005



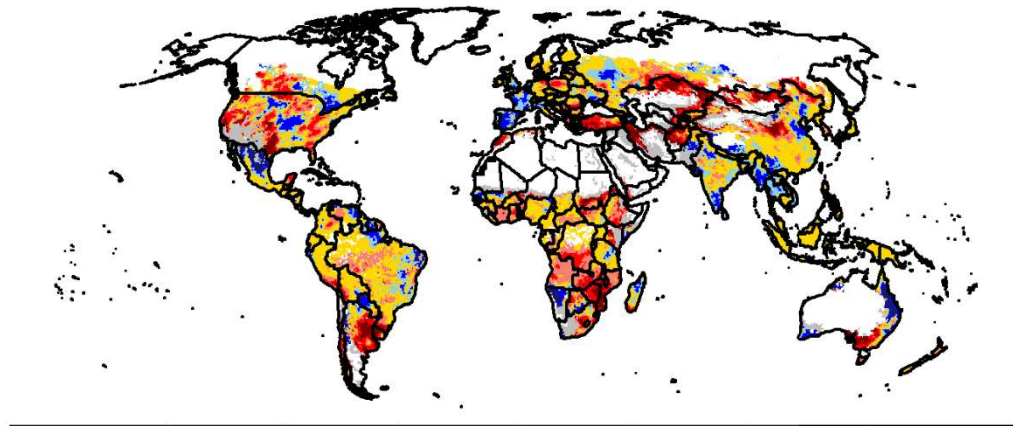
Year 2006



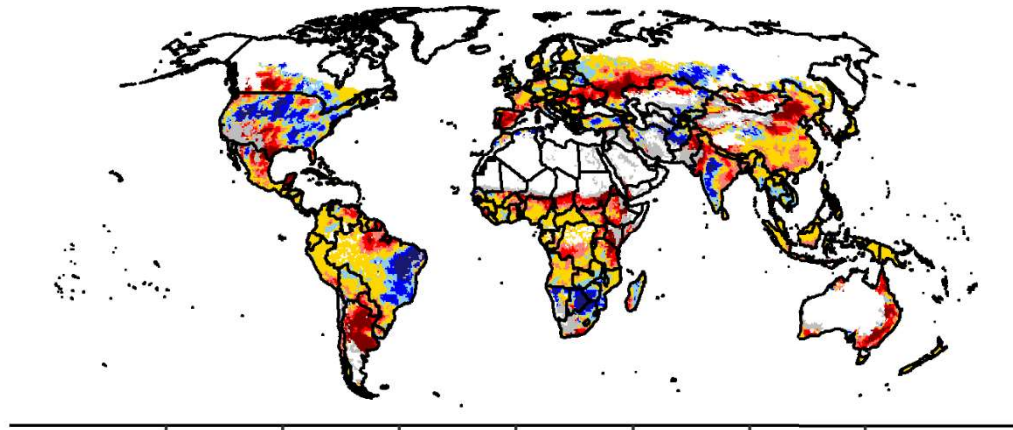
Year 2007



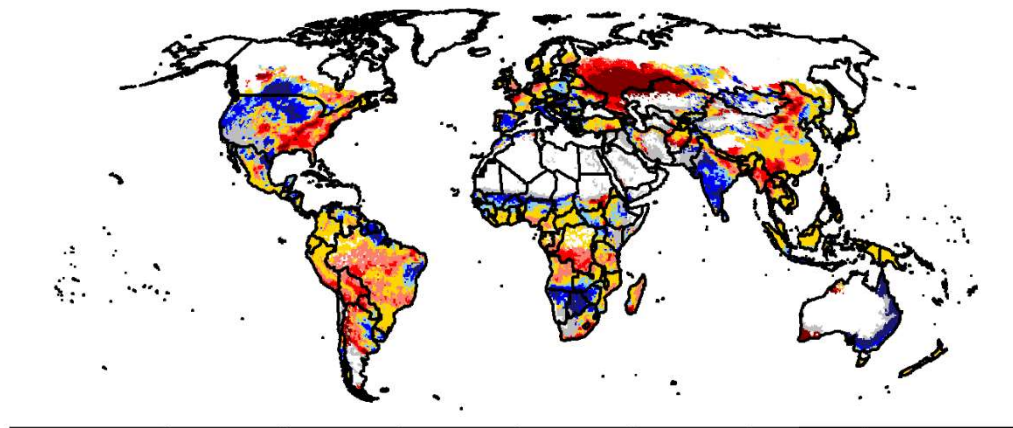
Year 2008



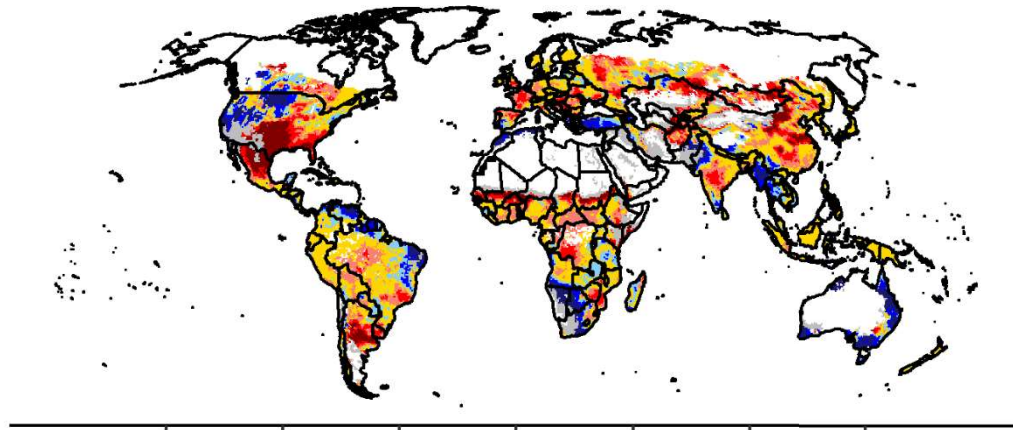
Year 2009



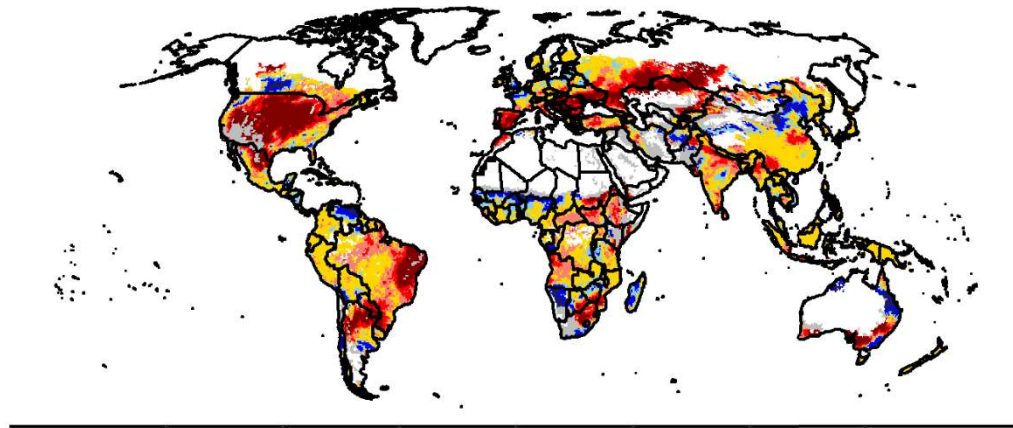
Year 2010



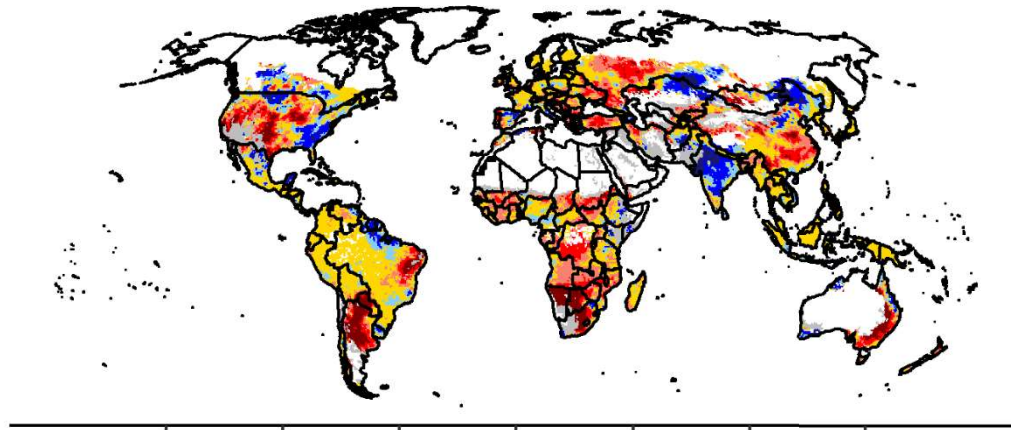
Year 2011



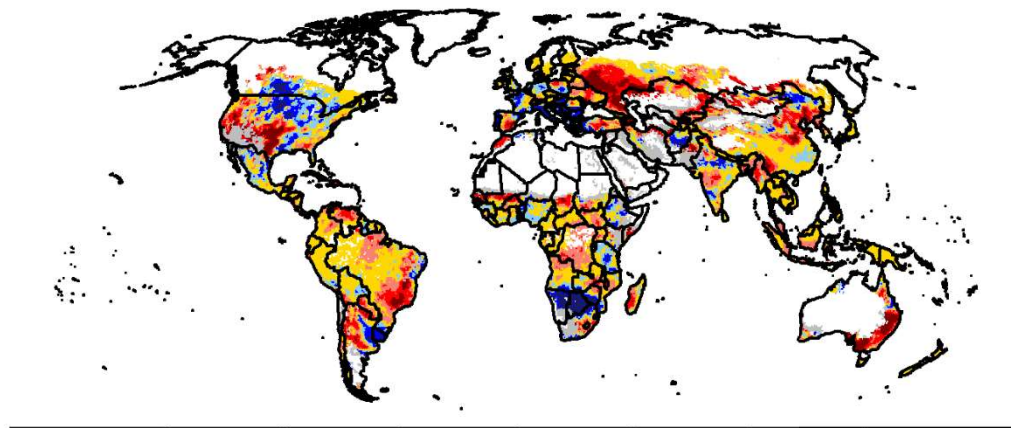
Year 2012



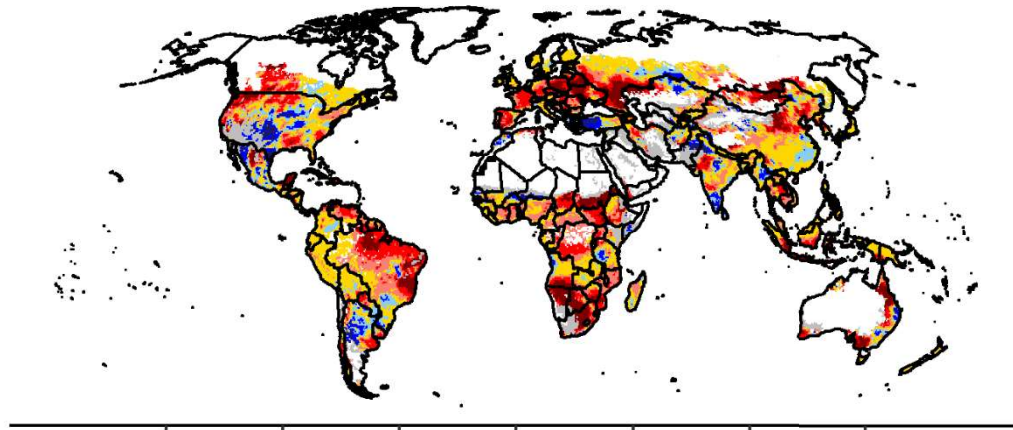
Year 2013



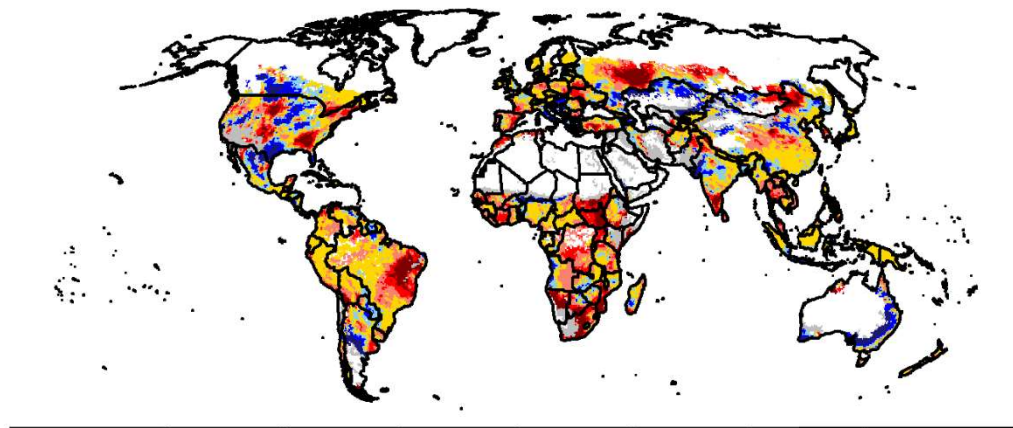
Year 2014



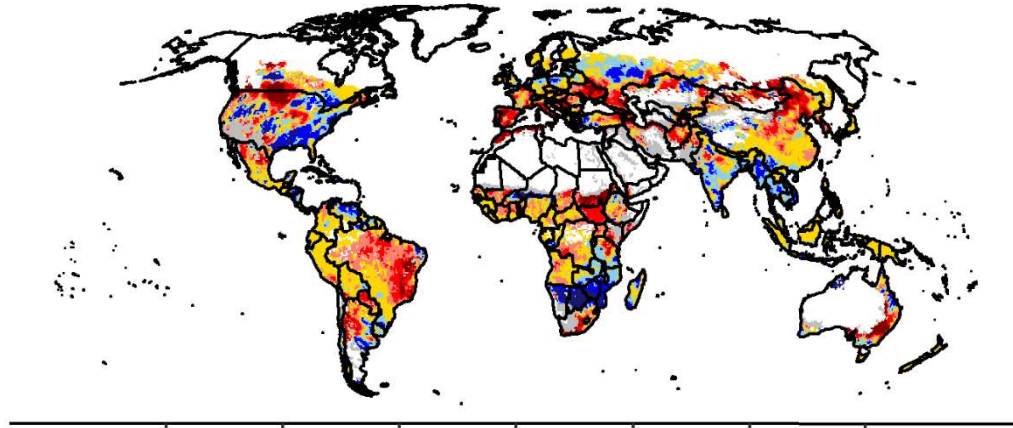
Year 2015



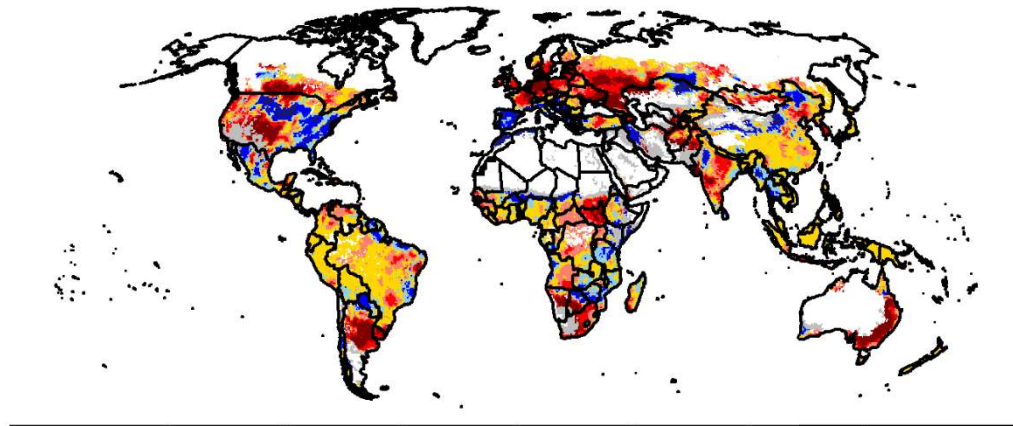
Year 2016



Year 2017

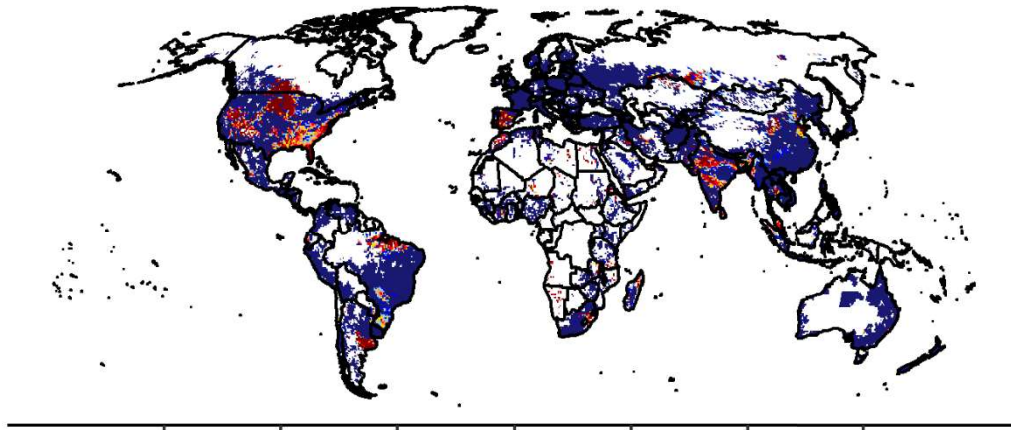


Year 2018

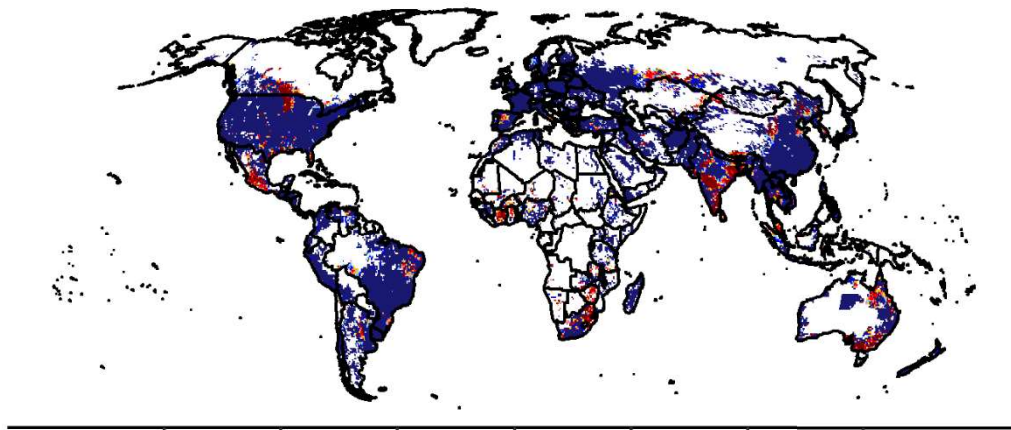


2. Irrigated agricultural systems

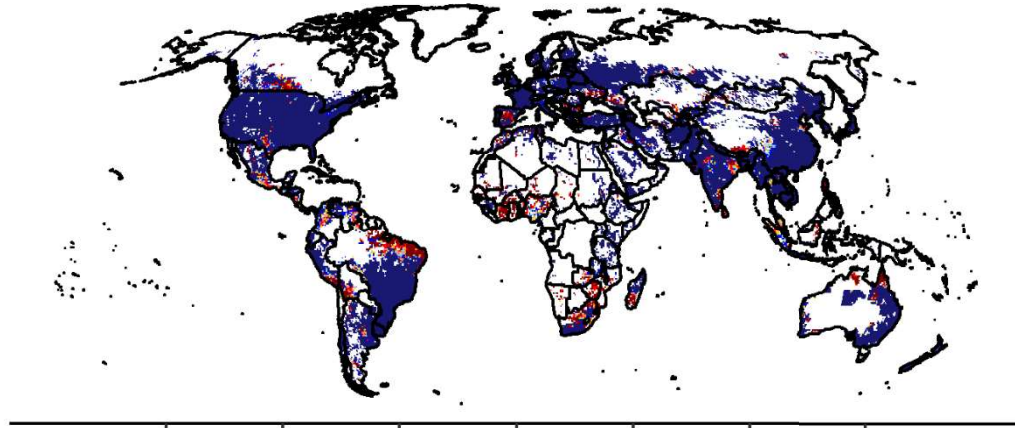
Year 1981



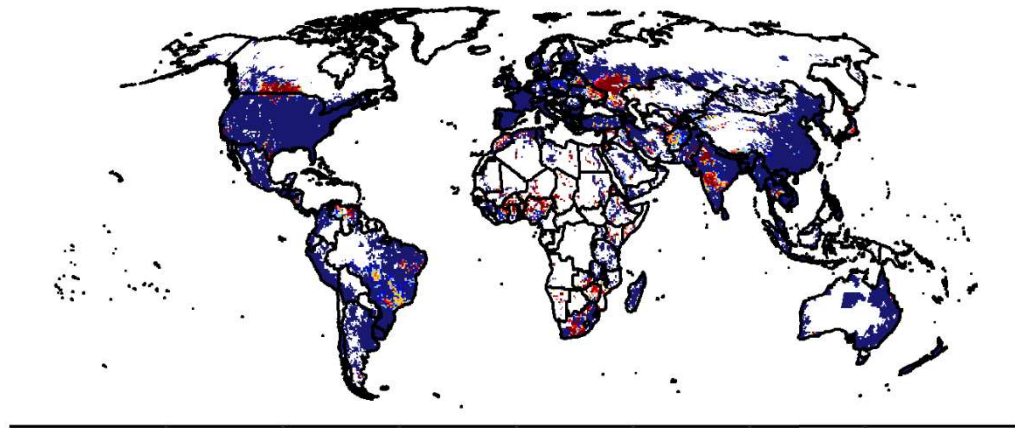
Year 1982



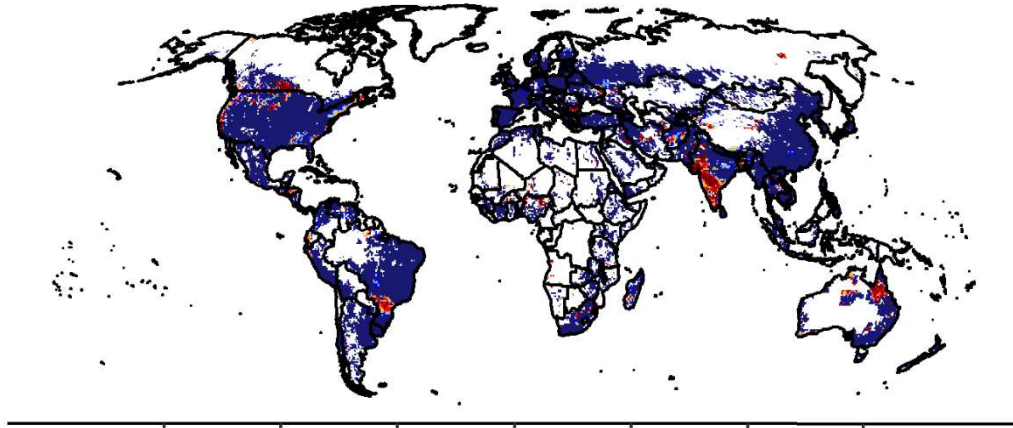
Year 1983



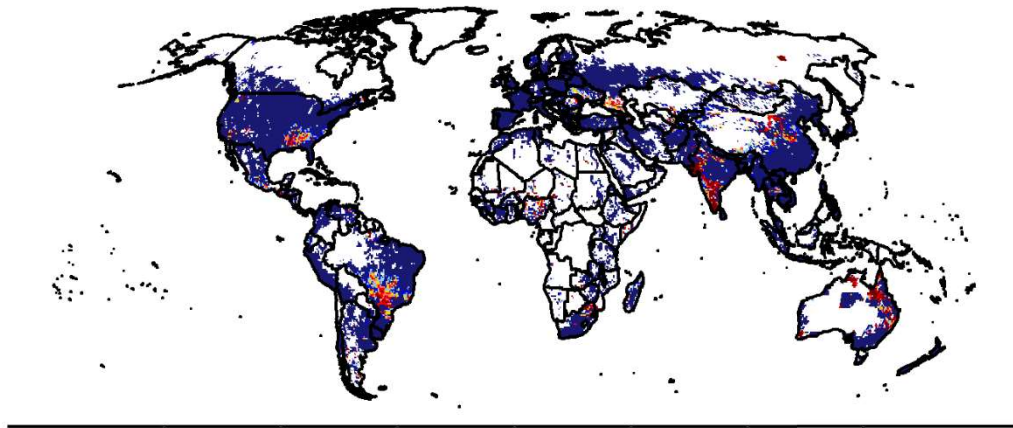
Year 1984



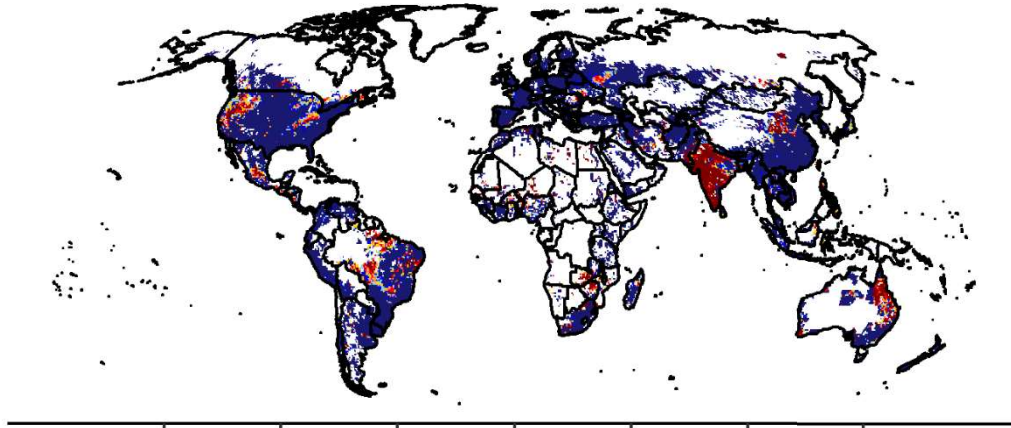
Year 1985



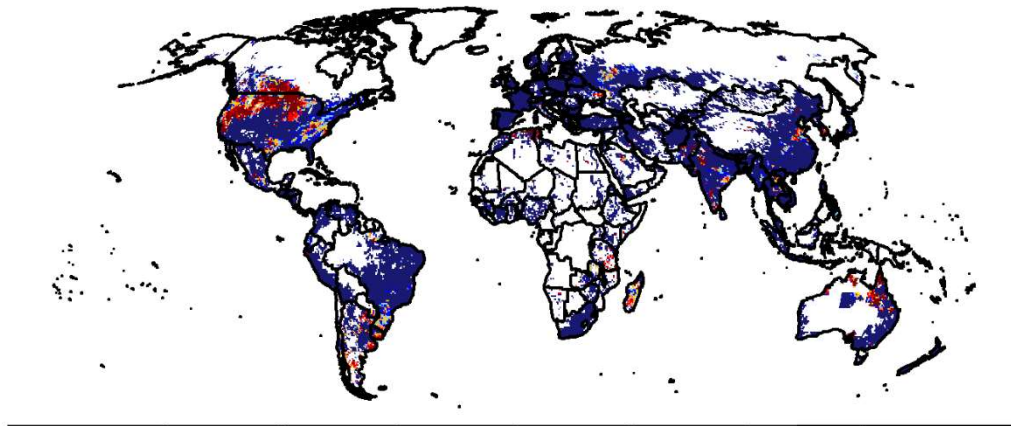
Year 1986



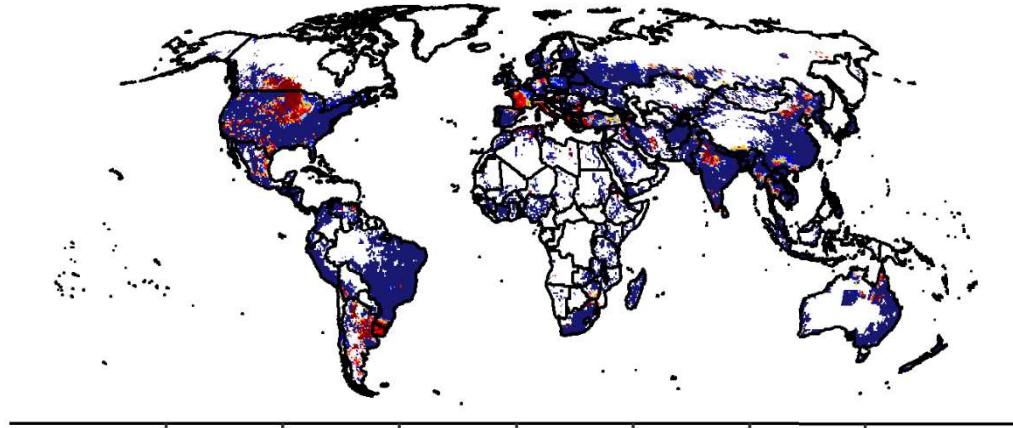
Year 1987



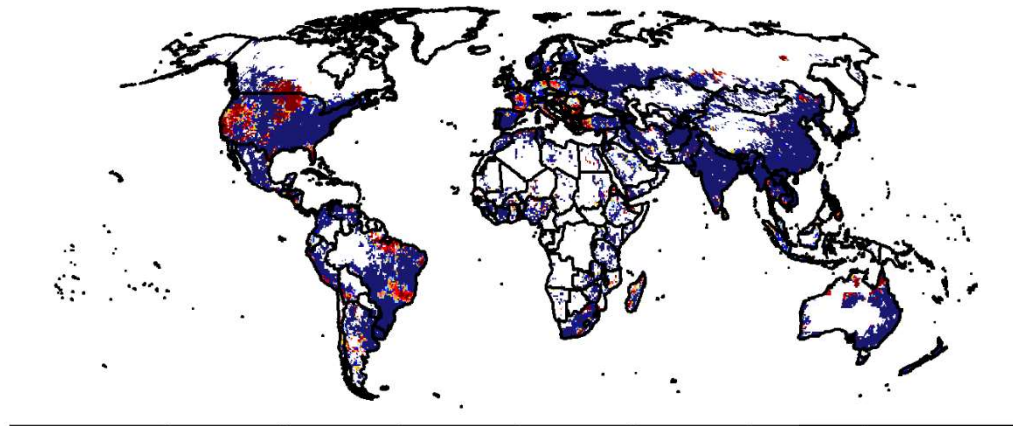
Year 1988



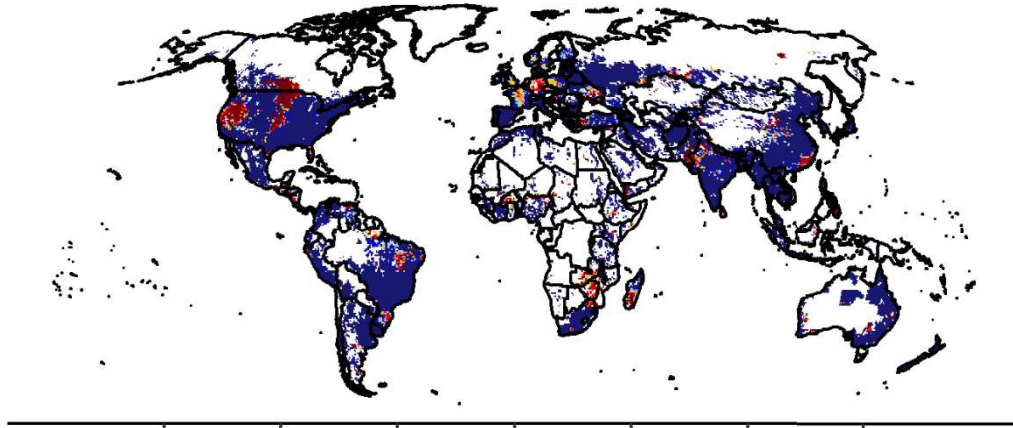
Year 1989



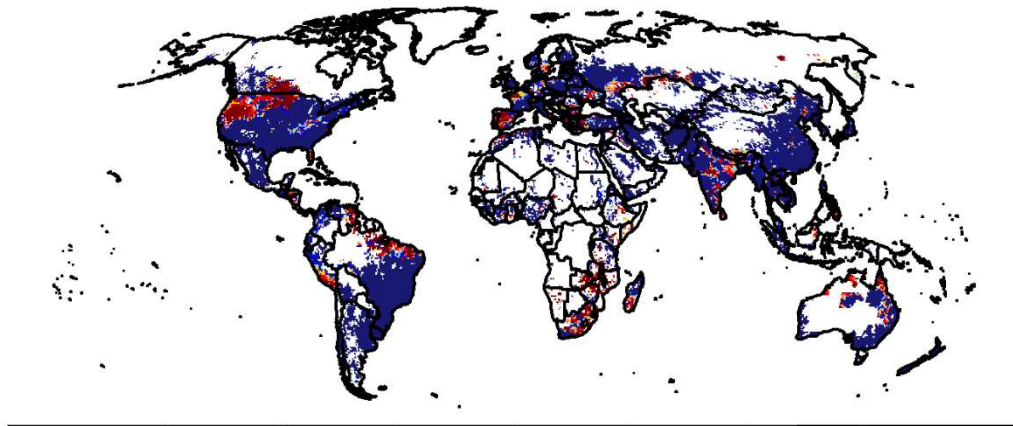
Year 1990



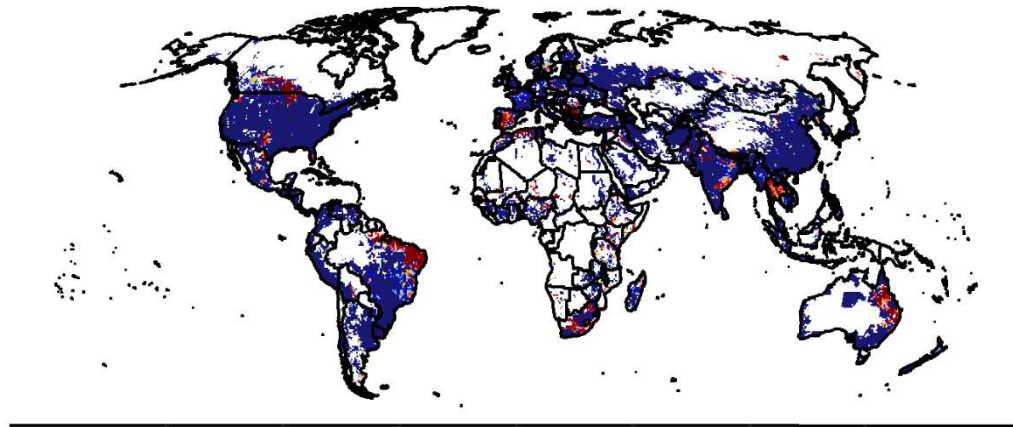
Year 1991



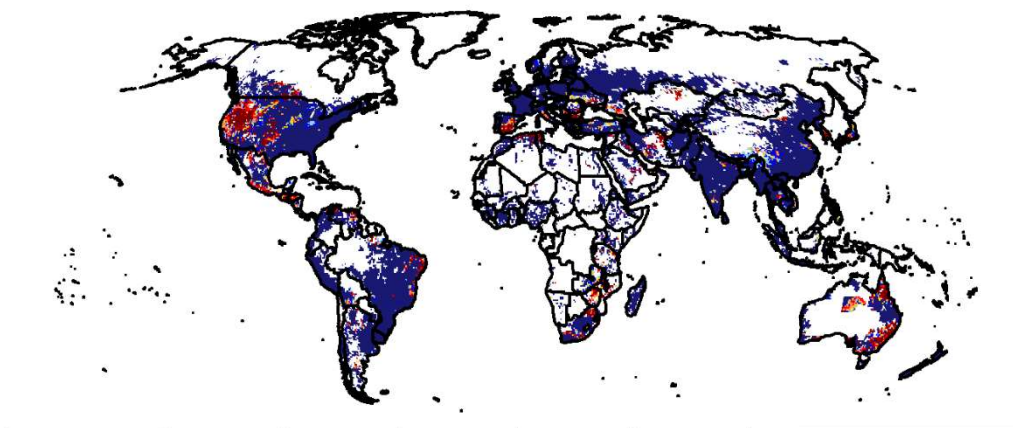
Year 1992



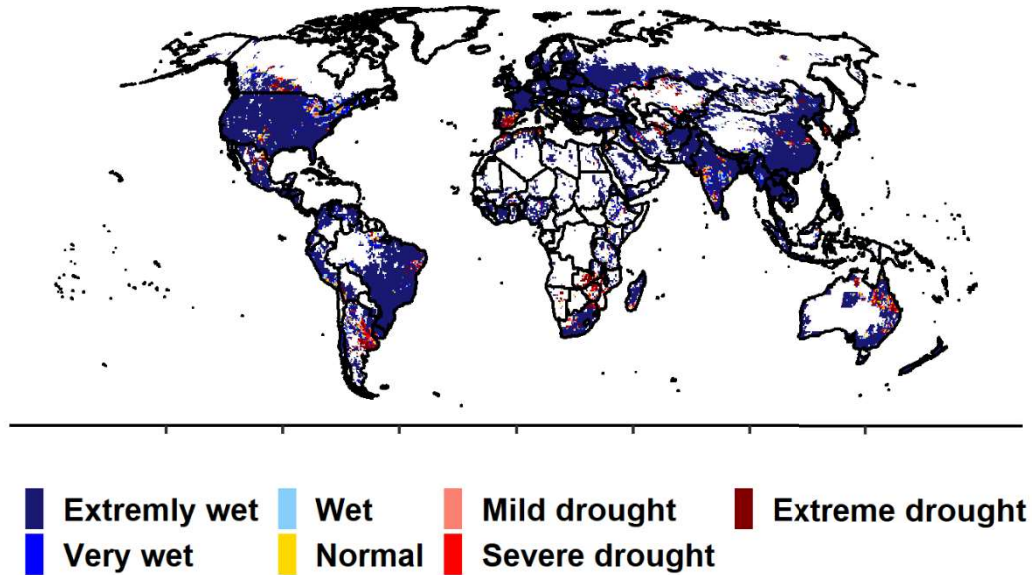
Year 1993



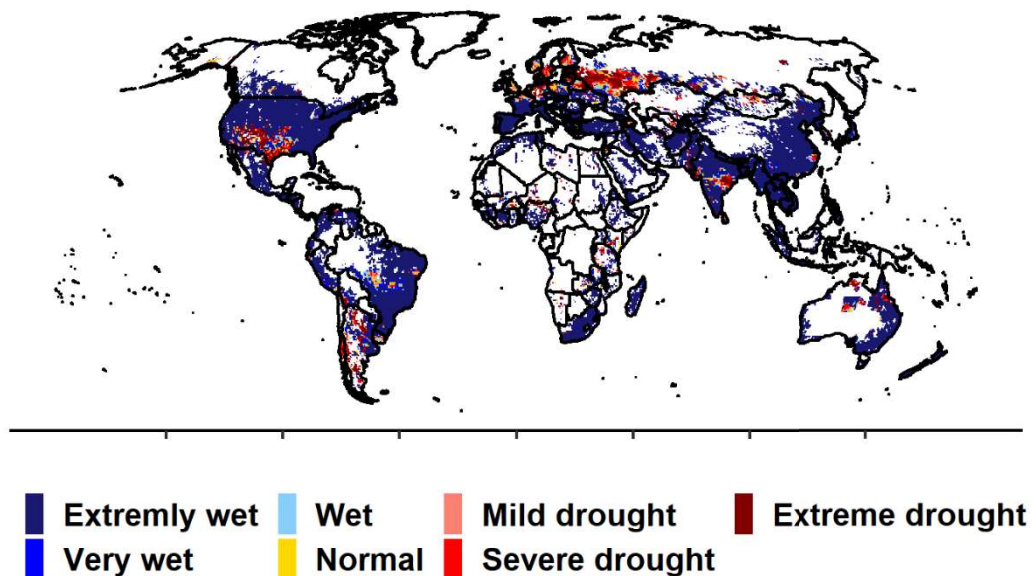
Year 1994



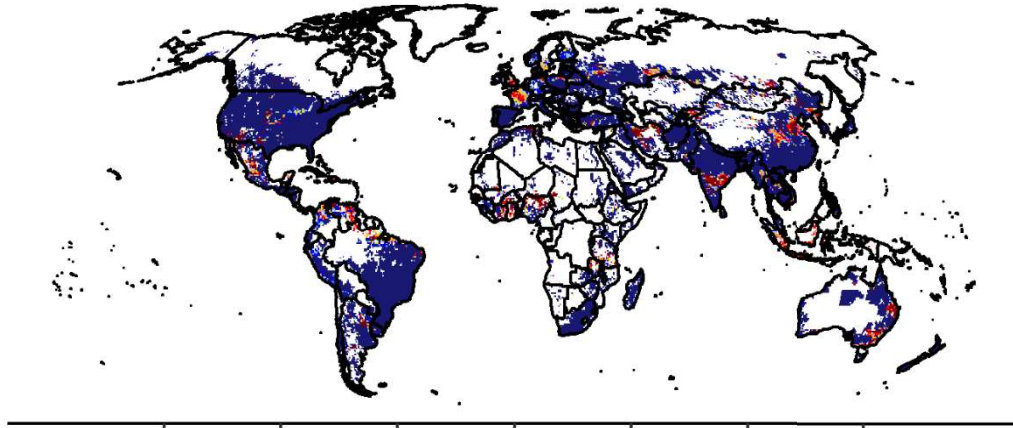
Year 1995



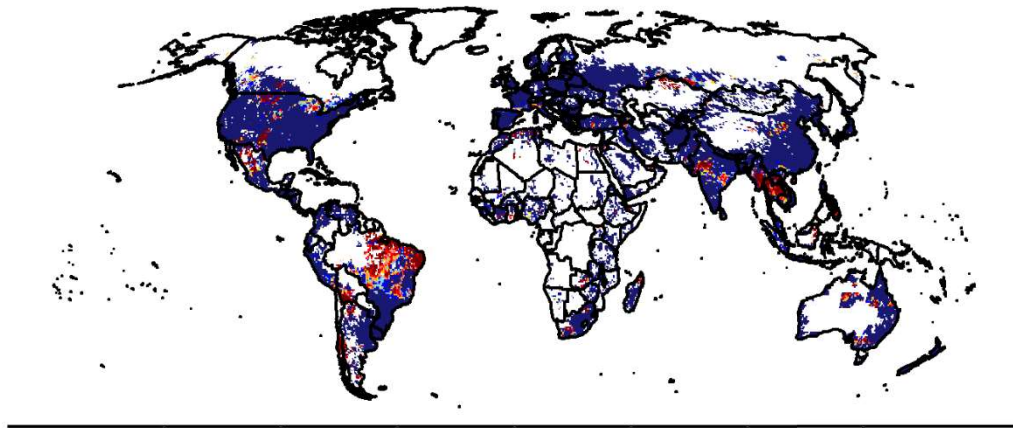
Year 1996



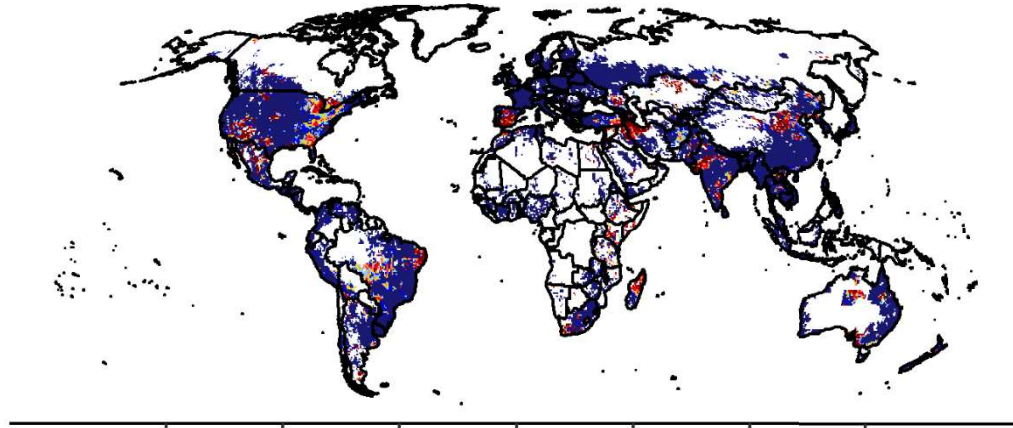
Year 1997



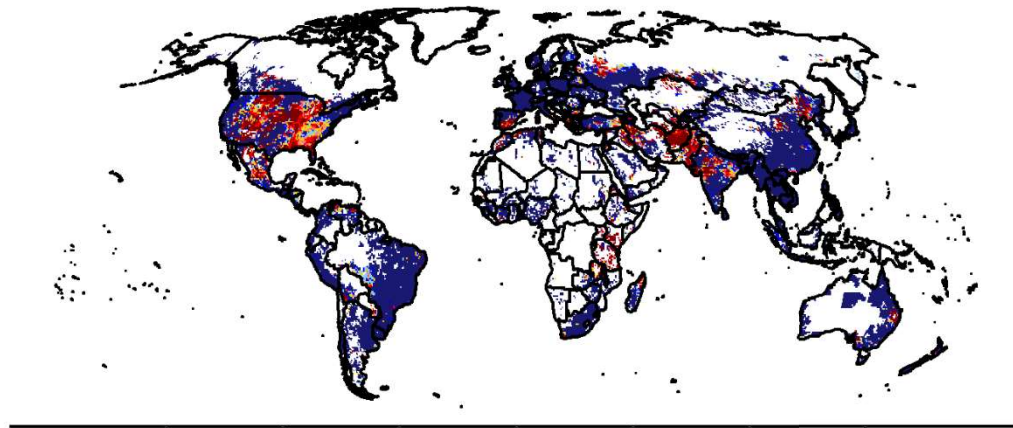
Year 1998



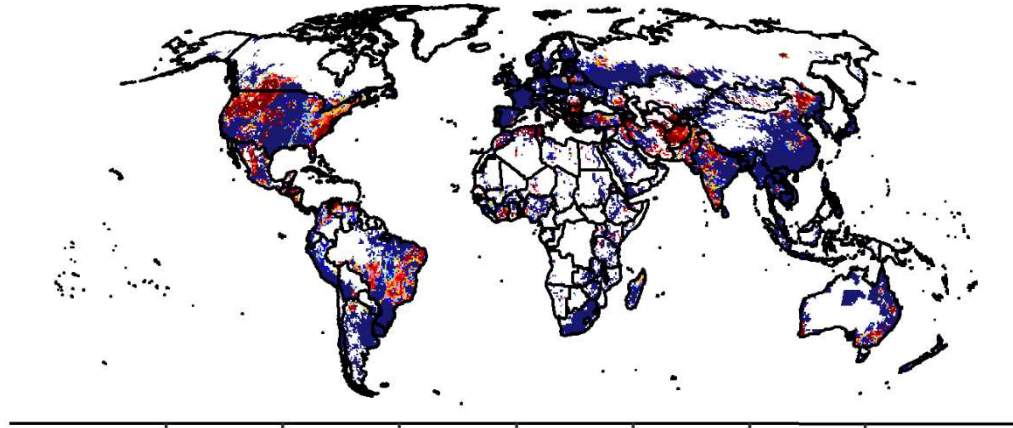
Year 1999



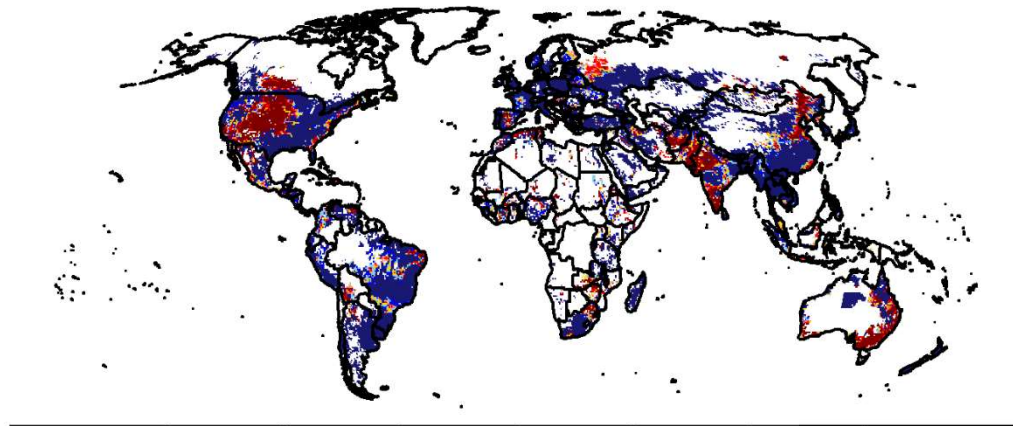
Year 2000



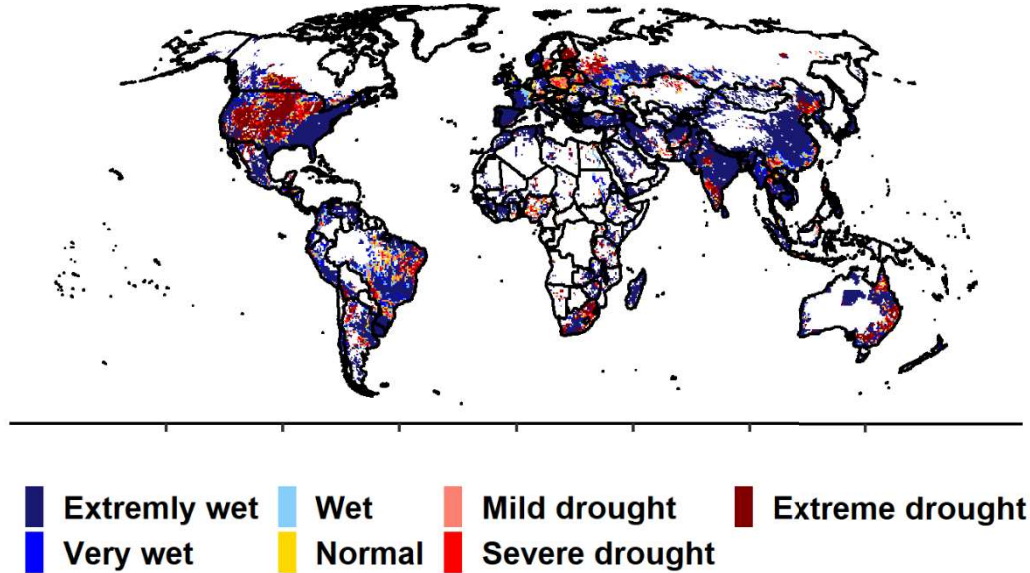
Year 2001



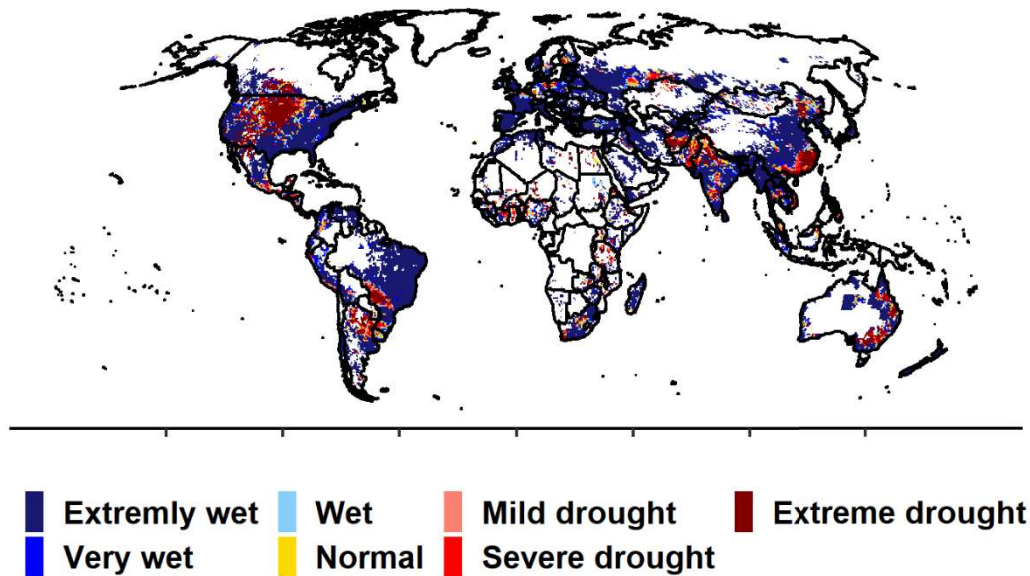
Year 2002



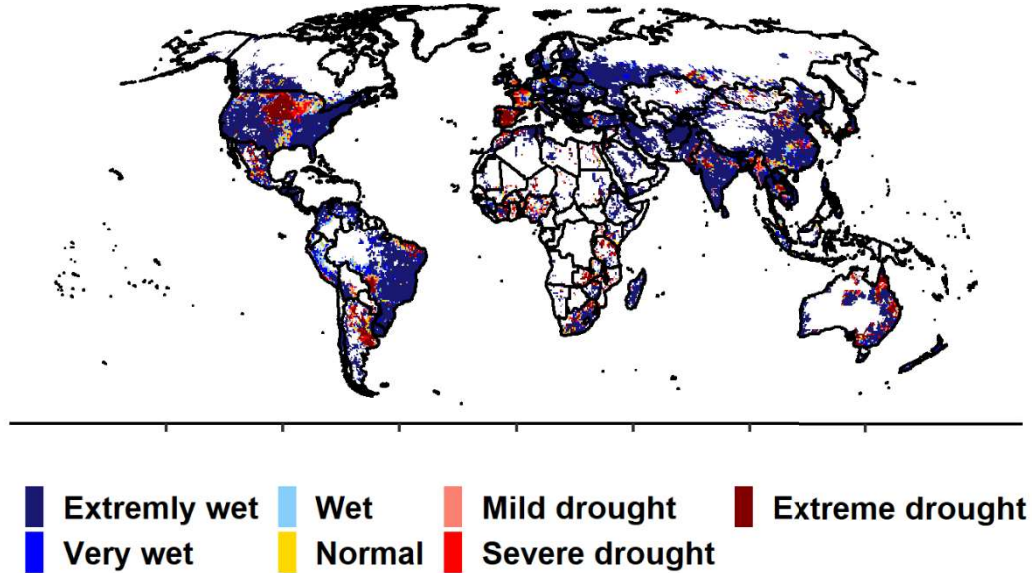
Year 2003



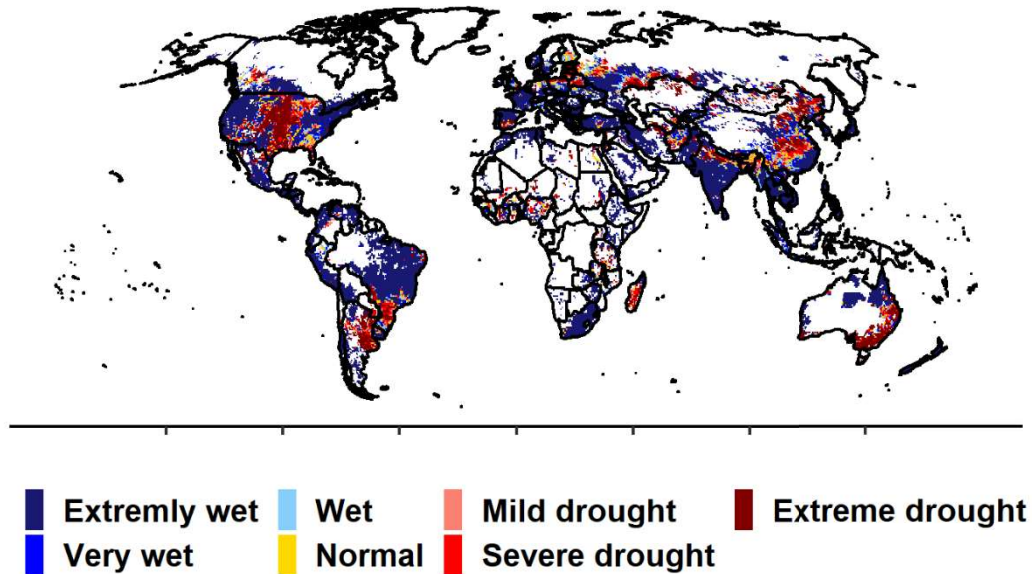
Year 2004



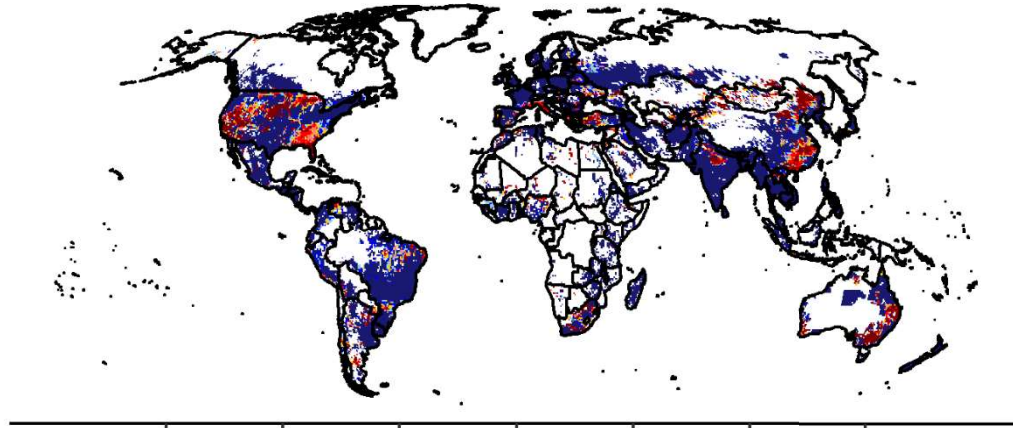
Year 2005



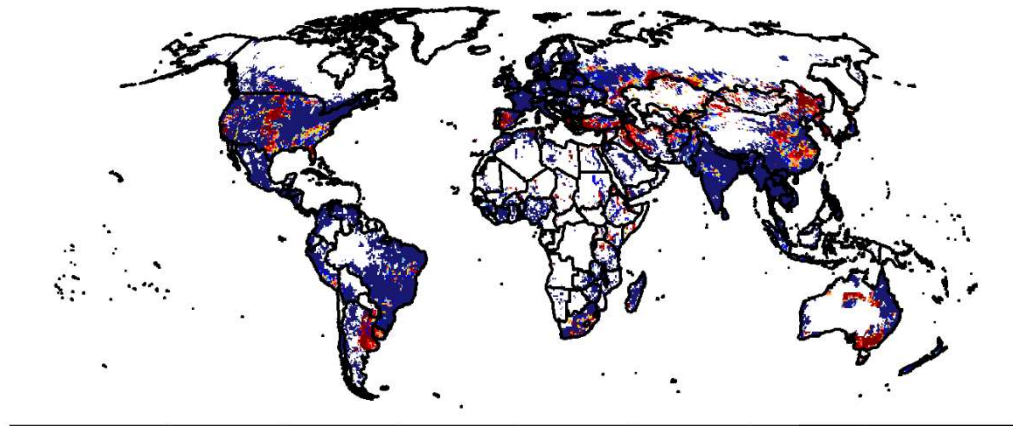
Year 2006



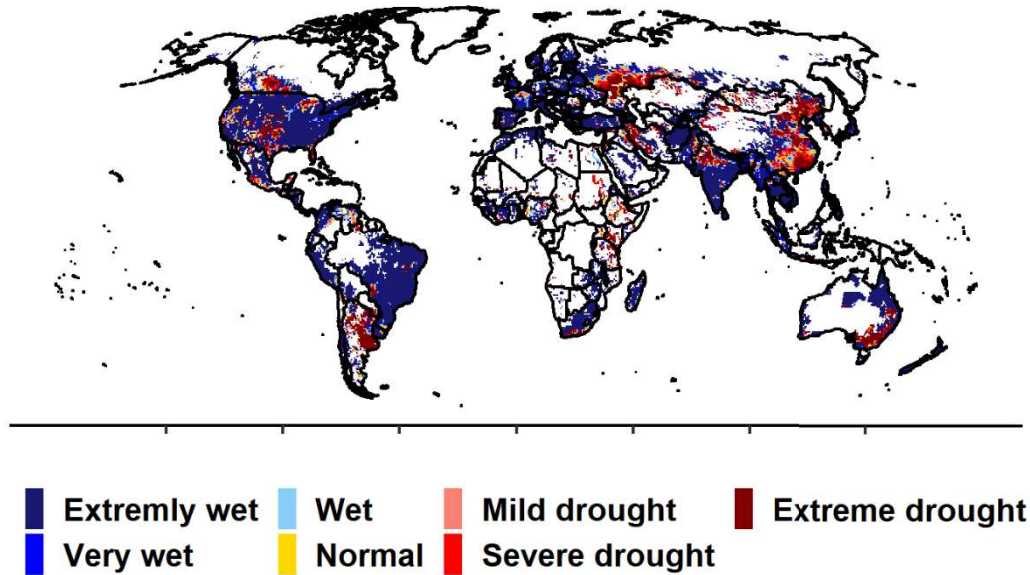
Year 2007



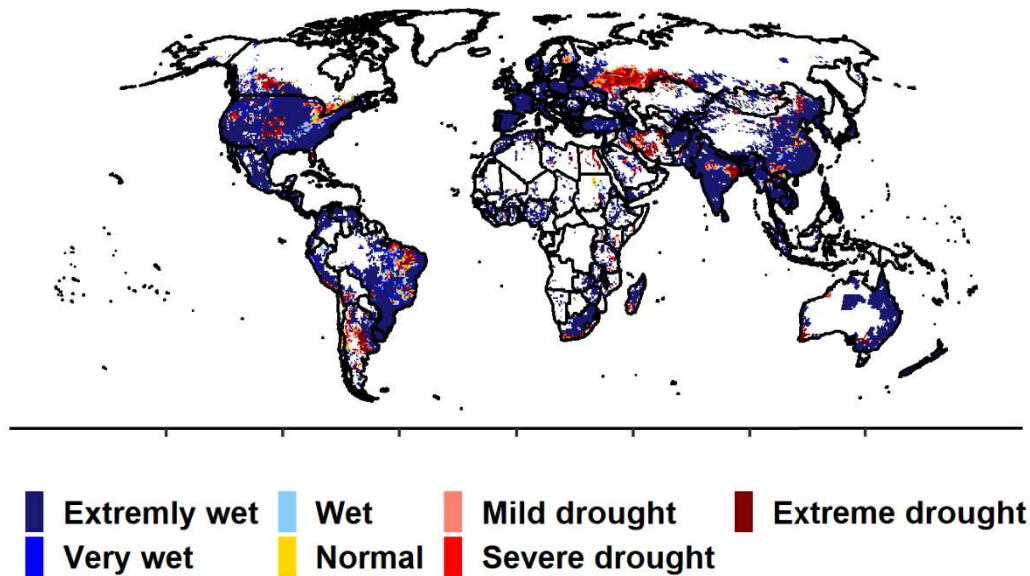
Year 2008



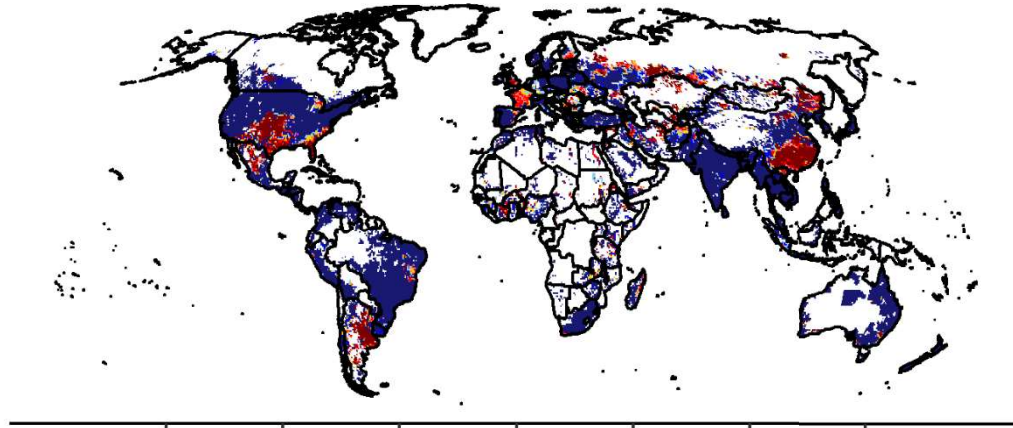
Year 2009



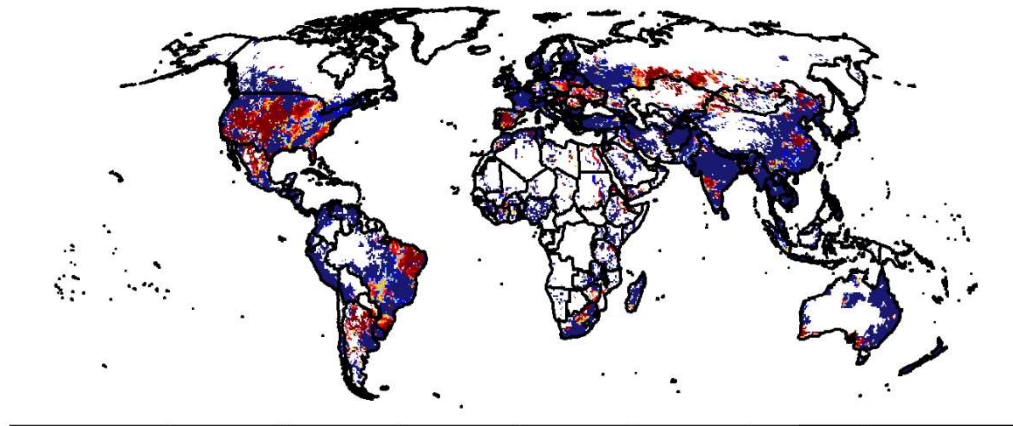
Year 2010



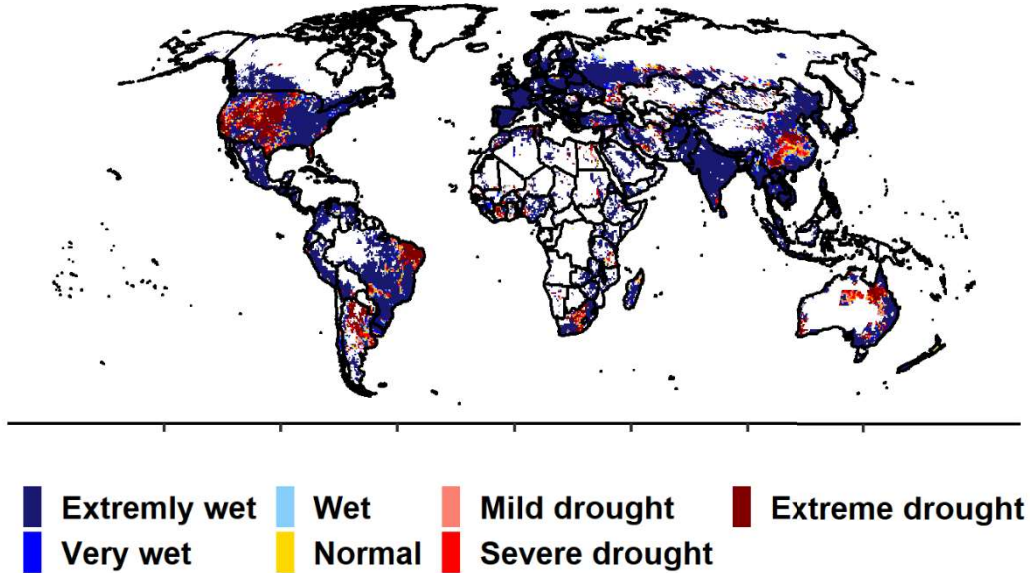
Year 2011



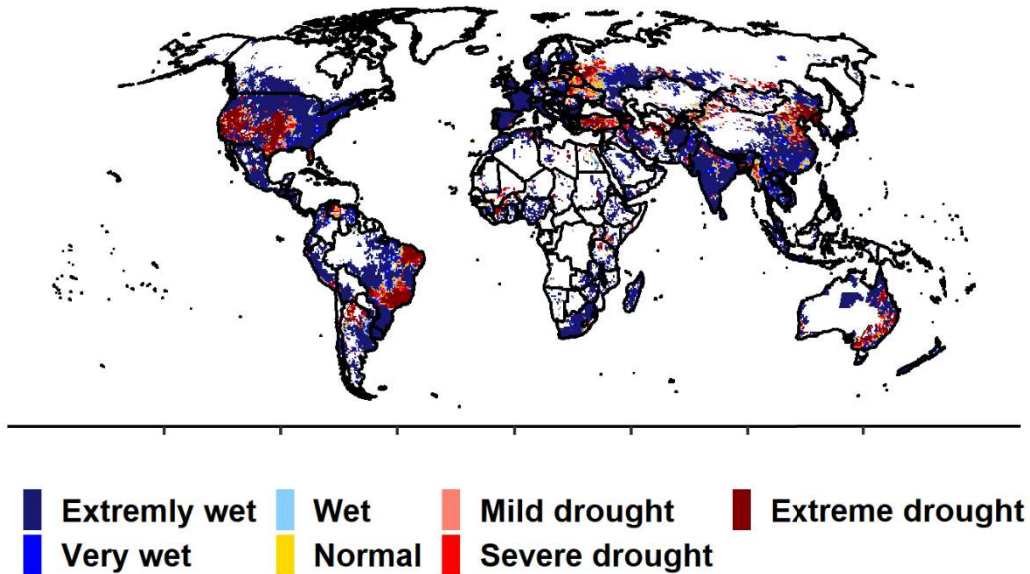
Year 2012



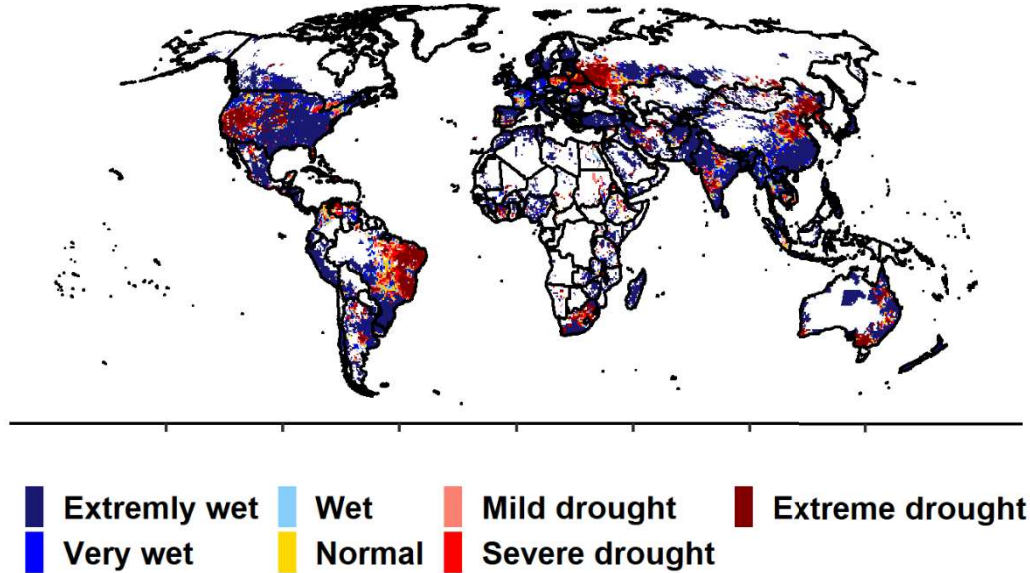
Year 2013



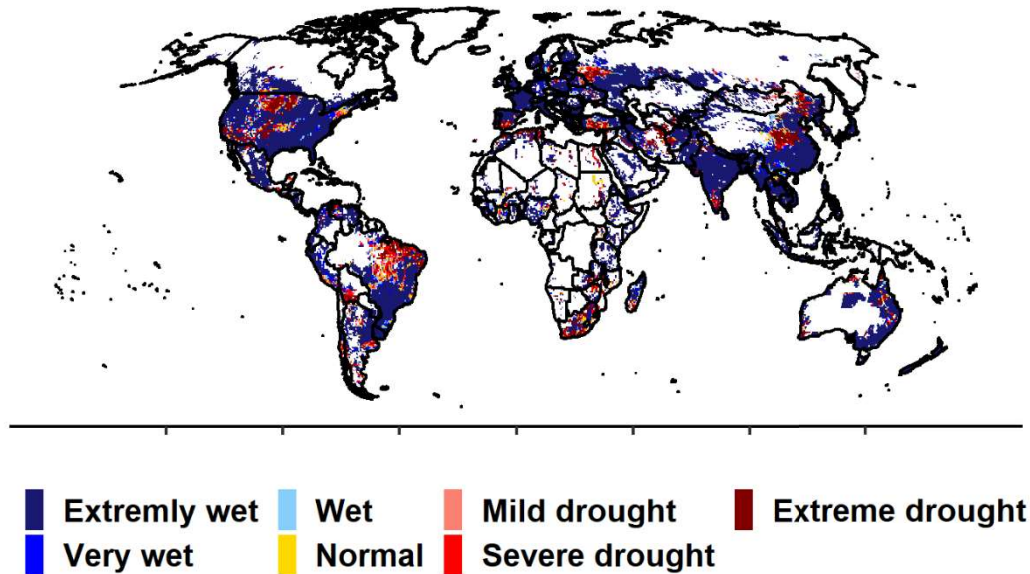
Year 2014



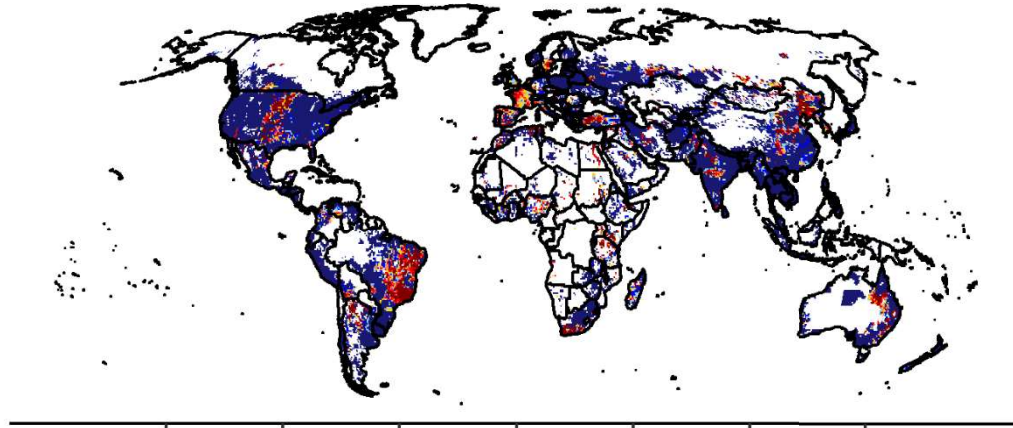
Year 2015



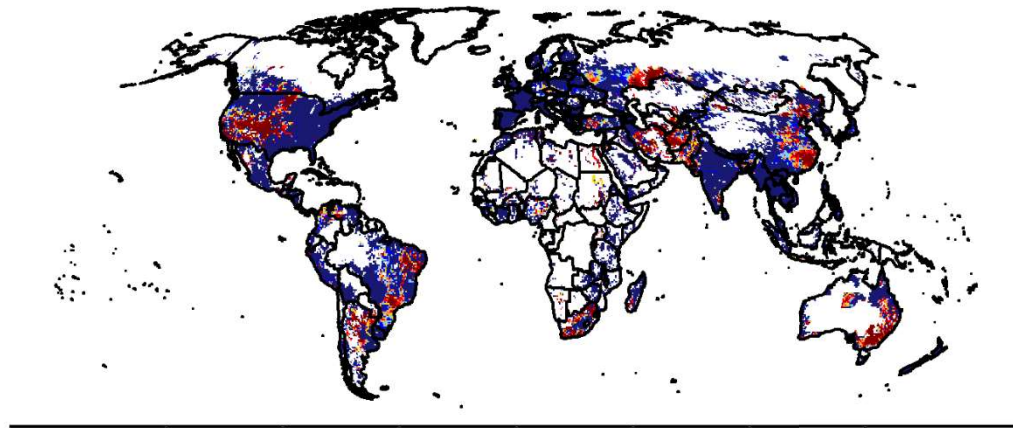
Year 2016



Year 2017



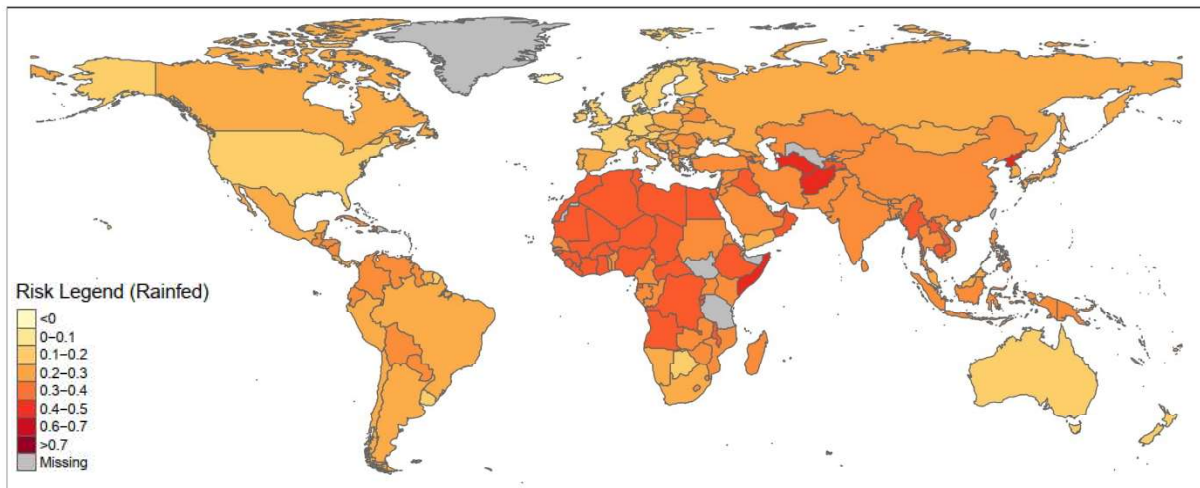
Year 2018



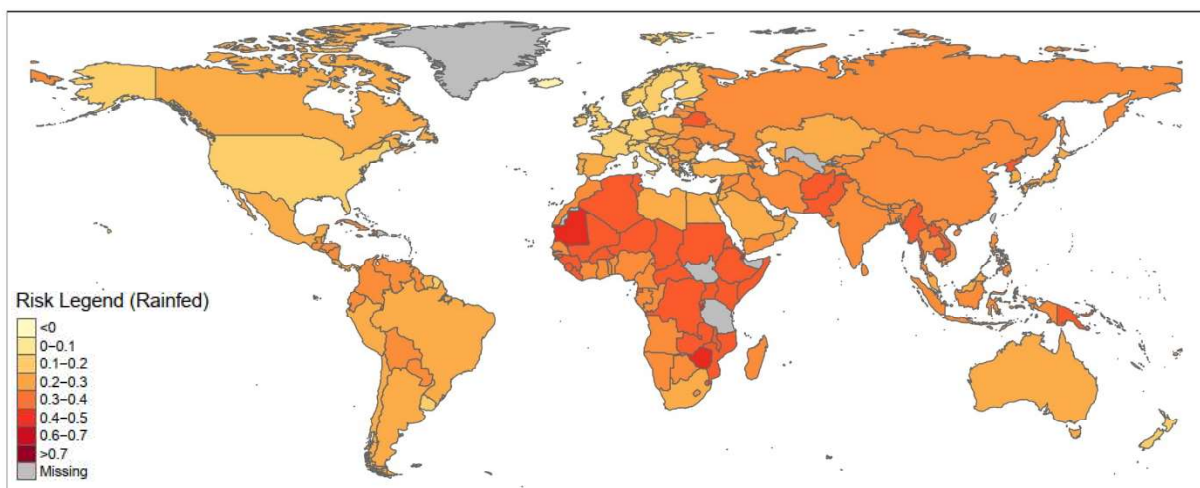
Appendix A2 - Time series of global drought risk at country level (2000-2018)

1. Rainfed agricultural systems

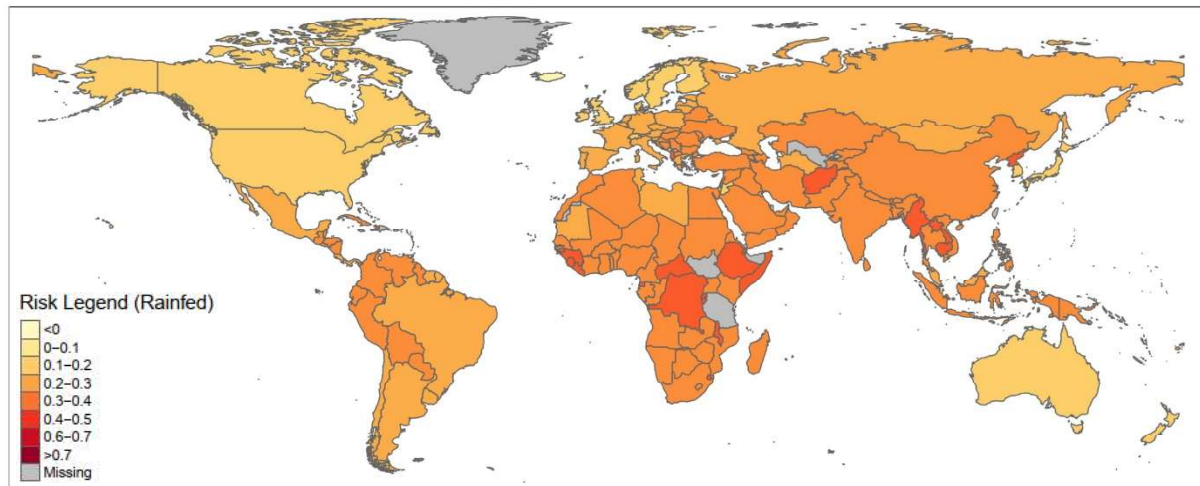
2001 – Drought risk of rainfed agricultural systems



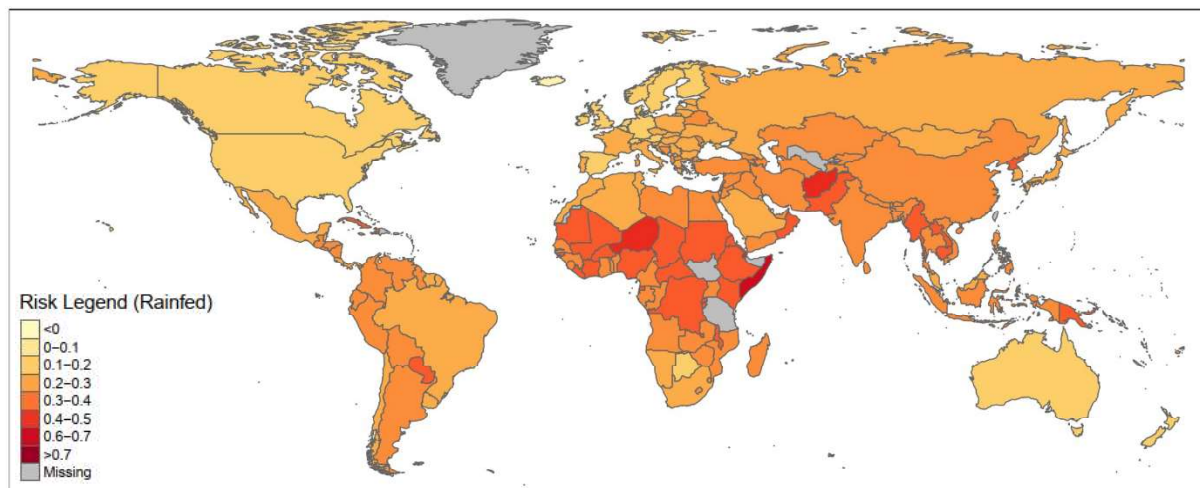
2002 – Drought risk of rainfed agricultural systems



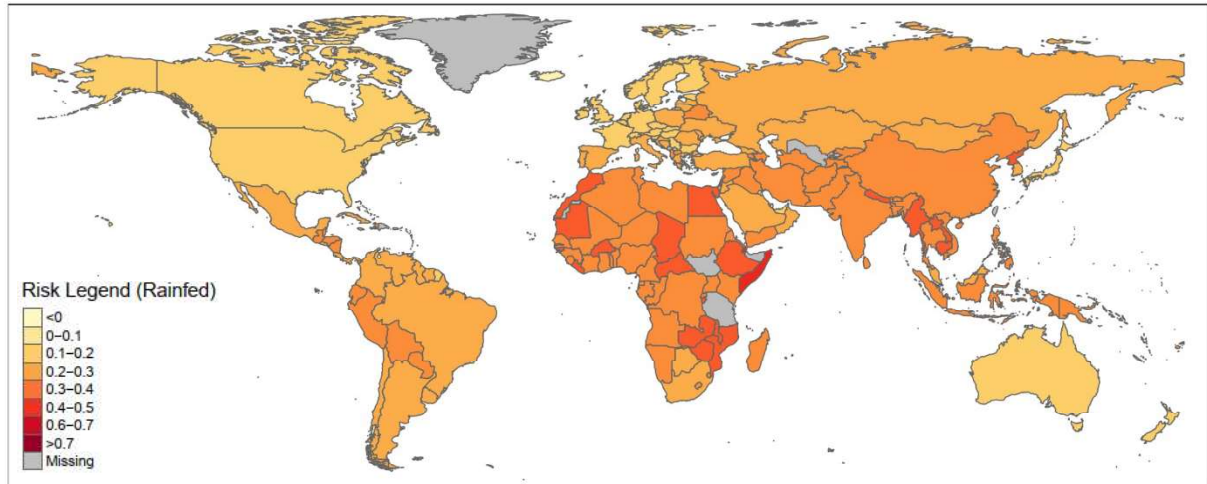
2003 – Drought risk of rainfed agricultural systems



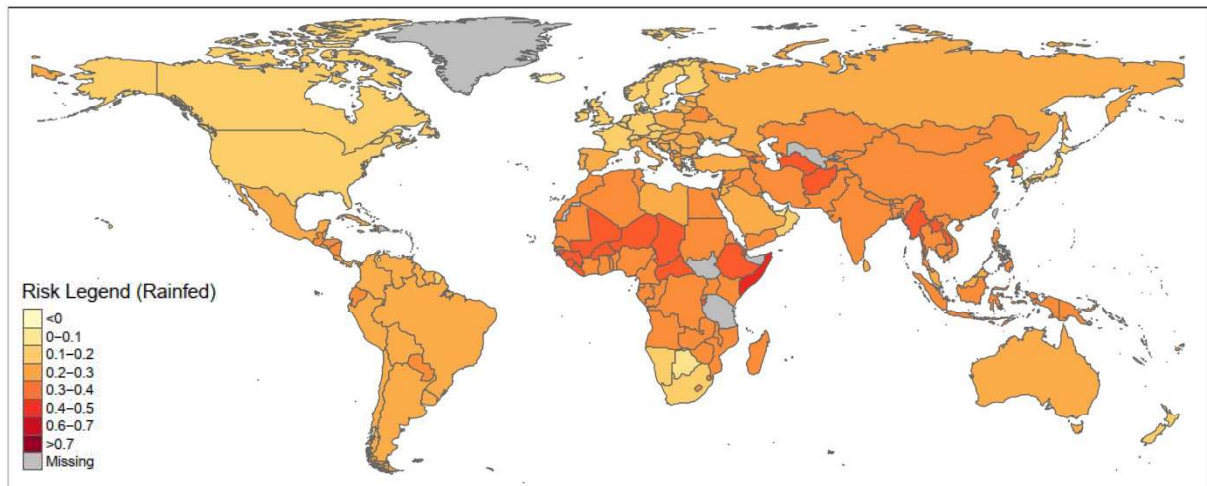
2004 – Drought risk of rainfed agricultural systems



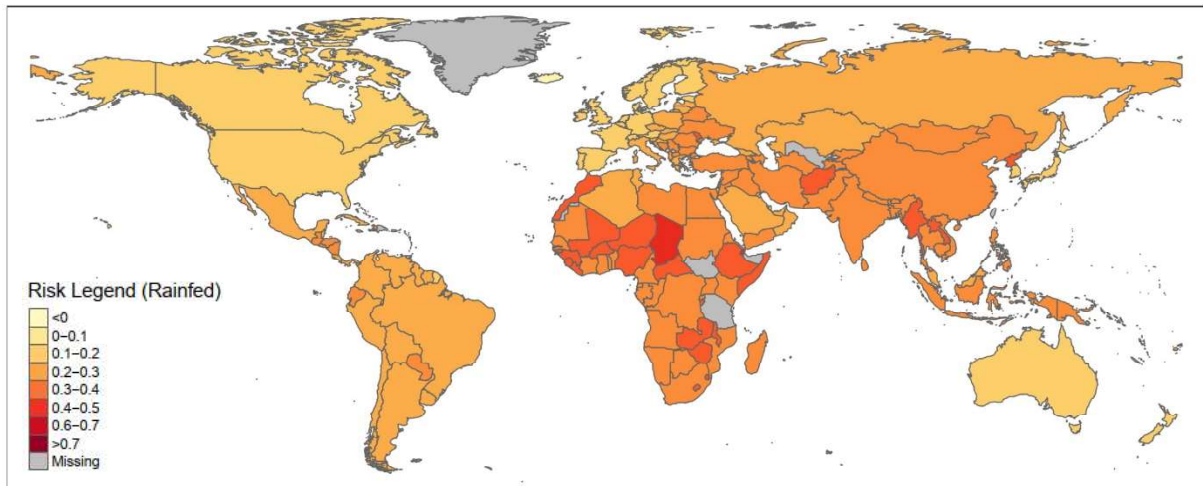
2005 – Drought risk of rainfed agricultural systems



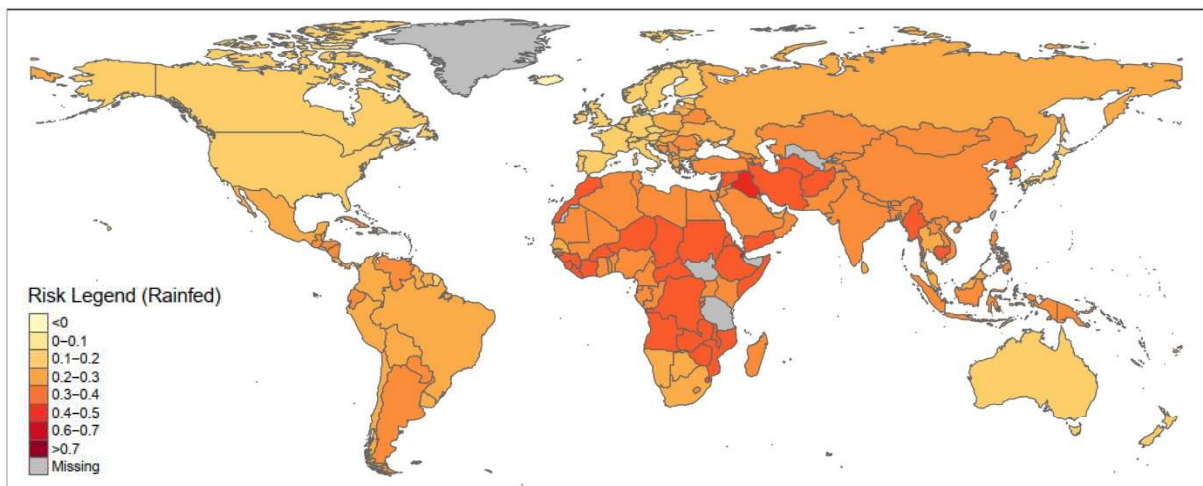
2006 – Drought risk of rainfed agricultural systems



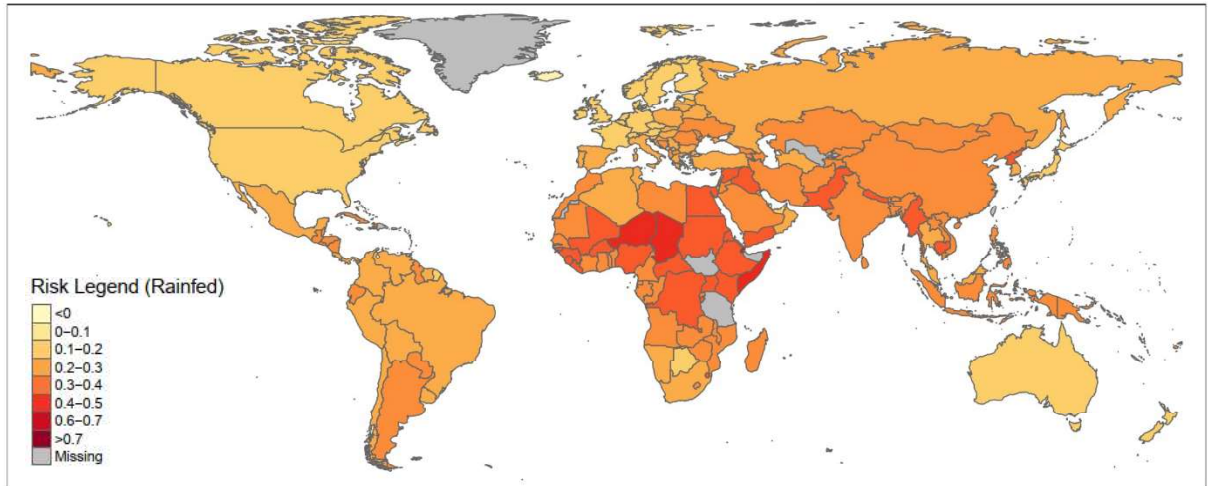
2007 – Drought risk of rainfed agricultural systems



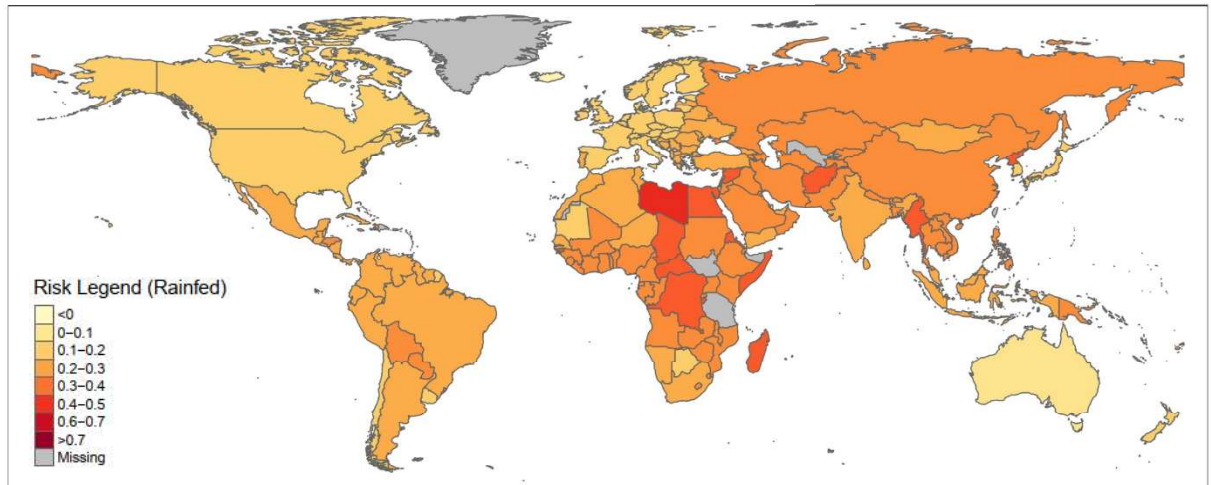
2008 – Drought risk of rainfed agricultural systems



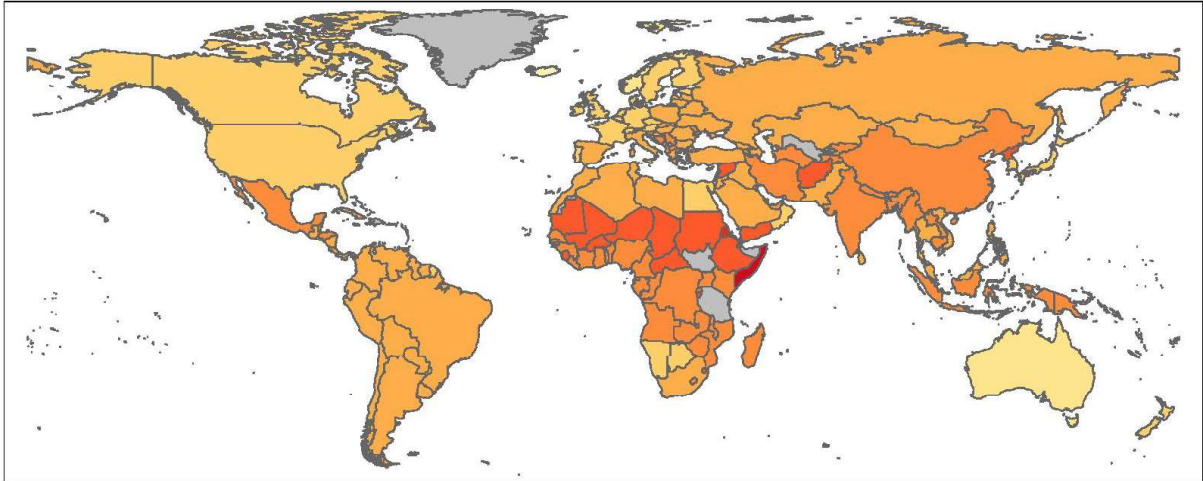
2009 – Drought risk of rainfed agricultural systems



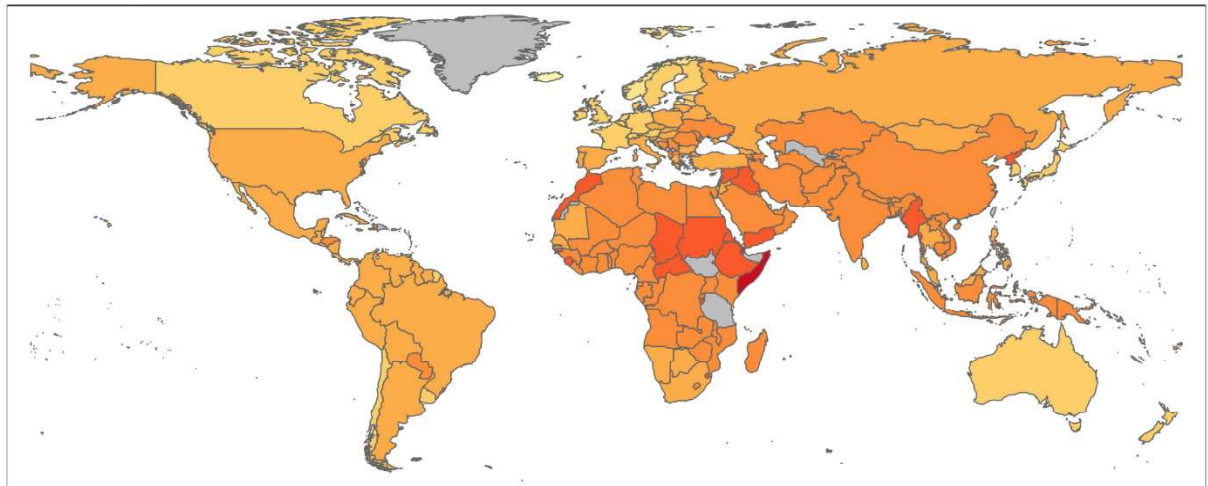
2010 – Drought risk of rainfed agricultural systems



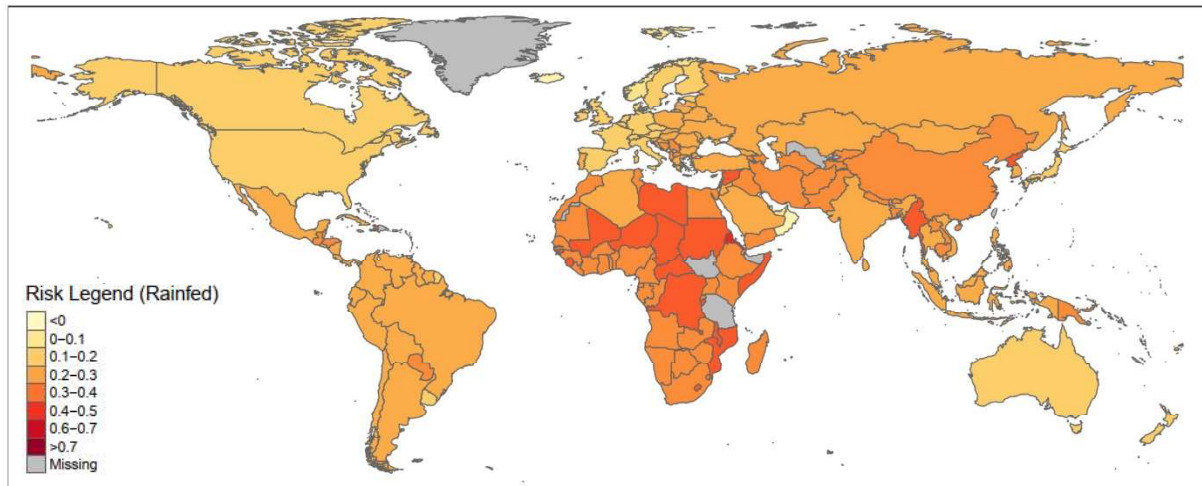
2011 – Drought risk of rainfed agricultural systems



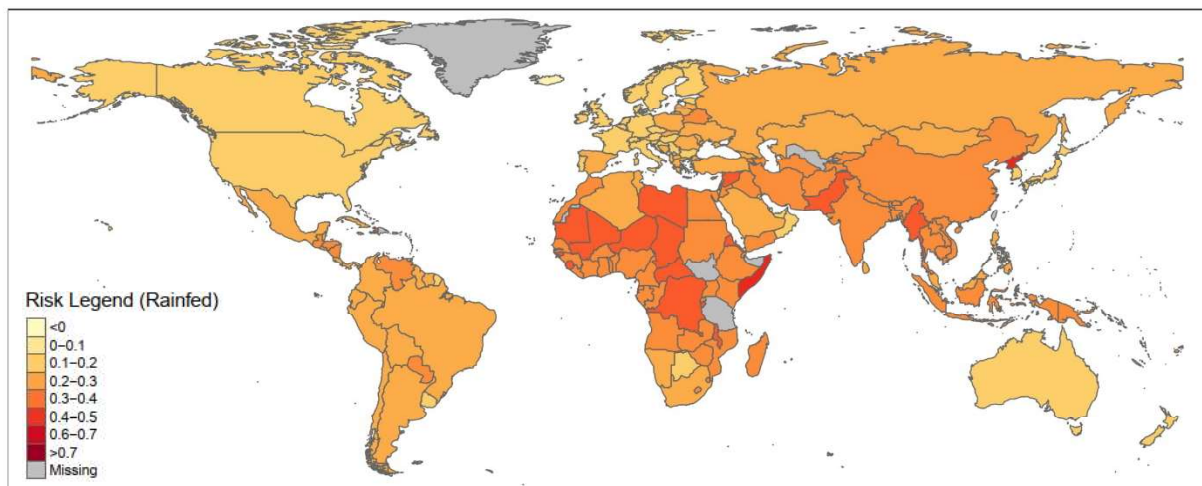
2012 – Drought risk of rainfed agricultural systems



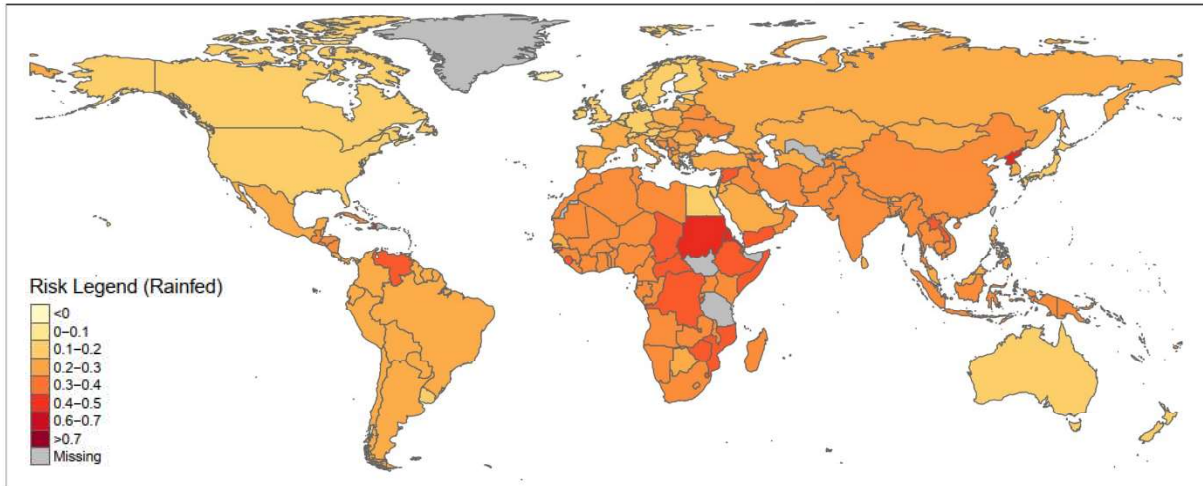
2013 – Drought risk of rainfed agricultural systems



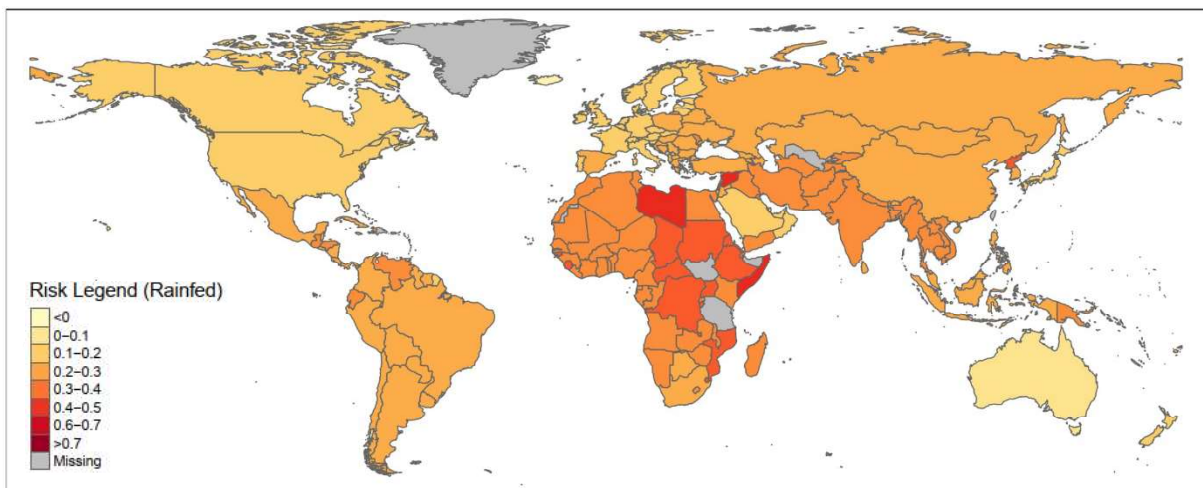
2014 – Drought risk of rainfed agricultural systems



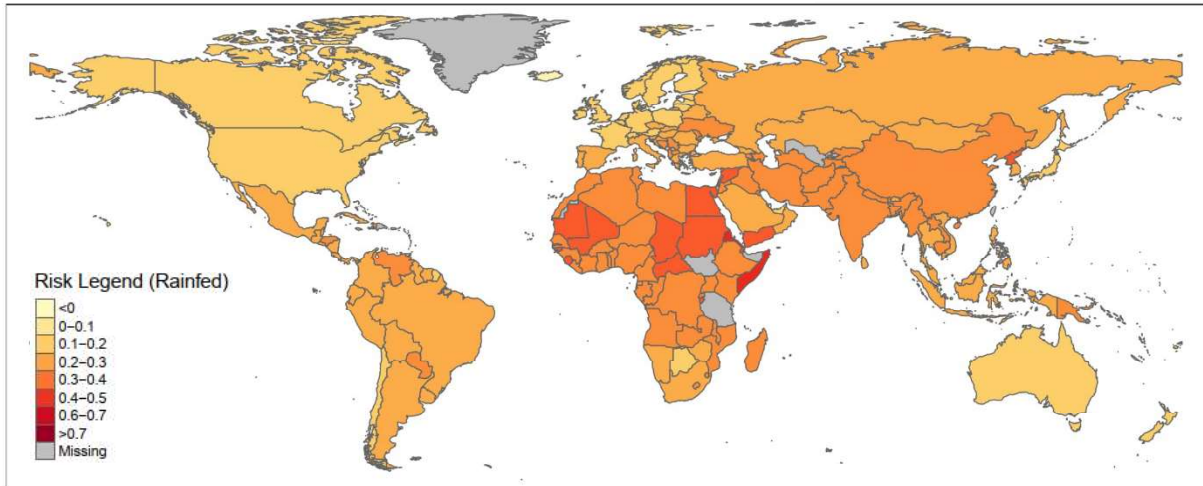
2015 – Drought risk of rainfed agricultural systems



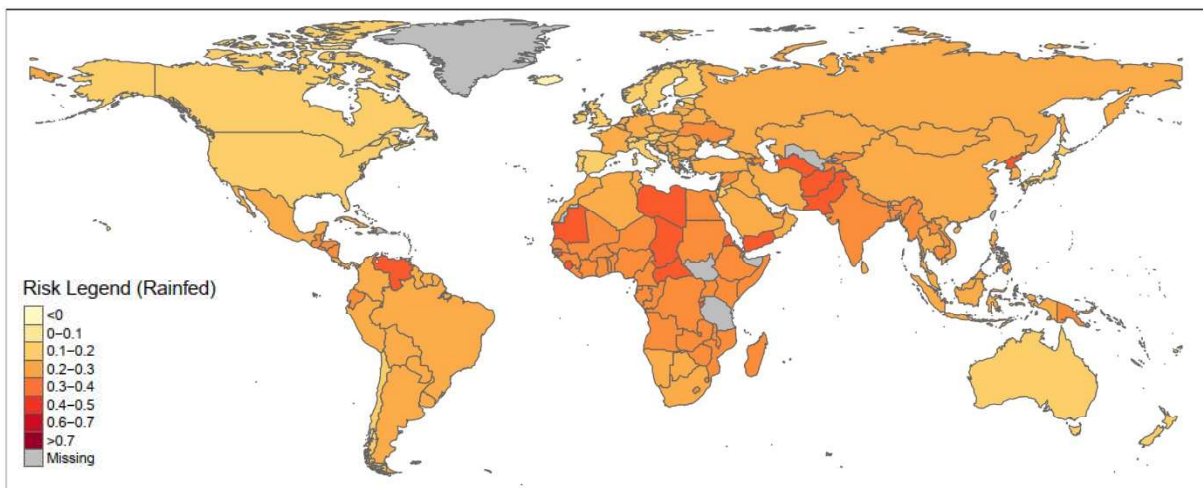
2016 – Drought risk of rainfed agricultural systems



2017 – Drought risk of rainfed agricultural systems

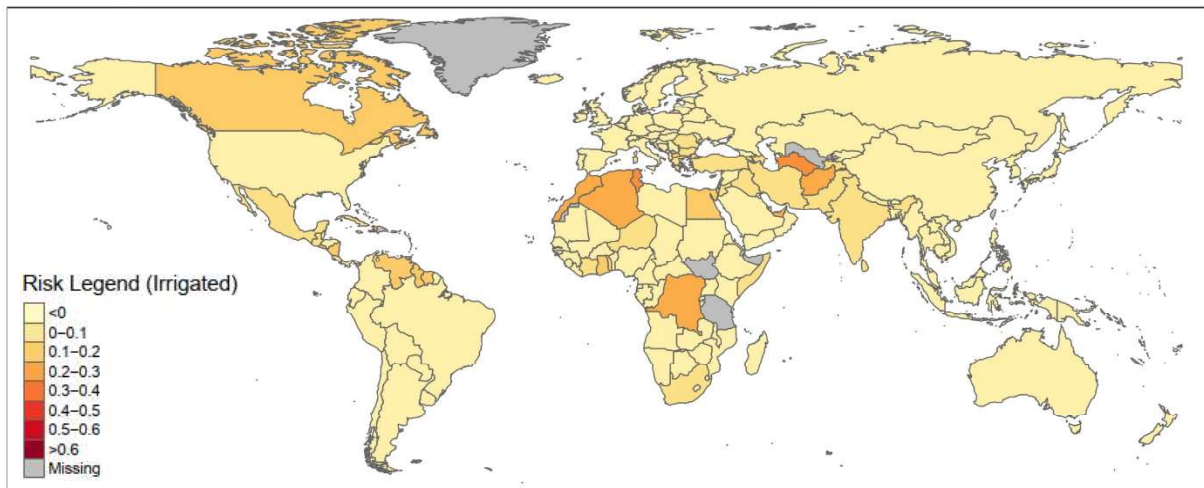


2018 – Drought risk of rainfed agricultural systems

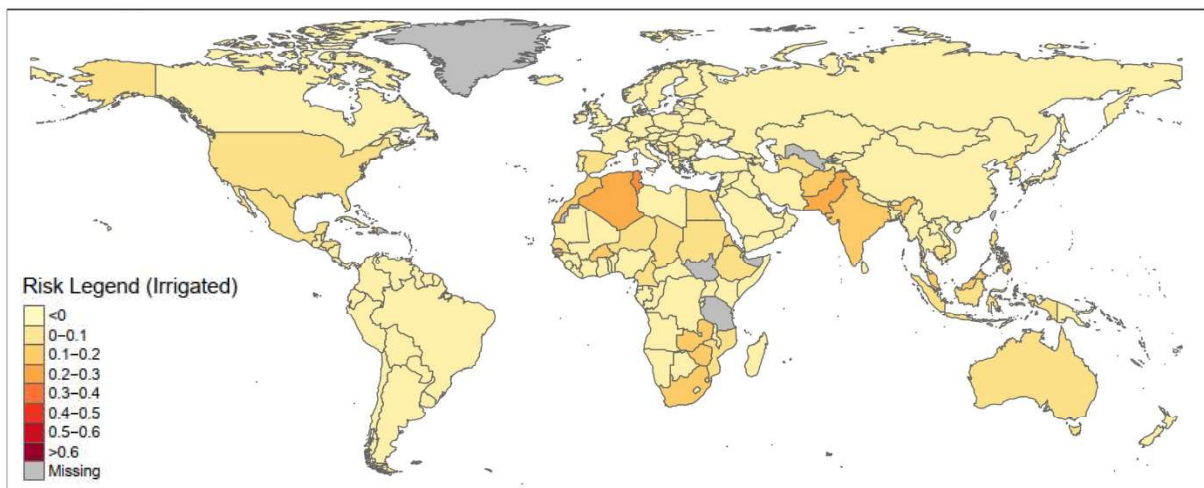


2. Irrigated agricultural systems

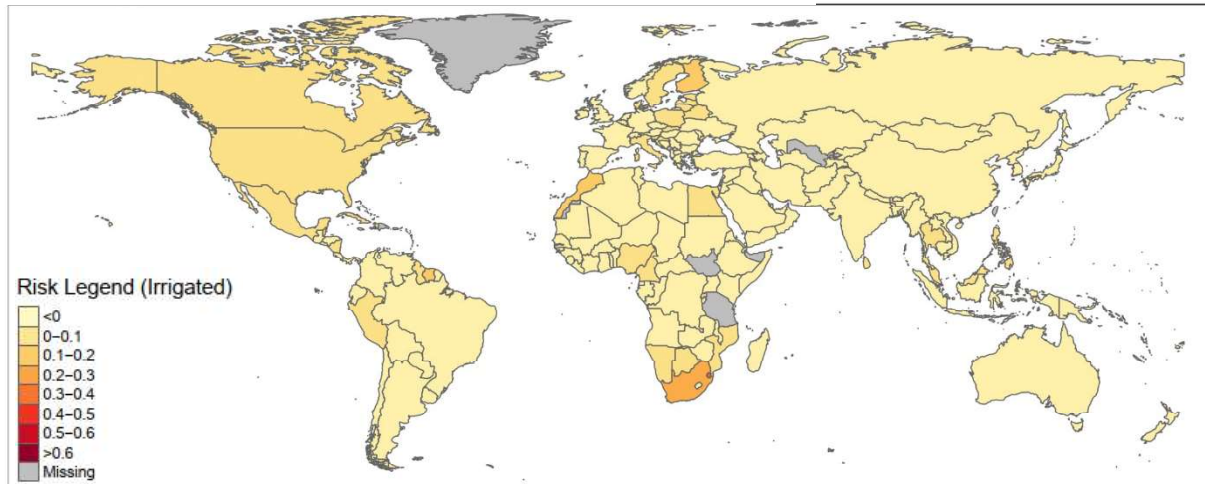
2001 – Drought risk of irrigated agricultural systems



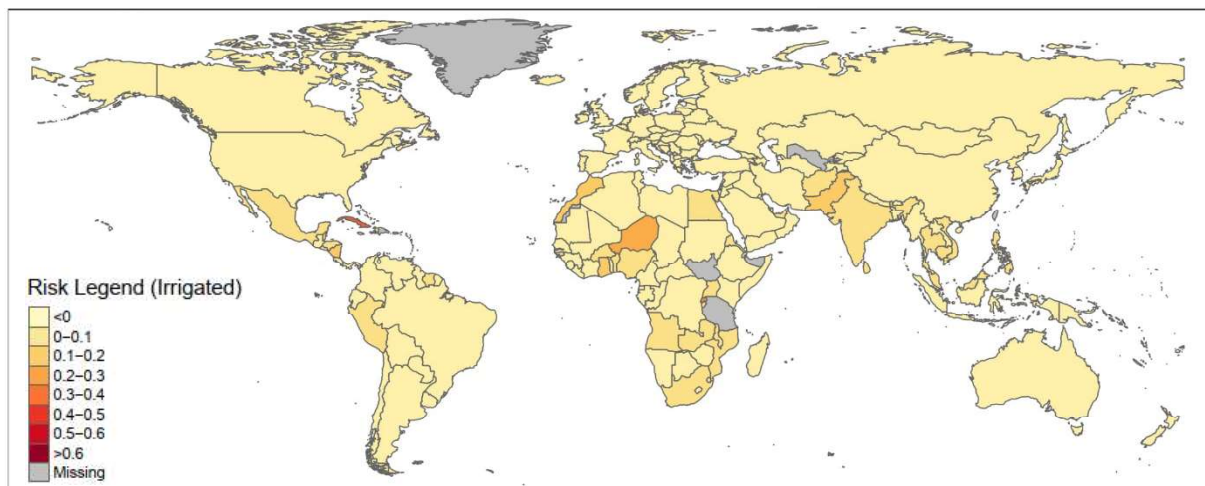
2002 – Drought risk of irrigated agricultural systems



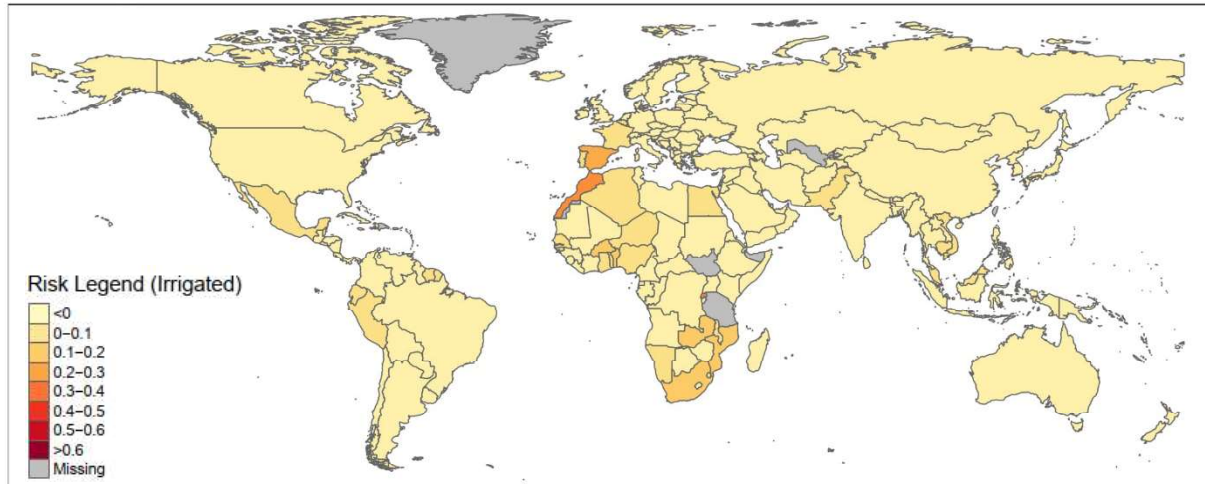
2003 – Drought risk of irrigated agricultural systems



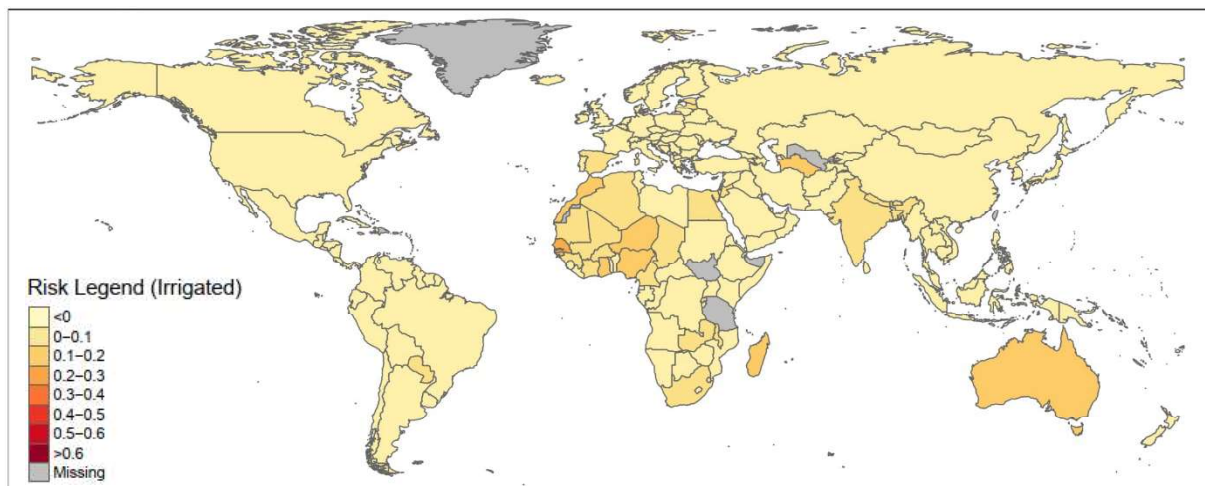
2004 – Drought risk of irrigated agricultural systems



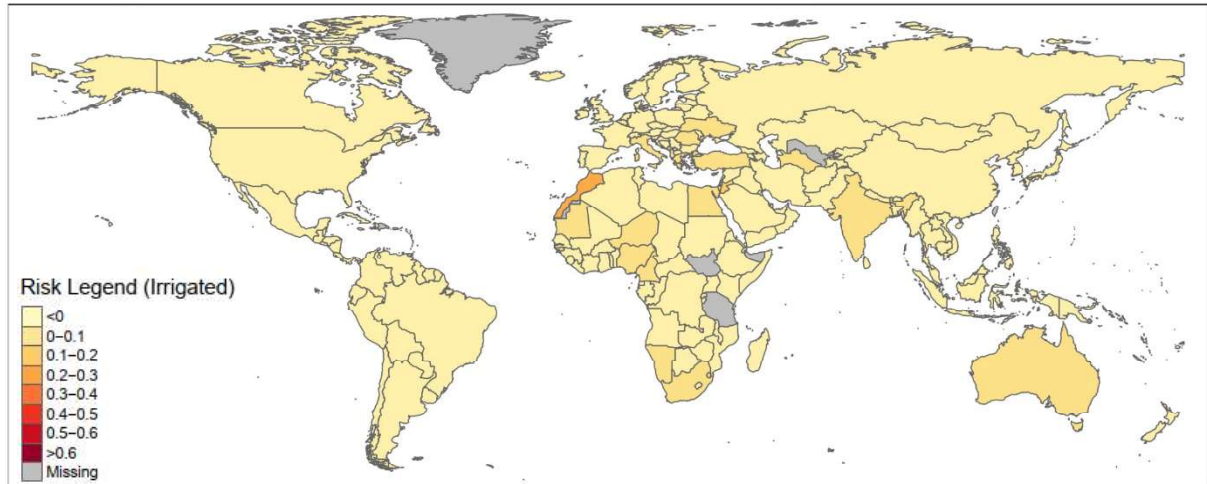
2005 – Drought risk of irrigated agricultural systems



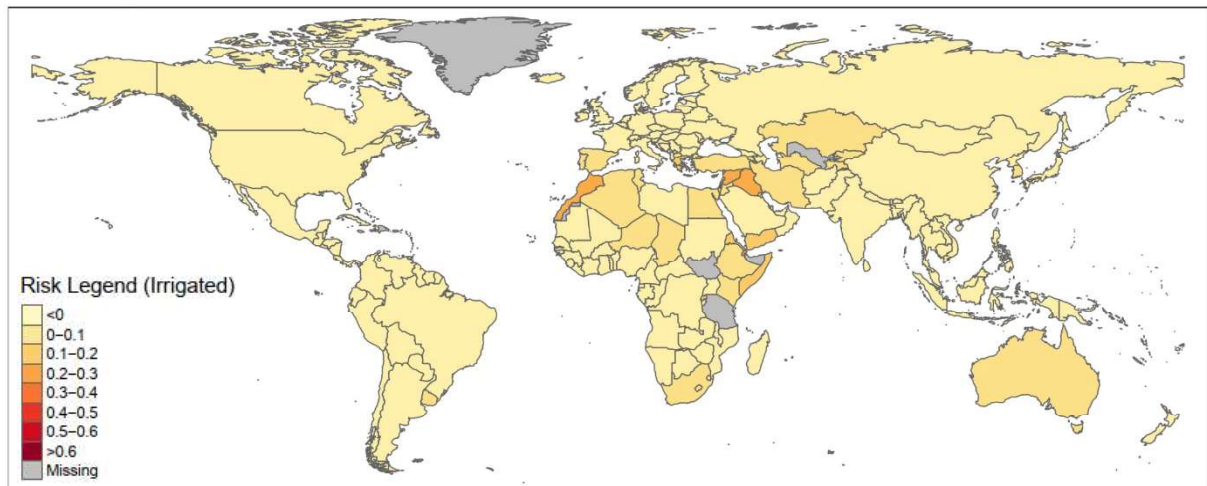
2006 – Drought risk of irrigated agricultural systems



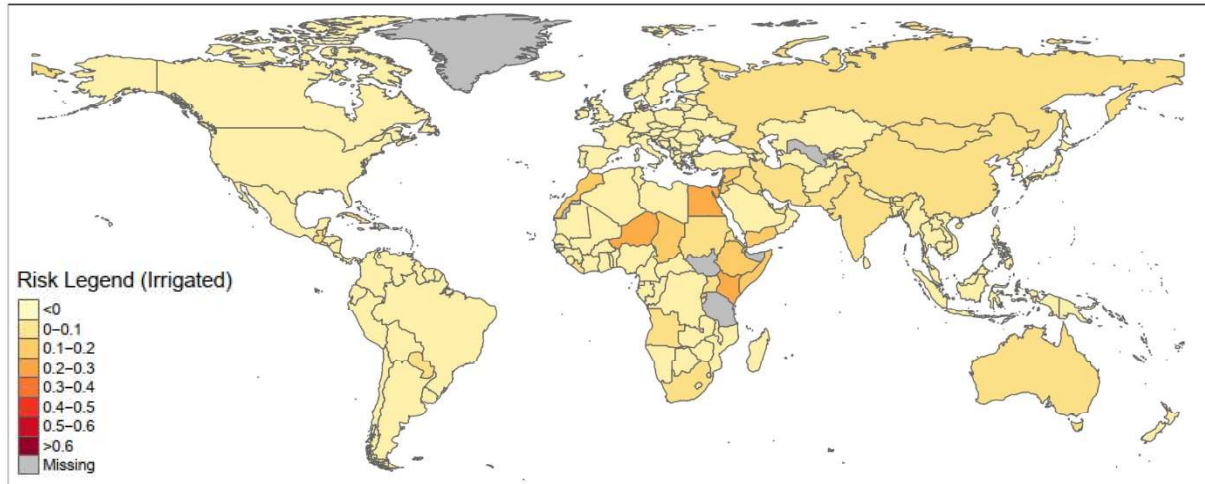
2007 – Drought risk of irrigated agricultural systems



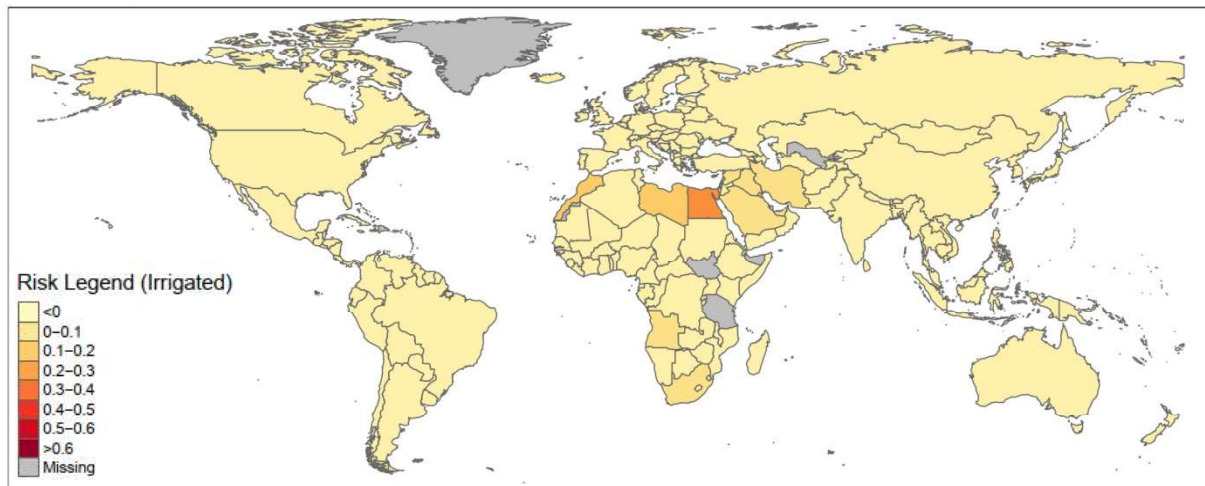
2008 – Drought risk of irrigated agricultural systems



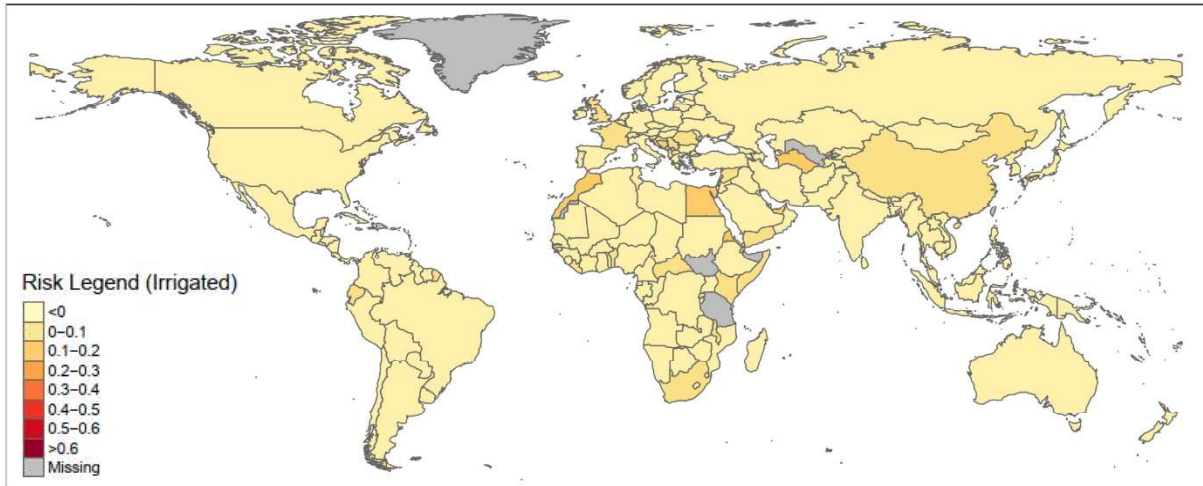
2009 – Drought risk of irrigated agricultural systems



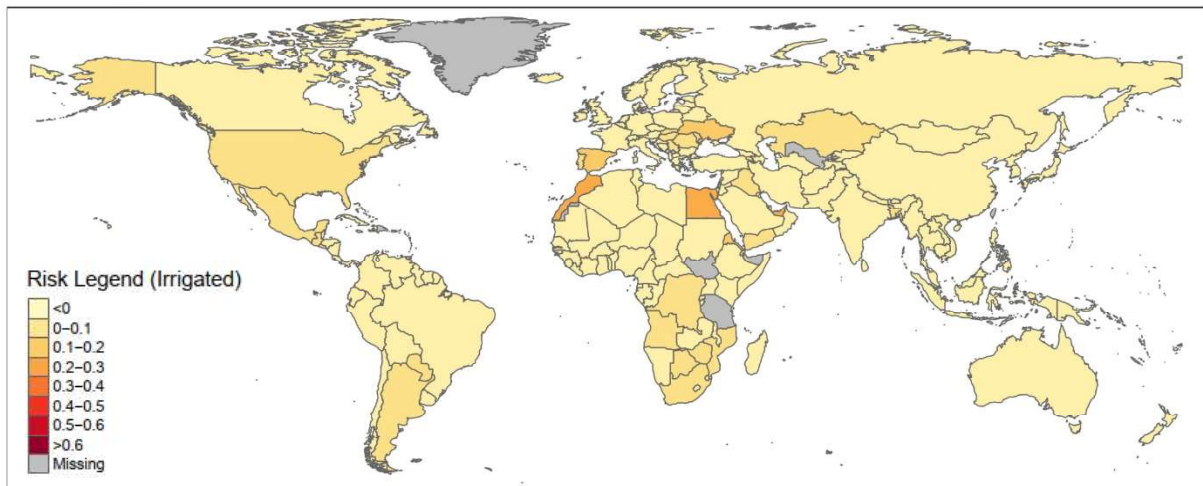
2010 – Drought risk of irrigated agricultural systems



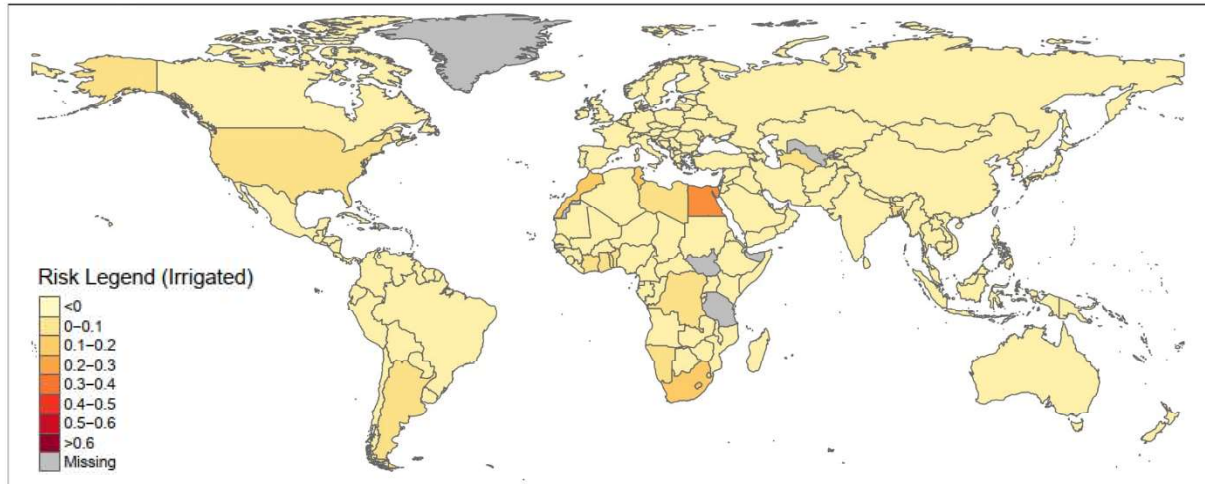
2011 – Drought risk of irrigated agricultural systems



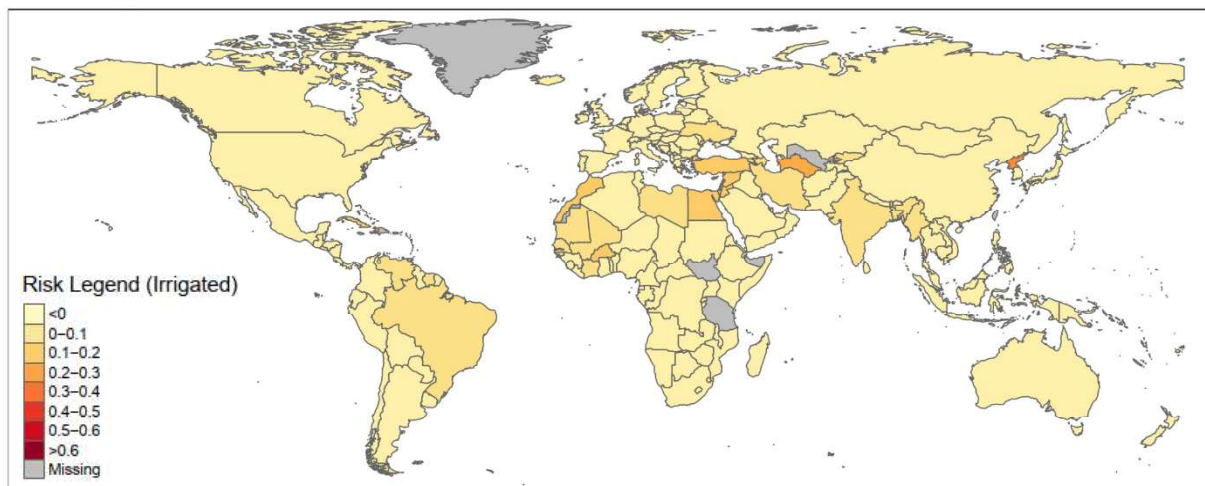
2012 – Drought risk of irrigated agricultural systems



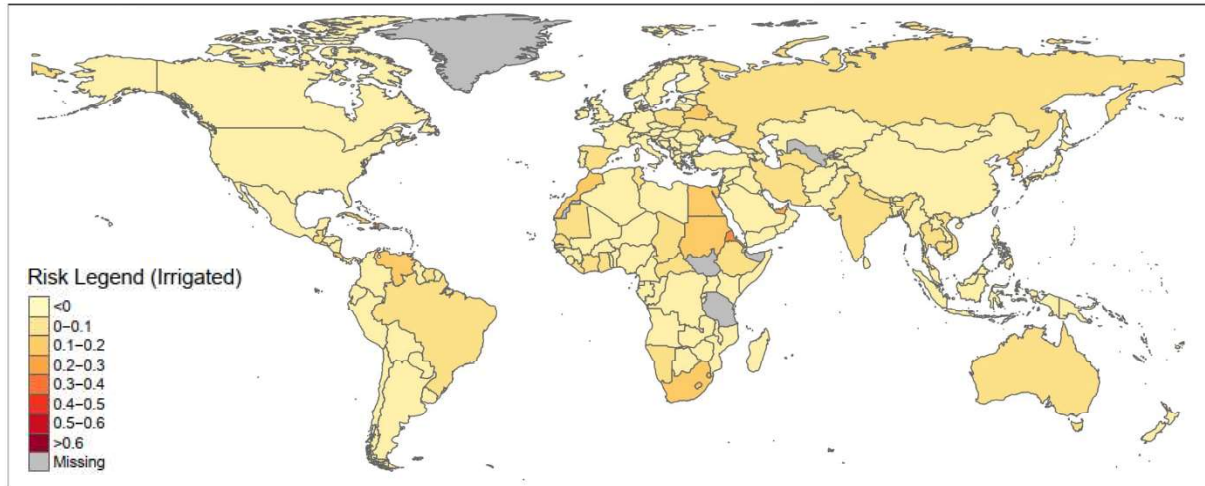
2013 – Drought risk of irrigated agricultural systems



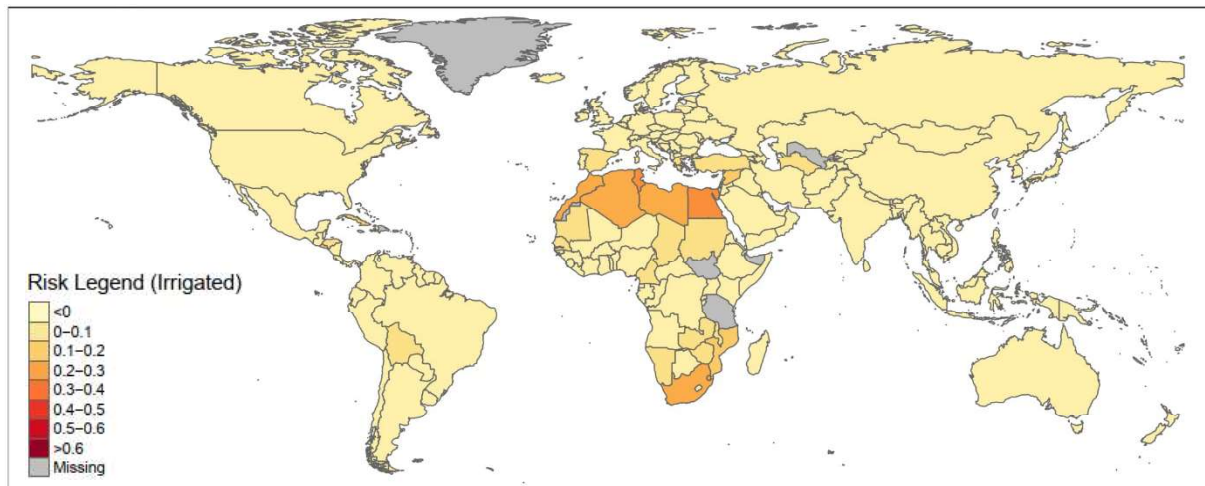
2014 – Drought risk of irrigated agricultural systems



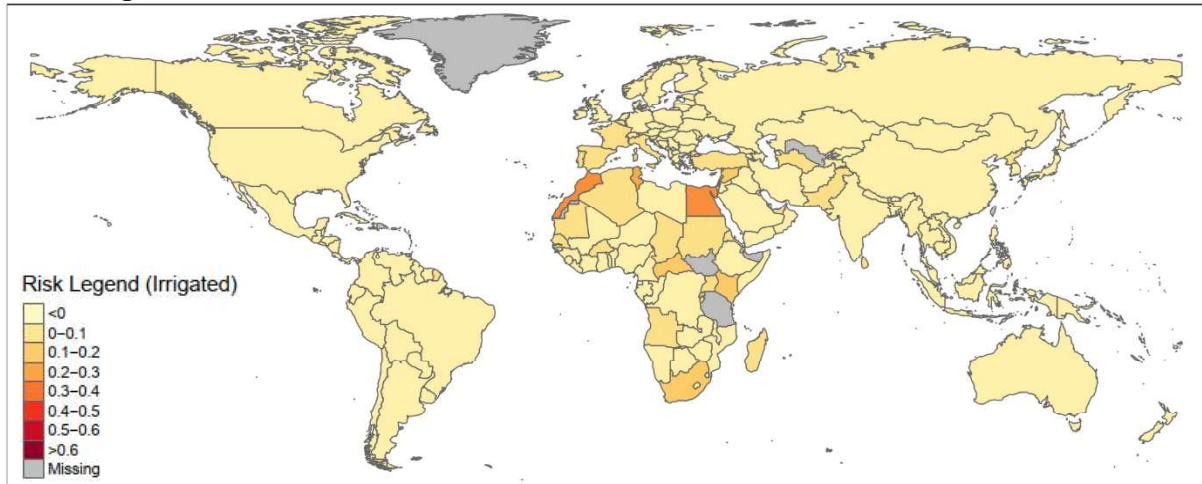
2015 – Drought risk of irrigated agricultural systems



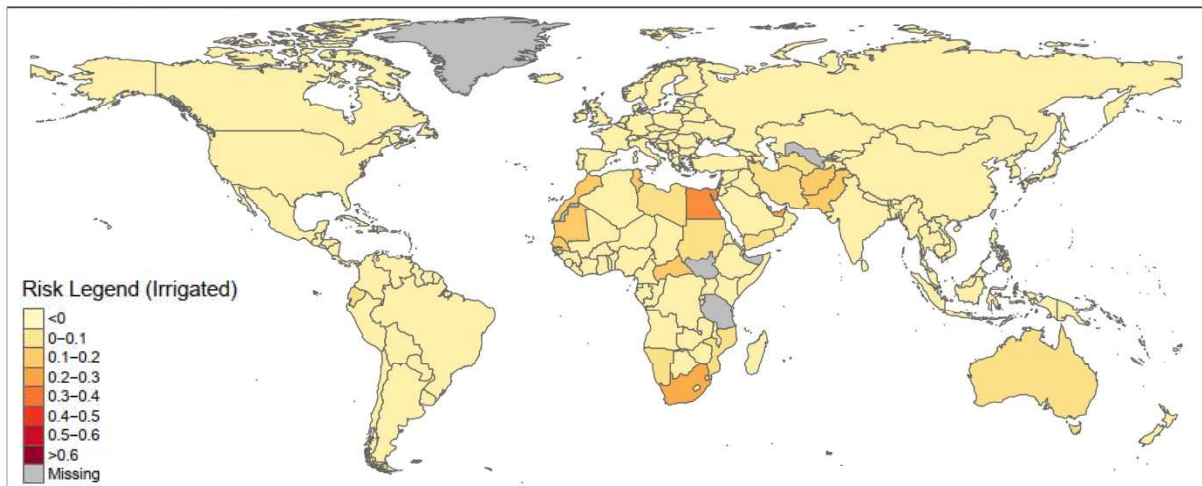
2016 – Drought risk of irrigated agricultural systems



2017 – Drought risk of irrigated agricultural systems



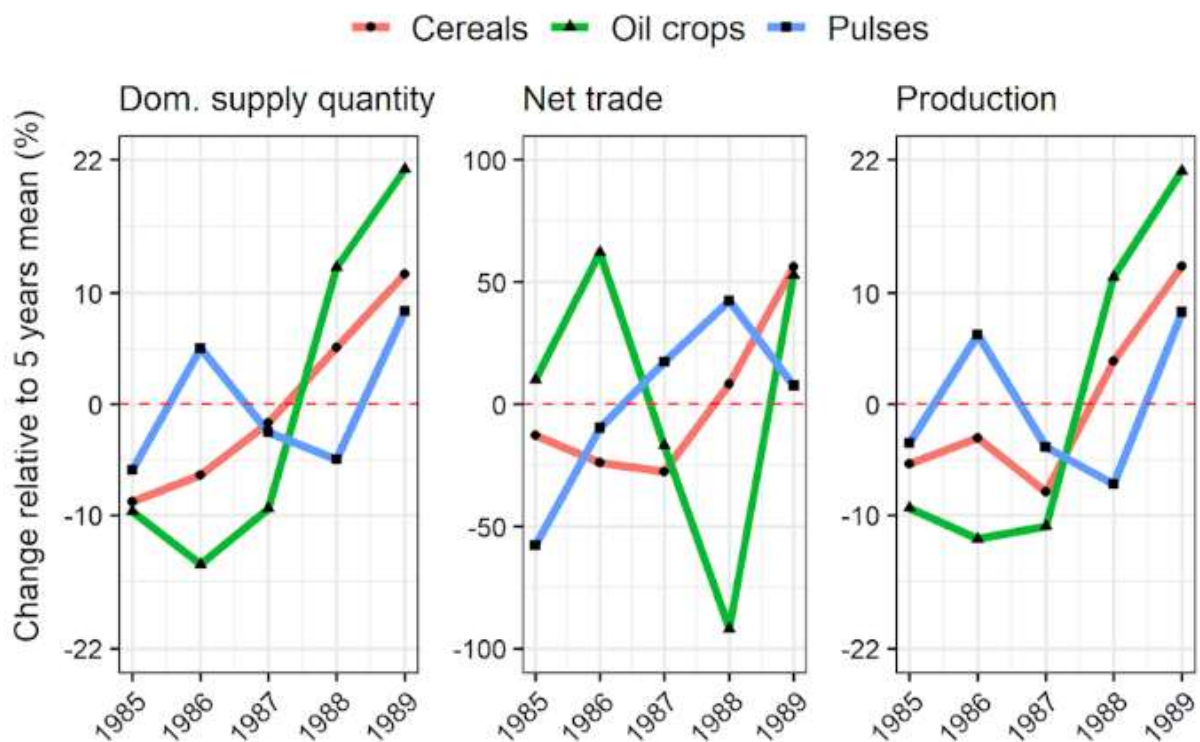
2018 – Drought risk of irrigated agricultural systems



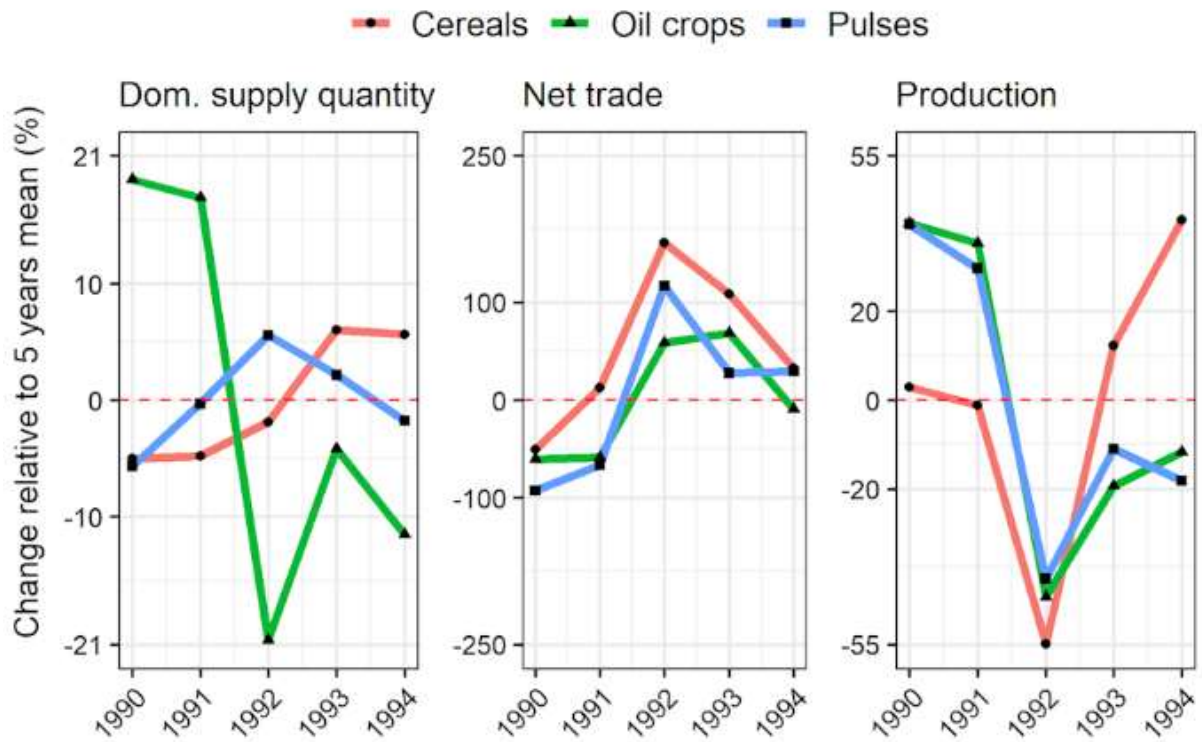
Appendix A3 - Drought impact analysis: regional anomalies in domestic food supply, net trade and production of cereals, oil crops and pulses

For three crop categories of cereals, oil crops and pulses, changes relative to the five years mean of three elements of domestic supply quantity, net trade and crop production were extracted from FAOSTAT for selected countries or regions for the years around their most extreme drought events (drought year, two years before and two years after).

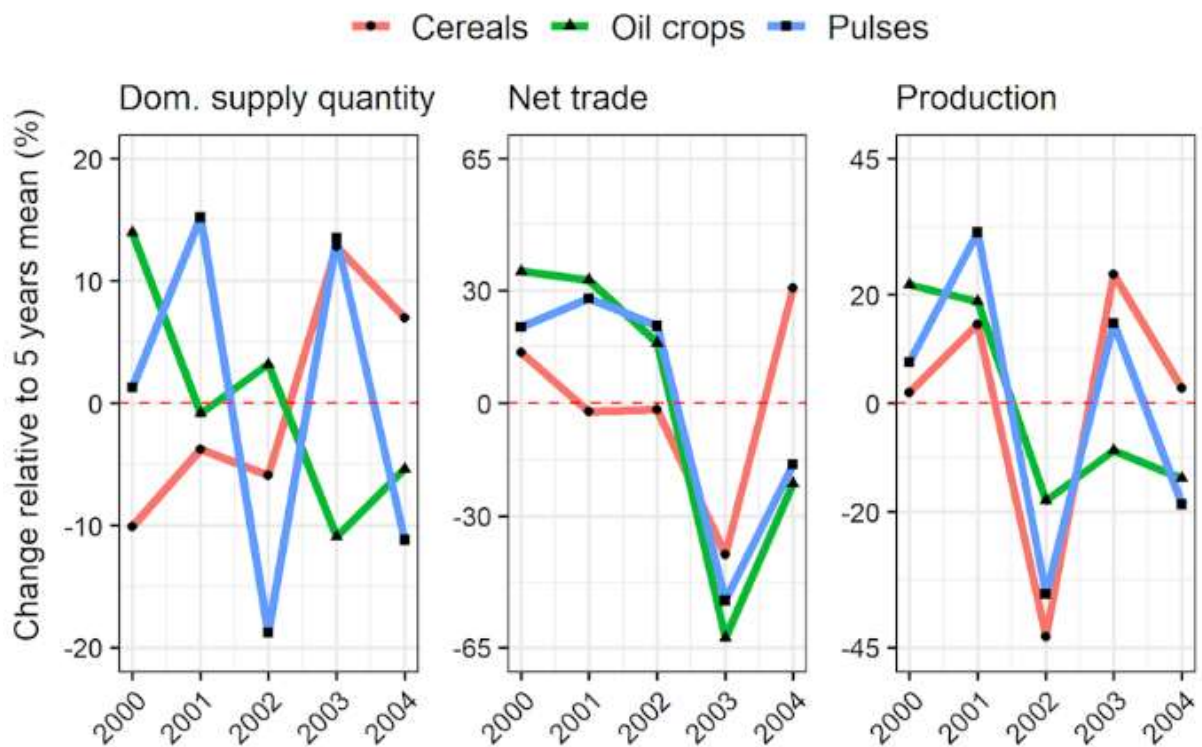
South Asia (1987)



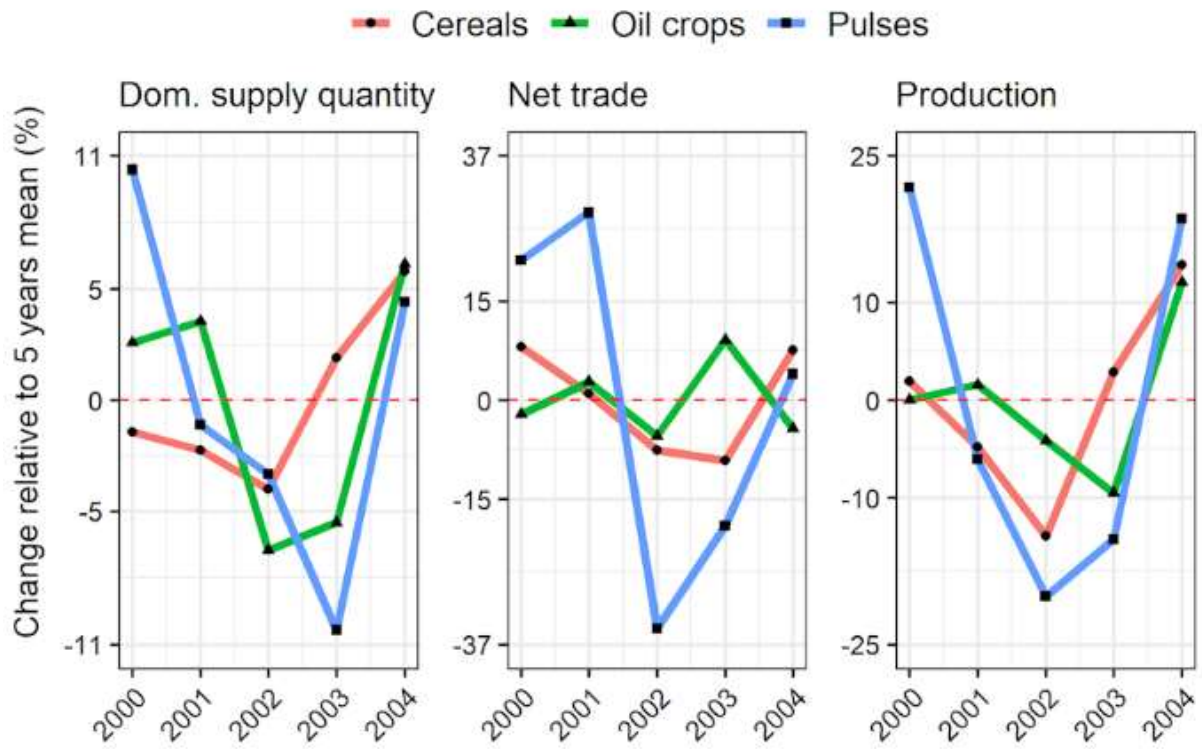
Southern Africa (1992)



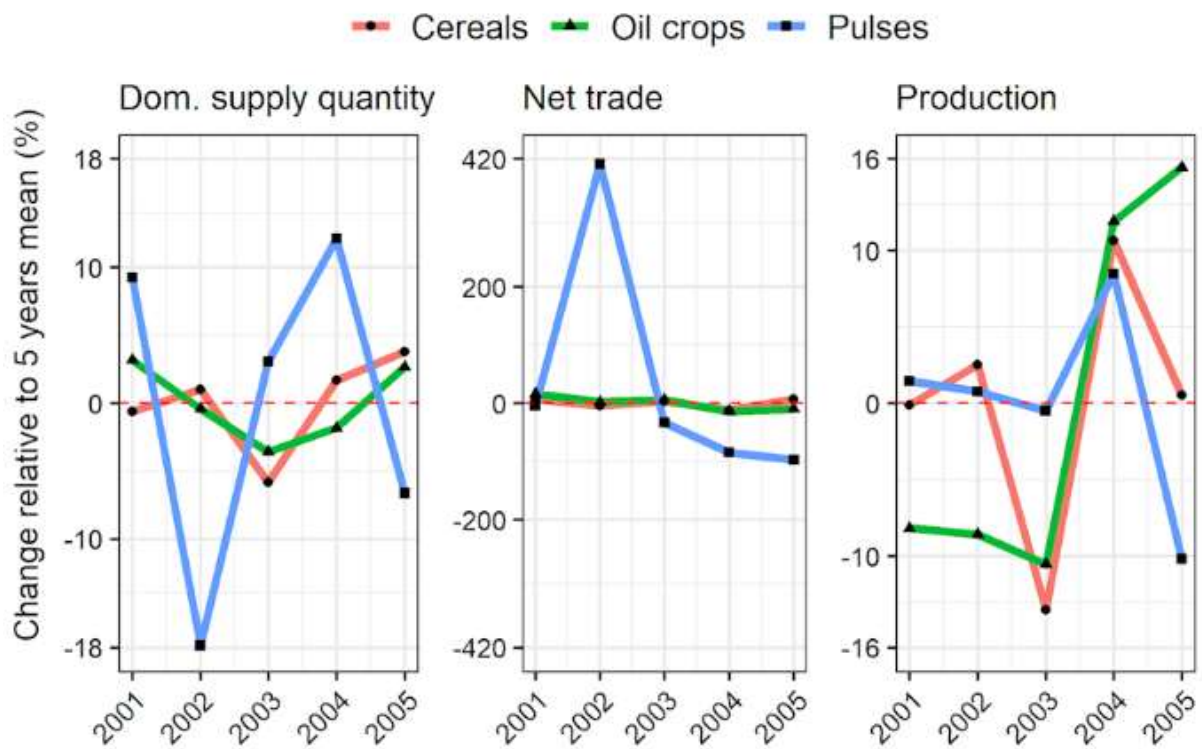
Australia (2002)



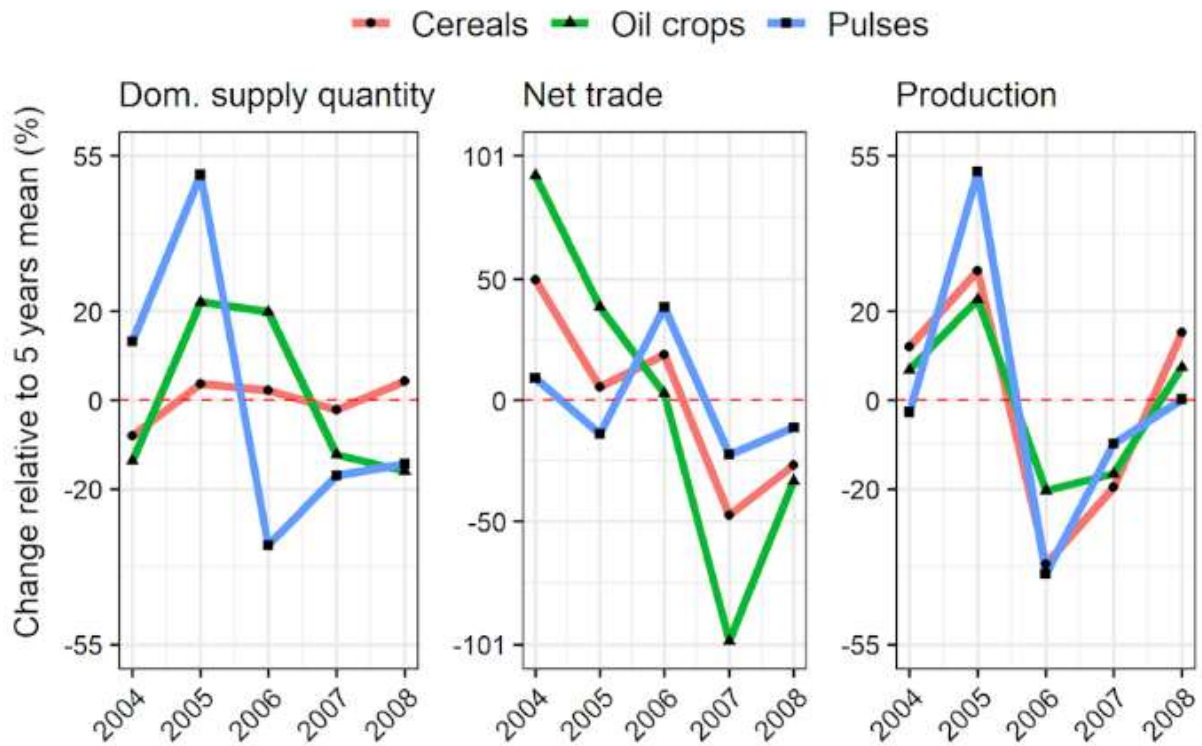
Northern America (2002)



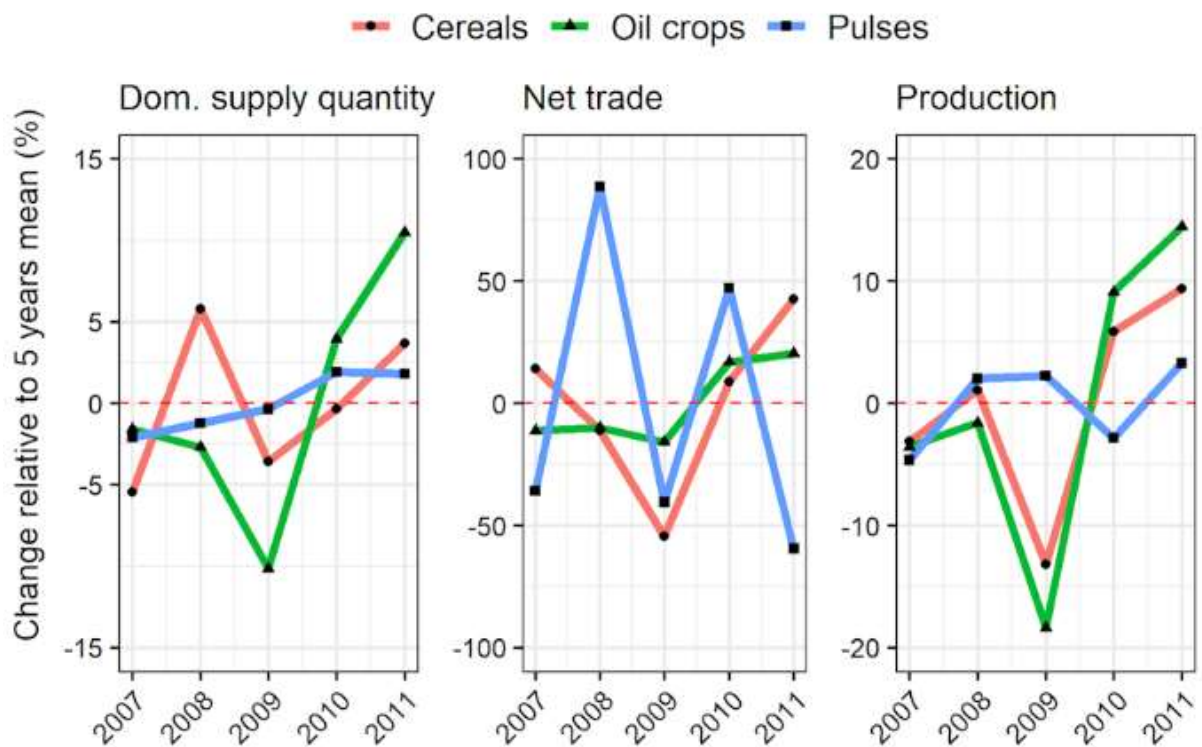
Western Europe (2003)



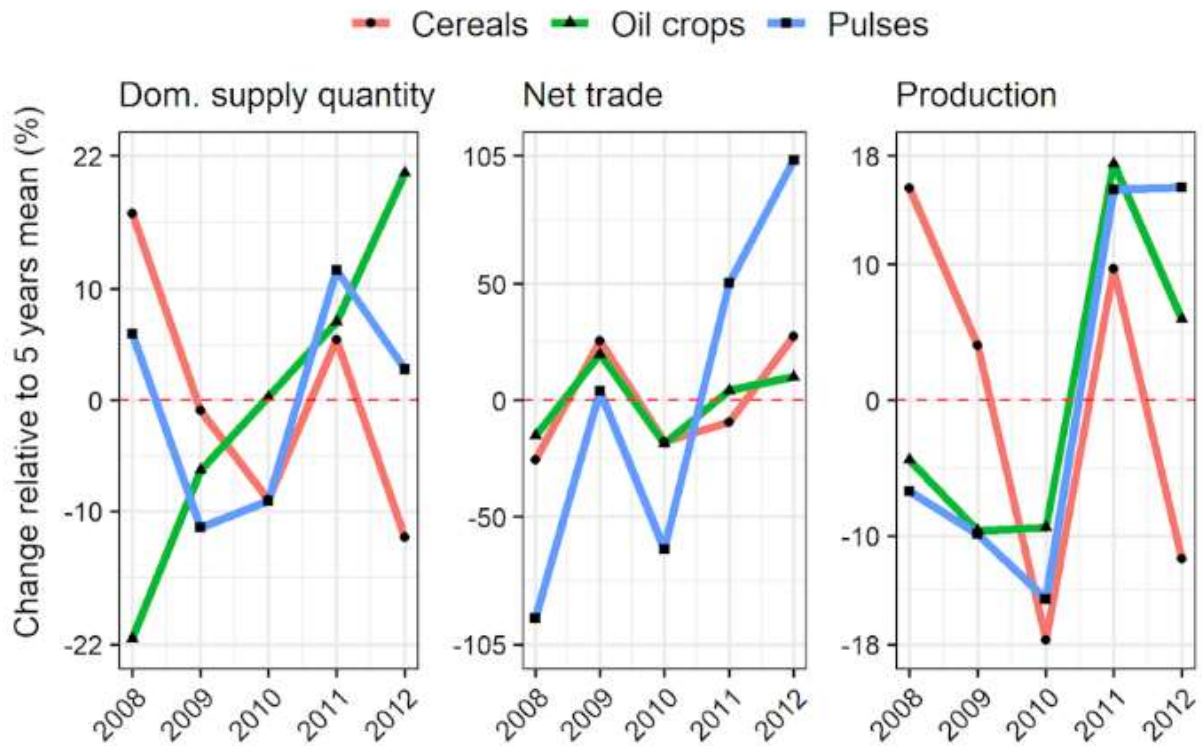
Australia (2006)



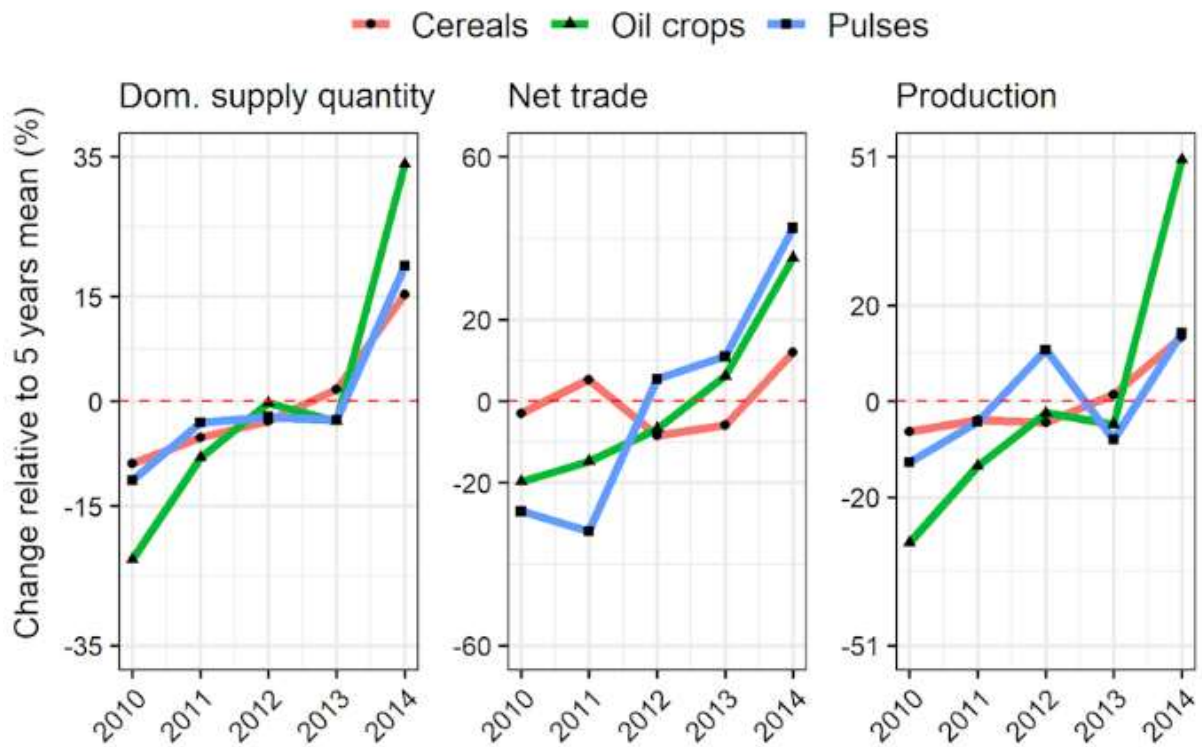
Southern America (2009)



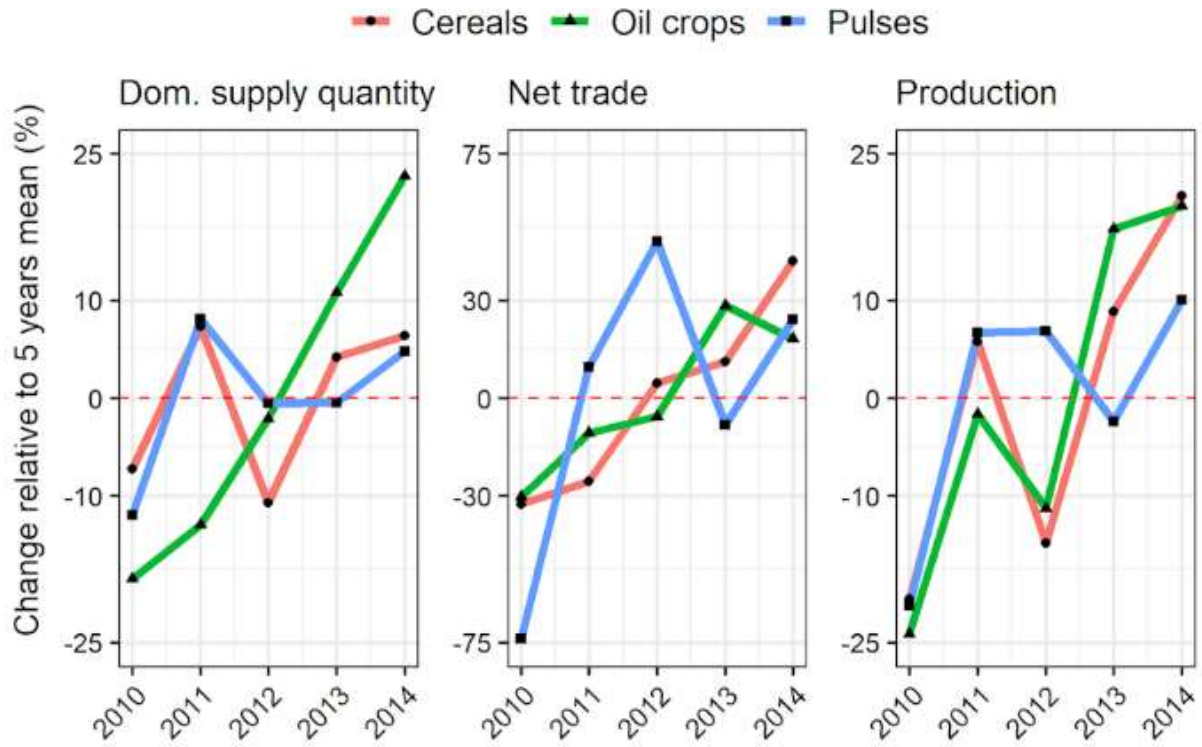
Eastern Europe (2010)



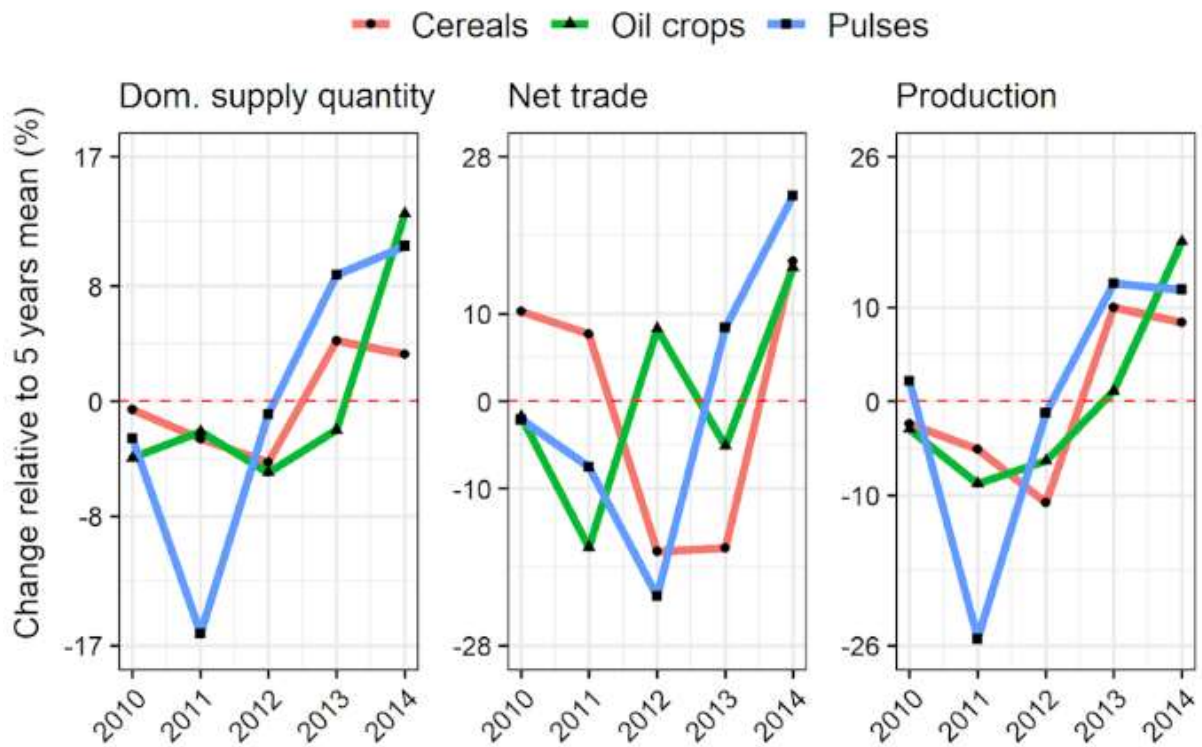
Eastern Africa (2012)



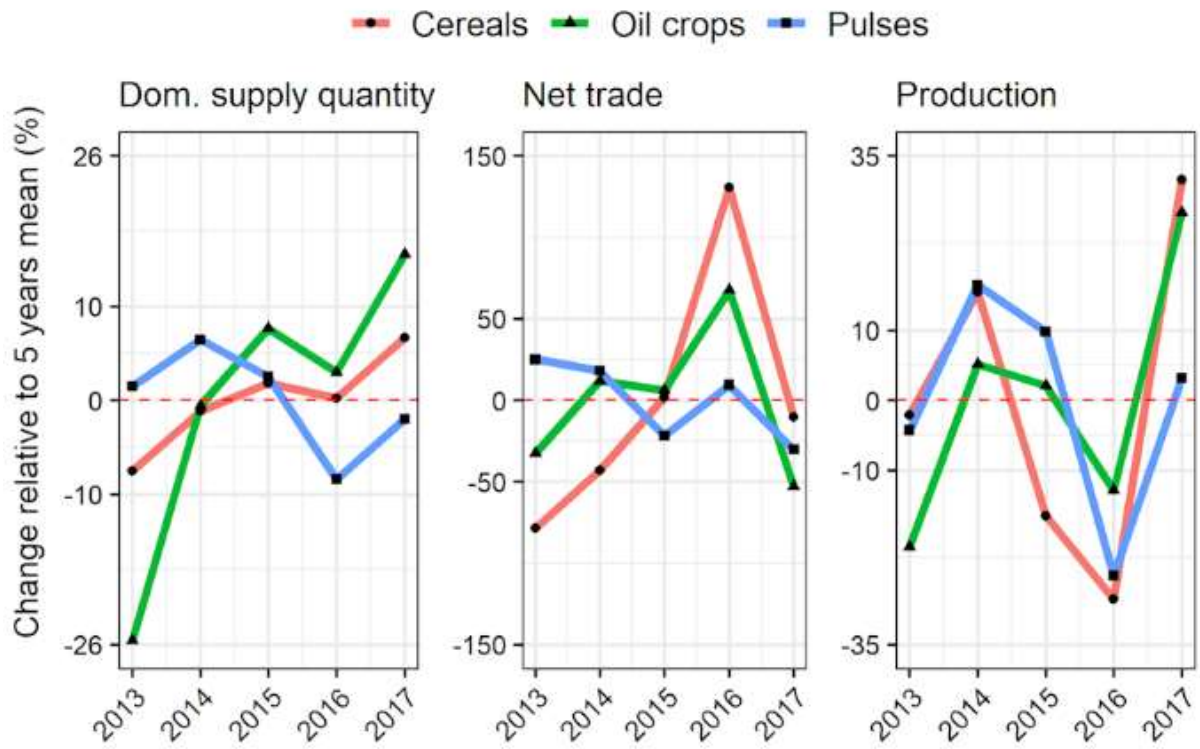
Eastern Europe (2012)



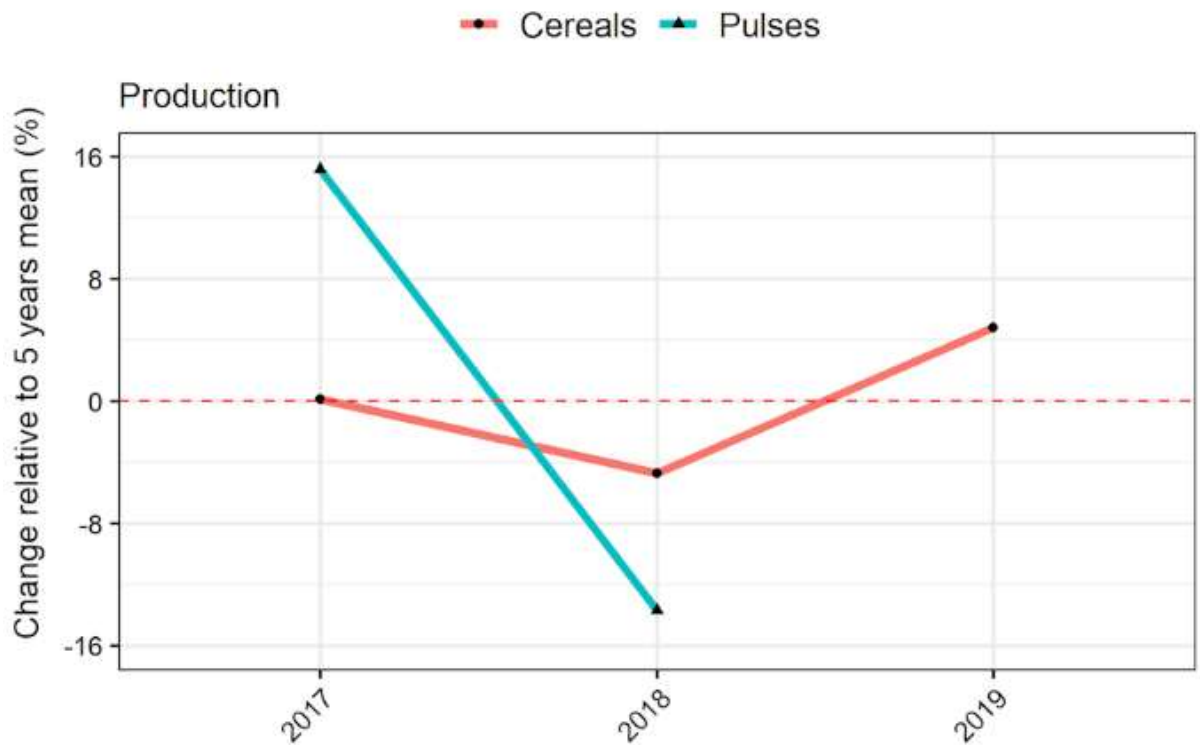
Northern America (2012)



Southern Africa (2015)



Western Europe (2018)*



* Data for year 2019 and 2020 not yet available

Appendix A4 - List of project publications

Berger, M., Campos, J., Carolli, M., Dantas, I., Forin, S., Kosatica, E., Kramer, A., Mikosch, N., **Nouri, H.**, Schlattmann, A., Schmidt, F., Scomberg, A., Semmling, E. (2021). Advancing the water footprint into an instrument to support achieving the SDGs – Recommendations from the “Water as a Global Resources” research initiative (GRoW). *Water Resource Management* 35, 1291–1298, <https://doi.org/10.1007/s11269-021-02784-9>

Dubovyk, O., Ghazaryan, G., González, J., Graw, V., Löw, F., & Schreier, J. (2019). Drought hazard in Kazakhstan in 2000–2016: a remote sensing perspective. *Environmental Monitoring and Assessment* 191, 510, <https://doi.org/10.1007/s10661-019-7620-z>

Eyshi Rezaei, E., Ghazaryan, G., González, J., Cornish, N., Dubovyk, O. Siebert, S. (2021). The use of remote sensing to derive maize sowing dates for large-scale crop yield simulations. *Int J Biometeorol* 65, 565–576, <https://doi.org/10.1007/s00484-020-02050-4>

Eyshi Rezaei, E., Ghazaryan, G., Moradi, R., Dubovyk, O., Siebert, S. (2021). Crop harvested area, not yield drives variability in crop production in Iran. *Environmental Research Letters* 16, 064058. <https://doi.org/10.1088/1748-9326/abfe29>

Eyshi Rezaei, E. and Lashkari, A. (2019). The consequences of change in management practices on maize yield under climate warming in Iran. *Theoretical and Applied Climatology* 137, 1001-1013. <https://doi.org/10.1007/s00704-018-2637-8>

Eyshi Rezaei, E., Siebert, S., Hüging, H., Ewert, F. (2018). Climate change effect on wheat phenology depends on cultivar change. *Scientific Reports* 8, 4891. <https://doi.org/10.1038/s41598-018-23101-2>

Eyshi Rezaei, E., Siebert, S., Manderscheid, R., Müller, J., Mahrookashani, A., Ehrenpfordt, B., Haensch, J., Weigel, H.-J., Ewert, F. (2018). Quantifying the response of wheat yields to heat stress: The role of the experimental setup. *Field Crops Research* 217, 93-103. <https://doi.org/10.1016/j.fcr.2017.12.015>

Frischen, J., Meza, I., Rupp, D., Wietler, K., Hagenlocher, M. (2020). Drought risk to agricultural systems in Zimbabwe: A spatial analysis of hazard, exposure, and vulnerability. *Sustainability* 12, 752, <https://doi.org/10.3390/su12030752>

Gerdener, H., Engels, O., Kusche, J. (2020). A framework for deriving drought indicators from the Gravity Recovery and Climate Experiment (GRACE). *Hydrology and Earth System Sciences* 24, 227–248. <https://doi.org/10.5194/hess-24-227-2020>

Ghazaryan G., Dubovyk O., Graw, V., Kussul N., Schellberg, J. (2020). Local-scale agricultural drought monitoring with satellite-based multi-sensor time-series. *GIScience & Remote Sensing* 57, 511-524, <https://doi.org/10.1080/15481603.2020.1778332>

Ghazaryan, G., König, S., Eyshi Rezaei, E., Siebert, S., Dubovyk, O. (2020). Analysis of drought impact on croplands from global to regional scale: A remote sensing approach. *Remote Sensing*, 12, 4030, <https://doi.org/10.3390/rs12244030>

Hagenlocher, M., Meza, I., Anderson, C., Min, A., Renaud, F.G., Walz, Y., Siebert, S., Sebesvari, Z. (2019). Drought vulnerability and risk assessments: state of the art, persistent

gaps, and research agenda. Environmental Research Letters 14, 083002. <https://doi.org/10.1088/1748-9326/ab225d>

Heino, M., Puma, M., Ward, P., Gerten, D., Heck, V., **Siebert, S.**, Kummu, M. (2018). Two-thirds of global cropland area impacted by climate oscillations. Nature Communications 9, 1257. <https://doi.org/10.1038/s41467-017-02071-5>

Keune, J., Sulis, M., Kollet, S., **Siebert, S.**, Wada, Y. (2018). Human water use impacts on the strength of the continental sink for atmospheric water. Geophysical Research Letters 45, 4068-4076. <https://doi.org/10.1029/2018GL077621>

Landmann, T., Eidmann, D., **Cornish, N.**, **Franke, J.**, **Siebert, S.** (2019). Optimizing harmonics from Landsat time series data: The case of mapping rainfed and irrigated agriculture in Zimbabwe. Remote Sensing Letters 10, 1038-1046, <https://doi.org/10.1080/2150704x.2019.1648901>

Meza, I., **Eyshi Rezaei, E.**, **Siebert, S.**, **Ghazaryan, G.**, **Nouri, H.**, **Dubovyk, O.**, **Gerdener, H.**, **Herbert, C.**, **Kusche, J.**, **Popat, E.**, Rhyner, J., Jordaan, A., **Walz, Y.**, **Hagenlocher, M.** (2021). Drought risk for agricultural systems in South Africa: Drivers, spatial patterns, and implications for drought risk management. Science of The Total Environment 799, 149505. <https://doi.org/10.1016/j.scitotenv.2021.149505>

Meza, I., **Hagenlocher, M.**, Naumann, G., Vogt, J., **Frischen, J.** (2019). Drought vulnerability indicators for global-scale drought risk assessments. Publications Office of the European Union, Luxembourg, <https://doi.org/10.2760/73844>

Meza, I., **Siebert, S.**, **Döll, P.**, **Kusche, J.**, **Herbert, C.**, **Eyshi Rezaei, E.**, **Nouri, H.**, **Gerdener, H.**, **Popat, E.**, **Frischen, J.**, Naumann, G., Vogt, J.V., **Walz, Y.**, **Sebesvari, Z.**, **Hagenlocher, M.** (2020). Global-scale drought risk assessment for agricultural systems. Nat. Hazards Earth Syst. Sci. 20, 695-712, <https://doi.org/10.5194/nhess-20-695-2020>

Popat, E. and **Döll, P.** (2021): Soil moisture and streamflow deficit anomaly index: an approach to quantify drought hazards by combining deficit and anomaly, Nat. Hazards Earth Syst. Sci., 21, 1337–1354, <https://doi.org/10.5194/nhess-21-1337-2021>.

Qin, Y., Abatzoglou, J.T., **Siebert, S.**, Huning, L.S., AghaKouchak, A., Mankin, J.S., Hong, C., Tong, D., Davis, S.J., Mueller, N.D. (2020). Agricultural risks from changing snowmelt. Nature Climate Change, 10, 459-465. <https://doi.org/10.1038/s41558-020-0746-8>

Schreier, J., **Ghazaryan, G.**, **Dubovyk, O.** (2020): Crop-specific phenomapping by fusing Landsat and Sentinel data with MODIS time series. European Journal of Remote Sensing 54, 47-58, <https://doi.org/10.1080/22797254.2020.1831969>

Schwarz M., **Landmann T.**, **Cornish N.**, **Wetzel K.-F.**, **Siebert S.**, **Franke J.** (2020). A spatially transferable drought hazard and drought risk modeling approach based on remote sensing data. Remote Sensing, 12, 237, <https://doi.org/10.3390/rs12020237>

Wan, W., Zhao, J., **Popat, E.**, **Herbert, C.**, **Döll, P.** (2021). Analyzing and monitoring the impact of streamflow drought on hydroelectricity production: A global-scale study. Water Resources Research 57, e2020WR028087, <https://doi.org/10.1029/2020WR028087>